The Amsterdam Bosbaan: a Top-class Rowing course?

A study of Lane Differences

June 1998

Linda M. van der Bend

Committee:

Prof. dr. ir. G.S. Stelling
Prof. dr. ir. J.A. Battjes
Dr. ir. J. van de Graaff
Ir. IJ.G. Haagsma
Ir. M.D.J.P. Bijvelds

TU Delft

Delft University of Technology
CiTG Subfaculty of Civil Engineering
Section Fluid Mechanics

ACKNOWLEDGEMENTS

This study was performed with valuable assistance and support.
First I want to thank prof. G.S. Stelling for accompanying and reviewing the (intermediate) results and the draft final report. His advice was not limited to Bosbaan issues. The personal interest in my proceedings and the hints for professional behaviour were extremely valuable for me. Prof. Stelling also arranged the computer, office facilities, and the DELFT3D model at the WL|DELFT HYDRAULICS institute. I like to thank the laboratory and S&O staff for this opportunity and their support. Also I thank my colleagues/roommates Jacqueline and Sylvio for the pleasant working atmosphere.

Next I thank the examination committee: Marco Bijvelds for helping me out, when the results appeared to be alarming again. Prof. J.A. Battjes, for reading and critically comment upon my draft report on such a short notice. IJsbrand Haagsma for teaching me some rowing knowledge, and dr. J. vd Graaff for valuable tips to increase the readability of my report.
I will thank the Municipality of Amsterdam for offering me this graduation subject and for the financial contribution during this period.

Additionally I want to thank some people in my neighbourhood who supported me during my study in general and this Bosbaan project especially. At first there is my boyfriend Joost. He often cheered me up when I was a bit down and motivated me in pursuing the project. From Saskia and Marianne I appreciate the warm friendship during my total study time very much.

Finally of course I thank my parents for their continuous support during the past years. Additional to facilitating my study in Delft they always were prepared to give special help and understanding.

Linda van der Bend

ABSTRACT

Introduction
The Amsterdam rowing course 'The Bosbaan' does not meet the requirements for international championships. The major concern is that under certain wind conditions, there is an unfairness between the racing lanes of the course, which is called lane difference. Lane differences in rowing contests are caused by inequalities in wind velocities, flow velocities, and wave heights between the lanes.

The international rowing federation, the FISA has proposed a widening of the course to 118 meters with 8 in stead of 6 lanes. They assume that this widening will decrease the lane differences. Objective of this study was to verify that assumption, and to propose additional measures to reduce the lane differences.

Method
The flow in the Bosbaan was computed with the 3-dimensional shallow-water solver DELFT3D-FLOW. The wind velocities above the course were implemented as surface boundary conditions. The influence of the computed flow velocities on the lane differences (arrival times of boats on the different lanes) is compared with the direct influence of wind on the basis of estimations of air- and water resistance forces.

Results
The trees around the Bosbaan cause differences in wind velocity above the course. In addition, this in-space-varying wind field induces a water circulation, with different flow velocities in different lanes. The differences in wave height between the lanes are of minor importance. The differences in wind- and flow velocity are maximal for the two outer lanes: lane 1 and lane 6, and increase with increasing wind speed.

These wind- and flow velocity differences result in differences in travel times between the lanes. Which of the two influences prevails, depends mainly on the direction of the wind: for adverse wind, the direct influence of wind on the rowers dominates, while for assisting wind, the larger part is caused by the differences in flow velocity.

The proposed widening in northern direction will yield somewhat higher wind- and flow velocities than nowadays. However, there will be an area with relatively lower flow velocity differences. For all wind directions, this area is at the north side of the course, and covers approximately 4 lanes. Compared with the existing situation, the lane differences increase for the lanes 3 to 8, but decrease with approximately 20% for the lanes 1 to 6. However, even with this improvement lane differences remain. Further widening is expected to increase the area with relatively lower lane differences and therefore decrease the lane differences between the lanes.

Additional measures to reduce the lane differences can be subdivided into measures to control the wind and measures to control the flow. The first category measures (not examined in this study) are most effective since they remove the cause. The best way to do that is an indoor facility. The second category measures just intend to influence the flow velocity differences. From exploration of likely measures, two realistic possibilities for further investigation arose: (i) lateral fences, slowing down the flow, and (ii) deepening of specific areas of the course, directing the flow.

SAMENVATTING

Inleiding
De Amsterdamse roeibaan 'de Bosbaan' voldoet niet aan de eisen voor internationale toernooien. Het grootste probleem is dat er onder bepaalde windcondities oneerlijkheid optreedt tussen de verschillende banen. Dit noemt men boeiverschil. Boeiverschillen tijdens roeiwedstrijden worden veroorzaakt door ongelijkheden in windsnelheden, stroomsnelheden en golfhoogten tussen de banen.

De internationale roeibond, de FISA, heeft een verbreding van de baan voorgesteld van 92 tot 118 meter met 8 in plaats van 6 banen. Daarbij wordt verondersteld dat deze verbreding de boeiverschillen zal verkleinen. Het doel van deze studie was om het effect van deze verbreding op de boeiverschillen te bepalen en te kijken naar eventuele andere methoden ter vermindering van het boeiverschil.

Methode
De stroming in de Bosbaan is gemodelleerd met het 3-dimensionale ondiep-water model DELFT3D-FLOW. De windsnelheden boven de baan zijn geïmplementeerd als randvoorwaarden op het oppervlak. De invloed van de berekende stroomsnelheden op de boeiverschillen (roeitijden van de boten per baan) is vergeleken met de directe invloed van wind, op basis van schattingen van de lucht- en water weerstandskrachten.

Resultaten
De bomen rond de Bosbaan veroorzaken verschillen in windsnelheid boven de baan. Daarnaast veroorzaakt dit in ruimte variërende windveld een watercirculatie met verschillende stroomsnelheden per baan. De verschillen in golfhoogte per baan zijn van ondergeschikt belang. De grootste verschillen in wind- en stroomsnelheid treden op tussen de twee uiterste banen, baan 1 en baan 6, en nemen toe met toenemende windsnelheid.

Deze verschillen in wind- en stroomsnelheid resulteren in verschillende roeitijden tussen de banen. Welk van deze twee invloeden overheerst, hangt voornamelijk af van de windrichting: in geval van tegenwind domineert de directe invloed van wind op de roeiers, terwijl in geval van meewind het grootste deel wordt veroorzaakt door de stromingsverschillen.

De voorgestelde verbreding in noordelijke richting leidt tot iets hogere wind- en stroomsnelheden dan nu. Er zal echter een gebied ontstaan met relatief lagere stroomsnelheidsverschillen. Voor alle windrichtingen ligt dit gebied aan de noordzijde van de baan, en beslaat ongeveer 4 banen. Vergeleken met de bestaande situatie zullen de boeiverschillen toenemen voor de banen 3 tot 8, maar afnemen met ongeveer 20% voor de banen 1 tot 6. Echter, ondanks deze verbreding zullen boeiverschillen blijven bestaan. Een verdere verbreding zal waarschijnlijk leiden tot een vergroting van het gebied met relatief lagere boeiverschillen, en dus tot een vermindering van het boeiverschil tussen 6 banen.

Additionele maatregelen ter vermindering van de boeiverschillen kunnen worden onderverdeeld in maatregelen ter beïnvloeding van de wind en maatregelen ter beïnvloeding van de stroming. De eerste categorie van maatregelen (niet onderzocht in deze studie) zijn het meest effectief want deze hebben betrekking op de oorzaak. De ideale oplossing in dit kader zou zijn een volledige overkapping van de Bosbaan. De tweede categorie van maatregelen zijn slechts bedoeld om de stroomsnelheidsverschillen te verminderen. Na inventarisatie van mogelijke maatregelen kwamen twee realistische maatregelen in aanmerking voor nader onderzoek: (i) bodemschermen in de breedte-richting van de baan ter afremming van de stroming, en (ii) verdiepen van bepaalde gebieden van de baan om de stroming te richten.

TABLE OF CONTENTS

LIST OF FIGURES

LIST OF TABLES

LIST OF SYMBOLS

Roman letters

Symbol	Description	Units
A	(wetted) surface area of the body	m^2
B	width of the Bosbaan	m
B	width of the racing shell	m
C_{2D}	2D Chézy coefficient	$m^{½}/s$
C_b	block coefficient	-
C_d	wind drag coefficient	-
C_f	friction coefficient due to skin friction on (wetted) surface	-
C_u	wind velocity coefficient	%
C_v	Viscous resistance coefficient	-
c	wave celerity	m/s
$c_{\mu'}$	constant in Kolmogorov-Prandtl's eddy viscosity formulation	-
c_μ	calibration constant in k-ε model	-
c_D	constant relating ε to L	-
$c_{1\varepsilon}$	calibrated constant related to production term in ε equation	-
$c_{2\varepsilon}$	calibrated constant related to dissipation rate in ε equation	-
D_x,D_y	diffusive terms in momentum equations in x- and y-direction respectively	?
d	depth below horizontal reference plane z = 0	m
F	fetch	m
F	friction force	N
F_{air}	total air resistance force	N
F_{row}	force delivered by the rowers	N
F_{water}	total water resistance force	N
Fr	Froude number	-
g	acceleration of gravity	N/kg
H	total water depth	m
H	wave height	m
i,j	integers indicating directions of the Cartesian coordinate system (x: i,j=1; y: i,j=2; z: i,j=3)	?
K	layer number (surface layer: K=1; bed layer K=Kmax)	-
k	turbulent kinetic energy per unit mass	m^2/s^2
k_s	Nikuradse roughness length	m
L	characteristic length scale	m
L	length of the Bosbaan	m
L	length of the racing shell	m
L	wave length	m
l_m	mixing length	m
M	mass of boat and rowers	kg
m,n,k	grid cell label, staggered grid	-
P	power	W
P	pressure	N/m^2
P_a	atmospheric pressure	N/m^2
Re	Reynolds number	-
T	wave period	s
T	travel time	s
T8-T3	lane difference between lane 8 and lane 3	s
T6-T1	lane difference between lane 6 and lane 1	s
t	time	s
t	wind duration	s
U	characteristic horizontal velocity	m/s
U_{10}	wind velocity measured at the meteorological institute at Schiphol	m/s

Symbol	Description	Units
u	flow velocity in x-direction	m/s
u_*	friction velocity	m/s
u_{*b}	bed friction velocity	m/s
u_{*s}	friction velocity at the free surface induced by wind stress	m/s
V	velocity of the flow around the body [m/s]	m/s
v	flow velocity in y-direction	m/s
v_b	boat velocity [m/s];	m/s
W	characteristic vertical velocity	m/s
w	flow velocity in z-direction	m/s
w	local wind velocity 1.75 m above the course [m/s	m/s
w_*	wind shear velocity	m/s
x_i	Cartesian coordinates (tensor notation)	-
(x,y,z)	Cartesian coordinate system	-
z_0	bottom roughness height	m
z_{w0}	wind roughness height	m
2DH	two-dimensional horizontal	-
2DV	two-dimensional vertical	-

Greek letters

δ	Kronecker delta	-
Δ	Laplace operator	-
Δh	draught of the racing shell	m
Δt	timestep of the computation	s
Δx, Δy	rectangular horizontal mesh sizes in x- and y-direction respectively	m
$\Delta\sigma(K)$	thickness of layer K (in percentage of the total depth)	%
ε	dissipation rate of turbulent kinetic energy per unit mass	m^2/s^3
ζ	water level above horizontal reference plane $z = 0$	m
κ	von Kármán constant	-
ν_m	the kinematic viscosity	m^2/s
ν_t	eddy viscosity	m^2/s
ν_t^H	horizontal component of eddy viscosity tensor	m^2/s
ν_t^V	vertical component of eddy viscosity tensor	m^2/s
ρ	density of water	kg/m^3
ρ_{air}	density of air	kg/m^3
σ	scaled vertical coordinate	-
σ_X	turbulent Prandtl/Schmidt number with reference to scalar X	-
τ_b	bottom stress	$kg/m/s^2$
τ_{bx},τ_{by}	component of bottom stress x- and y-direction respectively	$kg/m/s^2$
τ_{ij}	components of stress due to molecular viscosity	$kg/m/s^2$
τ_{ij}	components of the Cartesian stress tensor	$kg/m/s^2$
τ_s	wind surface stress	$kg/m/s^2$
τ_{sx},τ_{sy}	component of wind shear stress in x- and y-direction respectively	$kg/m/s^2$
ω	vertical component of the velocity vector in σ-transformed coordinate system	-

1. INTRODUCTION

1.1 General

The Mayor and Aldermen of the City of Amsterdam are willing to realise a top-class rowing course, qualifying Amsterdam to host international rowing championships. The Bosbaan, an existing rowing course situated in the Amsterdamse Bos, was designated for this plan. At present, however, the Bosbaan does not meet the requirements for international championships.

The major concern is the current unfairness between the racing lanes at certain wind conditions. This unfairness is called lane difference. It is defined as the difference in time that rowing crews which deliver the same amount of power need to cover the same distance on different lanes. Lane differences in rowing contests are caused by inequalities in wind velocities, flow velocities, and wave heights between lanes.

This project focuses on the second point, the differences in flow. It is assumed that the wind generates a horizontal circulation in the course. This means that during a contest, one rowing combination rows with the flow, while, at the same time, another rowing combination at the other side of the course rows against the flow.

The international Rowing Federation (FISA) has proposed a widening of the Bosbaan (from the present 92 m to 118 m). The FISA assumes this will cause a sufficient decrease in lane differences and make the Bosbaan eligible for hosting future World Championships.

This project was performed as a practical work assignment for the municipality of Amsterdam. WL|DELFT HYDRAULICS provided office facilities, computer facilities, and the flow model DELFT3D-FLOW.

1.2 Purpose of the study

Lane differences are caused by different conditions in the lanes of the rowing course. For the Bosbaan these differences are solely caused by the wind field, which varies strongly in space above the course, resulting in variable influences on rowers and their boats. As mentioned above, the following influences can be distinguished:

- the influence from wind directly on the rower(s) and on the part of the boat above water;
- the influence from flow (also generated by wind) on the part of the hull under water;
- the influence of wave action on the boat.

Wind pattern data are available from wind tunnel tests performed by TNO in 1989. This report presents predictions of the flow field in the Bosbaan for the normative wind conditions in summer. The flow in the Bosbaan is computed with the 3-dimensional shallow-water solver DELFT3D-FLOW, which has been made available by WL|DELFT HYDRAULICS. The influence of the computed flow velocities on the lane differences (travel times of the boats along the different lanes) is compared with the direct influence of wind, taking into account the spatial variations of wind- and flow velocities on the resistance forces on the rowers and their boats.

One possible way of reducing the lane differences might be the proposed widening of the course, resulting in the option to choose the six best lanes out of eight. The effect on the flow of this widening is estimated, with numerical computations. Other possible options to reduce the wind-induced flow are mentioned briefly.

1.3 Assumptions

A physical model is a simulation of the real world. On the basis of assumptions, physical phenomena can be expressed as differential equations. For shallow-water flow, these assumptions are e.g. hydrostatic pressure, and the Boussinesq approximation. Additional assumptions are needed to solve these equations numerically, e.g. turbulent closure assumptions. A numerical model therefore contains empirical parameters with values that vary from application to application, and thus from model to model. The only way to determine these values for a specific situation is to verify the model results with the prototype measurements (in the Bosbaan case: measurements of flow velocities for known wind conditions).

For the Bosbaan, measurements of an existing situation did not exist. Values of the empirical parameters are therefore determined as a best guess with the present knowledge, but not calibrated for an existing situation. With these 'best choice' values for the numerical parameters, the model is used to predict flow fields for the new widened situation. The results of these computations should therefore be used as a means to predict the tendencies of the changes, rather than as a comparison of exact numbers.

Other assumptions in this study:

- The local wind data used for the flow computations are considered to be correct, however they are also a result of (physical) modelling, containing its own uncertainties.
- The influence of the differences in wave action between the lanes on the total lane differences is assumed to be small in comparison to the two other influences.
- To determine the contribution of the other influences on the lane differences, travel times for a coxed four on 2000 meters are computed and compared. The boat velocity is calculated by estimation of the boat- and wind resistance, and the estimated delivered effective power of a rowing combination.

1.4 Outline of the report

This report can be divided into two parts. Part I, containing the Chapters 2 to 5, presents the problem and the modelling results. Part II, containing the Chapters 6 to 8, gives detailed information about the way the results were obtained (theoretical background and numerical model).

Part I

Chapter 2 describes the actual situation. First a detailed analysis of the problem is given, after which the numerical model is explained briefly. The remaining part of the Chapter presents the local wind fields together with the resulting flow fields for various Schiphol wind conditions. Also a comparison is made between the part of the lane differences caused by the direct influence of wind, and the part caused by the differences in flow velocity. Both parts are therefore expressed as differences in travel time of a four on 2000 meters.

Chapter 3 describes the resulting flow fields and lane differences for the widened Bosbaan. Chapter 4 discusses other ways to reduce the flow differences between the lanes. Chapter 5, gives concluding remarks in combination with recommendations.

Part II

Chapter 6 gives the mathematical-physical formulations that were used for the flow simulation. Special attention is paid to the turbulence closure assumptions. Chapter 7 explains briefly the solution method of DELFT3D-FLOW. Chapter 8 describes the details of the Bosbaan model and makes appropriate choices for the numerical and physical parameters on the basis of a sensitivity analysis. The last part of this Chapter discusses the numerical aspects of the hydrostatic pressure assumption.

2. THE PRESENT SITUATION

2.1 Introduction

Lane differences result from differences in wind, flow, and wave conditions; all result from the differences in wind conditions. Section 2.2 describes these aspects in relation to the present situation of the Bosbaan.

Section 2.3 discusses the two most important factors of the three: the wind and the flow. First it gives a description of the wind fields above the course, and explains the flow patterns which result from those wind fields. Both wind- and flow fields are related to measured wind conditions at Schiphol. The final part of this section determines the differences in both wind- and flow velocities between the lanes.

Section 2.4 explains to what degree those differences in wind- and flow velocity influence the travel times of rowing combinations in the different lanes (lane differences). Finally, section 2.5 presents a brief summary of this chapter.

2.2 The Problem

2.2.1 Description of the site

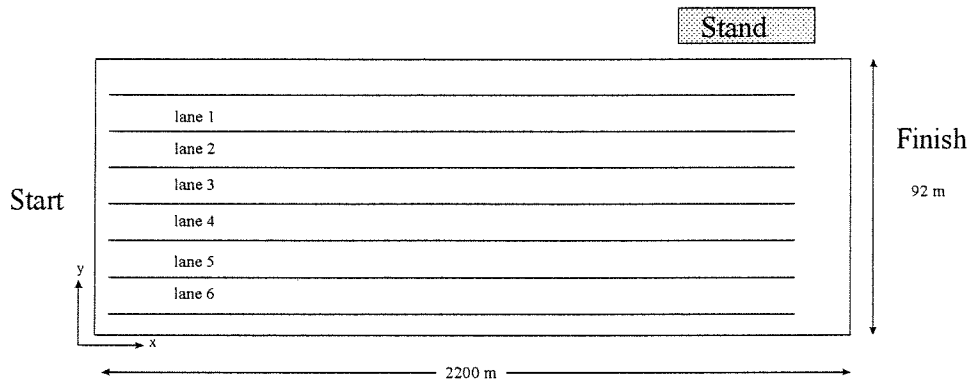

Figure 2.1: The Bosbaan lay-out

The Bosbaan was opened in 1936 as part of the Amsterdamse Bos. Originally, the course had a total width of 72 meters, and consisted of 5 lanes. In 1964, for the European Championships, it was widened to 92 meters, divided into 6 lanes of 12.5 meters each (total 75 meters). At the south side there remains a strip with a width of 5 meters; at the north side a 12 meters wide training lane remains. The length of the Bosbaan is 2200 meters, with a racing length of 2000 meters. The depth of the course is 2.2 meters. The banks consist of slopes planted with reeds. A plan of the course is shown in Appendix A.

The orientation of the course is from west-south-west to east-north-east (which is also the racing direction) at an angle of 13 degrees to the east, see Figure 2.2.

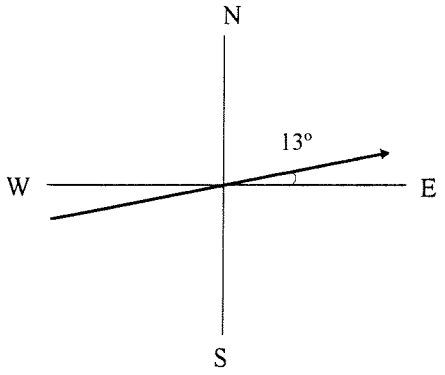

Figure 2.2: Orientation of the course

On the south side, the course is bounded by a strip of flat land, with a road on it. Next to this is a dike, with behind it trees along the full length of the course. On the north side the ground level is slightly sloping. This area is overgrown with trees, alternating with grassy plains. A cross-section is shown in Figure 2.3 (not drawn to scale).

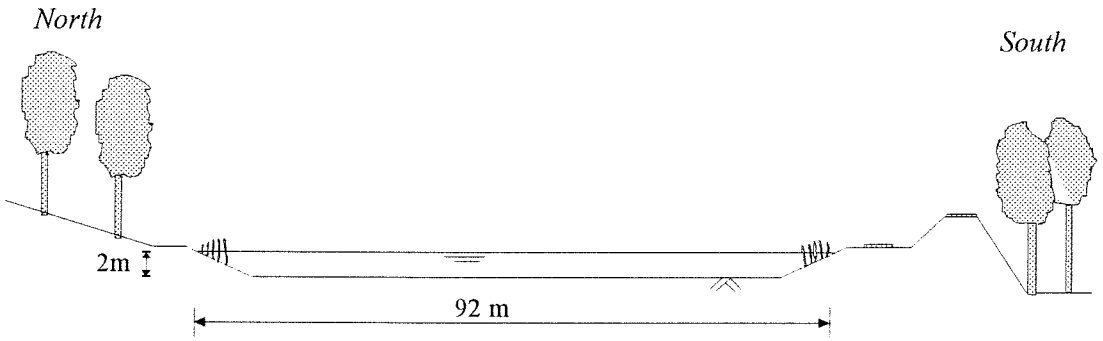

Figure 2.3: Cross-section of the Bosbaan

2.2.2 Lane difference

Lane differences in the Bosbaan are caused solely by wind. Wind effects however, can be separated into three parts: (i) the direct wind force on the rowing combination, (ii) flow forcing and (iii) wave forcing. The most important conclusions resulting from earlier research into lane differences on the Bosbaan (Van Melle (1989), Van der Zee (1985), Van Oort (1986), Van Elk/Husmann (1983), Bruijnen/Lageweg (1985), and Dekkers/Kerssens (1985)) are assimilated herein.

wind

The most important parameters are the wind speed, the wind direction and the spatial variations of the wind field above the course. Since only steady state computations will be performed, temporal variations are not taken into account. The trees along the course cause strong spatial variations in the local wind field, and thus differences in wind velocity between the lanes. The most unfavourable conditions occur at a head wind with a 45° angle to the course axis: lee side will have a disadvantage over the lanes at the opposite side; with wind in the back, lee side will have a small advantage. The differences generally increase with increasing wind speed, because the direct wind force on the rowing combination depends quadratically on the difference between boat speed and wind speed.

flow

When wind is blowing over a body of water the water near the surface will move in the wind direction, thus producing a windward lowering of the water level and a leeward rise, which is called

wind set-up. This tilt of the surface creates a pressure gradient which induces a bottom flow in the direction opposite to that generated by the wind. This so-called vertical circulation occurs when the wind blowing over the water surface is constant in space, and the depth is constant as well, see Figure 2.4a. The water is coflowing with the wind at the surface and counterflowing in the lower parts of the water column. The depth-averaged velocity over a cross-section is zero.

However, when the wind forces exerted on the water surface vary in space, horizontal shear stress gradients occur, inducing a combined horizontal and vertical circulation. Horizontal circulation causes lane differences. Both the horizontal and the vertical circulation are shown separately in Figure 2.4, as proposed by Van der Zee in his study of wind-induced flow in the Bosbaan (1985). In his study however, he strongly simplified the process, not taking into account the combined effect of both circulations, and the horizontal exchange of momentum. The present study, based upon 3-dimensional flow computations, does take these effects into account.

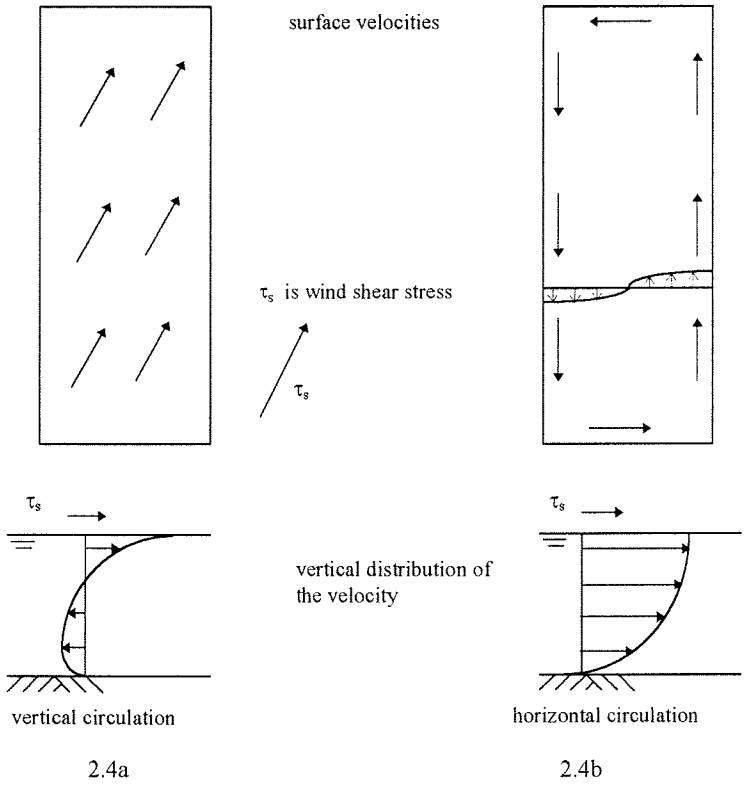

Figure 2.4: The complicated circulation pattern that occurs when the wind field varies in space can be separated into a vertical and a horizontal circulation, as was shown by Van der Zee (1985).

waves

When wind is blowing over a body of water, waves are generated. This process depends on the wind speed and the roughness of the water surface. In turn, the roughness of the water surface depends on the wave height. As wind comes up, the wave height grows over some stretch of water until the energy transfer from the water surface is equal to the rate of energy dissipation internally and by bottom friction. In case of the Bosbaan the wave height will be fetch limited: i.e. the wave height at some point mainly depends on the distance of that point from the upwind boundary.

The space-varying wind field above the course will generate waves with different heights in the different lanes. The restricted dimensions of the course, however, will prevent the waves to grow to such length as to influence the bottom friction, and thus the flow effectively. The only way that the differences in wave height may contribute to the lane differences is via the wave resistance.

2.3 Calculations of Velocities

2.3.1 The Bosbaan model

The flow in the Bosbaan is modelled with the 3D shallow-water solver DELFT3D-FLOW, which has been made available by WL|DELFT HYDRAULICS. All details concerning the numerical model are discussed in the second part of this report.

The Bosbaan has been covered with a numerical mesh with different mesh-sizes in x- and in y-direction. In vertical direction, a non-equidistant layer distribution with finer resolution near the surface and near the bottom, proved to be the only way to represent the vertical velocity profiles accurately. The internal stresses in DELFT3D-FLOW are modelled by means of the eddy viscosity concept, explained in chapter 6.

The velocity gradients for the Bosbaan model are considerable both in horizontal and in vertical directions, resulting in a large amount of momentum exchange between adjacent grid cells, due to turbulent vortices. The modelling of the eddy viscosity is therefore of major importance to describe the flow in the Bosbaan correctly. The model proved to be very sensitive to this eddy viscosity coefficient, both in vertical and in horizontal direction. In vertical direction a so-called 2-equation model has been applied: the k-ε model, which takes the production and dissipation of turbulent kinetic energy into account. In horizontal direction a best guess was used as estimate for the eddy viscosity. The lack of measurements must be mentioned in this respect.

The water in the Bosbaan starts to flow because of the wind. In DELFT3D-FLOW, wind forcing is imposed as a boundary condition at the water surface. At each grid point, wind velocities- and directions must therefore be prescribed.

2.3.2 Wind fields

The Bosbaan is surrounded by trees, at the north side alternating with grassy fields. The distance between the course and the water side is only a few meters. This close proximity of trees causes differences in wind velocity above the course. To quantify these differences, scale model measurements were performed in a boundary layer wind tunnel at TNO; see Van Melle (1989). The result of these measurements is a table of wind coefficients for 21 locations on the race course (lane 1, in between lane 3 and lane 4, and lane 6, at locations 250, 500, 750, 1000, 1250, 1500, 1750 and 2000 m), for all wind directions in steps of 15°, presented in Table 2.2 in the Appendix 'Tables'; wind direction 0° corresponds to north wind.

The wind coefficients relate the local wind velocities at the Bosbaan to the wind velocity U_{10} measured at the meteorological office at Schiphol by:

$$w = C_u * U_{10} / 100 \qquad (2.1)$$

where: w local wind velocity 1.75 m above the course [m/s], U_{10} wind velocity measured at the meteorological station at Schiphol at 10 m height [m/s], and C_u wind (velocity) coefficient [%]. The wind coefficients, and with them the wind velocities, vary strongly over the course, but are always less than they would have been in the open field where C_u = 70%. Generally, it can be stated that wind velocities at north winds are a bit higher than at south winds: at the north side, there are less trees, and therefore less sheltering for the wind. For south-west wind (210° measured at Schiphol) the distribution of wind coefficients is given in Figure 2.5.

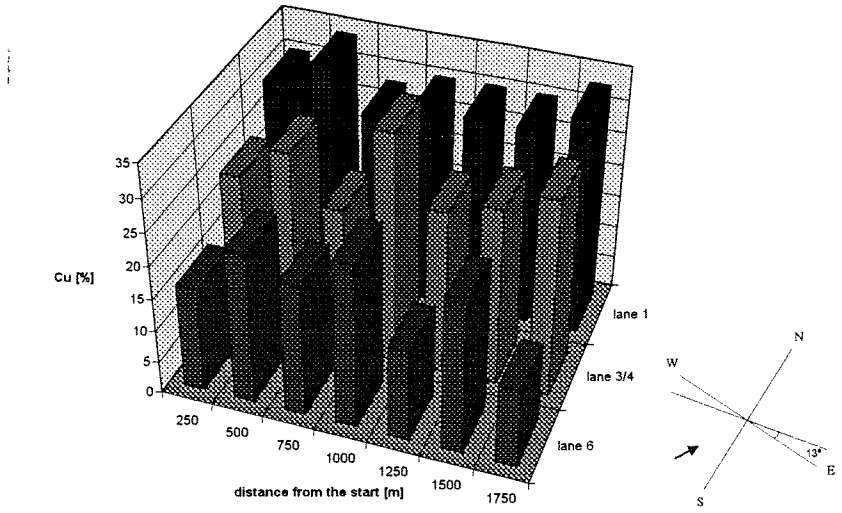

Figure 2.5: Wind field on the Bosbaan, wind direction Schiphol 210° (south-west wind)

The close proximity of trees also affects the local wind directions: the wind is 'tunnelled' in the direction of the course axis for most wind directions measured at Schiphol, as shown in Figure 2.6 (Van Melle, 1989 and Van Oort, 1986). Spatial variations of the wind directions above the course proved to be small; the local wind velocities just vary in magnitude, not in direction.

The differences in wind coefficients between lane 1 and lane 6 were determined for all measured wind directions, and are presented in Table 2.3 (Appendix 'Tables'). The last column gives the resulting differences in the rowing direction, which determine the differences in wind velocity between lane 1 and lane 6. Those differences are the largest at wind directions 45°, 120°, 210°, and 300°: wind with an angle of approximately 45° relative to the course axis. For those cases, the local wind direction is parallel to the course axis, as can be seen from Figure 2.6, in which those cases have been indicated with a thick line.

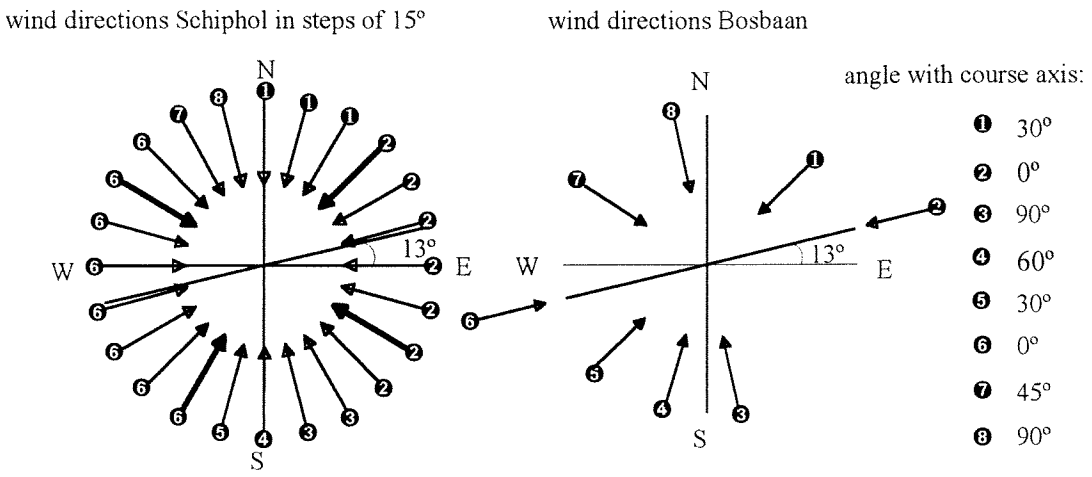

Figure 2.6: Local wind directions in relation to wind directions at Schiphol.

For the Bosbaan model, wind conditions at all grid points were needed as surface boundary conditions. These values were obtained by linear interpolation of the measured wind coefficients and multiplication with the concerned wind velocity measured at Schiphol. This way, local wind fields above the course are obtained, related to the wind conditions at Schiphol: for every wind condition at Schiphol (velocity and direction) there is a related wind field above the course.

Those wind fields, however, should not be looked upon as exact. The wind coefficients were obtained by physical modelling, containing its own uncertainties, and the linear interpolation of those coefficients was just an assumption. In addition, wind variations in time have been left out of consideration. Wind is a statistical matter, and hence, wind conditions are never the same. The wind fields used to model the flow are just one possible realisation of a stochastic experiment, related to an average wind velocity at Schiphol and will differ from realisation to realisation.

International rowing contests always take place in summer. The distribution of frequencies of wind conditions (wind velocity and wind direction) for the months July and August is given in Appendix B.

2.3.3 Flow patterns

Computations were performed with the Bosbaan model for the worst four wind directions (45°,120°, 210°, and 300°, which give the largest differences in wind velocity between the lanes) and six different wind speeds (2.5, 5, 7.5, 10, 12.5, and 15 $m.s^{-1}$) measured at the meteorological office at Schiphol. The local wind fields related to these wind conditions where obtained as described in section 2.3.2. The results for a wind velocity of 10 $m.s^{-1}$ (wind force 5), are presented in Figures 2.15 and 2.16 (Appendix 'Figures'), where a, b, c, and d correspond with the wind directions 45°,120°, 210°, and 300°, respectively.

Figures 2.15a-2.15d show the velocity vectors in the horizontal plane at 6 different depths: at the surface, at the bottom, and at 2, 16, 66, and 152 cm deep; these figures depict the Bosbaan on a strongly distorted scale. Figure 2.6 shows the computed surface velocities for the prevailing south-west wind. The surface velocity patterns show great similarity to the corresponding wind velocity fields, with the surface flow at the windward side being much smaller or even opposite to the flow at the lee-shore. At larger depths, complicated circulations patterns arise. At the bottom the flow direction is opposite to that at the surface, against the wind direction.

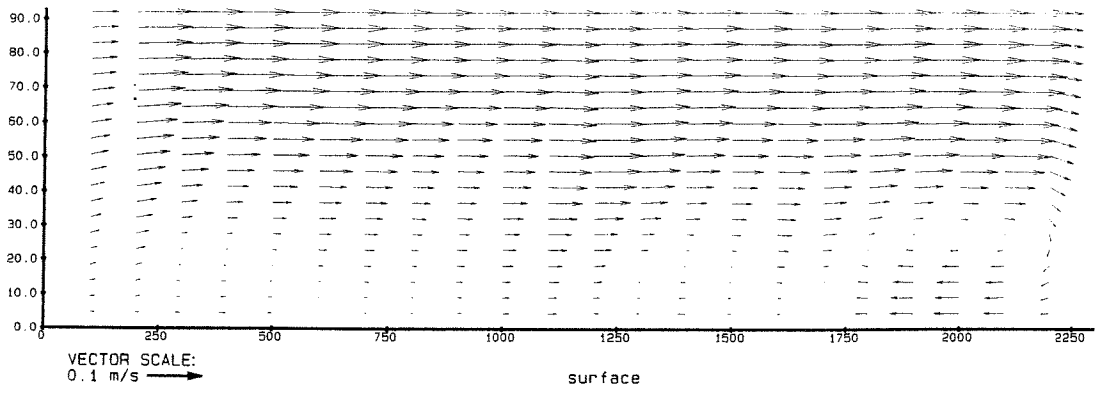

Figure 2.7: Bosbaan surface velocities, wind condition Schiphol 210°, 10 m/s

Figures 2.16a-2.16d compare the vertical distributions of velocity in x-direction (equivalent with the rowing direction) in the lanes 1, 3/4 (in between lane 3 and lane 4), and 6, on four locations at the course: 500, 1000, 1500, and 2000 meters from the start. The differences in velocity between lane 1 and lane 6 are considerable for all four wind directions. The velocity curve for lane 3/4 always lies in between those for lane 1 and lane 6. For a south-west wind of 10 m/s at Schiphol, the vertical distributions of velocity (in the rowing direction) for the 6 lanes are presented in Figure 2.8; the velocity curves present the average for each lane.

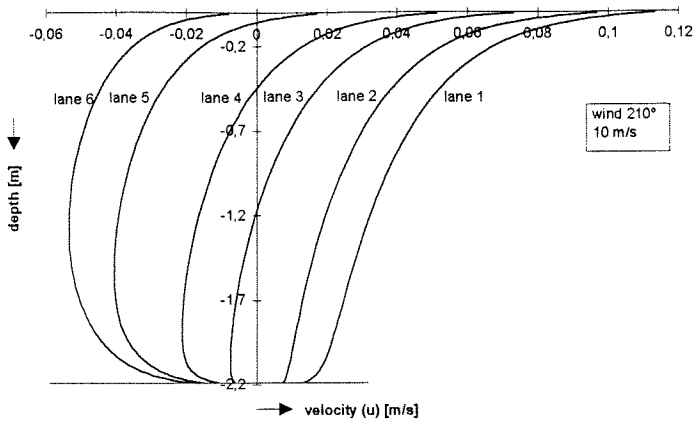

Figure 2.8: Vertical distributions of velocity for all lanes, wind condition Schiphol 210°, 10 m/s.

In lane 6, the windward side, the velocity is against the wind direction at the surface as well as at the bottom, while in lane 1, the velocity is in the wind direction at all depths. For those outer two lanes the horizontal circulation prevails. In the middle of the course, the velocities at the surface are in the opposite direction as the velocities at the bottom, yielding a small net depth-averaged velocity: the vertical circulation prevails. The maximum velocity difference is found between lane 1 and lane 6, thus for calculating lane differences, only those two lanes will be considered.

2.3.4 Differences in wind- and flow velocity

Differences in wind velocity

The wind velocities on lane 1 and on lane 6, on all grid points that form one lane, are presented in the Tables 2.4a, 2.4b, 2.4c, and 2.4d (Appendix 'Tables'). Table 2.4a presents the wind velocities for wind direction 45°, Table 2.4b wind direction 120°, Table 2.4c wind direction 210°, and Table 2.4d wind direction 300°. The wind directions 45° and 120° concern adverse wind (against the rowing direction) and are indicated with a negative sign. The last two rows of each table give the average wind velocity on the lane, and the difference in wind velocity between lane 6 and lane 1. The absolute values of these differences are taken and presented in Figure 2.9, for each examined wind direction. The wind velocities on the lanes increase linearly with the wind velocity at Schiphol (see equation 2.1), and so do the wind velocity differences. The differences are a bit larger for south winds, compared to north winds, but the velocities itself are larger for north winds.

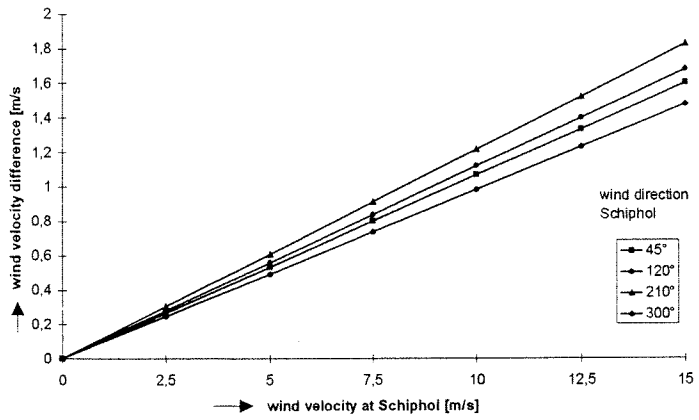

Figure 2.9: Absolute wind velocity differences between lane 1 and lane 6

Differences in flow velocity

The flow velocities on all grid points resulted from the computations with the Bosbaan model. Just the flow velocities on lane 1 and on lane 6 are needed to determine the lane differences, and of these two lanes just the upper part of the water column is used by rowers: depending on the type of racing shell, the draught varies between 10 cm for a skull to 20 cm for an eight. The exact value is not very important: as can be seen from Figure 2.8, the velocities decrease strongly and rapidly immediate below the surface for all lanes. The velocity-differences between the lanes decrease only a little with depths below 5 centimetres, as follows from Figure 2.10, which presents the flow velocity differences between lane 1 and lane 6 in the upper part of the water column, computed for Schiphol wind condition 210° and 10 m/s.

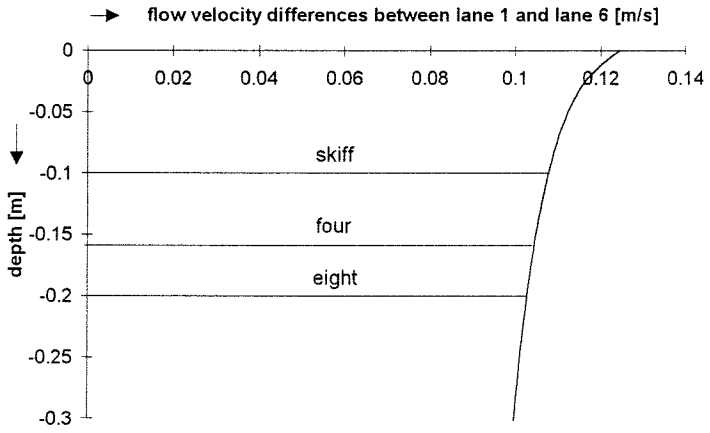

Figure 2.10: Flow velocity differences between lane 1 and lane 6 in the upper part of the water column.

The average velocity (in the rowing direction) in the upper ten cm of the water column are presented in the same manner as the wind velocities in Tables 2.5 (Appendix 'Tables'). Table 2.5a presents the flow velocities for wind direction 45°, Table 2.5b wind direction 120°, Table 2.5c wind direction 210°, and Table 2.5d wind direction 300°. Adverse flow velocities have been indicated with a negative sign. The last two rows of each table give the average flow velocity on the lane, and the difference in flow velocity between lane 6 and lane 1. The absolute value of those differences are taken and presented in Figure 2.11, the same way as the wind velocity differences in Figure 2.9.

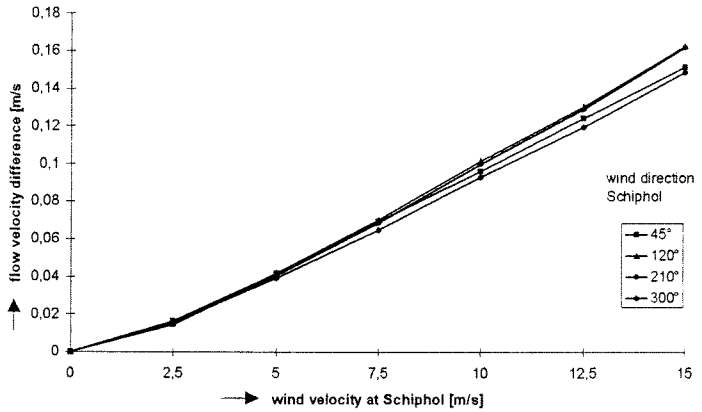

Figure 2.11: Absolute flow velocity differences between lane 1 and lane 6

The flow velocity differences between the two lanes are somewhat larger for south-west wind and for south-east wind: for both south wind conditions, the flow at the windward side is against the wind direction, while for the two north winds the flow at the windward side is small, but in the wind direction. This can be explained by the locations of the trees along the course: on the north side the areas with trees are varied with grassy plains, while on the south side the areas with trees form a close unit, and thus a larger shadow zone. Which lane has advantage at what wind direction is shown in Figure 2.12, in which the flow velocities have been indicated with arrows.

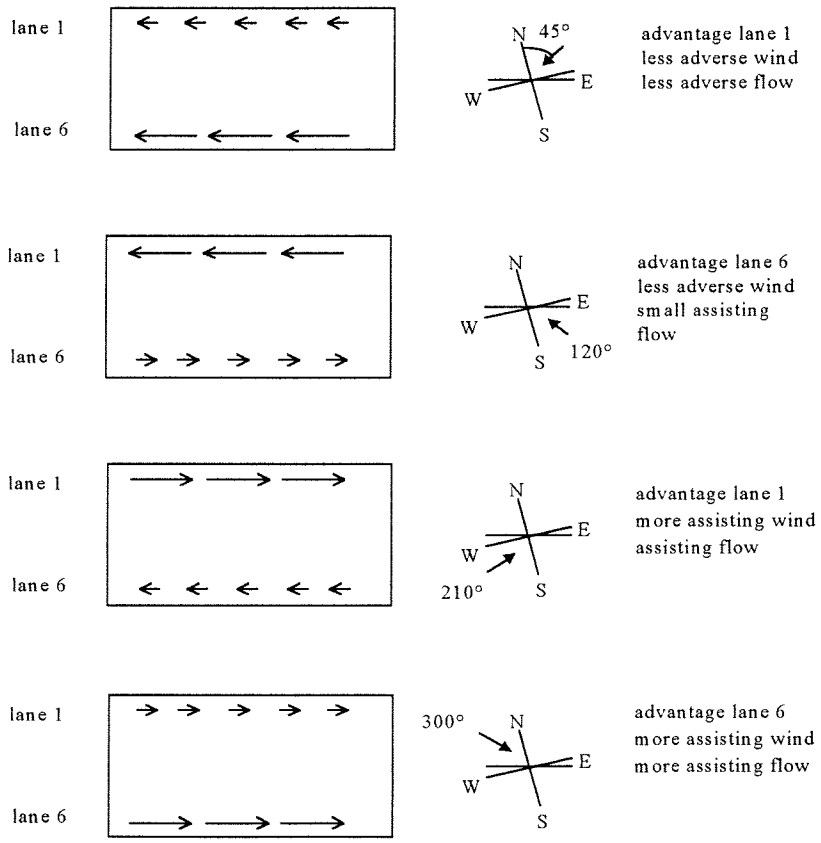

Figure 2.12: What lane is in favour?
Surface flow velocities in the Bosbaan at wind directions 45°, 120°, 210°, and 300°.

2.4 Estimation of lane differences

2.4.1 The rowing balance

In the previous section, the differences between the lanes were expressed as velocities. This suffices, when one is just interested in both influences separately. However, to determine the extent to which both influences contribute to the lane differences, the influences must be expressed in a quantity that can be compared. Therefore the lane differences were obtained by estimating the travel times for boats on lane 1 and on lane 6, on the basis of wind speed and flow velocity in both lanes. These wind speeds and flow velocities were determined in section 2.3.4.

The boat velocity results from the balance of the rowing force, the friction forces and wave resistance acting on the boat and the rowers. This balance is given by:

$$F_{row} + F_{water} + F_{air} = 0 \qquad (2.2)$$

where: F_{row} the force delivered by the rowers to overcome the resistance forces: F_{water} the flow resistance force, and F_{air} the air resistance force. These three forces are discussed in the sections 2.4.2, 2.4.3, and 2.4.4 respectively. The rowing balance is solved in section 2.4.6.

For the calculations of lane differences, a four-oars boat with coxswain has been chosen, that rows 2000 meters in 6'30" (390 seconds) in a situation without wind. The following data were taken from "Rowing" (1977).

- length L: 12 m
- width B: 0.5 m
- mass M: 470 kg (4 rowers of 85 kg each, coxswain 51 kg, boat 63 kg, oars 16 kg)
- wet surface A: 12 m* 0.5 m = 6 m^2
- block coefficient C_b: 0.5
- average boat velocity without wind v_b: 5.13 $m.s^{-1}$

The water displacement and the draught of the rowing combination can now be calculated as follows:

$F_{up} = M.g$ = 470 kg *9.81 N/kg = 4611 N

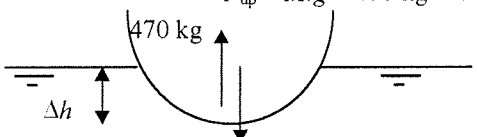

$F_{down} = \rho.g.C_b.\Delta h.B.L$ = 1000 kg/m^3 * 9.81 N/kg * 0.5 m * Δh * 0.5 m * 12 m

Equalisation of both forces gives: Δh = 0.157 m ≈ 16 cm.
The water displacement is then: $C_b.\Delta h.B.L$ = 0.5 * 0.157 m *12 m * 0.5 m = 0.47 m^3.

2.4.2 Delivered power of the rowing combination

In the present study, the power which must be delivered to overcome the total resistance on the hull and rowers is defined as:

$$P = F_{row} v_b \tag{2.3}$$

The calculations are aimed at determining the differences between the lanes and not at describing the race correctly. Therefore, speed variations due to racing conditions, as well as unsteady variations during an individual rowing stroke has been left out of consideration. In addition the effectively delivered amount of power is assumed constant over the race.

2.4.3 Water resistance

The major forces resisting the motion of the boat are the hydrodynamic resistance and the aerodynamic resistance, the former being responsible for about 90% of the total resistance at windless weather. In the present study, the hydrodynamic resistance is taken to be the sum of the viscous resistance, the wave resistance, and dynamic resistance due to the rowers' motion. The viscous resistance is the sum of the skin friction and the form resistance. Those various resistance forces have been estimated on the basis of the earlier mentioned article 'Boat resistance' in 'Rowing' (1977). A more detailed description of the water resistance is given in Appendix C.

Viscous resistance: skin friction
The main part of the water resistance (86%) is caused by skin friction between the wetted surface area of the hull entraining water along with the hull.

The basic formula for skin friction is:

$$F = \frac{1}{2}\rho V^2 C_f A \qquad (2.4)$$

in which: F: friction force [N]
V: velocity of the flow around the body [m/s]
C_f: friction coefficient due to skin friction on (wetted) surface [-]
A: (wetted) surface area of the body [m^2]

For streamlined bodies at high Reynolds numbers, the friction coefficient depends on the Reynolds number: $C_f \sim Re^{-0.15}$, see Hoerner (1965), Van der Zee (1985), and 'Rowing' (1977). The Reynolds number is given by: $Re = VL/\nu_\mu$, with L the length of the boat, and ν_μ the kinematic viscosity of water: 1.10^{-6} m^2/s. Four the four-oars boat, this yields: $Re = 6.1 \cdot 10^7$. In this case C_f is found to be 0.0023 ('Rowing' (1977) and Hoerner (1965).

Viscous resistance: form effects

The viscous resistance due to form effects is only 1% of the total water resistance for racing shells ('Rowing' 1977). This form resistance is caused by the pressure difference between the bow and the stern as a consequence of the growth of the viscous boundary layer. This leads to a resulting pressure force on the hull. In 'Rowing' (1977), this is taken into account by increasing the friction coefficient with: $1.5(B/L)^{1.5}$. For racing shells, the ratio B/L is 1/24, so the increase of the resistance coefficient is only 1%. Officially this form resistance must be related to the surface of the body normal to the flow direction, thus it can't be incorporated in equation (2.1) this way. However, the relative unimportance of this resistance makes it a reasonable approximation.

wave resistance

A moving boat generates a wave system, which starts at the bow (beginning with a crest), and a similar (but weaker) system from the stern (beginning with a trough). A part of the power delivered by the rowers is used in generating waves. Wave making is thus resistance against the motion of the boat. This wave resistance is depending upon whether the two systems interact or not, which depends on the length-based Froude number, given by: $Fr = V/(gL)^{1/2}$. The wave resistance amounts to approximately 8% of the total resistance ('Rowing', 1977).

The 8% mentioned above is the wave resistance in perfectly calm water. This may be affected due to wind generated waves. When a boat bumps into the waves, this will result in an additional loss of energy, and thus in an increase in wave resistance. Wave growth on the Bosbaan is examined in Appendix D, from which follows that the waves are strongly fetch limited, and therefore remain very short and small. Their celerity is much smaller than the speed of the racing shells. The shells cut as it were through the waves, so that the waves don't have the opportunity to influence the wave resistance effectively. This holds for all lanes, both on the leeward and on the windward side. The increase in wave resistance due to wind-generated waves on the Bosbaan is therefore neglected, and thus also the differences in wave resistance between the lanes.

Resistance due to dynamic forces

The dynamic resistance is the resistance due to the movement of the rowers, and leads to an additional component of the wave resistance. No exact data are known about the influence of this instationary resistance on the total water resistance. In this study the values are taken from the anonymous article "boat resistance". Those values were based on towing-tank measurements in Germany.

- 3% due to the vertical movement of the rowers;
- 1% due to horizontal movement of the centre of gravity of the rowers;
- 1% due to the strokes during which the velocity of the boat is not constant.

Total water resistance

In the case of the four-oars boat, as the skin friction dominates the total water resistance, the viscous resistance is approximately equal to:

$$F_{water} = \frac{1}{2}\rho(v_b + u)^2 C_f A_{wet} * 1.16 \qquad (2.5)$$

in which: F_{water}: water resistance force [N];
v_b: boat velocity [m/s];
u: flow velocity against boat direction [m/s];
C_f resistance coefficient due to skin friction
A_{wet}: wetted surface [m^2]

As has been explained in this section, the part of the water resistance caused by friction takes up 86% of the total water resistance. Therefore, the friction force given by equation (2.4) is multiplied by 1/0.86 = 1.16 to obtain the total water resistance.

For flow in the boat direction, u has a negative sign, resulting in a lower combined boat-plus-flow velocity, and thus in a lower resistance force.

2.4.4 Air resistance

Aerodynamic resistance on the crew and the above-water portion of the hull follows from a similar equation as the water resistance (equation 2.5):

$$F_{air} = \frac{1}{2}\rho_{air}(v_b + w)^2 C_f A \qquad (2.6)$$

where: ρ_{air}: density of air [kg/m^3]
w: wind velocity against the boat direction, for which the wind velocities at 1.75 m can be used, according to Van Melle (1989).

The air resistance is the sum of the air resistance on the rowers, and the resistance on the blades:

$$F_{air} = \frac{1}{2}\rho_{air}(v_b + w)^2 \left(C_{frowers} A_{rowers} + C_{fblades} A_{blades}\right) \qquad (2.7)$$

The rowers have been approximated by four cylinders with a surface of 0.4 m^2 each, placed behind each other, and a C_f of 0.8. Because they sit partly in each other's wake, only two of the four have been taken into account.

The force on the blades during the recover is the force on four rectangles of 0.1 m^2 each, and a C_f of 1.0. The blades move with a velocity which is greater than the boat velocity, but only during half the recover (when the blades are vertical).This effect is approximated by multiplication of this force by a factor 0.3.

Considering the mass-density ratio of water against air in the order of 1000, the air resistance of the rowers and the blades may not appear to be important. However, heading into the wind, the air resistance is proportional to the square of ship-plus-wind velocity. As a consequence this resistance can be an appreciable fraction of total resistance. This in contrast with assisting wind, when the air resistance can sometimes even be neglected: as wind velocity and boat velocity have the same

magnitude and direction. At windless weather, the air resistance amounts to approximately 7% of the total resistance (Van Melle, 1989).

2.4.5 Solving the rowing balance

Substitution of equations 2.3, 2.5, and 2.7 in equation 2.2 gives:

$$\frac{P}{v_b} + \frac{1}{2}\rho(v_b + u)^2 C_f A + \frac{1}{2}\rho_{air}(v_b + w)^2 \left(C_{frowers} A_{rowers} + C_{fblades} A_{blades}\right) = 0 \qquad (2.8)$$

The reference travel time (without wind and flow) was chosen as 390 s (6'30"). The average boat velocity is then 5.13 m/s. The power needed to overcome the total resistance follows from equation (2.8) with $u = w = 0$: $P = 1157$ W. This P is used to compute the boat velocity in situations with wind and flow, with u and $w \neq 0$.

An iterative solution procedure is needed to calculate the boat velocity from (2.8). This is done for all grid points in a lane, thus taking into account the spatial variations of wind- and flow velocity. For the iteration procedure the simple method of bisection is used: each new estimate is halfway the two previous ones (see Appendix E for the listing of the calculation program). Finally the travel times for the lanes 1 and 6 are calculated by integration of the calculated boat velocities over all consecutive grid cells that form one lane. The results are presented in the next section.

2.4.6 Resulting lane differences

Lane differences have been calculated both for wind and flow together, and for wind influence alone. The results are presented in the Tables 2.6 for the four examined wind directions 45°, 120°, 210°, and 300°, respectively. Each table presents the travel times for the lanes 1 and 6, and their difference, computed with a combined influence of wind and flow, or computed with the influence of wind alone; the flow velocity is assumed to be zero. The differences in travel times for the two lanes, T6-T1, are referred to as lane differences.

In the Tables 2.6 (Appendix 'Tables'), the lane difference caused by the combined influence of wind and flow is compared with the lane difference caused by wind alone. The latter is subtracted from the first to obtain the lane difference caused by flow alone. The results (absolute values) are summarised in Table 2.1: Table 2.1a shows the results for adverse wind, while Table 2.1b shows the results for assisting wind. The last columns (indicated with bold) reflect the percentage of the lane differences caused by the wind-generated flow alone.

	wind direction 45°				**wind direction 120°**			
w [m/s]	**both [s]**	**wind [s]**	**flow [s]**	**flow [%]**	**both [s]**	**wind [s]**	**flow [s]**	**flow [%]**
2.5	1.87	1.07	0.8	**43**	1.76	1.09	0.67	**38**
5	4.49	2.52	1.97	**44**	4.41	2.4	2.01	**46**
7.5	7.65	4.30	3.35	**44**	7.36	4	3.36	**46**
10	11.17	6.50	4.67	**42**	10.76	5.88	4.88	**45**
12.5	15.25	9.16	6.09	**40**	14.35	8.06	6.29	**44**
15	19.79	12.23	7.56	**38**	18.44	10.52	7.92	**43**

Table 2.1a: Comparison of absolute values of lane differences caused by wind and flow, wind, and flow separately, for adverse wind.

	wind direction 210°				wind direction 300°			
w [m/s]	both [s]	wind [s]	flow [s]	flow [%]	both [s]	wind [s]	flow [s]	flow [%]
2.5	1.58	0.92	0.66	**42**	1.42	0.69	0.73	51
5	3.51	1.56	1.95	**56**	2.94	1.08	1.86	**63**
7.5	5.26	2	3.26	**62**	4.24	1.2	3.04	**72**
10	6.93	2.24	4.69	**68**	5.43	1.01	4.42	**82**
12.5	8.29	2.16	6.13	**74**	6.37	0.67	5.7	**89**
15	9.63	1.93	7.7	**80**	7.76	0.77	6.99	**90**

Table 2.1b: Comparison of absolute values of lane differences caused by wind and flow, wind, and flow separately, for assisting wind.

For the wind velocities 5 and 10 m/s, which correspond with wind forces 3-4 and 5 Beaufort, the lane differences are presented in the Figures 2.13a and 2.13b, respectively.

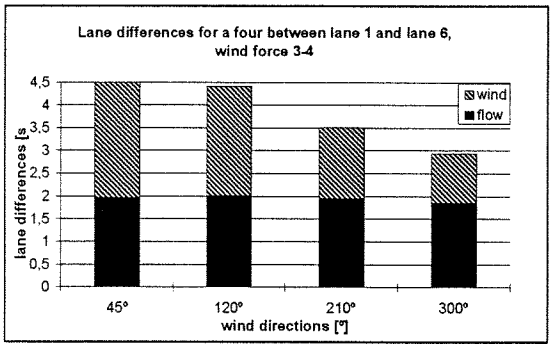

Figure 2.13a: Lane differences for a four, wind force 3-4.

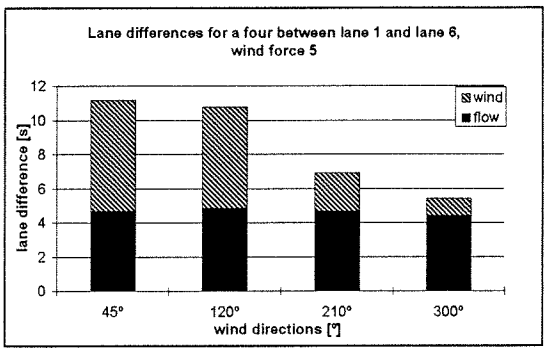

Figure 2.13b: Lane differences for a four, wind force 5.

The tables and figures indicate that:

- Adverse wind causes the largest lane differences, of which the larger part concerns the direct influence of wind on the rowers and their boat.
- Lane differences caused by the influence of wind-generated flow are of the same order of magnitude both for adverse and assisting wind.
- Lane differences caused by assisting wind consist for the larger part of the influence of wind-generated flow.
- Generally, the lane differences increase with increasing wind velocity. The development of the separate influences with increasing wind velocity is discussed below. For the two different situations (adverse and assisting wind), the development of the lane differences as a function of the wind velocities is given in Figures 2.14a, and 2.14b. The first for adverse wind (45° at Schiphol), and the second for assisting wind (210° at Schiphol).

Lane differences due to flow increase with the wind velocity, see Figure 2.14. For lane differences due to wind, a distinction has to be made between assisting and adverse wind. For adverse wind (air resistance proportional to the square of wind-plus-boat velocity), the lane differences due to wind increase with increasing wind velocity (Figure 2.14a), while for assisting wind (air resistance proportional to the square of wind-minus-boat velocity), the development of the lane differences depends on the absolute value of boat velocity minus wind velocity on the two lanes. Generally it can be said that the lane differences due to the direct effect of wind increase with increasing wind velocity for low wind velocities, reach a maximum (still a low value) when the wind velocity equals the boat velocity (in the lane with the higher wind velocities), and decreases for wind velocities higher than the boat velocity, see Figure 2.14b.

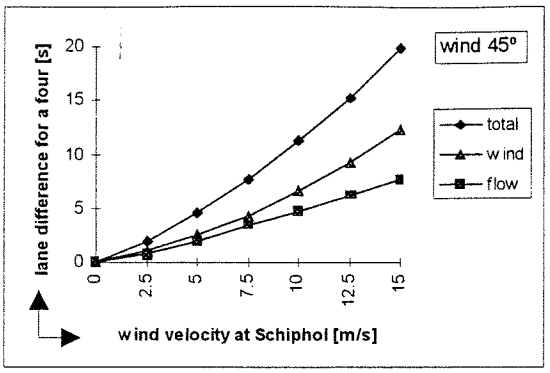

Figure 2.14a: Lane difference as a function of the wind velocity for north-east (adverse) wind

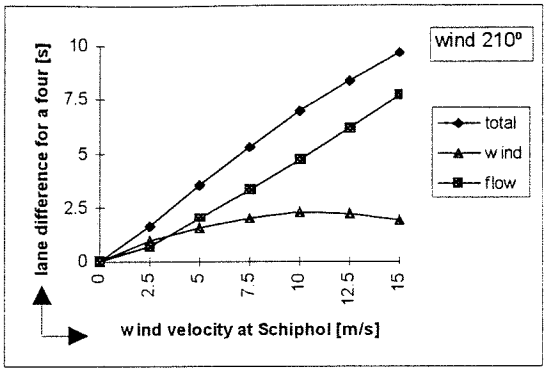

Figure 2.14b: Lane difference as a function of the wind velocity for south-west (assisting) wind

The calculations of the lane differences is based on various assumptions, concerning e.g. the resistance coefficients of boat and rowers, the delivered effective power of the rowing combination, and the percentages of the various water resistance forces. A change of those values will influence the results, for example, a larger resistance coefficient will increase the rowing time. But this larger resistance coefficient will effect both the boat in lane 1 and the boat in lane 6; hence, this larger resistance coefficient will only affect the differences between the lanes to a small extend. This also holds for changes in the other assumptions.

The choice of a four was a rather arbitrary. If another type of racing shell was chosen, the exact numbers would differ a little, but the tendencies would stay the same.

2.5 Conclusions

Due to the trees around the course, the wind is partly tunnelled in the course direction. The wind velocities above the course are always lower than they would have been in the open field, but vary strongly over the course, from almost zero at the shadow zone to a maximum at the lee shore. The largest differences in wind velocity occur at Schiphol wind directions 45°, 120°, 210°, and 300°; wind with an angle of approximately 45° to the course axis.

For these four wind directions, the flow velocities in the Bosbaan have been computed with the shallow-water solver. The wind velocities that vary above the course induce a horizontal circulation in the Bosbaan, with the flow at the windward side being much smaller or even opposite to the flow at the lee shore. The wave heights in the course may vary as well, but are considered to be of minor importance.

The maximum wind and flow velocity differences occur between lane 1 and lane 6. Those differences increase linearly with increasing wind speed, as was seen from Figures 2.9 and 2.11. Wind from the south-west and from the south-east cause a bit larger wind- and flow velocity differences than wind the from north-west and from the north-east, because at the south side the trees form a serried row and thus a larger shadow zone than at the north side, where the areas with trees are alternated with grassy planes. For the same reason, the wind velocities above the course (related to the same wind velocity at Schiphol) are larger for north winds.

The wind- and flow velocity differences result in differences in air- and water resistance on the different lanes, and thus in differences in travel times between the lanes. Those differences are larger for adverse (east) wind than for assisting (west) wind and increase with increasing wind speed. Which of the two influences prevails, depends mainly on the direction of the wind. Actually, the differences caused by the direct influence of wind are direction dependent, the part caused by flow is of the same

order of magnitude both for adverse and for assisting wind. Therefore, for adverse (east) wind, the direct influence of wind on the rowers dominates, while for assisting (west) wind the larger part is caused by the differences in flow velocity.

3. THE WIDENED COURSE

3.1 Introduction

The FISA has proposed to widen the course in northern direction with 26 meters to 118 meters: 8 lanes of 13.5 meters each, and 5 meters of clear water on each side, between the buoy-line and the edge of "any obstruction". After this five meters, the required depth of 2.2 meters must be reached. Several engineering offices have already worked out plans for this widening, but nothing has been decided yet. It has been assumed that the lane differences will be reduced due to this widening. The aim of this study is to verify this assumption.

The flow is again computed with the shallow-water solver DELFT3D-FLOW. All parameters were kept the same, except the number of grid points in y-direction: in this direction some more points were needed in order to keep the same mesh sizes as for the present course. The chosen grid is described in section 8.4.

Wind fields above the widened course were again obtained by linear interpolation of wind coefficients. How those wind fields differ from those above the present course is explained in section 3.2.1. Section 3.2.2 presents the resulting flow patterns, and compares the resulting flow velocities with those in the present-day course, after which section 3.2.3 discusses to what extent the widened Bosbaan affects the lane differences. Finally, section 3.3 presents some concluding remarks concerning the widening.

In race contests, only 6 of the 8 lanes will be used: of course, the 6 lanes with the smallest differences between them are preferred. All comparisons between the widened, and the present-day course are therefore based upon the differences between the two lanes of the 6 with the largest differences.

3.2 Comparison of the widened course with the present-day course

3.2.1 Wind velocities above the widened course

The widening of the Bosbaan was suggested already in 1984 by the FISA, to upgrade the course to Olympic standards. In 1989 measurements have been performed in a boundary layer wind tunnel in view of the possible differences in wind velocity on the widened course. However, then the emphasis was on less trees, and the intention was to widen the course to 125 meters. Now, the plan is to remove as few trees as possible, and the new width will be 118 meters. This future configuration is therefore different from the ones that have been measured.

Wind fields on this widened course had to be estimated, on the basis of the configurations examined in 1989. This was done by evaluating the differences in wind velocity due to widening in other configurations, see Van Melle (1989). The result is a table of wind coefficients for 28 locations on the future course (lane 1, in between lane 3 and lane 4, lane 6 and lane 8, at locations 250, 500, 750, 1000, 1250, 1500, 1750 and 2000 m), presented in Table 3.4 (Appendix 'Tables').

Comparison of these results with the wind fields on the present Bosbaan shows that the velocity coefficients on the future race course will be somewhat higher than nowadays, and by far not constant over the course. The local wind directions are assumed to be tunnelled in the course direction the same way as in the present-day situation, see Figure 2.6. The distribution of wind coefficients for south-west wind (210° measured at Schiphol) is given in Figure3.1.

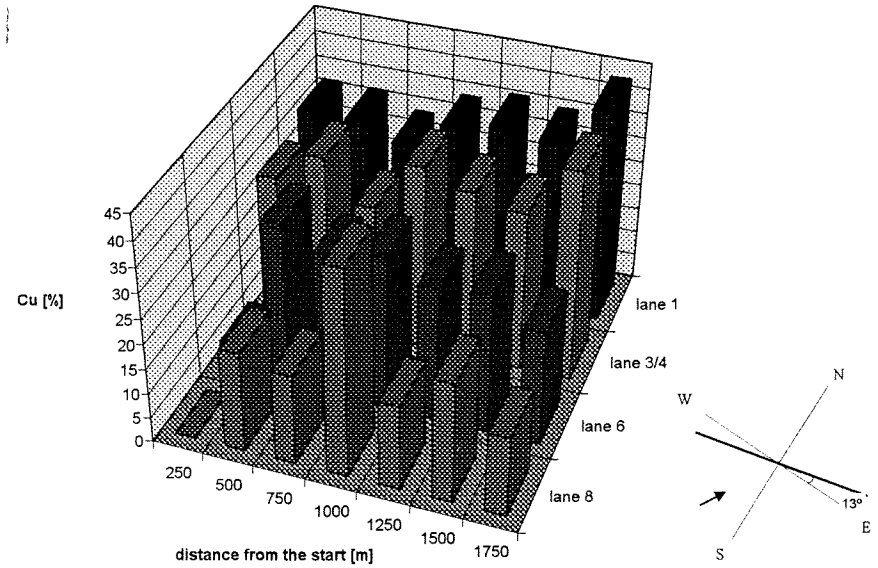

Figure 3.1: Wind field on the widened Bosbaan, wind direction Schiphol 210°

Those wind velocity coefficients relate the local wind velocities at 1.75 m above the course, to the wind velocities measured at the meteorological institute at Schiphol as explained in section 2.3.2. The local wind velocities on the grid points were again obtained by linear interpolation of those wind coefficients and multiplication with the wind velocity measured at Schiphol. It is chosen here to examine the same wind conditions as were examined for the present-day situation: wind directions 45° (north-east), 120° (south-east), 210° (south-west), and 300° (north-west), and the wind velocities ranging from 2.5 to 15 m/s, in steps of 2.5 m/s, corresponding to the wind forces 2-7. The local wind direction for those cases is parallel to the course axis, as for the present-day situation (Figure 2.6).

The local wind velocities increase linearly with the wind velocity at Schiphol, see section 2.3.4. Therefore, just one Schiphol wind velocity is taken to compare the local wind velocities on the widened course with the wind velocities on the present course: 10 m/s corresponding to wind force 5, a rather strong wind in summer. Tables 3.5a-3.5d (Appendix 'Tables') present the local wind velocities on lane 1, 3, 6, and 8 for the four examined wind directions. The average values for those four lanes are presented in Table 3.1; the values for the present course have been added for comparison. Wind velocities against the rowing direction have been indicated with a negative sign (wind from the east).

118 m wide course

	45°	**120°**	**210°**	**300°**
lane 1	-3.2	-3.6	3.4	3.6
lane 3	-3.5	-3.4	3.4	3.9
lane 6	-4.0	-2.6	2.3	4.2
lane 8	-4.5	-2.1	1.8	5.0
differences between the lanes				
6-1	0.8	1.0	1.1	0.6
8-3	1.0	1.3	1.6	1.1
8-1	1.3	1.5	1.6	1.4

92 m wide course

	45°	**120°**	**210°**	**300°**
lane 1	-3.1	-3.3	3.1	3.2
lane 6	-4.1	-2.2	1.9	4.2
difference between lane 1 and lane 6				
6-1	1.0	1.1	1.2	1.0

Table 3.1: Average wind velocities per lane [m/s] for wind 10 m/s

The differences in wind velocity between the lanes (absolute values) have also been indicated in this Table 3.1. The differences between the outer two lanes (lane 1 and lane 8) will be larger than they are in the present-day situation (between lane 1 and lane 6). The velocity differences between lane 3 and

lane 8 will also be larger than in the present situation. However, the differences between lane 1 and lane 6 will be smaller in the widened situation compared with the present-day situation. This especially holds for north-west and north-east winds. In the present situation, there are already less trees on the north side than on the south side, and due to this widening, even more trees will be removed on this side. The shadow zone is therefore smaller, the wind velocities higher, but the differences in wind velocity smaller.

3.2.2 Flow velocities in the widened course

Figures 3.6a-3.6d (Appendix 'Figures') present the resulting flow patterns for a wind velocity of 10 m/s (corresponding to wind force 5), where a, b, c, and d correspond with the wind directions 45°, 120°, 210°, and 300° respectively. These figures show the velocity vectors at the surface, at the bottom, and at depths 2, 16, 66 and 152 cm. Figure 3.2 shows the surface velocity vectors for the prevailing south-west wind (210°). From these figures it can be seen that the surface velocities still differ strongly over the course. Circulation patterns contain larger gradients than in the case of the present course, see Figures 2.15a-2.15d (Appendix 'Figures').

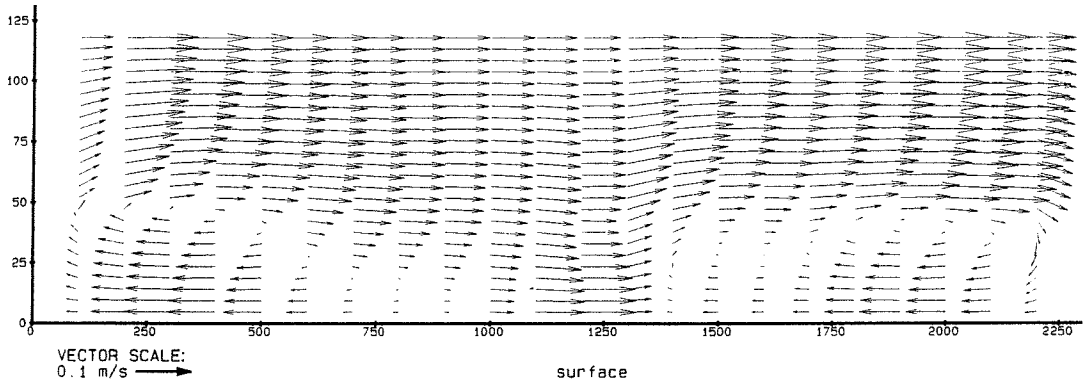

Figure 3.2: Widened Bosbaan surface velocities, wind condition Schiphol 210°, 10 m/s

Figures 3.7a-3.7d (Appendix 'Figures') compare the vertical distributions of velocity in x-direction (equivalent with the rowing direction) for the lanes 1, 3, 6, and 8 on four locations at the course: 500, 1000, 1500, and 2000 meters from the start. Again, a, b, c, and d correspond with the wind directions 45°, 120°, 210°, and 300° respectively, all with Schiphol wind velocity 10 m/s (wind force 5) It is noteworthy that for all four wind directions, the velocity differences between lane 1 and lane 6 are smaller than the differences between lane 3 and lane 8.

For south-west wind (210°) and wind velocity 10 m/s, Figure 3.3 presents the vertical distributions of velocity in x-direction (in the rowing direction) in all 8 lanes of the widened Bosbaan; the curves present the average distribution for each lane. The differences between the lanes 1 to 4 on the north side (lee side) are small, but increase strongly for the lanes 5 to 8. This is different from the present-day course, where the differences between two adjacent lanes are always approximately the same, as was seen from Figure 2.8. In rowing contests, 6 lanes are used: either lane 1 to lane 6 or lane 3 to lane 8, dependent on which option causes the smallest differences. The option of using lane 2 to 7 is not examined, because it will always be worse than an option which uses the area near a bank.

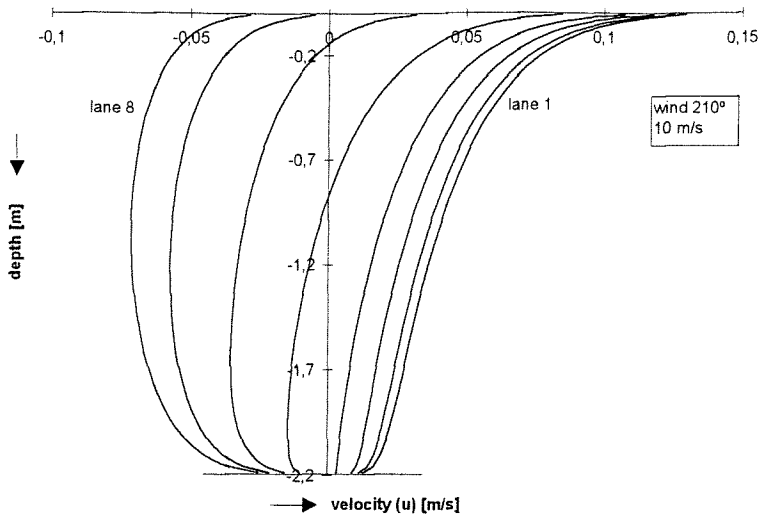

Figure 3.3: Vertical distributions of velocity for all lanes of the widened Bosbaan, wind condition Schiphol 210°, 10 m/s.

Tables 3.6 (Appendix 'Tables') summarise the computed flow velocities on the lanes 1, 3, 6, and 8, in the upper part of the water column. The average values for those four lanes are presented in Table 3.2; the values for the present course have been added for comparison. The last rows give the flow velocity differences between the lanes. As with the wind velocity differences, the differences between lane 1 and lane 6 for the widened course will be a bit smaller than in the present-day situation, regardless of the wind direction. The differences between lane 8 and lane 3 will be larger than in the present-day situation.

118 m wide course

	45°	120°	210°	300°
lane 1	-0.006	-0.113	0.10	0.017
lane 3	-0.029	-0.092	0.089	0.037
lane 6	-0.095	-0.020	0.018	0.085
lane 8	-0.143	0.031	-0.027	0.144
differences between the lanes				
6-1	0.089	0.093	0.082	0.068
8-3	0.114	0.123	0.116	0.107
8-1	0.137	0.144	0.127	0.127

92 m wide course

	45°	120°	210°	300°
lane 1	-0.016	-0.093	0.088	0.019
lane 6	-0.112	0.009	-0.012	0.111
difference between lane 1 and lane 6				
6-1	0.096	0.102	0.10	0.092

Table 3.2: Average flow velocities per lane [m/s] for wind 10 m/s

Figures 3.8a-3.8d (Appendix 'Figures') present the distribution of surface flow velocities (in the upper part -10 cm- of the water column, averaged in length-direction) over the width of the course; each figure shows the flow velocities for both the present and the widened course, resulting from the same wind condition at Schiphol: 10 m/s. The present course (92 m wide) is indicated with dashed lines, the widened course (118 m wide) with solid lines. Figures a-d correspond with the wind directions 45°, 120°, 210°, and 300° respectively. The lanes of the future course are wider than those of the present-day situation, 13.5 m and 12.5 m, respectively. Both are indicated in the figures, the widened course left, with solid lines, the present-day course right, with dashed lines. For convenience, the surface flow velocity distributions for south-west wind (210°) are also presented in Figure 3.4.

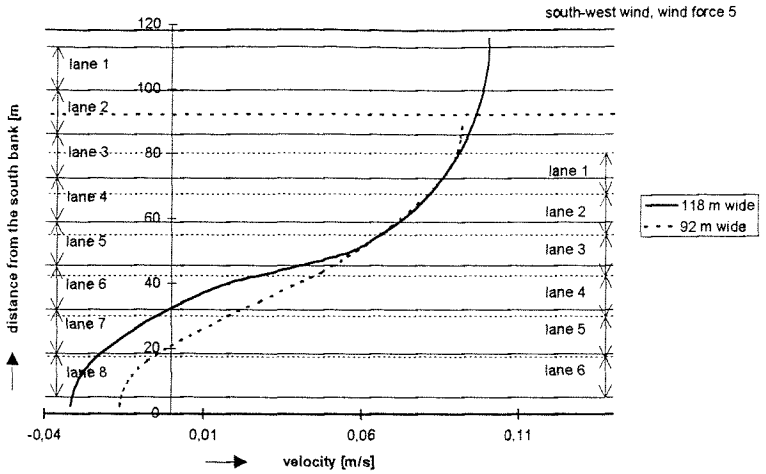

Figure 3.4: Average flow velocity distribution over the width of the course at south-west wind, 10 m/s

From these figures it can be concluded that:

- The differences in flow velocity between the opposite sides of the course increase. As was seen in section 3.2.1, local wind velocities above the course will be higher in the future situation than they are now. In addition, the widened Bosbaan has a larger surface on which the wind stress acts. These two effects together create a stronger circulation than in the present-day course, and with a stronger flow in the wind direction, the return current will be stronger as well.
- As for the present-day situation, a distinction can be made between the winds from the north and the winds from the south. The flow velocities for north winds are in the wind directions, even at the windward shore, while for south winds, the flow velocities are against the wind direction at the windward shore. This is because on the north side of the course, there are less trees than at the south side, creating less sheltering for the wind, and thus higher wind velocities. This holds even more for the widened course: because of the widening in northern direction, less trees remain on this northern side.
- For all wind directions, the strongest gradients in flow velocity occur roughly at the same place, for both the present and the widened course: in lane 5 of the widened course. From lane 1 to lane 4 the differences in flow velocity are rather small, but for the lanes 5 and 6, the differences increase relatively more than in the present-day situation. As in rowing contests only 6 of the 8 lanes are used: the lanes 1 to 6 are preferred to the lanes 3 to 8, for all wind directions. It should be noted, however, that in this case lane 6 has got relatively more disadvantage than the other lanes, because of the stronger gradient, see Figure 3.4.
- Summarising: the differences in flow velocity between lane 1 and lane 6 are still considerable for the 118 m wide course, although less than for the present course.

3.2.3 Lane differences for the widened Bosbaan

With the known wind- and flow fields for this widened Bosbaan, the travel times for a four have been calculated, the same way as explained in section 2.4. All assumptions concerning air- and water resistance forces and the delivered power of the rowing combination were kept the same. The same Schiphol wind conditions were examined as for the present-day situation (wind directions 45°, 120°, 210°, and 300°, and wind velocities: 2.5m/s, 5m/s, 7.5m/s 10m/s, 12.5m/s and 15m/s). Table 3.7 (Appendix 'Tables') present the computed travel times, for the combined influence of wind and flow as well as for the influence of wind alone. The last three columns of each table present the absolute differences between the outer two of the 6 lanes, either lane 8 and lane 3 (indicated with T8-T3) or lane 6 and lane 1 (indicated with T6-T1). The differences caused by the influence of flow alone were obtained by subtracting the wind influence of the total. For comparison, the differences between lane

6 and lane 1 in the present-day situation have been indicated as well, in the column 92m indicated as T6-T1.

For three wind forces (wind force 2, corresponding to a wind velocity of 2.5 m/s, wind force 3-4, corresponding to a velocity of 5 m/s, and wind force 5, corresponding to a velocity of 10 m/s), those data are presented in the Figures 3.5a, 3.5b and 3.5c. Per wind direction there are three bars; the first one gives the difference between lane 8 and lane 3, the second one the difference between lane 6 and lane 1, both for the widened Bosbaan. The third bar gives the difference between lane 6 and lane 1 for the present-day Bosbaan. In addition, each bar is divided into two parts: the lower part presents the lane differences due to flow alone, and the above part the lane differences due to wind alone.

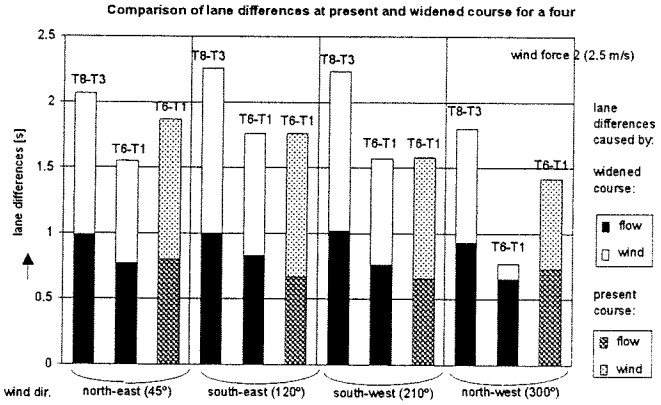

Figure 3.5a: Comparison of lane differences at present and widened course for a four at wind force 2.

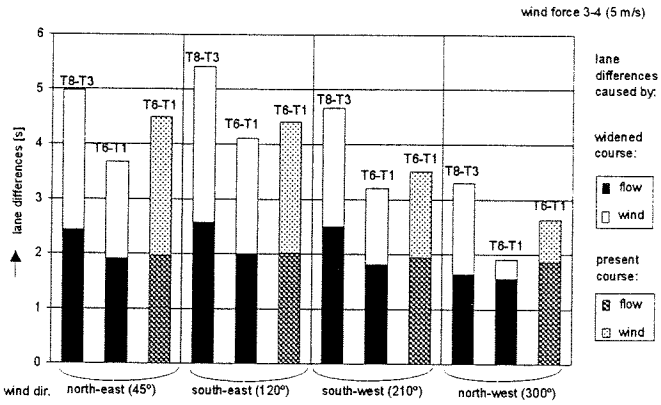

Figure 3.5b: Comparison of lane differences at present and widened course for a four at wind force 3-4.

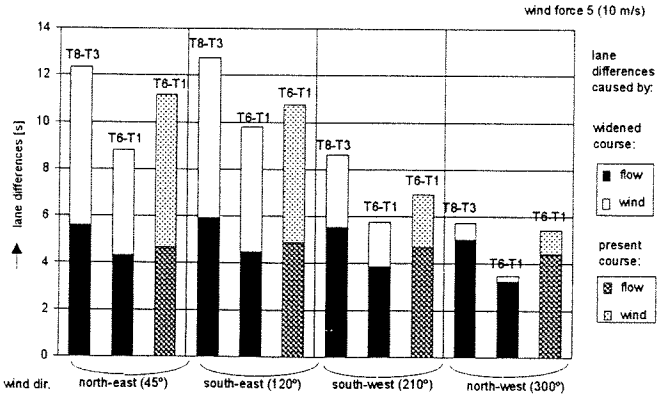

Figure 3.5c: Comparison of lane differences at present and widened course for a four at wind force 5.

As can be seen from these figures, and from Table 3.7 (Appendix 'Tables'), the lane differences for the widened course will always be less than in the present-day situation, provided that lane 1 to 6 are used. The differences between lane 3 and lane 8 will always be larger than in the present-day situation, as was already observed with the differences in wind- and in flow velocity. To what extent the lane differences decrease depends on the wind direction- and velocity. For the wind velocities of 5 and 10 m/s, the percentages of improvement are indicated in Table 3.3.

	45°	120°	210°	300°
5 m/s	18	12	8	35
10 m/s	21	10	17	35

Table 3.3: Improvement [%] of the widened course in comparison with the present-day course.

For south-east wind (120°) the improvement is the smallest: about 10%, and the lane differences remain large. For north-west wind (300°) the improvement is the largest, approximately 35%. Especially for high winds, the differences due to the direct influence of wind will almost entirely be cancelled. For the predominant wind direction in Holland, south-west wind, the improvement is less than 20%. The improvement is larger for higher winds, because the wind resistance decreases (for assisting winds) as the wind velocity is of the same order of magnitude as the boat velocity, as explained in section 2.4.5.

3.3 Conclusions

Due to the widening in northern direction, the wind velocities above the course will be somewhat higher than nowadays (less trees on the north side, and a larger area). The differences in wind velocity between lane 1 and lane 6 (the northern part of the course) will be smaller than in the present-day situation, while the differences between lane 3 and lane 8 will be larger, regardless of the wind direction.

The average wind force per unit surface will increase, causing stronger horizontal circulations, see Figure 3.8 (Appendix 'Figures'). This figure also shows that the widened Bosbaan has a larger area for which the differences in flow velocity are smaller, but this area is not large enough to hold six lanes. For all wind directions, this area is at the north side of the course, and the most rapid change in flow velocities occurs near lane 5. Therefore, as for the wind velocities, the lanes 1 to 6 are preferred to the lanes 3 to 8.

The widened Bosbaan affects the lane differences (expressed as the difference in travel times for a four on different lanes) in the same way as the wind- and flow velocity differences: the situation deteriorates for the lanes 3 to 8 and improves for the lanes 1 to 6, for which an average improvement of about 20% is reached. But even with this improvement, differences between the lanes remain.

4. REDUCE LANE DIFFERENCES

4.1 Introduction

Lane differences are caused primarily by differences in wind velocity between the lanes, resulting in differences in wind resistance force (direct effect) and differences in flow velocity (indirect effect). Cancelling the wind velocity differences is therefore by far the most effective way to create equal circumstances. Of course, an indoor facility would be the best solution; no wind means no differences in conditions. This is not a realistic option for the Bosbaan. Earlier studies into lane differences in the Bosbaan mention several methods intended to reduce the lane differences. These, and some other methods, are evaluated briefly hereafter. Section 4.2 discusses methods to reduce the differences in wind velocity, which will, at the same time, reduce the differences in flow velocity. Section 4.3 discusses methods just aimed at reducing the differences in flow velocity. Concluding remarks are given in section 4.4.

4.2 Methods to reduce the wind velocity differences

Differences in wind velocity above the course occur predominantly as a result of the trees around the course, creating a shadow-zone with lower wind velocities than on the opposite side of the course. A course situated in the open field would yield much higher wind velocities above the course, but with smaller differences. Only very small differences in velocity occur due to the lower roughness of the water surface in relation to the bank (with roughness heights: 0.03 m for the open field and 0.0002 m for the water surface, the velocity at the windward side is about 1.1 times the velocity at the lee side, see equation (8.7)).

For the Bosbaan, removal of the trees is not realistic. And even so, there will still be a dike on the south side creating a shadow zone. Even high reeds at the banks may cause lane differences. In addition, a course situated in the open field has its own problems: without trees or other obstacles next to the course the wind velocities are not slowed down and can be very high. The waves generated by this high wind velocities will also increase.

Van Melle (1989) suggested the placement of trees, or fences with the same height as the trees, on the glades at the north side of the course. This is not a good option. As was found in section 2.3.2, winds from the north cause higher local wind velocities but smaller differences in wind velocity, just because there are less trees on that side. By placing trees or fences, a larger shadow zone is formed on this side, and thus larger velocity differences. The differences for winds from the north directions will then be as high as for the south directions. In fact, the situation worsens for north winds.

As was seen in section 3.2.1, the planned widening in northern direction will result in higher wind velocities above the course, but in lower wind velocity differences between six lanes. A further widening in northern direction will increase this effect. For the 118 m wide course, the lanes 1 to 6 (the northern lanes) are always favourable in the case of the widened course. When even more trees will be removed from this side, a larger improvement is expected.

A horizontal, half transmitting cover above the Bosbaan is also a good option, according to Van Melle (1989). Indeed, anything that can be constructed above the course, like fences, cover, or spoilers should affect the lane differences positively. The principle of these methods is to shift the wind boundary layer upwards, till above the rowers. The rowers stay underneath the cover, in the lee, with much smaller wind velocities, and wind velocity differences.

4.3 Methods to reduce the flow velocity differences

Several methods aimed at reducing the flow velocity differences have been mentioned in earlier studies concerning lane differences in the Bosbaan (Van der Zee, 1985, W. Op den Velde, 1988, Klerks, 1997)). These, and some other methods are evaluated here. Some methods could be rejected immediately, while others had to be examined a bit more carefully. However, the conclusions have been based upon simple reasonings and calculations, because the time was lacking to execute extensive numerical computations.

It should be mentioned that these alternatives, if of any influence at all, are just meant to reduce the flow velocity differences between the lanes. The differences in wind resistance will not be influenced, and may still cause unacceptable lane differences.

Wider ends of the course
In the Keulen rowing course (Klerks, 1997), the course-width increases near the start and near the finish, in order to enhance the horizontal mixing. This does, however, not reduce the differences in flow velocity between the lanes. The surface flow velocities will still follow the local wind velocities above the course; if the wind velocities show a large variation, the surface flow velocities will as well.

Banks without vegetation
Banks without vegetation have been applied in the rowing courses in Keulen and in Harkstede, in order to reduce the horizontal circulation (Klerks, 1997). For the Bosbaan this won't have any effect, because the lane differences are not caused by the vegetation at the banks, but by the trees along the course. In addition, banks without vegetation are not preferred for their bad wave reflecting properties.

Spill-way channel around the Bosbaan
This channel can be built along the complete outline of the Bosbaan (W. Op den Velde, 1988), with its edge at the water level of the Bosbaan. The idea is, that such no wind set-up can develop: the surplus of water is released into the channel via a spillway. No horizontal circulation can then be driven.
This is unfortunately not what happens in practice: a new equilibrium will be reached, including a new wind-set-up, but now with lower water levels (below the edge of the channel). There will still be a horizontal circulation.

Return channel separate from the Bosbaan
A return channel is built to hold the counterflow caused by the wind set-up (W. Op den Velde, 1988) It should therefore have a discharge capacity profile of at least the same size as the Bosbaan, with a much smaller fetch. This has been applied at the course in Moskow. But as was seen there, the counterflow did not go through the specially built return channel, but took the easy way through the big basin (rowing course). So no improvements should be expected from this return channel.

Deepening of the entire course
By deepening of the course, the total volume of water is enlarged, while the same amount of energy from the wind is imparted to the water surface. The flow velocities will therefore decrease. Whether this also holds for the surface velocities is examined for Schiphol wind direction 210° with wind velocity U_{10}: 10 m/s. The vertical distributions of velocity in x-direction (equivalent with the rowing

direction) at the lanes 1 and 6 are presented in Figure 4.1, for the course depths 3, 5, 7, and 10 m. The velocity distribution obtained at the original depth of 2.2 m has also been indicated.

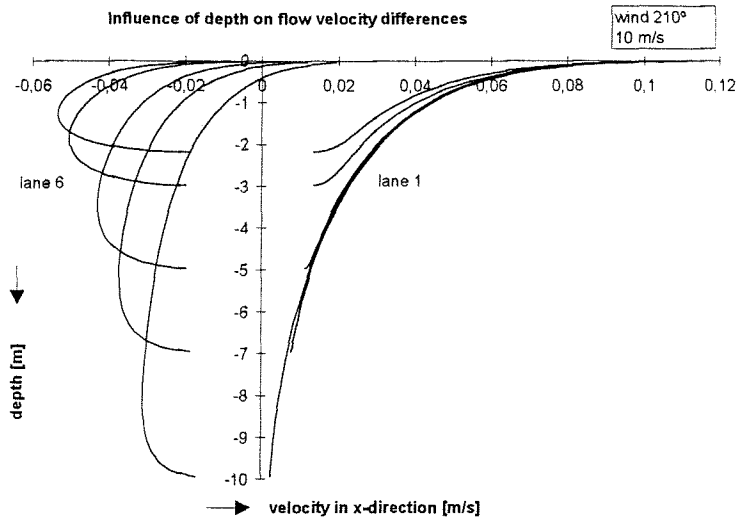

Figure 4.1: Influence of course depth on the flow velocity differences. The vertical distributions of flow velocity result from the Schiphol wind condition: 210°, 10 m/s.

The vertical profiles keep approximately the same shape, but are spread over a larger depth. Due to the larger volume available for the vertical circulation, the horizontal circulation is weakened a bit. The surface velocities, however, still show large differences between the lanes, in keeping with the wind velocities. Table 4.1 gives the flow velocities for lane 1 and for lane 6, the differences between those two lanes, and the lane differences calculated for a four. The direct influence of wind has been incorporated in the lane differences; this is constant 2.24 s for this wind condition.

depth	flow velocity lane 6 [m/s]	flow velocity lane 1 [m/s]	flow vel. difference[m/s]	lane difference [s]
2.2	-0.012	0.088	0.10	6.9
3	-0.004	0.091	0.095	6.7
5	0.009	0.089	0.080	6
7	0.018	0.086	0.068	5.4
10	0.026	0.083	0.057	4.9

Table 4.1: Influence of the course depth on the flow velocities. The values were obtained with the Schiphol wind condition: 210°, 10 m/s.

As can be seen from this table, the differences decrease slowly with increasing course depth. A substantial improvement can only be reached with a really deep Bosbaan.

Deepening of certain parts of the course

When a constant wind is blowing over a closed basin with uniform depth, the flow at the surface is in the wind direction, while the flow at the bottom is in the opposite direction. By deepening for example half of the course, it is possible to direct the flow, as is shown in Figure 4.2. Figure 4.3 presents the vertical distributions of velocity both for the situation with a shallow and a deep half, and for uniform depths, shallow and deep.

At the shallow half, the flow is in the wind direction, at the surface as well as at the bottom; the flow velocities at the surface are larger than they would have been in a basin with a constant depth. At the deeper half, the flow velocities at the surface are smaller than in the case of a constant depth, but in the wind direction. At a small depth below the surface the velocity turns against the wind direction

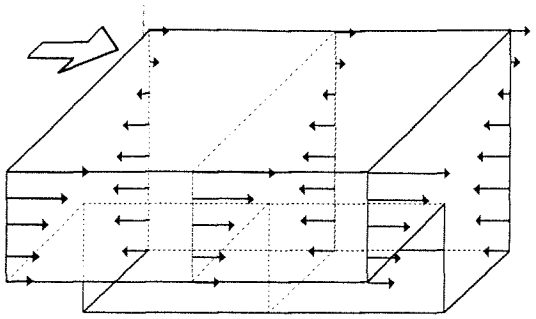

Figure 4.2: Constant wind blowing over a basin with non-uniform depth

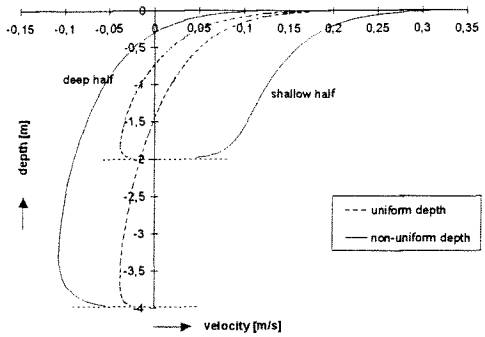

Figure 4.3: Vertical distributions of velocity, resulting for the situation in Figure 4.2, together with those for a constant depth.

Thus, at shallow parts, the flow is in the wind direction for the whole depth, while the deeper part is merely used for the counter current. Deepening of specific parts of the course is therefore a powerful means to influence the flow patterns, and might be used to reduce the flow velocities between the lanes. When, for example the northern half of the Bosbaan is deepened, the situation improves for south winds: At the lee side (deep), the flow is slowed down by the vertical circulation, while at the windward side (shallow), the flow is directed in the wind direction. However, for north winds, the situation deteriorates: the horizontal circulation is enhanced.

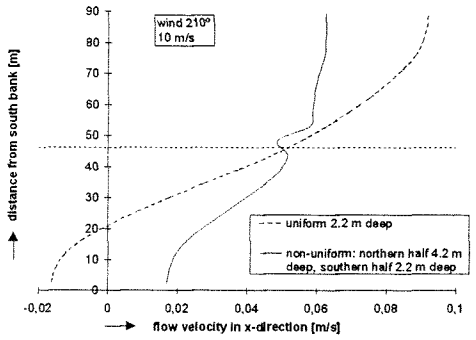

Figure 4.4a: Influence of deepening of the north half of the Bosbaan on the average surface flow velocity distribution over the width of the course at south-west wind (10m/s).

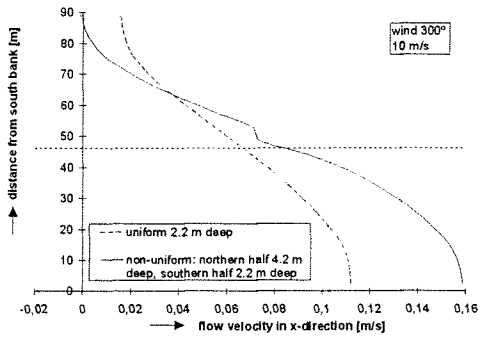

Figure 4.4b: Influence of deepening of the north half of the Bosbaan on the average surface flow velocity distribution over the width of the course at north-west wind (10m/s).

This is shown in the Figures 4.4a and 4.4b, which present the surface velocity distributions (upper 10 cm of the water column) over the width of the course in the Bosbaan model for south-west and north-west wind (both with wind force U_{10} = 10m/s). The northern half of the Bosbaan is deepened to 4.2 meters, while the southern half is still 2.2 meters. The results for a constant depth of 2.2 meters have been indicated for comparison. The numbers for those two wind directions are summarised in Table 4.2.

	depth [m]	flow velocity lane 6 [m/2]	flow velocity lane 1 [m/s]	flow vel. difference[m/s]	lane difference [s]
210°	**2.2/4.2**	0.024	0.062	0.038	4.03
	2.2	-0.012	0.088	0.1	6.93
300°	**2.2/4.2**	0.161	0.009	0.152	8.23
	2.2	0.112	0.019	0.093	5.43

Table 4.2: Influence of deepening of the north half on the surface flow velocity differences. Both north-west and south-west wind have been examined with U_{10} = 10 m/s.

The last column gives the resulting lane differences for a four; the influence of wind has been incorporated, which is 2.24 s for 210°, and 1.01 s for 300°. As can be seen from these values, the improvement for south-west wind is of the same order of magnitude as the deterioration for north-west wind. The same can be said of south-east and north-east wind. With a deepening of the northern half, the south wind directions improve at the expense of the north wind directions. But, taking into account the frequency of appearance of wind directions in summer, it can be chosen to improve the situation for the prevailing wind directions, at the expense of the less frequent wind directions.

Deepening of certain parts of the widened course

For this wider course two extra lanes are available, which aren't used during races. Here it is examined if the extreme (large or small) flow velocities can be restricted to those to lanes by deepening of specific parts. First it is examined if the return current can be restricted to two deeper lanes at the windward side. On the contrary, a shallow windward side can be used to direct the flow, as was shown above. To cancel the negative effect for north winds, a symmetric deep/shallow course is examined: deep in the middle with shallow parts near both banks. Both methods have been examined for one wind condition: 210° (south-west) with U_{10}: 10 m/s.

- Deepening of the windward side

  For south-west wind the strongest gradient in surface flow velocity occurs between lane 5 and lane 6. This gradient may move southwards by deepening lane 8 (or 8 and 7): enlarging the flow profile increases the return current on that spot, and decreases it elsewhere. Figure 4.5 shows the surface velocities over the width of the course for south-west wind, 10 m/s.

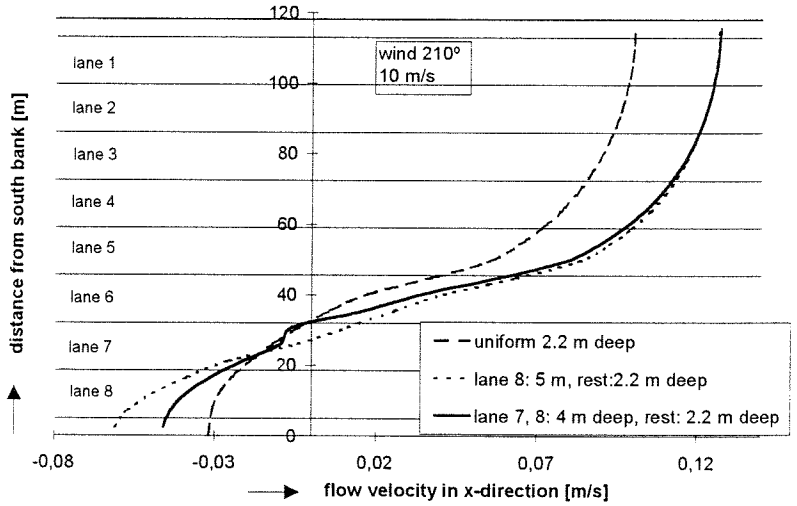

Figure 4.5: Influence of deepening of the south part of the widened course on the distribution of surface flow velocities over the with of the course at south-west wind, 10 m/s

As can be seen from Figure 4.5, the situation does not get any better. Indeed, the gradient has moved a little southwards, but the differences between lane 1 and lane 6 increase. Lane 1 to 7 (1 to 6) are shallow (compared with the south side), increasing the flow velocity considerably, while the flow in the deeper part is stronger against the wind direction.

- Deepening of the middle part

  As was seen for the 92 m wide course, a deepening of the north-half is favourable for winds from the south, but unfavourable for winds from the north. For this wider course it might be better to deepen the middle part, and keep both sides shallow. Two possibilities have been examined:

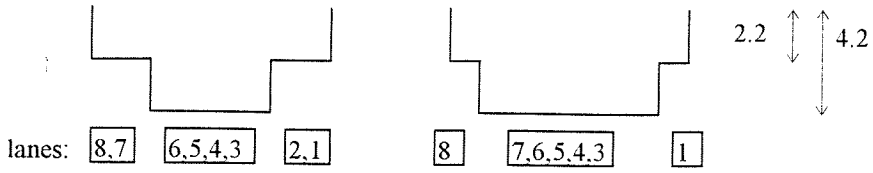

The resulting distributions of surface velocities over the width of the course are given in Figure 4.6, again for the Schiphol wind condition 210° (south-west) and U_{10}: 10 m/s. The flow velocities for the second variant are summarised in Table 4.3, and compared with the original situation with a uniform depth of 2.2 meters.

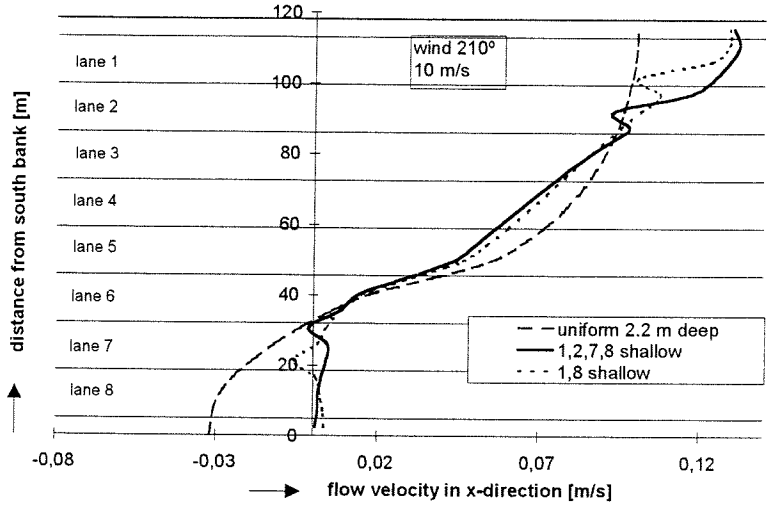

Figure 4.6: Influence of deepening of the middle part of the course on the distribution of surface flow velocities over the width of the course at south-west wind, 10 m/s.

	flow velocity lane 8 [m/s]	**flow velocity lane 6 [m/s]**	**flow velocity lane 3 [m/s]**	**flow velocity lane 1 [m/s]**	**differences 8-3 [m/s]**	**differences 6-1[m/s]**
new	0	0.019	0.084	0.12	0.08	0.1
old	-0.027	0.018	0.089	0.10	0.12	0.08

Table 4.3: Influence of deepening of the middle part of the widened course on the surface flow velocities at south-west wind, 10 m/s.

The profit gained for the lanes 8 to 3 is lost for the lanes 6 to 1. In the shallow part at the windward side, the flow is not longer against the wind direction, and therefore the lanes 8 to 3 are now in favour in contrast with the original situation. Due to the shallow part at the lee side, the flow at that side increases, increasing the differences as well. The differences between the six best lanes (8-3 in the new situation, and 6-1 in the old situation) remain the same.

Fences on the course bottom

- In the longitudinal direction, between the lanes to canalise the flow.

Fences in the length direction, that end approximately 50 cm below the water surface can be used to canalise the flow. When the fences are placed between the lanes, all lanes can be considered as separate units, in which the flow direction is parallel to the fences. The distribution of flow velocities over the width of the course becomes discontinuous: the smallest flow velocity occurs above the fences and a the largest flow velocity occurs between the fences. The differences in flow velocity between the lanes (separate units) will still be present in the above part of the water

column, because the surface velocities will still follow the wind velocities. The benefit of this measure is therefore expected to be small.

- In the lateral direction, to slow down the flow.

  Fences in the width direction can be used to slow down the flow, by creating small vertical circulation cells, see Figure 4.7. Now the flow velocities are discontinuous in the longitudinal direction of the course. The flow, averaged over a lane is therefore smaller, decreasing the differences between the lanes. How much, should be determined by computational modelling with for example, DELFT3D-FLOW. A more extended model than was used in this study is then needed. Also the effect of the hydrostatic pressure assumption on the flow near the fences is expected to be considerable. A non-hydrostatic model is therefore advised for modelling the influence of fences on the course bottom.

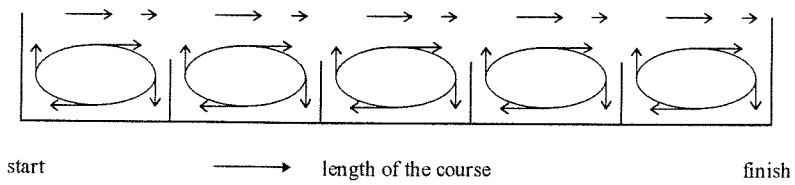

Figure 4.7: Cross-section of the Bosbaan in length direction, with fences placed on the course bottom

Water in-take at the start and out-let at the finish

This with the intention to create a flow at the windward side with the same velocities as in the other lanes. For example for south-west wind the flow in the Bosbaan decreases strongly from the north bank to the south bank where the flow is even in the opposite direction. The idea is to create an artificial flow at this south side, with the same velocity as in the other lanes, by taking in water from the Nieuwe Meer at the start, and pumping this water out at the finish as shown in Figure 4.8a. For north winds this artificial flow must be at the north side, and for east winds, the artificial flow must be the other way around.

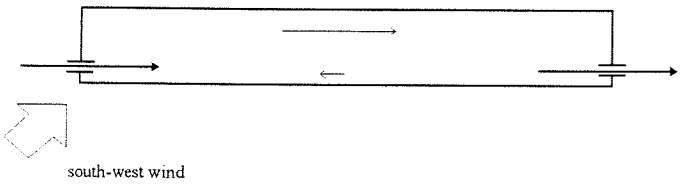

Figure 4.8a: Artificial flow in order to create the same velocity in all lanes.

Another possibility to reduce the differences in flow velocity might be to create an artificial flow against the wind-induced flow as shown in Figure 4.8b.

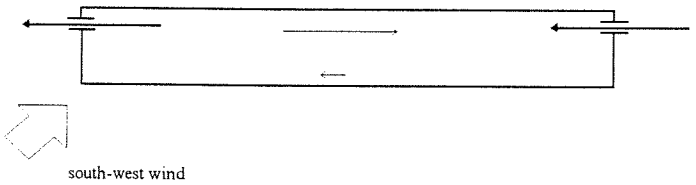

Figure 4.8b: Artificial flow in order to cancel the wind-induced flow.

Those methods are both rather complicated and costly: several structures and an extensive regulation system are needed, considering the large water level differences between the Bosbaan, the Nieuwe Meer and the remaining part of the Amsterdamse Bos. Another disadvantage is that the water from

the Nieuwe Meer is filthier than the water in the rest of the Amsterdamse Bos. Moreover, it should be questioned whether these methods really reduce the flow velocity differences. Some simple tests performed with DELFT3D-FLOW have shown that the water which is taken in, is spread in horizontal direction, increasing the overall flow velocities; the differences between the lanes will not differ much. This spreading process is strongly dependent on the horizontal exchange coefficient, which is still an uncertain parameter in the model. It is therefore recommended to calibrate the original Bosbaan model on the basis of measurements in the real Bosbaan, in order to determine so the value of this influential exchange coefficient.

Additional widening in northern direction

An additional widening in northern direction will increase the effect caused by the already planned widening to 118 meters: the wind velocities increase, as does the surface area at which the wind stress acts. The flow velocities will therefore increase as well. As for the differences in wind velocity, there is an area for which the differences in flow velocity are relatively lower than for the rest of the course. This area is always on the north side, thus the lanes 1 to 6 are always in favour of the lanes 3 to 8. For an additional widening in northern direction, it is expected that this area will increase. There will be more lanes with relatively less lane difference. Hence, this additional widening is favourable both for the lane differences due to the direct influence of wind, and for those due to the differences in flow velocity.

Mixing up the surface flow

The problem is that the surface flow velocities will always follow the wind velocities. The differences in surface flow velocity can be directly reflected to the differences in wind velocity. Effective ways to reduce these flow velocity differences can be sought in mixing up these surface velocities, in order to create a more uniform flow field. Ways to accomplish this are e.g. cross jets, or bubble screens. It should be questioned, however, if these measures are favourable for rowers.

4.4 Conclusions

By cancelling the differences in wind velocity over the course, there will be no lane differences anymore. This is, however, hard to achieve. Only an indoor facility would create completely equal circumstances between the lanes. A course situated in the open field will not have much lane difference but is not a realistic option for the Bosbaan. Moreover, it should be questioned if this is to be preferred: in that situation all lanes have will have bad conditions at high adverse winds. The only possibility (concerning the wind velocity differences) that is worth examining further are structures constructed above the course to shift the wind boundary layer upwards till above the rowers; the rowers stay in the lee, with very low wind velocities.

With just reducing the flow velocity differences, the differences in wind resistance may still cause lane differences. Besides, reducing the differences in flow velocity is not an easy task. The surface flow velocities result directly from the wind velocities, and show approximately the same patterns: high at the windward side and low at the lee side. An exploratory study into possible methods proved that it is very difficult to influence these surface velocities. The results of this study are summarised here:

No effect can be expected from:

- Banks without vegetation, or wider ends of the course in order to reduce the horizontal circulation.
- A channel around the course, both along the length and the width, with the edge at the water level of the Bosbaan in order to prevent the wind-set-up.
- A return channel separate from the Bosbaan, that is supposed to hold the counterflow caused by the wind set up.

- Longitudinal fences to canalise the flow and thus prevent the horizontal circulation.

Minor effect can be expected from:

- Slowing down the flow by deepening the entire course. A substantial improvement can only be reached with a radical deepening.
- Directing the flow by deepening specific parts of the course. A deepening of lee side is favourable, a deepening of the windward side is unfavourable. Hence, a deepening of one side of the course is favourable for half of the wind directions, but unfavourable for the other wind directions. However, it can be chosen to improve the situation for the prevailing wind direction in summer, at the cost of the less frequent wind directions.
- Directing the flow, and/or creating a larger area with smaller flow velocity differences by deepening specific parts of the widened course. A situation that is favourable for all wind directions can not be obtained this way.
- Directing the flow by taking in water from the "Nieuwe Meer" at the start and letting out this water at the finish, or the other way around to create an artificial flow against the wind-generated flow. Both methods will be hard to realise, and their use should be questioned. The artificial flow may be spread in horizontal direction, increasing the overall flow velocities. The differences in flow velocity will not be affected much.

Further studies are needed to determine the effect of:

- Slowing down the flow by lateral fences on the course bottom. To determine the exact effect of this, numerical computations with a non-hydrostatic numerical model are recommended.
- Creating a larger area with relatively small flow differences by an additional widening in northern direction. The influence of such an extreme measure should be examined carefully. Additional wind studies are necessary to determine the wind fields above this wider course.

5. CONCLUSIONS AND RECOMMENDATIONS

5.1 The present situation

The trees around the Bosbaan cause differences in wind velocity above the course. In addition, this spatially varying wind field induces a water circulation, with different flow velocities in the different lanes. Depending on the wind conditions, the flow at the windward side of the course may even be in opposite direction to that at the lee side. Both the differences in wind and in flow velocity cause the lane differences. The wave heights, which may also differ between the different lanes, are of minor importance. The differences in wind- and in flow velocity are maximal for the two outer lanes: lane 1 and lane 6, and increase with increasing wind speed.

These wind- and flow velocity differences result in differences in air- and water resistance for the different lanes, and thus in differences in travel times between the lanes. Those differences in travel times are larger for adverse (east) wind than for assisting (west) wind and increase with increasing wind speed. Which of the two influences prevails, depends mainly on the direction of the wind. Actually, it are the differences caused by the direct influence of wind that are direction dependent, the part caused by flow is of the same order of magnitude both for adverse and for assisting wind. Therefore, for adverse wind, the direct influence of wind on the rowers dominates, while for assisting wind the larger part is caused by the differences in flow velocity.

The prevailing wind direction in summer is south-west, hence assisting wind. For a four, the differences in travel time on 2000 meters then range from 2 seconds for wind force 2 to 7 seconds for wind force 5. East winds are not very common in summer, and if they occur, the wind force will generally be low. For north-east wind, the lane differences for a four range from 2 seconds for wind-force 2 to 8 seconds for wind force 4. These numbers are just meant to give an indication of the order of magnitude, and should not be considered as exact numbers.

5.2 The widened Bosbaan

The widening from 92 meters to 118 meters, as proposed by the FISA, will yield somewhat higher wind velocities above the course than in the present situation (less trees on the north side, and a larger area). Regardless of the wind direction, the wind velocity differences between lane 1 and lane 6 will be smaller than for the existing situation. The differences between lane 3 and lane 8 will be larger than for the existing situation.

Those higher wind velocities acting on a larger surface area induce stronger horizontal circulations, but there is an area with relatively lower flow velocity differences. For all wind directions, this area is at the north side of the course, and covers approximately 4 lanes; the most rapid change in flow velocity occurs near lane 5. The lanes 1 to 6 always have a smaller lane difference than the lanes 3 to 8.

Compared with the existing situation, the lane differences increase for the lanes 3 to 8, but decrease with approximately 20% for the lanes 1 to 6. Therefore, the lanes 1 to 6 are preferred over the lanes 3 to 8, regardless of the wind direction. But in spite of this improvement, the differences between the lanes remain.

5.3 Possible further improvements

Further widening
An additional widening in northern direction will increase both the wind and the flow velocities, but it will also increase the area with relatively less wind- and flow velocity difference. Therefore, this will lead to a further reduction of the lane differences between 6 lanes (starting at the north side of the course).

Measures to control the wind
Lane differences are caused primarily by differences in wind velocity between the lanes. Measures above the water are therefore most effective in reducing the unfairness. Removing the wind is the best, but only an indoor facility can do that. For the Bosbaan, one can think of structures above the course that can decrease the wind velocities, and thus the wind velocity differences, above the water surface.

The differences in wind velocity above the course result mainly from the trees which create a wake. Removing the trees will therefore decrease the wind velocity differences, but it will increase the wind velocities. At high wind velocities, bad conditions will result for all lanes.

Measures to control the flow
Measures under the water are aimed at reducing the differences in flow velocity between the lanes. Several methods can be thought of, that will influence the overall flow patterns, but the surface velocities will always, to a large extent, follow the wind velocities: when the wind velocities above the course vary in space, the surface flow velocities do as well.

Deepening specific parts of the course will affect the flow most: e.g. a deepening of the north side of the course reduces flow velocity differences at south winds (including the prevailing south-west wind) with approximately 50%. This at the expense of the north winds, for which the flow velocity differences increase with approximately 50%.

Lateral fences on the course bottom slow down the flow above these fences, so that the average velocity in a lane is reduced. To determine to what extent these fences influence the surface velocities, extensive numerical computations will be needed.

The same holds for methods to create an artificial flow in the Bosbaan. Moreover, the feasibility of this kind of measures should be questioned.

5.4 Recommendations

The computations performed in this study give an impression of the orders of magnitude of the lane differences. To obtain more precise data, the following is recommended:

- The numerical model must be calibrated for several known situations: local wind fields together with the flow patterns they generate. The vertical layer distribution and the horizontal eddy viscosity coefficient can then be determined more precisely, while in this study a best estimate was applied without calibration.
- These known situations can only be obtained by measurements in the field: both wind- and flow measurements must be performed at various locations above- and in the course. These measurements should be performed in summer (during the rowing season) at various Schiphol wind conditions.
- As was seen in section 8.3, the hydrostatic pressure assumption does influence the flow. It is therefore recommended to execute the numerical computations with a model that solves all three momentum equations.

The calibrated Bosbaan model can be extended with e.g. fences on the bottom or a deeper half. A further widening of the course can only be examined after determining the wind field above the widened course.

Most benefit in reducing the lane differences is expected from structures above the course, e.g. fences, spoilers, or a cover. The rowers stay in the lee of these structures, where the wind velocities remain small, as do the wind velocity differences. The flow velocities and flow velocity differences that result will be small as well. After making an inventory of the structures that are feasible, wind tunnel tests, and if possible, field measurements are needed to determine their influence on the local wind velocities. Numerical computations will again determine the flow conditions.

Finally a very simple recommendation: With the discussion about lane differences going on already for a very long time, it is remarkable that nobody kept statistics of rowing contests: the travel times for the rowers, together with the lane numbers. If this was done for several years, the lane differences would have been known now. It is therefore recommended to start with gathering these statistics as soon as possible.

6. THEORETICAL ASPECTS

6.1 Introduction

This chapter gives a mathematical-physical description of the shallow-water flow model that was used to generate flow data.

The basic equations describing the flow are the Navier-Stokes equations presented in section 6.2. For shallow-water flow, these Navier-Stokes equations can be simplified. The assumptions discussed in section 6.3 result in the governing equations that describe shallow-water flow. One of these assumptions, viz. ensemble averaging, gives rise to additional terms in the equations: the so-called Reynolds stresses. These stresses can be modelled using the eddy viscosity assumption explained in section 6.4. The unknown eddy viscosity can be described in terms of known quantities in several ways, as summarised in section 6.5. The equations thus obtained need to be fixed by the boundary conditions discussed in section 6.6.

6.2 Navier-Stokes equations

The Navier-Stokes equations describe conservation of mass and momentum. Conservation of mass is expressed through:

$$\frac{\partial \rho}{\partial t} + \frac{\partial}{\partial x}(\rho u) + \frac{\partial}{\partial y}(\rho v) + \frac{\partial}{\partial z}(\rho w) = 0 \tag{6.1}$$

With ρ the density of water, and t is time.
The coordinate system (Figure 6.1) is (x,y,z), with z positive upward and velocity components (u,v,w).

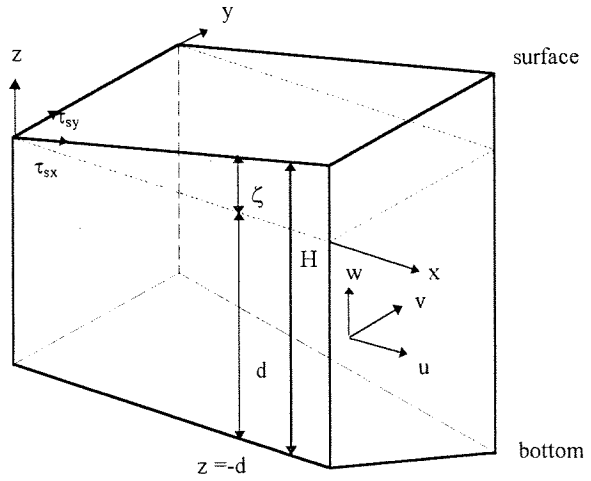

Figure 6.1: Definition of coordinate system and boundaries

Equation (6.1) can be rewritten as:

$$\frac{D\rho}{Dt} + \rho\frac{\partial u}{\partial x} + \rho\frac{\partial v}{\partial y} + \rho\frac{\partial w}{\partial z} = 0 \tag{6.2}$$

where D/Dt is the material derivative. For an incompressible fluid $D\rho/Dt = 0$ (This does not mean that $\partial\rho/\partial t = 0$ or $\partial\rho/\partial x_i = 0$), and (6.2) reduces to the continuity equation:

$$\frac{\partial u}{\partial x}+\frac{\partial v}{\partial y}+\frac{\partial w}{\partial z}=0 \tag{6.3}$$

The equations expressing the conservation of momentum is written as:

$$\frac{\partial}{\partial t}(\rho u)+\frac{\partial}{\partial x}(\rho u^2)+\frac{\partial}{\partial y}(\rho uv)+\frac{\partial}{\partial z}(\rho uw)=-\frac{\partial P}{\partial x}+\frac{\partial \tau_{xx}}{\partial x}+\frac{\partial \tau_{xy}}{\partial y}+\frac{\partial \tau_{xz}}{\partial z} \tag{6.4a}$$

$$\frac{\partial}{\partial t}(\rho v)+\frac{\partial}{\partial x}(\rho uv)+\frac{\partial}{\partial y}(\rho v^2)+\frac{\partial}{\partial z}(\rho vw)=-\frac{\partial P}{\partial y}+\frac{\partial \tau_{xy}}{\partial x}+\frac{\partial \tau_{yy}}{\partial y}+\frac{\partial \tau_{yz}}{\partial z} \tag{6.4b}$$

$$\frac{\partial}{\partial t}(\rho w)+\frac{\partial}{\partial x}(\rho uw)+\frac{\partial}{\partial y}(\rho vw)+\frac{\partial}{\partial z}(\rho w^2)=-\frac{\partial P}{\partial z}-\rho g+\frac{\partial \tau_{xz}}{\partial x}+\frac{\partial \tau_{yz}}{\partial y}+\frac{\partial \tau_{zz}}{\partial z} \tag{6.4c}$$

local inertia *momentum flux* *pressure gradient* *gravity* *viscous stresses*

where P is pressure and g the acceleration due to gravity.

If ν_m is the kinematic viscosity, then the viscous stress tensor τ_{ij} can be expressed in terms of the rate of deformation of a fluid element by the motion:

$$\frac{\tau_{ij}}{\rho}=\nu_m\left(\frac{\partial u_i}{\partial x_j}+\frac{\partial u_j}{\partial x_i}\right) \tag{6.5}$$

where x_j stands for (x,y,z) and u_j for (u,v,w) if j = 1,2,3.

6.3 Three-dimensional shallow-water equations

In DELFT3D-FLOW the flow is modelled by the 3D shallow-water equations. Several approximations are used to formulate these equations, the most important of which are treated below.

Boussinesq approximation

Density variations affect the velocity through the momentum equations. It is assumed that density variations are small: $\Delta\rho/\rho << 1$. Such small variations have no important consequences in the inertia terms of (6.4) nor in the viscous terms. The so-called Boussinesq approximation assumes that the influence of density variations is only envisaged in the gravity term. For all other terms, a reference density ρ_0 is used.

Turbulence averaging

Equations (6.4) together with the continuity equation (6.3) form a closed system, describing all details of turbulent motion. However, to resolve all turbulent length scales present in the flow, an extremely fine resolution in space and time is required, especially if the Reynolds number (ratio of inertia to viscous terms) $Re = UH/\nu_m$, is large (with H the water depth, and U a typical horizontal flow velocity). Unfortunately, this is the case in essentially all applications in hydraulics. To avoid such an extremely fine resolution in numerical simulations an additional simplification is applied, which models the influence of small scale motion on the large scale motion (turbulence modelling). This statistical approach, as suggested by Reynolds, assumes that each variable can be split into a slowly

varying mean value (indicated with ¯) and a random variation about it (indicated with '). This gives for example for the velocity in x-direction:

$$u = \bar{u} + u' \tag{6.6}$$

The important thing to note is that the mean of a product is not the product of the means, e.g.:

$$\overline{uv} = \bar{u}\bar{v} + \overline{u'v'} \tag{6.7}$$

Substituting the splitting of all variables into the Navier-Stokes equations (6.3) and (6.4) and taking the average gives what is called the Reynolds equations for the statistical average of a turbulent flow. These equations have the same form as the original Navier-Stokes equations; the difference is that additional terms called Reynolds stresses appear in the momentum equations, representing the exchange of momentum between fluid elements by turbulent motion. They occur in exactly the same way as the viscous stresses, and can be combined in:

$$\frac{\tau_{ij}}{\rho} = \nu_m \left(\frac{\partial \bar{u}_i}{\partial x_j} + \frac{\partial \bar{u}_j}{\partial x_i} \right) - \overline{u'_i u'_j} \tag{6.8}$$

These Reynolds stresses ($\overline{u'u'}, \overline{u'v'}$, etc) are a-priori unknown, and must be described in terms of known quantities to obtain a well-posed problem. How this can be done is described in section 6.4.

Shallow-water

Shallow-water flows are classified as flows in which the horizontal length scale of phenomena is much larger than the vertical one (the curvature of the streamlines in z-direction must be small). The assumption of shallowness gives rise to further simplified flow equations. Some terms are neglected as a result of rewriting the equations in dimensionless form. The following characteristic relations are distinguished:

1) $\frac{H}{L} << 1$ The characteristic horizontal length scale (L) is much larger than the water depth (H).

2) $W = \frac{H}{L} U$ The characteristic vertical velocity component (W) is small in comparison with the horizontal velocity component (U).

Under these additional assumptions the vertical momentum equation reduces to the hydrostatic pressure relation.

Summarising the results, the 3D shallow-water equations become, omitting the bars (-).

The continuity equation

$$\frac{\partial u}{\partial x} + \frac{\partial v}{\partial y} + \frac{\partial w}{\partial z} = 0 \tag{6.9a}$$

The momentum equation in x-direction

$$\underbrace{\frac{\partial u}{\partial t}+u\frac{\partial u}{\partial x}+v\frac{\partial u}{\partial y}+w\frac{\partial u}{\partial z}}_{\text{inertia}}=\underbrace{-\frac{1}{\rho_0}\frac{\partial P}{\partial x}}_{\text{press.}}+\underbrace{\nu_m\Delta u}_{\text{visc.}}-\underbrace{\left(\frac{\partial u'^2}{\partial x}+\frac{\partial u'v'}{\partial y}+\frac{\partial u'w'}{\partial z}\right)}_{\text{Reynolds stresses}} \tag{6.9b}$$

by mean values | *by turbulent fluctuations*

The momentum equation in y-direction

$$\frac{\partial v}{\partial t}+u\frac{\partial v}{\partial x}+v\frac{\partial v}{\partial y}+w\frac{\partial v}{\partial z}=-\frac{1}{\rho_0}\frac{\partial P}{\partial y}+\nu_m\Delta v-\left(\frac{\partial v'u'}{\partial x}+\frac{\partial v'^2}{\partial y}+\frac{\partial w'v'}{\partial z}\right) \tag{6.9c}$$

with Δ the Laplace operator. The momentum equations are written in nonconservative form. They are obtained by performing the differentiations in (6.4a) and (6.4b) and using the continuity equation (6.3) to cancel a number of terms.

The hydrostatic pressure relation (as a result of the simplified momentum equation in z-direction):

$$\frac{\partial P}{\partial z}=-\rho g \tag{6.9d}$$

The water level is denoted with $z = \zeta$, the bottom with $z = -d$ (see also Figure 6.1). Then, by definition, the water depth equals:

$$H=\zeta+d \tag{6.10}$$

In case of constant density equation (6.9d) becomes

$$P(z)=P_a+\rho g(\zeta-z) \tag{6.11}$$

with P_a the atmospheric pressure at the water surface. The characteristic hydraulic pressure is recognised after insertion of $z = -d$ in equation (6.11).

Using (6.11), and assuming constant density, the pressure gradients in the horizontal momentum equations can be written as

$$\begin{aligned}\frac{1}{\rho_0}\frac{\partial P}{\partial x}&=g\frac{\partial \zeta}{\partial x}\\ \frac{1}{\rho_0}\frac{\partial P}{\partial y}&=g\frac{\partial \zeta}{\partial y}\end{aligned} \tag{6.12}$$

The equations given in (6.9) are ready for numerical implementation as soon as the Reynolds stresses are quantified and the boundary conditions are given. The boundary conditions specify additional driving forces of the fluid flow, such as wind shear stresses exerted on the free water surface. A detailed description of turbulence modelling is given in the sections 6.4 and 6.5. The boundary conditions are described in section 6.6.

6.4 The Reynolds stresses

6.4.1 The closure problem

The Navier-Stokes equations (6.3) and (6.4) are supposed to describe all details of turbulent motion, but, for practical situations in civil engineering, they can be solved only after an additional simplification has been applied. Numerical solution methods approximate these equations with respect to a predefined grid. To obtain consistent approximations, the grid must be chosen such that all characteristic motions are resolved. For turbulent motion, however, this is an unreasonable requirement, because important processes take place at very small length scales. Dissipation of turbulent energy, for instance, occurs at a characteristic length scale of 0.1 mm. To model an area of 1 cm^3 , at least 10^6 grid points would be needed. But since we are mostly interested in the large-scale features only, the Navier-Stokes equations can be averaged over a time scale which is long compared with that of the turbulent motions. The resulting Reynolds equations describe the distribution of mean velocity and pressure. These mean quantities vary more gradually in space, so that a less fine grid is needed. The averaging process, however, introduces correlations between fluctuating velocities $\overline{u_i' u_j'}$ in the equations (see (6.9a) and (6.9b)). Since these are not known, additional equations are needed to obtain a closed system of equations. This is called the turbulence closure problem.

Physically, these correlations, multiplied by the density, represent the transport of momentum due to the fluctuating (turbulent) motion; they act as stresses on the fluid and are therefore called turbulent or Reynolds stresses; e.g. $\overline{\rho u_i' u_j'}$ is the transport of x_i-momentum in the direction of x_j (or vice versa). These stresses can be divided into normal stresses (i = j) and shear stresses (i ≠ j). Except in a thin viscous layer near the bottom or wall, the viscous stress components can be neglected compared to the turbulent shear stress components, when developed turbulent flow is considered. The gradients of the normal turbulent stresses, however, can be neglected compared to the gradient of the normal pressure P.

Equations (6.9) can be solved for the mean values of velocity and pressure only when the turbulence correlations can be determined in some way. In fact, the determination of these correlations is one of the main problems in calculating turbulent flows. Exact transport equations can be derived for $\overline{u_i' u_j'}$, but these equations contain turbulence correlations of the next higher order. Therefore, closure of the equations cannot be obtained by resorting to equations, for correlations of higher and higher order occur. Instead, a turbulence model must be introduced which approximates the correlations of a certain order in terms of lower order correlations and/or mean-flow quantities. These laws described by a turbulence model simulate the averaged character of real turbulence; these laws are expressed in differential and/or algebraic equations, which, together with the mean flow equations (6.9), form a closed set.

6.4.2 Nature of turbulence

Before focusing on models for turbulent transport processes, let's consider the basic nature of turbulence. Turbulence is an eddying motion, which, at the high Reynolds numbers usually prevailing, has a wide spectrum of eddy sizes and a corresponding spectrum of fluctuation frequencies. Its motion is always rotational and can be thought of as a tangle of vortex elements whose vorticity vectors can be aligned in all directions and are highly unsteady. The largest eddies, which are associated with low-frequency fluctuations, are determined by the boundary conditions of the flow and their size is of the same order of magnitude as the flow domain. The smallest eddies, associated with high-frequency fluctuations, are determined by de viscous forces.

The large eddies interact with the mean flow (because the length scales of both are similar), thereby extracting kinetic energy from the mean motion and feeding it into the large-scale turbulent motion. Eddies can be considered as vortex elements which stretch each other. Due to this vortex stretching, which is an essential feature of the 3D-turbulent motion, energy is passed on to smaller and smaller eddies until viscous forces become active and dissipate the energy into heat. This process is called energy cascade and is shown in Figure 6.2, see also Schiereck (1995).

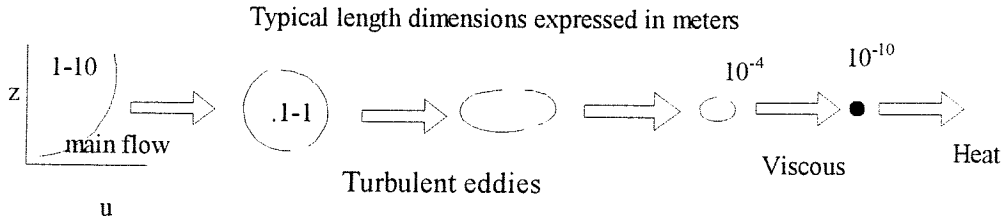

Big whirls have little whirls which feed on their velocity; and little whirls have smaller whirls and so on to viscosity. (L.F. Richardson)

Figure 6.2: Energy cascade

The rate at which mean-flow energy is fed into turbulent motion is determined by the large-scale motion. Only this amount of energy can be passed on to smaller scales and finally be dissipated. Therefore, the rate of dissipated energy is also determined by the large-scale motion. It is important to note that viscosity does not determine the amount of dissipated energy but only the scale at which dissipation takes place. The smaller the effect of viscosity (i.e. the larger the Reynolds number), the smaller are the dissipative eddies relative to the large-scale eddies.

Hence, it is mainly the large scale turbulent motion that transports momentum and contributes to the turbulence correlations $\overline{u_i' u_j'}$. Therefore it is this large-scale motion that has to be simulated in a turbulence model for the determination of $\overline{u_i' u_j'}$; the velocity and length scales introduced in turbulence models are parameters which characterise this motion.

6.4.3 Boussinesq's eddy viscosity

The turbulence correlations $\overline{u_i' u_j'}$ can be taken into account by assuming that the Reynolds stresses are proportional to the strain rate of the mean flow. In analogy to molecular viscosity, the proportionality coefficient is referred to as eddy viscosity. The latter is generally found to be many orders of magnitude larger than the molecular one, and worse, it is not a property of the fluid but rather of the flow. Applying the eddy viscosity concept the Reynolds stresses can be modelled according:

$$-\overline{u_i' u_j'} = \nu_t \left(\frac{\partial \overline{u_i}}{\partial x_j} + \frac{\partial \overline{u_j}}{\partial x_i} \right) - \frac{2}{3} k \delta_{ij} \qquad (6.13)$$

where ν_t is the turbulent or eddy viscosity.

The difference between the characteristic horizontal and vertical length scales gives rise to the distinction between two eddy viscosities ν_t^H, and ν_t^V denoting the horizontal and vertical eddy viscosity respectively.

The eddy viscosity concept was conceived by presuming an analogy between the molecular motion, which leads to Stokes' viscosity law in laminar flow, and the turbulent motion. The turbulent eddies were thought of as lumps of fluid which, like molecules, collide and exchange momentum. The molecular viscosity is proportional to the average velocity and mean free path of the molecules. Accordingly, the eddy viscosity [m^2s^{-1}] is considered proportional to a velocity characterising the fluctuation motion, U, and to a typical length of this motion, L.

$$\nu_t^{\nu} \propto LU \tag{6.14}$$

However, the analogy between molecular and turbulent motion cannot be correct in principle, because the turbulent eddies are not rigid bodies which retain their identity, and because the large eddies responsible for the momentum transfer, and consequently their "free paths", are not small compared with the flow domain, as required by the kinetic gas theory. In spite of these conceptual objections, the eddy viscosity concept has often been found to work well in practice.

The term involving the Kronecker delta δ_{ij} is necessary to make the expression applicable to normal stresses (when i = j). The first part of (6.13) involving the velocity gradients would yield the normal stresses:

$$\overline{u'^2} = -2\nu^H_t \frac{\partial u}{\partial x} \quad , \quad \overline{v'^2} = -2\nu^H_t \frac{\partial v}{\partial y} \quad , \quad \overline{w'^2} = -2\nu^V_t \frac{\partial w}{\partial z} \tag{6.15}$$

whose sum is zero because of the continuity equation. However, all normal stresses are by definition positive quantities, and their sum is twice the kinetic energy k of the fluctuating motion:

$$k = \frac{1}{2}\left(\overline{u'^2} + \overline{v'^2} + \overline{w'^2}\right) \tag{6.16}$$

Inclusion of the second part of the eddy viscosity expression (6.13) assures that the sum of the normal stresses is equal to $2k$. The normal stresses act like pressure forces, thus the second part of (6.13) constitutes a pressure. Therefore, when equation (6.13) is used to eliminate $\overline{u_i' u_j'}$ in the momentum equations (6.9) and (6.9c) this second part can be absorbed by the pressure gradient terms, yielding equations (6.17b) and (6.17c).

The continuity equation

$$\frac{\partial u}{\partial x} + \frac{\partial v}{\partial y} + \frac{\partial w}{\partial z} = 0 \tag{6.17a}$$

The momentum equation in x-direction

$$\begin{aligned} \frac{\partial u}{\partial t} + u\frac{\partial u}{\partial x} + v\frac{\partial u}{\partial y} + w\frac{\partial u}{\partial z} &= -\frac{1}{\rho_0}\frac{\partial P}{\partial x} \\ &+ 2\frac{\partial}{\partial x}\left(\nu_t^H \frac{\partial u}{\partial x}\right) + \frac{\partial}{\partial y}\left(\nu_t^H\left(\frac{\partial u}{\partial y} + \frac{\partial v}{\partial x}\right)\right) + \frac{\partial}{\partial z}\left(\nu_t^V \frac{\partial u}{\partial z}\right) \end{aligned} \tag{6.17b}$$

The momentum equation in y-direction

$$\frac{\partial v}{\partial t}+u\frac{\partial v}{\partial x}+v\frac{\partial v}{\partial y}+w\frac{\partial v}{\partial z}=-\frac{1}{\rho_0}\frac{\partial P}{\partial y} +\frac{\partial}{\partial x}\left(\nu_t^{H}\left(\frac{\partial u}{\partial y}+\frac{\partial v}{\partial x}\right)\right)+2\frac{\partial}{\partial y}\left(\nu_t^{H}\frac{\partial v}{\partial y}\right)+\frac{\partial}{\partial z}\left(\nu_t^{V}\frac{\partial v}{\partial z}\right) \tag{6.17c}$$

The hydrostatic pressure relation

$$\frac{1}{\rho}\frac{\partial P}{\partial z}=-g \tag{6.17d}$$

Note that the viscous shear, which is small compared to the Reynolds stresses, is neglected. For convenience the continuity equation and the hydraulic pressure distribution are repeated here. As a consequence of the shallow-water assumptions, the terms involving $\partial w/\partial x$ and $\partial w/\partial y$ in the Reynolds stress terms of the horizontal momentum equations are being neglected. This set of equations (6.17) will be used further and can be solved once the eddy viscosities ν_t^H and ν_t^V are quantified and the boundary conditions are given.

Also turbulence models exist, which do not make use of the eddy viscosity concept but employ differential transport equations for the turbulent momentum- see e.g. Rodi (1984) or Booij (1992). This way, the different development of the various Reynolds stresses (representing various velocity scales in complex flows) and their transport can properly be taken into account. These Reynolds stress models were not implemented in DELFT3D-FLOW, the shallow-water solver that was used for the Bosbaan computations, and will therefore not be discussed in this study.

The introduction of the eddy viscosity provides a framework for constructing a turbulence model, but it does not itself constitute a complete model. The eddy viscosity still has to be expressed in terms of known or calculable quantities, for which many methods exist - see Rodi (1984). Some frequently applied descriptions of eddy viscosities are described in the following section.

6.5 Turbulence closure models

6.5.1 Introduction

In this section some possible choices for the arising eddy viscosities are outlined. Special attention will be paid to the turbulence closure models available in the shallow-water flow solver DELFT3D-FLOW which has been used for this study.

Especially in shallow-water embayment, the effect of the horizontal eddy viscosity (ν_t^H) on the flow pattern is much smaller than the effect of the vertical one (ν_t^V). The effect of small horizontal viscosity terms is often obscured by numerical diffusion. Many shallow-water solvers presume ν_t^H = constant. However, in the case of a space varying wind, ν_t^H may become important, see section 8.2.2.

Turbulence closure models can be divided into four categories: (i) constant eddy viscosity; (ii) zero-equation models, which express the eddy viscosity in terms of known quantities by means of algebraic expressions; (iii) one-equation models, which use the differential transport equation of turbulent kinetic energy to determine the turbulent mean velocity, and an algebraic expression to prescribe the length scale; (iv) two-equation models, which for example use two coupled differential equations for

the turbulent kinetic energy and the dissipation of this energy. In DELFT3D-FLOW all four models are available.

The first one (i) is a simple closure based on a constant eddy viscosity (independent of the vertical position z). This is sometimes called the quasi-laminar approximation, since it leads to a parabolic velocity distribution as in the laminar case, see section 8.1.2. For the case of turbulent flow, the eddy viscosity is a function of z, so that this is not a realistic option.

The following three turbulence closure schemes are based on the so-called eddy viscosity concept of Kolmogorov and Prandtl, which is obtained by introducing the time-averaged turbulent kinetic energy per unit mass, k (6.16) in the eddy viscosity relation (6.14).

According to (6.16), k is a direct measure of the intensity of the turbulent fluctuations in the three directions. As the energy k is contained mainly in the large-scale fluctuations, $k^{1/2}$ is a velocity scale for the large scale turbulent motion. The Kolmogorov-Prandtl expression is given by:

$$\nu_t^v = c_{\mu'} L\sqrt{k} \tag{6.18}$$

where $c_{\mu'}$ is a numerical constant. The turbulence closure schemes differ in their prescription of the turbulent kinetic energy k, the dissipation of energy ε and/or the length scale L.
The three models (ii), (iii) and (iv) are discussed in the sections 6.5.2, 6.5.3 and 6.5.4 respectively.

6.5.2 Zero equation model

In zero equation models algebraic expressions are used for L and k. The length scale L is a typical distance along which the most energetic eddies/vortices "remember" their history. The geometric interpretation is that L should be less than the nearest distance to the free surface, the bed or a wall. For free surface flows in shallow-water, this geometrical restriction of L is conveniently exploited in the form of the Bakhemetev length scale distribution:

$$L = \kappa(z+d)\sqrt{1-\frac{z+d}{H}} \tag{6.19}$$

with κ the von Kármán constant ($\kappa \approx 0.4$), and d and H defined as in Figure 6.1. The turbulent kinetic energy k depends on the (friction) velocities or velocity gradients. The zero order closure scheme available in DELFT3D-FLOW is called Algebraic Eddy Viscosity Model (AEM) and is a combination of two separate models: the algebraic closure model (ALG) and the Prandtl's mixing length model (PML).

In the algebraic closure model (ALG) the turbulent kinetic energy k is determined on the basis of the shear stresses at the bed and at the free surface. The following algebraic equation is used:

$$k = \frac{1}{\sqrt{c_\mu}}\left[[u_{*_b}]^2\left(1-\frac{z+d}{H}\right)+[u_{*_s}]^2\frac{z+d}{H}\right] \tag{6.20}$$

In this formulation

c_μ	a calibration constant, $c_\mu \approx 0.09$
u_{*s}	the friction velocity at the free surface
u_{*b}	the bed friction velocity

Given k of (6.20) and L of (6.19) the eddy viscosity ν_t^V is prescribed by (6.18). The eddy viscosity is parabolic and gives in the case of a wind-driven circulation, a double logarithmic vertical velocity profile (see section 8.1.2)

In Prandtl's mixing length model (PML) the eddy viscosity is supposed to depend on the local velocity gradient and the mixing length l_m. In this case $L = l_m$:

$$\nu_t^V = l_m^2 \sqrt{\left(\frac{\partial u}{\partial z}\right)^2 + \left(\frac{\partial v}{\partial z}\right)^2} \tag{6.21}$$

The mixing length, like the eddy viscosity is a property of the flow. For convenience, equation (6.21) is written in the form of the turbulent kinetic energy, using equation (6.18):

$$k = \frac{1}{\sqrt{c_\mu}} l_m^2 \left[\left(\frac{\partial u}{\partial z}\right)^2 + \left(\frac{\partial v}{\partial z}\right)^2\right] \tag{6.22}$$

For a stationary logarithmic velocity profile, without wind, (6.20) and (6.22) give a linear distribution of k.

Both the ALG and the PML model are not suitable when processes of convective or diffusive transport of turbulence are important. The PML model has an additional disadvantage: it yields a zero eddy viscosity at the position of zero mean velocity gradient (wind-driven flows). This is physically incorrect. More generally, both models are of little use in complex flows because of the great difficulties in specifying L/l_m.

In DELFT3D-FLOW the two algebraic models ALG and PML are combined into one algebraic model. The eddy viscosity is calculated following ALG and PML and the maximum of those two eddy viscosities is taken.

6.5.3 One equation model

The length scale L is prescribed analytically, again using the Bakhemetev distribution (6.19). However, to find the kinetic energy k, a transport equation is solved. This turbulence closure model is known as the k-L model.

The equation for k can be derived in exact form from the Navier-Stokes equation and has the following form:

$$\underbrace{\frac{\partial k}{\partial t}}_{(a)} + \underbrace{\overline{u_i}\frac{\partial k}{\partial x_i}}_{(b)} = \underbrace{-\frac{\partial}{\partial x_i}\left[\overline{u'_i\left(\frac{u'_j u'_j}{2} + \frac{p}{\rho}\right)}\right]}_{(c)} \underbrace{-\overline{u'_i u'_j}\frac{\partial \overline{u_i}}{\partial x_j}}_{(d)} \underbrace{-\nu_m \frac{\overline{\partial u'_i}}{\partial x_j}\frac{\overline{\partial u'_i}}{\partial x_j}}_{(e)} \tag{6.23}$$

in which
(a) rate of change
(b) convective transport
(c) diffusive transport
(d) production by the Reynolds stresses
(e) viscous dissipation

The rate of change of k is balanced by: the convective transport due to the mean motion, the diffusive transport due to velocity and pressure fluctuations, the production of k by interaction of Reynolds stresses and mean-velocity gradients, and the dissipation of k by viscous action into heat. The production term represents the transfer of kinetic energy from the mean motion to the turbulent motion. It appears with opposite sign as a sink term in the equation for the kinetic energy of the mean motion. The viscous dissipation ε transfers kinetic energy of the fluid and is always a sink term.

This equation cannot be used in a turbulence model yet, because additional correlations appear in the diffusion and dissipation terms. To obtain a closed set of equations, model assumptions must therefore be introduced for these terms. The diffusion flux (term (c)) is often assumed proportional to the gradient of k:

$$\frac{\nu_t^{\nu}}{\sigma_k}\frac{\partial k}{\partial x_i} \tag{6.24}$$

where σ_k is an effective Prandtl number with a value approximately equal to unity. The dissipation ε is usually modelled by the expression:

$$\varepsilon = c_D \frac{k\sqrt{k}}{L} \tag{6.25}$$

in which c_D is a numerical constant. In literature values for c_D and c_μ, (6.18) in the k-L model are found to be are around 0.3.

In shallow-water flow, it can be assumed further that:

- The gradients of the vertical velocity w can be neglected with respect to the gradients of the vertical velocity components u and v;
- The horizontal gradients in the production term can be neglected in comparison with the vertical gradients;
- In horizontal direction, the numerical diffusion is more important than the physical diffusion. Horizontal diffusion is therefore not implemented. In the vertical direction, the numerical diffusion is small, due to small vertical grid sizes and velocities.

With the above model assumptions and the eddy viscosity assumption the k equations reads (omitting the bars):

$$\frac{\partial k}{\partial t} + u\frac{\partial k}{\partial x} + v\frac{\partial k}{\partial y} + w\frac{\partial k}{\partial z} = \frac{\partial}{\partial z}\left(\frac{\nu_t^{\nu}}{\sigma_k}\frac{\partial k}{\partial z}\right) + \nu_t^{\nu}\left[\left(\frac{\partial u}{\partial z}\right)^2 + \left(\frac{\partial v}{\partial z}\right)^2\right] - c_D\frac{k\sqrt{k}}{L} \tag{6.26}$$

The mixing length model mentioned earlier is a special case of the k-L model: if both the advective and diffusive transport terms are negligible. In that case:

$$\nu_t^{\nu}\left[\left(\frac{\partial u}{\partial z}\right)^2 + \left(\frac{\partial v}{\partial z}\right)^2\right] = c_D\frac{k\sqrt{k}}{L} \tag{6.27}$$

When (6.27) is used to eliminate k in the Kolmogorov-Prandtl expression (6.18), there results:

$$\nu_t^{\nu} = \left(\frac{c_{\mu'}^{3}}{c_D}\right)^{1/2} L^2 \sqrt{\left(\frac{\partial u}{\partial z}\right)^2 + \left(\frac{\partial v}{\partial z}\right)^2} \tag{6.28}$$

which is the mixing length formula introduced in (6.21). The mixing length l_m can be seen to be $(c_{\mu'}{}^3/c_D)^{1/4}$ times the length scale L. This derivation clearly shows that the mixing length model is suitable only for flows where the turbulence is in local equilibrium.

6.5.4 Two equation model

In this model, the eddy viscosity is calculated by solving two coupled differential equations for the turbulent kinetic energy k and its dissipation ε. This k-ε model is more complex than the others but does not require a-priori knowledge of the distribution of the length scale L.

The length scale is determined from ε according to:

$$L = c_D \frac{k\sqrt{k}}{\varepsilon} \tag{6.29}$$

The transport equations for k and ε are non-linearly coupled by means of the eddy diffusivity and dissipation terms. The ε-equation is generally taken to be of the following form:

$$\frac{\partial \varepsilon}{\partial t} + u\frac{\partial \varepsilon}{\partial x} + v\frac{\partial \varepsilon}{\partial y} + w\frac{\partial \varepsilon}{\partial z} = \frac{\partial}{\partial z}\left(\frac{\nu_t^{\nu}}{\sigma_\varepsilon}\frac{\partial \varepsilon}{\partial z}\right) + c_{1\varepsilon}\nu_t^{\nu}\frac{\varepsilon}{k}\left[\left(\frac{\partial u}{\partial z}\right)^2 + \left(\frac{\partial v}{\partial z}\right)^2\right] - c_{2\varepsilon}\frac{\varepsilon^2}{k} \tag{6.30}$$

in which σ_ε is the effective Schmidt number, $c_{1\varepsilon}$ and $c_{2\varepsilon}$ are numerical constants.

k is given in the following form:

$$\frac{\partial k}{\partial t} + u\frac{\partial k}{\partial x} + v\frac{\partial k}{\partial y} + w\frac{\partial k}{\partial z} = \frac{\partial}{\partial z}\left(\frac{\nu_t^{\nu}}{\sigma_k}\frac{\partial k}{\partial z}\right) + \nu_t^{\nu}\left[\left(\frac{\partial u}{\partial z}\right)^2 + \left(\frac{\partial v}{\partial z}\right)^2\right] - \varepsilon \tag{6.31}$$

The viscosity ν_t^{V} is given by:

$$\begin{aligned} \nu_t^{\nu} &= c_{\mu'} L\sqrt{k} \\ &= c_\mu \frac{k^2}{\varepsilon} \qquad with \quad c_\mu = c_D c_{\mu'} \end{aligned} \tag{6.32}$$

The standard k-ε model was used in literature (Tsanis, 1989 and Rodi, 1984) with model constants $c_\mu = 0.09$, $\sigma_k = 1.0$, $\sigma_\varepsilon = 1.3$, $c_{1\varepsilon} = 1.44$ and $c_{2\varepsilon} = 1.9$ to calculate wind-induced channel flow.

The eddy viscosity based on k-ε is more complex, but does not require a priori knowledge of the distribution of the turbulent length scale L.

6.6 Boundary conditions

In order to get a well-posed problem a set of boundary conditions for water levels and velocities must be specified. The surface and bottom conditions come in two kinds: kinematic conditions and dynamic conditions. The kinematic conditions say that water particles will not cross either boundary. For the solid bottom, this means that the normal velocity component must be zero:

$$-u\frac{\partial d}{\partial x}-v\frac{\partial d}{\partial y}-w=0 \quad \text{at } z=-d \tag{6.33}$$

At the free surface it is a bit more complicated as the surface may be moving by itself. Then the relative normal velocity must be zero, given by:

$$\frac{\partial \zeta}{\partial t}+u\frac{\partial \zeta}{\partial x}+v\frac{\partial \zeta}{\partial y}-w=0 \quad \text{at } z=\zeta \tag{6.34}$$

Secondly there are dynamic boundary conditions which say something about the forces acting at the boundaries. At the bottom it may be assumed that the viscous fluid "sticks" to the bottom, i.e.:

$$u=v=0 \quad \text{at } z=-d \tag{6.35}$$

which is called the "no slip" condition.

At the free surface, continuity of stresses is assumed, i.e. the stresses in the fluid just below the surface are assumed to be the same as those in the air just above. This means that the surface tension is not taken into account. For the pressure this gives

$$P=P_a \quad \text{at } z=\zeta \tag{6.36}$$

On the free surface a shear stress may act due to wind. The shear stress (τ_{sx} ,τ_{sy}) tangent to the water surface is

$$\tau_{sx}=-\tau_{xx}\frac{\partial \zeta}{\partial x}-\tau_{xy}\frac{\partial \zeta}{\partial y}+\tau_{xz} \quad \text{at } z=\zeta \tag{6.37}$$

and similarly for the y-direction. The wind stress vector on the left-hand side is supposed to be known as an external force. The stresses τ_{ij} are defined using the eddy viscosity concept as:

$$\frac{\tau_{ij}}{\rho_0}=\nu_t\left(\frac{\partial u_i}{\partial x_j}+\frac{\partial u_j}{\partial x_i}\right), \quad (i,j=1,2,3) \tag{6.38}$$

With the assumption that the free surface slopes $\partial\zeta/\partial x$ and $\partial\zeta/\partial y$ are small enough to neglect the contribution of the horizontal momentum diffusion to the vertical flux of momentum at the free surface, equations (6.37) and (6.38) constitute a boundary condition on the velocity field:

$$\frac{\left(\tau_{sx},\tau_{sy}\right)}{\rho_0}=\nu_t^{V}\frac{\partial}{\partial z}(u,v) \quad \text{at } z=\zeta \tag{6.39}$$

At the bottom a similar relation defines the bottom shear stress which is not known and must be a result of the model.

The total differential order of the momentum, pressure and continuity equations in z-direction is 4, so 4 boundary conditions would be expected. That there are 5 is because the level of the free surface ζ is still unknown. This surface level elevation is computed from the surface conditions which is a global or integrated continuity equation. This is obtained by integrating the continuity equation (6.17a) from the bottom to the surface. This gives:

$$w(x,y,\zeta,t) - w(x,y,-d,t) = -\int_{-d}^{\zeta} \frac{\partial u}{\partial x} dz - \int_{-d}^{\zeta} \frac{\partial v}{\partial y} dz \tag{6.40}$$

Next, we substitute equations the kinematic boundary conditions (6.33) and (6.34) into the left-hand side, and use Leibniz' rule on the right-hand side. After rearranging, we obtain the following condition, which is independent of the vertical velocity w:

$$\frac{\partial \zeta}{\partial t} = -\frac{\partial}{\partial x}\left[\int_{-d}^{\zeta} u\, dz\right] - \frac{\partial}{\partial y}\left[\int_{-d}^{\zeta} v\, dz\right] \tag{6.41}$$

this relation is called the surface condition from which the surface elevation is calculated.

7. NUMERICAL ASPECTS OF DELFT3D-FLOW

7.1 Introduction

This chapter discusses the implementation of the shallow-water equations within the simulation program DELFT3D-FLOW. This shallow-water solver was made available by WL|DELFT HYDRAULICS.

The shallow-water equations as discussed in the previous chapter are not yet ready for numerical treatment. First they are transformed in accordance with the chosen grid that covers the physical domain of interest. Section 7.2 discusses how this is done in DELFT3D-FLOW. Secondly, the shallow-water equations in transformed coordinates must be discretized in space as well as in time. This is done based upon finite difference approximations, explained in section 7.3. Finally section 7.4 discusses the boundary conditions in transformed coordinates.

7.2 Grid choice

This section discusses the shallow-water equations in transformed coordinates, in accordance with the Bosbaan. The course has got a rectangular shape, thus only a vertical transformation, called σ-transformation is applied, explained in section 7.2.1. The grid used by DELFT3D-FLOW is a staggered boundary-fitted grid, discussed in section 7.2.2.

7.2.1 σ-Transformation

For numerical solutions, the shallow-water flow region is covered with a computational mesh. This is not a straight-forward task because most engineering applications deal with complicated flow regions such as irregular boundaries and a moving free surface. In DELFT3D-FLOW, the numerical treatment of the shallow-water flow equations is based upon boundary-fitted coordinates. For that purpose the shallow-water equations are transformed. The Bosbaan has a rectangular shape, so that it can be covered with a rectangular grid in the horizontal plane with grid sizes Δx, Δy. No coordinate transformation in the horizontal plane is therefore needed. However, to realise boundary fitted coordinates in z-direction, the so-called σ-coordinate transformation is used. The vertical z-coordinate is replaced by σ defined as:

$$\sigma = \frac{z-\zeta(x,y,t)}{H(x,y,t)} \quad or \quad z = \sigma H(x,y,t) + \zeta(x,y,t) \tag{7.1}$$

in which ζ denotes the water level elevation above the plane of reference $z = 0$. The bottom topography is expressed by d below that plane.

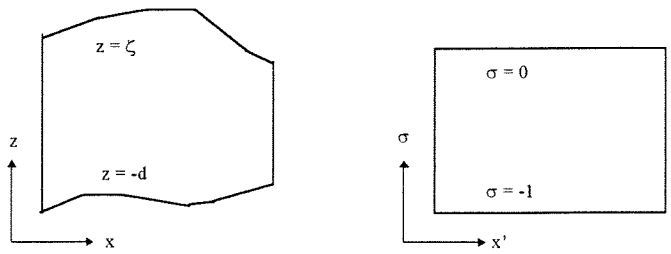

Figure 7.1: Physical domain and σ-transformation

At the bed $\sigma = -1$ and at the free surface $\sigma = 0$. The vertical grid consists of *KMAX* layers $\Delta\sigma(K)$ with $1 \le K \le KMAX$. Their thickness $H.\Delta\sigma(K)$ depends on the total water depth $H = d+\zeta$. This means that over the entire computational area, irrespective of the local water depth, the number of layers is constant. (see Figure 7.1) The grid points move up and down with the surface level. The relative layer thickness can be non-uniformly distributed, which allows for more resolution in the zones of interest, such as near the surface - Vreugdenhil (1993).

The following chain rule is frequently used in σ-transformation

$$\left(\frac{\partial}{\partial x}\right)_{y,x,t} = \left(\frac{\partial}{\partial x^*}\right)_{y^*,\sigma,t^*} + \left(\frac{\partial \sigma}{\partial x}\right)_{y,z,t} \cdot \left(\frac{\partial}{\partial \sigma}\right)_{x^*,y^*,t^*} \tag{7.2}$$

A very beneficial property of the σ-transformation is that the material derivative remains functionally the same provided the vertical component w of the velocity is replaced by the alternative component ω:

$$\frac{\partial}{\partial t} + u\frac{\partial}{\partial x} + v\frac{\partial}{\partial y} + w\frac{\partial}{\partial z} = \frac{\partial}{\partial t^*} + u^*\frac{\partial}{\partial x^*} + v^*\frac{\partial}{\partial y^*} + \frac{\omega}{H}\frac{\partial}{\partial \sigma} \tag{7.3}$$

where

$$u^*(x^*,y^*,\sigma,t^*) = u(x,y,z,t) \quad , \quad v^*(x^*,y^*,\sigma,t^*) = v(x,y,z,t) \tag{7.4}$$

and

$$\omega = w - H\left(\frac{\partial \sigma}{\partial t} + u\frac{\partial \sigma}{\partial x} + v\frac{\partial \sigma}{\partial y}\right) \tag{7.5}$$

The definition of the vertical velocity component ω may be visualised using Figure 7.2 -see Uittenbogaard et al. (1992). Consider in a vertical plane a streamline for a steady flow, going through point $\underline{x}$ and the σ-plane upon which $\underline{x}$ lies. Now ω in $\underline{x}$ is the difference between Cartesian component w and the vertical velocity of its vertical projection on the σ-plane passing through $\underline{x}$.

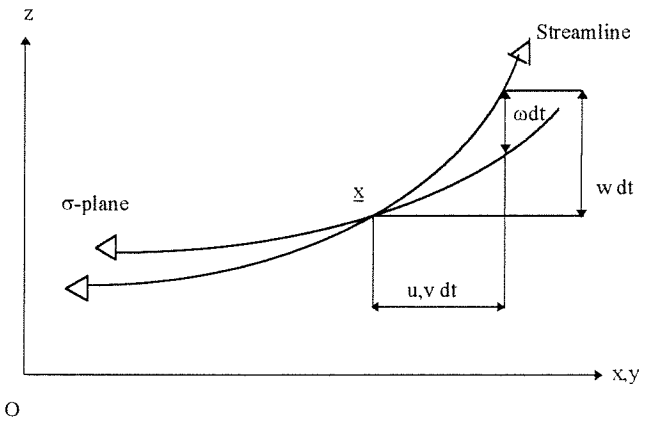

Figure 7.2: Graphical definition of vertical velocity ω in σ-coordinates

Transformation of the continuity equation (6.17a) and using the definition of ω yields (omitting the *)

$$\frac{\partial H}{\partial t} + \frac{\partial}{\partial x}(Hu) + \frac{\partial}{\partial y}(Hy) + \frac{\partial \omega}{\partial \sigma} = 0 \tag{7.6a}$$

Transforming the momentum equation in x-direction gives (omitting the *)

$$\frac{\partial u}{\partial t}+u\frac{\partial u}{\partial x}+v\frac{\partial u}{\partial y}+\frac{\omega}{H}\frac{\partial u}{\partial \sigma}=-\frac{1}{\rho_0}\frac{\partial P}{\partial x}+ D_x(\nu_t^H)+\frac{1}{H^2}\frac{\partial}{\partial \sigma}\left(\nu_t^V\frac{\partial u}{\partial \sigma}\right) \tag{7.6b}$$

and similarly in y-direction

$$\frac{\partial v}{\partial t}+u\frac{\partial v}{\partial x}+v\frac{\partial v}{\partial y}+\frac{\omega}{H}\frac{\partial v}{\partial \sigma}=-\frac{1}{\rho_0}\frac{\partial P}{\partial y}+ D_y(\nu_t^H)+\frac{1}{H^2}\frac{\partial}{\partial \sigma}\left(\nu_t^V\frac{\partial v}{\partial \sigma}\right) \tag{7.6c}$$

The hydrostatic pressure distribution becomes

$$\frac{\partial P}{\partial \sigma}=-g\rho H \tag{7.6d}$$

The horizontal viscosity terms have become a bit more complicated:

$$\begin{aligned} D_x &= \frac{\partial \tau_{xx}}{\partial x}+\frac{\partial \tau_{xx}}{\partial \sigma}\frac{\partial \sigma}{\partial x}+\frac{\partial \tau_{xy}}{\partial y}+\frac{\partial \tau_{xy}}{\partial \sigma}\frac{\partial \sigma}{\partial y} \\ D_y &= \frac{\partial \tau_{xy}}{\partial x}+\frac{\partial \tau_{xy}}{\partial \sigma}\frac{\partial \sigma}{\partial x}+\frac{\partial \tau_{yy}}{\partial y}+\frac{\partial \tau_{yy}}{\partial \sigma}\frac{\partial \sigma}{\partial y} \end{aligned} \tag{7.7}$$

The arising transformed Reynolds stresses satisfy:

$$\begin{cases} \tau_{xx}=2\,\nu_t^H\left(\dfrac{\partial u}{\partial x}+\dfrac{\partial u}{\partial \sigma}\dfrac{\partial \sigma}{\partial x}\right) \\ \tau_{xy}=\nu_t^H\left(\dfrac{\partial u}{\partial y}+\dfrac{\partial u}{\partial \sigma}\dfrac{\partial \sigma}{\partial y}\right)+\nu_t^H\left(\dfrac{\partial v}{\partial x}+\dfrac{\partial v}{\partial \sigma}\dfrac{\partial \sigma}{\partial x}\right) \\ \tau_{yy}=2\,\nu_t^H\left(\dfrac{\partial v}{\partial y}+\dfrac{\partial v}{\partial \sigma}\dfrac{\partial \sigma}{\partial y}\right) \end{cases} \tag{7.8}$$

For the case of the Bosbaan, the horizontal length scale is much larger than the water depth; the shear stresses along the closed boundaries may be neglected. The horizontal viscosity terms $D_x(\nu_t^H)$ and $D_y(\nu_t^H)$ may then be simplified to:

$$\begin{aligned} D_x &= \nu_t^H\left(\frac{\partial^2 u}{\partial x^2}+\frac{\partial^2 u}{\partial y^2}\right) \\ D_y &= \nu_t^H\left(\frac{\partial^2 v}{\partial x^2}+\frac{\partial^2 v}{\partial y^2}\right) \end{aligned} \tag{7.9}$$

Finally, it is assumed that the bottom does not change due to morphological changes. Then the water depth satisfies:

$$\frac{\partial H}{\partial t}=\frac{\partial \zeta}{\partial t} \tag{7.10}$$

This expression can be inserted into the continuity equation.
With the equations (7.6) a complete mathematical-physical description of the three-dimensional shallow-water equations is given. The description is such that its numerical implementation may make use of a boundary-fitted mesh. Further numerical considerations will be discussed in the following section.

7.2.2 The staggered grid

To solve the shallow-water equations numerically a staggered boundary-fitted grid is introduced. A grid cell is labelled with *(m,n,k)*. *k=1* represents the top-layer. The water level points (pressure points) are defined in the centre of a (continuity) cell, whereas the velocity components are defined on the faces of this cell, see Figure 7.3.

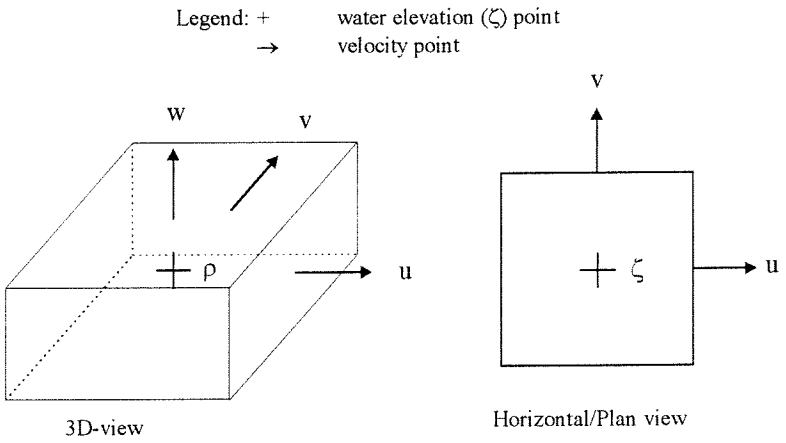

Figure 7.3: Grid staggering

This way the grids for the water levels and velocities are staggered. In the vertical the position of the velocity points is also staggered with the position of the pressure points.

The grid staggering is defined as:

- in the (x,y)-plane with σ is constant

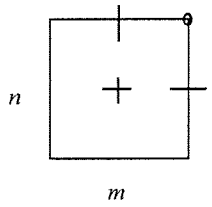

\- location of $u_{m+1/2,n,k}$
| location of $v_{,nm+1/2,k}$
\+ location of $\zeta_{m,n}$, $(\nu_t^H)_{m,n,k}$, $k_{m,n,k}$ and $\varepsilon_{m,n,k}$
° location of $d_{m+1/2,n+1/2}$ with $d = H - \zeta$

- in the (x, σ)-plane with y is constant

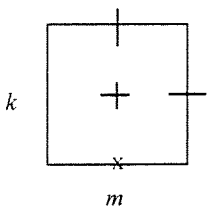

\- location of $u_{m+1/2,n,k}$
| location of $\omega_{m,n,k-1/2}$
x location of $(\nu_t^V)_{m,n,k+1/2}$

- the staggering in the (y, σ)-plane, with x is constant, is identical.

At the u- and v-locations also roughness quantities are defined. The choice of the location of the discrete variables is mainly based on accuracy considerations. Vertical viscosity terms arise in the momentum equations in x- and y-direction. Therefore $\partial/\partial\sigma(\nu_t^V(\partial u/\partial\sigma))$ must be evaluated at every u-location. The second order discretization for a physical quantity φ

$$\left.\frac{\partial\varphi}{\partial\sigma}\right|_k = \frac{\varphi_{k-1/2} - \varphi_{k+1//2}}{\Delta\sigma_k} \tag{7.11}$$

with $\Delta\sigma_k$ the relative layer thickness of layer k, immediately gives rise to position ν_t^V in the horizontal plane $k+1/2$. In general it is not known whether $\nu_t^V(\partial u/\partial\sigma)$ or $\nu_t^V(\partial v/\partial\sigma)$ is dominant, so, ν_t^V is located at the centre of the bottom side.

Staggered grids have several advantages such as:

- boundary conditions can be implemented rather simply, the boundary of the physical domain intersects with the u- and v-locations;
- it is possible to use a smaller number of discrete state variables in comparison with discretizations on non-staggered grids, to obtain the same accuracy;
- staggered grids prevent spatial oscillations of in the water levels.

7.3 The solution method for the 3D shallow-water equations

The shallow-water equations in transformed coordinates are solved using a finite difference spatial discretization, discussed in section 7.3.1, and the Alternating Direction Implicit time-integration method, discussed in section 7.3.2.

7.3.1 Spatial discretization

Spatial derivatives are approximated by means of finite differencing. Each equation is approximated at fixed points within the Eulerian mesh. Average operators have to be used to address a physical quantity to the point under consideration. For instance,

$$u_{m,n,k} = \frac{1}{2}\left(u_{m+1/2,n,k} + u_{m-1/2,n,k}\right) \tag{7.12a}$$

$$\zeta_{m+1/2,n} = \frac{1}{2}\left(\zeta_{m,n} + \zeta_{m+1,n}\right) \tag{7.12b}$$

Expression (7.12b) uses information of two adjacent grid cells.

The DELFT3D-FLOW version with which the computations were performed differs from the standard version. In this version, the following spatial discretizations are applied:

- advection: first-order upwind along streamlines;
- diffusion: central second-order symmetric.

7.3.2 Integration in time

The horizontal velocities of adjacent vertical layers are coupled by the vertical advection term and the vertical viscosity term. The σ-coordinate system can lead to very thin layers in shallow areas. To prevent instabilities induced by the vertical viscosity term, a fully implicit integration is used for the vertical exchange terms. Together with the surface and bottom boundary conditions, this results in a

simple tridiagonal system of equations in the vertical, which can be solved efficiently using the Thomas or double-sweep algorithm.

An efficient numerical scheme is obtained by considering tridiagonal sets of equations in both horizontal directions as well. This is realised by a two step method, called Alternating Direction Implicit, in which the horizontal directions are treated implicitly in alternating order. The procedure marches forward in discrete time steps with increment Δt. Grid quantities are computed at time levels $t + \Delta t$ as well as at intermediate time levels $t + 1/2\Delta t$. The direction in which the integration is implicit changes each half time step. In both steps the horizontal viscosity terms are treated explicitly.

Implicit numerical treatment of non-linear terms gives rise to an iteration procedure, again to assure that only tridiagonal matrix systems have to be considered - see DELFT3D-FLOW manual (1996). The procedure (not the standard version of DELFT3D-FLOW) is summarised as follows:

Step 1: marching from time level t to time level $t + \frac{1}{2} \Delta t$.
1. First, v- velocities are computed explicitly from the momentum equation in y-direction.
2. Second, the momentum equation in x-direction is integrated in z-direction. The resulting depth-averaged momentum equation is substituted into the surface condition. The obtained systems of tridiagonal equations along rows of grid points can be solved implicitly. An iterative procedure yields the approximate water level elevation.
3. Third, back-substitution of the calculated water levels in the momentum equation in x-direction yields tridiagonal systems which can be solved by column, giving the individual u-velocities.
4. Fourth, these u- velocities are substituted into the continuity equation to calculate the ω-velocities.

Step 2: marching from time level $t + 1/2\Delta t$ to time level $t + \Delta t$.
The second step is similar to the first, except that u and v as well as x and y are interchanged.

The discretization method is second order accurate in space and time, except for the ω-velocities and the advection; these are first order accurate. Due to the explicit treatment of the horizontal viscous terms the scheme looses its property of being unconditionally stable.

7.4 Boundary conditions

The boundary conditions as discussed in section 6.6 are also subjected to the σ-transformation. Vertical, bed, and surface boundary conditions are discussed in the sections 7.4.1, 7.4.2, and 7.4.3. The physical domain is also bounded by walls, discussed in section 7.4.4. Dependent on the chosen turbulence closure scheme, additional boundary conditions are needed for the transport equations of turbulent kinetic energy k and its dissipation rate ε, discussed in section 7.4.5.

7.4.1 vertical boundary conditions

In the σ-coordinate system, the free surface and the bottom are σ-planes. The vertical kinematic boundary conditions for the continuity equation (6.33) and (6.34) simplify to:

$$\omega(-1) = 0 \quad \textit{and} \quad \omega(0) = 0 \tag{7.13}$$

7.4.2 Bed boundary conditions

The viscous shear stresses have been neglected so far, but near the bottom they may become important. In case of a smooth bottom the viscous shear stress becomes dominant close to the bottom,

in the viscous sublayer: the turbulent fluctuations die out near the bottom and are equal to zero at the bottom. Above the viscous sublayer the flow is turbulent. The most important turbulent sublayer is the turbulent boundary layer. Between the viscous sublayer and the boundary layer there is a transition sublayer, sometimes called the bufferlayer. Above the boundary layer sublayer there is an outer sublayer (see Figure 7.4)

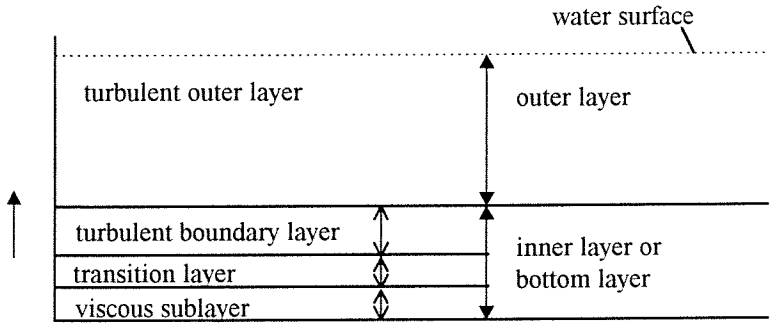

Figure 7.4: Areas in turbulent wall flow

The roughness elements on the bottom mainly influence the velocity distribution close to the bottom, because they generate eddies with the same size, which affect the turbulence structure and hence the velocities close to the bottom. Further away the eddies will rapidly be absorbed in the general existing turbulence pattern. The type of flow regime (hydraulically smooth or rough) depends on the size of the roughness elements on the bottom and the length scale of the viscous sublayer. In most civil engineering applications the flow regime is hydraulically rough: the roughness elements are larger than the viscous sublayer. The velocity distribution near the bottom is then not dependent on the molecular viscosity (ν_m), but solely on the size of the roughness elements.

At the bottom, the fluid sticks to the bottom, resulting in the no-slip condition (eq. 6.36). However, in numerical models this condition leads to very strong velocity gradients (logarithmic profile) near the bottom, which are difficult to resolve. A common alternative in turbulence modelling is using the 'law of the wall' (also indicated as drag law, partial-slip or mixed boundary condition). It assumes that in the turbulent boundary layer, the turbulent shear stress is constant and equal to the bottom stress τ_b. The bed boundary conditions for the momentum equations then become:

$$\frac{\nu_t^V}{H}\frac{\partial u}{\partial \sigma}\bigg|_{\sigma=-1} = \frac{\tau_{bx}}{\rho_0} \tag{7.14a}$$

$$\frac{\nu_t^V}{H}\frac{\partial v}{\partial \sigma}\bigg|_{\sigma=-1} = \frac{\tau_{by}}{\rho_0} \tag{7.14b}$$

with τ_{bx} and τ_{by} the components of the bed stress in x- and y-direction, respectively.

τ_b is defined as:

$$\tau_b = \rho_0 u_*^2 \tag{7.15}$$

The friction velocity u_* is determined by the assumption of a logarithmic velocity distribution in the turbulent boundary layer:

$$u(z) = \frac{u_*}{\kappa}\ln\left(\frac{z+z_0}{z_0}\right) \tag{7.16}$$

with z_0 the roughness height of the bed.
The first grid point above the bed is assumed to lie in the turbulent boundary layer so that:

$$u_b = \frac{u_*}{\kappa} \ln\left(1 + \frac{\frac{1}{2}\Delta z_b}{z_0}\right) \tag{7.17}$$

with u_b the velocity in the computational bed layer, and Δz_b the thickness of the computational bed layer (velocities are computed in the centre of the layer). To prevent the velocity at the bottom to become infinite a vertical transformation of z_0 has been applied.

Parameter z_0 can be linked to the actual geometric roughness as a fraction of the rms-value of the sub-grid bed fluctuations. Nikuradse found that:

$$z_0 = \frac{k_s}{30} \tag{7.18}$$

k_s is known as the Nikuradse roughness length scale.

7.4.3 Surface boundary conditions

At the free surface on which a wind stress acts, a similar assumption as at the bed can be made. The velocity profile in the upper layers can be expressed as a logarithmic function by assuming that the fluid shear stress is constant and equal to the wind shear stress, yielding:

$$\frac{\nu_t^V}{H}\frac{\partial u}{\partial \sigma}\bigg|_{\sigma=0} = \frac{\tau_{sx}}{\rho_0} \tag{7.19a}$$

$$\frac{\nu_t^V}{H}\frac{\partial v}{\partial \sigma}\bigg|_{\sigma=0} = \frac{\tau_{sy}}{\rho_0} \tag{7.19b}$$

with τ_{sx} and τ_{sy} the components of the surface stress in x- and y-direction, respectively.
The magnitude of the wind shear stress is defined as

$$|\tau_s| = \rho_0 u_{*s}^2 \tag{7.20}$$

with u_{*s} the magnitude of the wind friction velocity.

The wind stress vector τ_s is usually related to the wind speed U_{10}, measured 10 meters above the mean free surface. Its magnitude is defined as:

$$|\tau_s| = \rho_{air} C_d U_{10}^2 \tag{7.21}$$

In DELFT3D-FLOW ρ_{air} is invariably taken as 1,205 kg/m^3.

C_d is the drag coefficient of the free surface which depends on the spectrum of surface waves and slightly on the stratification conditions in the air above the free surface. The momentum transfer from wind to the water body is balanced by the generation of surface saves and turbulence. The ratio between turbulence production and the generation of surface waves depends both on the sea state and the fetch (upwind distance to the shore). In DELFT3D-FLOW it is assumed that the energy transfer from wind to water is entirely spent on turbulence generation.

Although measurements indicate that C_d depends on U_{10} and wave parameters, C_d is taken constant 0.0026 in DELFT3D-FLOW.

7.4.4 Shear stresses at closed boundaries

Along the side walls the tangential shear stress is calculated again, based on the logarithmic law of the wall.

$$\tau_{xy} = \tau_{yx} = \rho_0 u_*^2 \tag{7.22}$$

The shear velocity u_* is determined by the log-law for a rough wall, with roughness length z_0 and the distance normal to the boundary x:

$$u(x) = \frac{u_*}{\kappa} \ln\left(\frac{x}{z_0}\right) \tag{7.23}$$

However, in the case of the Bosbaan, the influence of the shear stresses along lateral boundaries can be neglected. Free slip is applied for all lateral boundaries, i.e. $\tau_{xy} = 0$ at the walls.

7.4.5 Boundary conditions for the turbulent kinetic energy and its dissipation rate

Depending on the turbulence closure scheme, additional boundary conditions are needed.
To solve the transport equation for the turbulent kinetic energy k, k must be specified at the bed and at the surface. In the turbulent boundary layer above the bed the Reynolds stresses are assumed constant. In this region advection and diffusion are negligible so that local equilibrium prevails: production = dissipation. This leads to the following Dirichlet boundary condition at $\sigma = -1$:

$$k|_{\sigma=-1} = \frac{u_{*b}^2}{\sqrt{c_\mu}} \tag{7.24}$$

The friction velocity u_{*b} at the bed is determined from the magnitude of the velocity of the grid point near the bed, under the assumption of a logarithmic velocity profile, see equation (7.17).

In case of wind forcing, a similar boundary condition is prescribed for the turbulent kinetic energy k at the free surface:

$$k|_{\sigma=0} = \frac{u_{*s}^2}{\sqrt{c_\mu}} \tag{7.25}$$

In the absence of wind the turbulent kinetic energy k is set to zero.

In the turbulent boundary layer above the bed, the dissipation rate ε equals the production k and becomes:

$$\varepsilon|_{\sigma=-1} = \frac{u_{*b}^3}{\kappa z_0} \tag{7.26}$$

and at the surface the dissipation ε is prescribed by

$$\varepsilon|_{\sigma=0} = \frac{{u_*}_s^3}{\kappa \frac{1}{2}\Delta z_s} \tag{7.27}$$

In case of no wind the dissipation ε is set to zero at the free surface.

8. THE BOSBAAN MODEL

This chapter presents the results of a sensitivity analysis. To limit the computing time, the first tests were performed with a 2-dimensional model (x-z). Section 8.1 describes the results of this simplified model, after which section 8.2 presents the sensitivity analysis for the 3-dimensional Bosbaan model with wind varying in space. Section 8.3 discusses the effect of the hydrostatic pressure assumption, first in general, and secondly, specific for the Bosbaan model. Finally, section 8.4 summarises the parameters that have been established in this chapter.

The coordinate system for the Bosbaan is defined as in Figure 8.1.

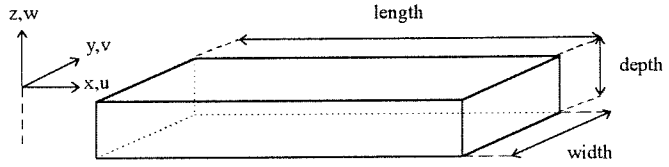

Figure 8.1: Coordinate system of the Bosbaan

8.1 2DV Bosbaan model

In the sections that follow, the results of the sensitivity analysis for the 2DV-Bosbaan are summarised. The tests referred to in this section were performed with the computational model described in section 8.1.1. Section 8.1.2 discusses the important choice of an appropriate turbulence closure model. The vertical layer distribution proved to be very influential as well, as described in section 8.1.3. Section 8.1.4 discusses the bottom roughness, which proved to be less influential. Finally, in section 8.1.5, the Bosbaan model is extended to a 3D model.

8.1.1 2DV-Computational area

In DELFT3D-FLOW, the number of grid points is defined as the number of solid lines connecting the depth points in both directions. In addition, DELFT3D-FLOW requires that boundary conditions are defined outside the model boundaries. Consequently, the grid dimension must be one greater than the model boundaries. The Bosbaan has a length of 2200 meters. With grid sizes of 100 meters in the length direction, 24 points were needed in M-direction (equivalent with x-direction). In N-direction (equivalent with y-direction), just one computational cell was used, with grid size 92 meters (the width of the Bosbaan). According to the boundary definition, two extra cells were needed. Figure 8.14 (Appendix 'Figures') shows the computational cells of this 2DV-course; the cells needed for the boundary definition are skipped. The depth of the model was taken uniform: 2 meters. The tests described in the next section were performed with a uniform vertical layer distribution of 20 layers. The wind was kept steady -10 m/s along the main axis of the course.

8.1.2 Sensitivity to the turbulence model

Turbulent mixing in case of the Bosbaan is preliminary caused by wind which is the principle source of mechanical energy. When a constant wind is acting at the surface of a water body, drift currents are caused in the direction it blows, thus causing a lowering of the water level at the windward side and a rise at the lee side. The difference of water levels creates a pressure gradient which induces a bottom flow in the direction opposite to that generated by wind, as is shown in Figure 8.2. In this

closed basin, the velocity is constant along the length of the course, and the depth-averaged velocity is zero.

For this two-dimensional case, the shallow-water equations (6.17) can be strongly simplified, see Appendix F. The two remaining terms in the equations of motion are the pressure gradient which is balanced by vertical shear, see equation F1b. For an eddy viscosity which is constant over the depth, the velocity distribution can easily be solved by integration of the momentum equation, using the no slip condition at the bottom, and the prescribed wind stress at the surface. The unknown surface gradient can be found using the continuity equation. This procedure, shown in Appendix F, leads to a parabolic velocity distribution as with laminar flow, and a linear shear stress distribution. The wind drift current decreases linearly with depth while the gradient current increases quadratically with depth (see equation F.11). The bottom stress comes out to half the wind stress (equation F.15). The turning point of velocity direction occurs at one third counting from the free surface.

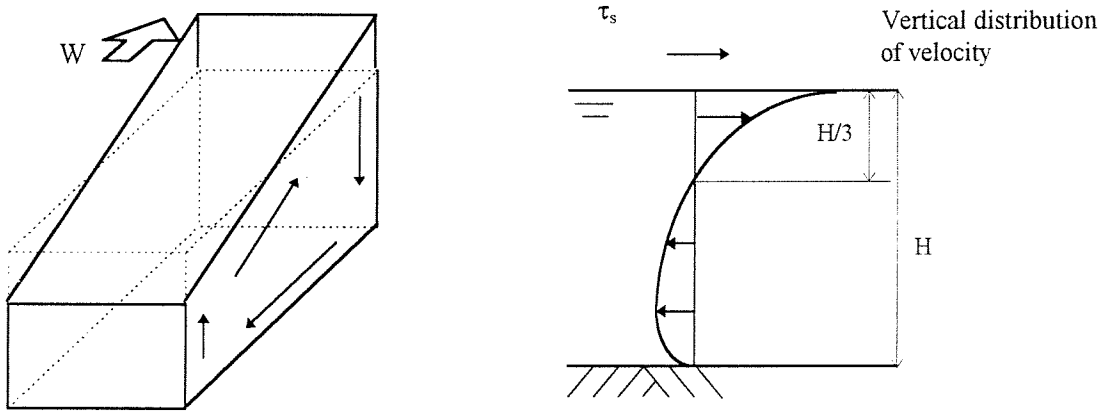

Figure 8.2: Constant wind acting on the Bosbaan surface

However, the assumption of an eddy viscosity which is constant over the depth is not correct. In the case of turbulent flow, the eddy viscosity is a function of the depth. For instance, a parabolic distribution of the eddy viscosity over the depth corresponds to a logarithmic velocity distribution, or double-logarithmic when wind stress is involved (Tsanis, 1989). In this case the bottom stress is about ten percent of the surface stress. Tsanis compared solutions for several eddy viscosity models in wind-induced currents and showed that the resulting velocity distributions varied substantially.

To obtain an appropriate vertical distribution in vertical cross-section for the 2DV-Bosbaan case, numerical experiments were carried out with two eddy-viscosity models:

algebraic (combination of algebraic turbulence model and mixing length model)

k - ε

Both turbulence models have been described in the sections 6.5.2 and 6.5.4 respectively.

Except for the turbulence model, the model set-up was kept the same, and the computations were carried out until the steady state was reached. For a constant wind in space, the flow velocities are constant along the course axis, so it suffices to compare the results at just one point, for which the middle point is chosen. Figure 8.15 (Appendix 'Figures') compares the vertical distributions of velocity, and shows that the vertical profiles obtained with the *algebraic* model differ substantially from those obtained with the k-ε model. With the *algebraic* model, the velocity in the uppermost layer is much smaller, and the turning point of velocity direction is situated in the middle of the water column, whereas with the k-ε model it is situated at about one third of water column (counting from the free surface). The velocity distribution obtained with the k-ε model agrees with the expected double-logarithmic profile.

Figure 8.15 also compares the vertical distributions of eddy viscosity obtained with both eddy viscosity models, which, as the vertical distributions of velocity, differ substantially. The eddy viscosity distribution obtained with the k-ε model agrees with the expected parabolic distribution, with the maximum occurring at half depth. The eddy viscosity distribution obtained with the *algebraic* model has a completely different shape: its maximum is much larger than the one obtained with the k-ε model, and it is located near the surface in stead of at half depth. This larger eddy viscosity means a larger vertical mixing, and thus a much steeper, and thus more uniform velocity distribution in the vertical. From this experiment it is clear that in the case of wind-driven flow, usage of the *algebraic* turbulence model can lead to substantial inaccuracies. The k-ε model will therefore be used in all further computations. It should be noted that this approach is much more time consuming than the *algebraic* model because in each grid point, two extra differential equations (k and ε) must be solved.

8.1.3 Optimising distribution of layers in case of k - ε model

Some preliminary runs showed that the velocity in the upper layer in case of wind-driven currents is very sensitive to its thickness. To obtain an appropriate vertical distribution of the velocity, it is necessary to refine the vertical grid. First some numerical experiments were carried out with several equidistant layer distributions:

- 10 layers with relative thickness of 10 %, u10;
- 20 layers with relative thickness of 5 %, u5;
- 50 layers with relative thickness of 2 %, u2;
- 100 layers with relative thickness of 1 %, u1.

Except for the layer distribution the model set-up was kept the same. Figure 8.16 (Appendix 'Figures') compares the obtained vertical distributions of velocity and eddy viscosity in the middle point of the course; the vertical profiles of velocity end below the water surface because the velocities are plotted halfway the layers. A finer layer distribution always leads to more accurate results than a coarser distribution: the smaller the layer thickness, the larger/better the surface velocity. In addition, the eddy viscosity at the surface is not equal to zero at large layer thicknesses. The best results (of those four computations) were obtained with the finest resolution: 100 layers with a relative thickness of 1%. These vertical profiles of velocity and eddy viscosity will be used as prototype vertical profiles.

However, for the case of the Bosbaan, with also quite a number of grid points in y-direction, this many layers will be very time consuming. It is therefore worth trying to limit the number of layers, but still keeping the same (or nearly the same) vertical profiles. This can be obtained by refining the layers in the regions of interest: near the surface and near the bottom, in comparison with the remaining layers. To find the optimum number of layers and the 'best' distribution in comparison with 100 equidistant layers, several runs with different layer distributions were carried out. The tested layer distributions, shown in Table 8.1, differ in number of layers, in thickness of layers, and in smoothness of the distribution.

Figures 8.17-8.20 (Appendix 'Figures') present the computation results for the layer distributions shown in Table 8.1. Figures 8.17-8.19 show both vertical distributions of velocity and eddy viscosity, while Figures 8.20 just show the velocity profiles. It is visible that both, the thickness of the upper layer and the smoothness of the distribution play an important role. Figure 8.17 shows cases with 20 layers but with different layer thicknesses, which lead to very different vertical profiles. Figure 8.18 shows that several cases with a large variation in layer thickness lead to very similar results, but not similar with the case with 100 equidistant layers, see Figure 8.20b. Especially in the above part of the water column, which is important for the rowers, the profiles differ substantially (see Figure 8.20c).

Cases with a smooth distribution do not differ much from the case with 100 equidistant layers, see Figures 8.19, 8.20a, and 8.20c.

From these figures, it can be concluded that the layer distribution near the surface is decisive for reproducing correctly the vertical profiles of wind-induced flow. The middle part and bottom area are less important. From all presented results, the conclusion can be drawn that to reproduce correctly the vertical profile with a minimum number of layers, it is necessary to use about 20 layers with a smooth distribution, e.g. distribution as in case nu8.

	run nr.							
layer nr.	nu1	nu2	nu3	nu4	nu5	nu6	nu7	nu8
1	0.5	1	0.5	0.5	0.5	0.5	0.5	0.6
2	2	1.5	2	2	2	2	0.6	0.8
3	2.5	2	2.5	2.5	2.5	2.5	0.7	1.1
4	5	3	5	2.5	2.5	2.5	0.9	1.6
5	5	4	5	2.5	2.5	2.5	1	2.2
6	5	4.5	5	5	5	2.5	1.2	3.1
7	5	6	5	5	5	2.5	1.5	4.4
8	5	6	5	5	5	2.5	1.8	6.1
9	5	6	5	5	5	2.5	2.1	8.6
10	5	6	5	5	5	2.5	2.6	8.6
11	7.5	6	5	5	5	2.5	3.1	8.6
12	7.5	6	5	5	5	2.5	3.7	8.6
13	7.5	6	5	5	5	2.5	4.4	8.6
14	7.5	6	5	5	5	2.5	5.3	8.6
15	7.5	6	5	5	5	2.5	5.3	8.6
16	5	6	5	5	5	2.5	5.3	8.6
17	5	6	5	5	5	2.5	5.3	5.2
18	5	6	5	5	5	2.5	5.3	3.1
19	5	6	5	5	5	2.5	5.3	1.9
20	2.5	6	5	5	5	2.5	5.3	1.1
21			5	5	5	2.5	5.3	
22			5	5	2.5	2.5	5.3	
23				2.5	2.5	2.5	5.3	
24				2	2.5	2.5	5.3	
25				0.5	2	2.5	5.3	
26					0.5	2.5	5.3	
27						2.5	3.2	
28						2.5	1.9	
29						2.5	1.2	
30						2.5	0.7	
31						2.5		
32						2.5		
33						2.5		
34						2.5		
35						2.5		
36						2.5		
37						2.5		
38						2.5		
39						2.5		
40						2.5		
41						2		
42						0.5		
sum	100	100	100	100	100	100	100	100

Table 8.1: Non-equidistant layer distributions

8.1.4 Sensitivity to bottom roughness

The bottom roughness height z_0 needed for the bed boundary condition (see equation 7.17) can be related to the Chézy coefficient obtained with 2D-computations (depth-averaged), by assuming that the bed shear-stresses of the 3D-computations equal the bed shear-stresses obtained with the 2DH-code. The velocity distribution without wind is logarithmic:

$$u(z) = \frac{u_*}{\kappa} \ln\left(\frac{z}{z_0}\right) \tag{8.1}$$

The magnitude of bed shear-stress τ_b^{3D} in the 3D-computations is defined as:

$$\tau_b^{3D} = \rho_0 u_*^2 \tag{8.2}$$

The bed shear-stress in the 2DH-computations τ_b^{2D} follows from:

$$\tau_b^{2D} = \frac{\rho_0 g}{C_{2D}^2}\left(\overline{U}\right)^2 \tag{8.3}$$

The assumption of equality of both shear stresses, and elimination of u_* using equation 8.1 gives the required expression for z_0.

$$z_0 = H \exp\left(-\left(1 + \frac{\kappa}{\sqrt{g}} C_{2D}\right)\right) \tag{8.4}$$

A default value for C_{2D} in DELFT3D-FLOW is 65m$^{1/2}$/s, which leads to a z_0 of 2.10^{-4} m. This is a rather small roughness height for the shallow Bosbaan (only 2 meters deep): shallow-water results in relatively more influence of the bottom roughness, and thus in a higher bottom roughness height and a smaller C_{2D}.

When C_{2D} is 45m$^{1/2}$/s, for example, z_0 becomes 2.10^{-3} meters. Using White-Colebrook:

$$C_{2D} = 18 log\left(\frac{12H}{k_s}\right), \tag{8.5}$$

gives a Nikuradse roughness height of 7.5 cm. This is a realistic value for a sand bed.

The 2DV-Bosbaan model was tested for three values of z_0: 0.0002m, 0.002m and 0.02m, and for a Chézy coefficient of 65m$^{1/2}$/s. The resulting vertical velocity- and eddy viscosity profiles differ a little, and only at the bottom, see Figure 8.21. As expected, the resulting vertical profiles for z_0 = 0.0002 m and C_{2D} = 65 m$^{1/2}$/s are exactly the same. The vertical distribution of velocity is mostly determined by the surface shear; the bottom shear has only little influence (less than ten percent of the surface shear). The velocities near the bottom are small, as are the velocity gradients. Thus, wind profiles with a zero depth-averaged velocity are not sensitive to the bottom roughness.

8.1.5 Extension of the number of points in *y*-direction

As an extension to the 2DV-model, the number of grid points in *y*-direction were increased, resulting in a 3D-model. The Bosbaan width is 92 meters, with 6 lanes of 12.5 meters each. In order to represent correctly the expected horizontal circulation, grid sizes of 4.6 meters have been chosen. This leads to 20 computation cells + 2 for the boundary definition is 22 cells in *y*-direction. Thus, as the Bosbaan itself, the grid cells have a much larger length than width.

With the other model parameters still the same, and the wind still constant in the direction of the course axis, this model gives exactly the same results as the model with just one computation cell in *y*-direction. With a constant wind in space, no velocities and no velocity gradients occur in *y*-direction. Therefore, Δy, and the number of points in *y*-direction have no influence at all. What happens if the wind is varying in space, is explained in the next section.

8.2 The 3D Bosbaan model

In reality, the wind field above the Bosbaan is not constant; it varies strongly is space, as was shown in section 2.3.2. Section 8.2.1 discusses how these wind data have been used in the Bosbaan model, and explains how they will induce the flow. This process strongly depends on the horizontal eddy viscosity coefficient, for which an appropriate first choice is made in section 8.2.2. The influence of this parameter on the results, can only be determined after appropriate choices have been made for the numerical parameters. The sections 8.2.3, 8.2.4, and 8.2.5 discuss the time step influence, the number of points in x-direction, and the number of points in y-direction, respectively. After these numerical parameters have been established, the physical parameters are examined: section 8.2.6 discusses the 2D eddy viscosity, after which section 8.2.7 discusses the bottom roughness.

For the sensitivity analysis discussed in this section, 12 monitoring points were chosen, divided over the course. Their names and locations have been indicated in Table 8.2.

→ distance from the start [m]

	500	1000	1500	2000
lane 1	nw	nm1	nm2	ne
lane 3/4	mw	mm1	mm2	me
lane 6	sw	sm1	sm2	se

Table 8.2: Locations and names of the monitoring points used in the sensitivity analyses

8.2.1 Space-varying wind velocities

Assume a rectangular shaped basin with wind velocities in the direction of the course axis, which vary in space, see Figure 8.3. As with a constant wind in space, wind set-up up occurs. However, the wind set-up on the side with the larger wind velocities is larger than the wind set-up on the side with the smaller wind velocities. In this case, there are also surface gradients in y-direction, causing a horizontal water circulation in addition to the vertical circulation, which still occurs. Both circulations are shown in Figure 8.3.

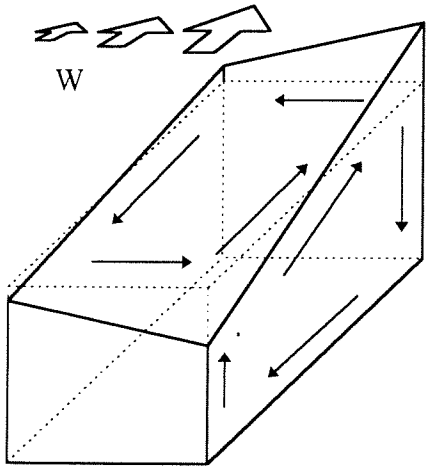

Figure 8.3: Space varying wind field acting on the Bosbaan surface

distance from start [m]

wind 30°			
	lane 1	**lane 3/4**	**lane 6**
250	21	29	45
500	35	29	34
750	15	27	38
1000	26	37	34
1250	22	25	28
1500	16	24	29
1750	18	25	22
mean	21.9	28	32.9

Table 8.3: Wind velocity coefficients [%], with wind direction 30°

These extra velocities due to this horizontal circulation are as it were added to the wind-induced vertical circulation, increasing the flow at the lee side, and decreasing the flow at the windward side, as is shown in Figure 8.4. The depth averaged flow is no longer zero everywhere in the course, but circulates: at the lee side the flow is in the wind direction, while at the windward side the flow is

against the wind direction. In the middle of the course, the depth averaged velocities are approximately zero.

For the sensitivity analysis, the Schiphol wind condition 30° (north-east wind), with wind velocity 10 m/s was chosen. The corresponding wind coefficients at the Bosbaan, as measured by van Melle in a boundary layer wind tunnel, are shown in Table 8.2. The local wind directions were assumed in the direction of the course-axis. Multiplication with the wind velocity at Schiphol (10 m/s for this case) gives the local wind velocities at 1.75 meters above the course.

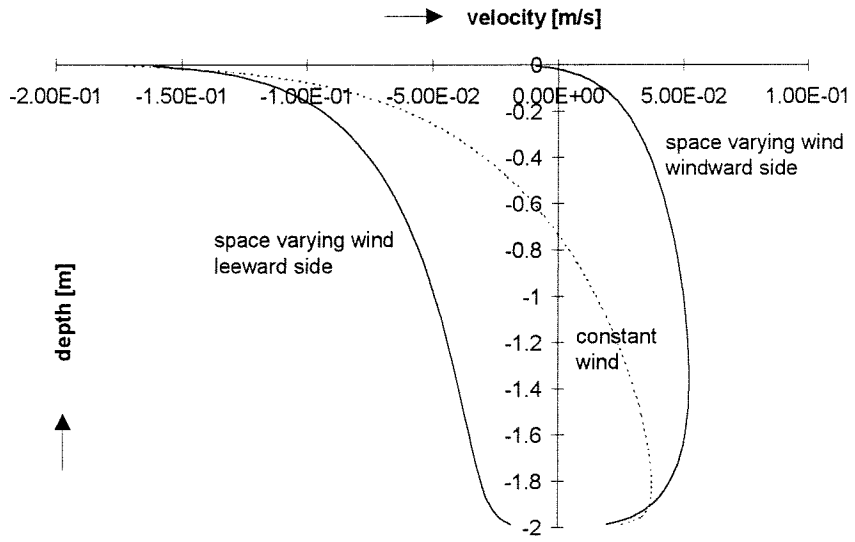

Figure 8.4: Velocity profile changes by space varying wind.

In DELFT3D-FLOW, wind forcing is determined using the following widely used quadratic expression, see also section 7.4.3.

$$|\tau_s| = \rho_{air} C_d U_{10}^2 \tag{8.6}$$

The wind velocities, measured at 1.75 meters above the water surface must therefore be transformed to wind velocities at 10 meters above water surface. In the atmospheric boundary layer the wind velocity distribution is logarithmic:

$$w(z) = \frac{w_*}{\kappa}\left(\frac{z}{z_{w0}}\right) \tag{8.7}$$

in which
$w(z)$ the wind velocity at height z
w_* the wind shear velocity
z_{w0} the wind roughness height

In an open field, z_{w0} is approximately equal to 0.03 meters, see Wieringa and Rijkoort (1983). The ratio of the wind velocity at 1.75 meters to the wind velocity at 10 meters follows from:

$$\frac{w(1.75)}{U_{10}} = \frac{\ln(1.75/z_{w0})}{\ln(10/z_{w0})} \tag{8.8}$$

which yields, U_{10} = 1.4 w(1.75). However, a multiplication of all local wind velocities with 1.4, has the same effect as a multiplication of C_d with $(1.4)^2 = 2$. Thus, in stead of a wind stress coefficient of 0.0025 as in the previous cases with a constant wind, a value 0.005 will be used for the space-varying wind fields. The wind velocity coefficients were measured at 21 points divided over the course. These values were interpolated linearly to obtain values for the wind velocities at the 24*22 grid points.

Theoretically, when wind velocities differ in space, the air pressure must differ in space as well: according to Bernoulli:

$$\frac{P}{\rho_{air} g} + \frac{U^2}{2g} = \text{constant , along a streamline.} \tag{8.9}$$

where U is the flow velocity along the streamline. This holds both for flow and air: a larger wind velocity means a lower pressure. The pressure correction due to the wind velocity differences results from:

$$\Delta P = -\rho_{air} \Delta(w)^2 \tag{8.10}$$

where ρ_{air} is the density of air, and w the wind velocity just above the course. For the chosen wind condition (30°, 10 m/s measured at Schiphol), the maximum wind velocity is 4.5 m/s while the minimum wind velocity is 1.8 m/s. The maximum pressure correction for this situation is only 10 N/m^2, which can be neglected in comparison with the atmospheric pressure. The pressure field above the course is therefore assumed to be constant and equal to the atmospheric pressure.

8.2.2 Horizontal eddy viscosity

Wind velocities, which vary in space above the course, cause flow velocities that vary in space as well, resulting in horizontal velocity gradients. For this case, the horizontal viscosity terms may become important. In DELFT3D-FLOW, this terms have been implemented as follows, see also section 7.2.1:

$$\begin{aligned} D_x &= \nu_t^H \left(\frac{\partial^2 u}{\partial x^2} + \frac{\partial^2 u}{\partial y^2} \right) \\ D_y &= \nu_t^H \left(\frac{\partial^2 v}{\partial x^2} + \frac{\partial^2 v}{\partial y^2} \right) \end{aligned} \tag{8.11}$$

In the case of the Bosbaan, especially $\partial u/\partial y$ becomes large, because U>>V and L>>B.

In DELFT3D-FLOW, a distinction is made between horizontal and vertical eddy viscosity, which is referred to as 2D-turbulence and 3D-turbulence, respectively. The eddies related to 3D-turbulence, that are mainly generated at the bed and at the surface, have characteristic length scales smaller than or equal to the water depth. Therefore, if a turbulence model is required, then at least a "3D-turbulence' model is needed. For small scale applications, this may be sufficient.

However, for flows with much larger horizontal extension there is a "gap" between the horizontal resolution of the flow and the 3D-turbulent vortices mentioned before. In this gap the fluctuating motions are almost horizontal and are defined as sub-grid 2D-turbulence, assuming that the fluctuating motions at scales one order of magnitude larger than the horizontal mesh sizes are well represented.

In DELFT3D-FLOW the horizontal viscosity is assumed to be a superposition of the two parts: the part due to "2D-turbulence" and the part due to "3D-turbulence" see Uittenbogaard et al., (1992). Therefore $\nu_t^H = \nu_t^{2D} + \nu_t^V$, where ν_t^V is referred to as three-dimensional turbulence and is computed following the turbulence closure model that is used. For ν_t^{2D} an appropriate estimate has to be made. In the case of the Bosbaan, especially the horizontal u-momentum exchange in y-direction is important (see equations 8.11). The grid sizes in this direction are only a little larger than the water depth, and the "gap" is therefore not very big. A crude estimate for ν_t^{2D} is obtained by assuming it proportional to the friction velocity and a typical length scale, in this case the grid distance Δy. An upper limit for ν_t^{2D} is thus obtained: $\nu_t^{2D} \approx u_* \Delta y \approx 1/10u\ \Delta y = 1/10*0.2*4.6 \approx 0.1 m^2/s$. A lower limit is obtained by assuming isotopic viscosity, $\nu_t^H = \nu_t^V$, and $\nu_t^{2D} = 0$. In the latter case, an equally fine resolution is needed in y-and in z-direction. As a first estimate a value in between those two limits is chosen: $\nu_t^{2D} = 0.05\ m^2/s$. The sensitivity of the Bosbaan model to the horizontal eddy viscosity is analysed in section 8.2.6. In the sections prior to this section, the sensitivity to numerical parameters, as time step and horizontal grid-distances is discussed.

8.2.3 Sensitivity to the time-step

Since only steady state computations will be performed, the results are not affected by the time step. Of course, the time step should be chosen such that the steady state is reached. The DELFT3D-FLOW version with which the Bosbaan computations were performed, integrates the advective terms explicitly. This reduces the computation time per step considerably, but the time step becomes restricted by:

$$\Delta t \leq \frac{\Delta x}{u} \tag{8.12}$$

Thus, the smaller the grid distances, the smaller time step is needed. The decisive grid distance is Δy, which is 4.6 meters. With an advection velocity of approximately 0.20 m/s (follows from previous computations), Δt must be smaller than 23 seconds (0.4 minute). To choose an appropriate value for the time step, computations were performed with 3 different time steps: 0.5 minute, 0.1 minute, and 0.05 minute. Figures 8.22 (Appendix 'Figures') show the resulting spin-up times for three monitoring stations, located in lane 6 near the start (sw), in between lane 3 and lane 4 in the middle (mm1), and in lane 1 near the finish (ne). As was expected, the steady state was not reached for $\Delta t = 0.5$ minutes, as shown in Figure 8.22a for station (mm1). For the other two tested time-steps the steady state was reached after 600 minutes. With time-steps 0.1 and 0.05 the same results were obtained, see Figure 8.22b for (sw), and 8.22c for (ne). Therefore a time step of 0.1 minute has been chosen for all further calculations.

8.2.4 Sensitivity to the number of point in x-direction

To check the sensitivity of the Bosbaan model to the number of grid points in x-direction, and thus to the grid sizes Δx, a computation was performed with half grid sizes: $\Delta x = 50$ meters in stead of 100 meters. In that case, 2200/50 = 44 + 2 boundary points = 46 points were needed. Figure 8.23 (Appendix 'Figures') compares the vertical distributions of velocity in x-direction for both values of Δx for the 12 monitoring points. The resulting velocity differences between lane 1 and lane 6, obtained with $\Delta x = 100$ meters are larger than the velocities differences obtained with $\Delta x = 50$ meters. This holds especially for the points at 500 meters distance from the start, where the velocities are the largest.

Finer grids always lead to more accurate results. Best is to use a grid with the same size in x- and y-direction, but that would increase the number of grid cells with a factor 20. The computation power to compute such a large model was not available for this study. Since this study is aimed at obtaining qualitative more than quantitative data, it is chosen to keep Δx =100 meters, with the advantage of not increasing the computation time with a factor 2.

8.2.5 Sensitivity to the number of points in y-direction

The sensitivity to the number of points in y-direction was also checked with a computation using half grid sizes Δy: 2.3 meters in stead of 4.6 meters. As was seen in section 8.2.2, the estimate of the horizontal viscosity was based on the grid size Δy. Therefore, it had to be checked as well, if better results were obtained with a smaller value of ν_t^{2D}: 0.025m^2/s in stead of 0.05. Figure 8.24a (Appendix 'Figures') compares the vertical distributions of velocity in x-direction obtained with Δy = 4.6 meters for the 12 monitoring points with those obtained with Δy = 2.3 meters and ν_t^{2D} = 0.025m^2/s. Figure 8.24b (Appendix 'Figures') does the same but this time the results with Δy = 2.3 meters were obtained without scaling ν_t^{2D} (ν_t^{2D} was kept 0.05m^2/s). From these results it can be seen that the Bosbaan model is not sensitive to the grid size Δy: the profiles differ only a little. For most monitoring points, the results obtained without scaling of ν_t^{2D} are better than those obtained with scaling of ν_t^{2D}. The sensitivity of the Bosbaan model to this horizontal eddy viscosity, which is expected to be large, is examined in the next section.

8.2.6 Sensitivity to the 2D-viscosity coefficient

Previous runs have shown that models with a space varying wind are very sensitive to the 2D, or horizontal eddy viscosity coefficient. This coefficient acts as a spreading and smoothing mechanism. This means that when this coefficient is chosen zero, there is little mixing in horizontal direction: the momentum exchange by the Reynolds stresses is zero. The surface velocities, like the wind velocities, are non-homogeneously distributed, with large differences between the velocities on opposite sides, sometimes even in the opposite direction. The horizontal circulation predominates the vertical circulation. On the contrary, when a large value is taken for the horizontal eddy viscosity, there is much horizontal mixing of turbulent energy. The surface velocities are more homogeneously distributed and the vertical circulation predominates. However, such a large value for this horizontal eddy viscosity is not very realistic for the Bosbaan model, as was discussed in section 8.2.2.

To test the sensitivity of the Bosbaan model to this coefficient, computations were performed with four values of this coefficient: 1, 0, 0.1, and 0.05 m^2/s. The Figures 8.25-8.26 present the results: Figures 8.25a-d (Appendix 'Figures') show flow patterns for the various horizontal eddy viscosity coefficients, and Figures 8.26a-b (Appendix 'Figures') compare vertical distributions of velocity in x-direction in the monitoring points. From these figures it can be seen that an eddy viscosity of 1 m^2/s gives completely different results from an eddy viscosity of 0, 0.05, and 0.1 m^2/s , which results differ only a little. From Figure 8.26a, it can be seen that the velocities (in x-direction) for ν^{2D} = 0.05 m^2/s lie in between the results for ν^{2D} = 0.1m^2/s and ν^{2D}= 0m^2/s. Therefore ν^{2D} = 0.05 m^2/s seems an appropriate choice, and will be used further.

8.2.7 Sensitivity to the bottom roughness

The sensitivity analysis for the bottom roughness was performed with the same four values for the bottom roughness as were used for the 2DV-course in section 8.1.5: z_0 = 0.02, 0.002, and 0.0002 meters and Chézy = 65m^{½}/s. Figure 8.27 (Appendix 'Figures') presents the vertical distributions of velocity for the monitoring points (sw) and (nw). The resulting vertical profiles for the different

values of the bottom roughness differ more than in the case with a constant wind in the 2DV-model, because the depth-averaged velocity is no longer zero. As is explained in section 8.1.5, the resulting profiles with $z_0 = 0.0002$ meters coincide with profiles with Chézy = 65m$^{1/2}$/s. Because 0.002 is a more realistic value for z_0 than 0.0002, this first value is chosen.

8.3 Hydrostatic pressure assumption

This section analyses whether the hydrostatic pressure assumption is a correct assumption in the case of the Bosbaan. First, the aspects of this assumption are explained in general in section 8.3.1, after which section 8.3.2 demonstrates to what results this assumption may lead, on the basis of some simple numerical tests. Finally, section 8.3.3 explains how this assumption might affect the Bosbaan results.

8.3.1 General implications

The software package DELFT3D-FLOW is meant for 3-dimensional simulation of free surface flows in shallow seas, estuaries, rivers, and lakes. It makes use of the shallow-water theory, which requires that the horizontal length scale of the important flow phenomena is significantly larger than the vertical length scale. The approximating theory involves the shallow-water assumptions, which basically demand that streamlines are hardly curved in vertical direction. A necessary assumption of the shallow-water flow model is that the pressure is approximated by the hydrostatic pressure distribution. Or equivalently: the weight of the water right above a point in the water determines the pressure at that point. The hydrostatic pressure law replaces the vertical momentum equation, and as a consequence only two in stead of three momentum equations have to be solved.

For the Bosbaan, this hydrostatic pressure assumption seems correct: the horizontal length scale of the flow is much larger then 2 meters, the largest vertical length scale. This is however not the case near the closed boundaries; there the streamlines are strongly curved in vertical direction, and vertical accelerations do influence the pressure distribution, and accordingly, the horizontal and vertical velocities. In DELFT3D-FLOW, the influence of vertical acceleration is not taken into account, and the flow notices the side wall only at the last grid cell before the wall, as shown in Figure 8.5.

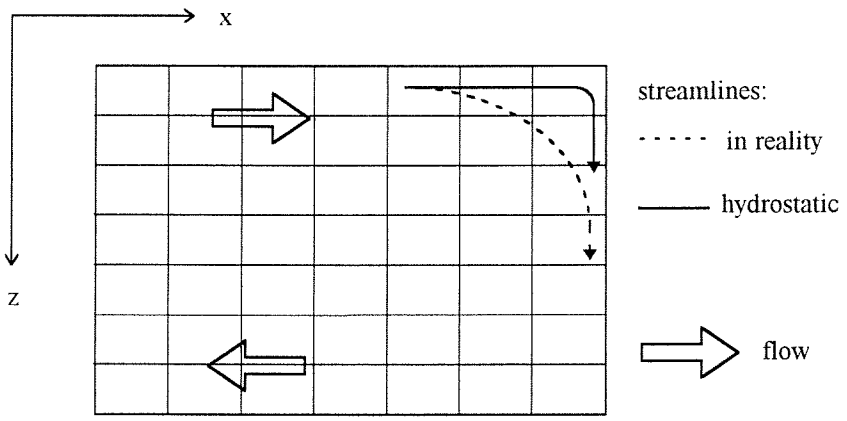

Figure 8.5: Effect of hydrostatic pressure assumption on streamlines

The vertical velocities are computed from the continuity equation, and just act as a closure term. For the above example, continuity of the upper right cell holds: $w = u^*\Delta z/\Delta x$, see Figure 8.6.

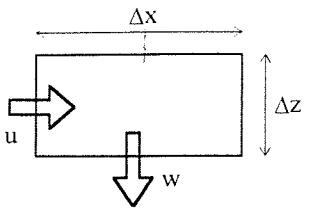

The smaller the grid distances Δx, the larger the vertical velocity w. This way, unrealistic high vertical velocities may result, which influence the vertical transport of horizontal momentum via the vertical advection terms. For wind-induced flow, this process is examined in the next sections.

Figure 8.6: Continuity of the upper right grid cell

8.3.2 Numerical tests

Some numerical tests were performed to determine the influence of this wall effect on wind-generated flow in closed basins. Several rectangular shaped basins were modelled, with a constant wind blowing diagonally over the course (angle 45°). Then, at the surface, the flow is in the wind direction, while at the bottom, the flow is in the opposite direction. The velocity turning point is at about one third of the depth; no variations occur in space. Near the side walls the flow is upwards or downwards, as indicated in Figure 8.7.

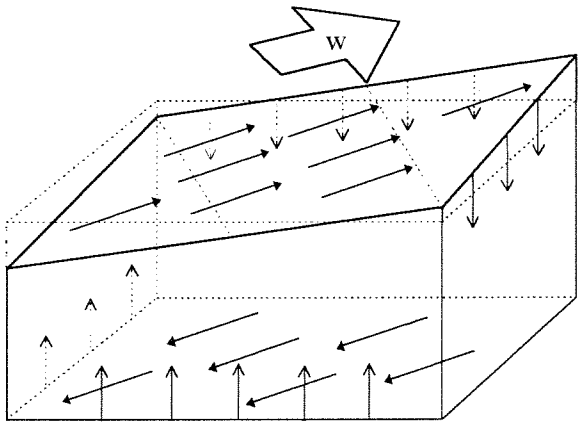

Figure 8.7: Wind blowing with an angle of 45° to a closed basin

The following computations where performed:

testno.	length [m]	width [m]	Δx [m]	Δy [m]	M	N
V1	100	100	10	10	10	10
V2	200	100	10	10	20	10
V3	400	100	10	10	40	10
V4	400	100	40	10	10	10
V5	1000	100	100	10	10	10

Table 8.4: Test computations to determine the effect of the hydrostatic pressure assumption on a closed basin with wind-induced flow.

Figures 8.28 to 8.32 (Appendix 'Figures') show the resulting velocity patterns at several depths. From these figures it can be concluded that the hydrostatic pressure distribution near the walls does not lead to a correct representation of the flow patterns: At all depths the velocities differ in direction over the course. For the surface and bed velocities, this is shown in Figure 8.8.

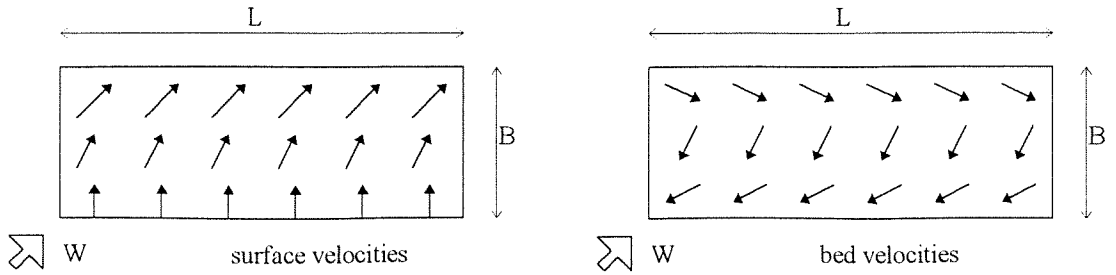

while the respective patterns should be like this:

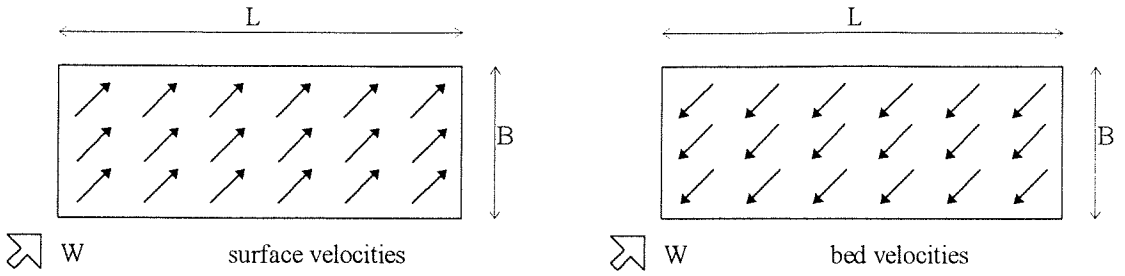

Figure 8.8: Velocity patterns with hydrostatic pressure assumption (above), compared with assumed reality (below)

The surface velocities in y-direction are the same over the course, while the velocities in x-direction increase from zero near the south wall to a value with the same order of magnitude as v at the north wall. This results in a horizontal circulation, which in reality does not exists. The longer the basin in proportion to the width, the stronger this circulation. The symmetric basin (test case v1) gives the best results, but not correct: the velocity vectors turn near the walls.

The explanation of this lies in the above mentioned vertical advection terms, and the high vertical velocities near the walls. Figure 8.33 (Appendix 'Figures') shows the vertical distributions of vertical velocity (w) at the walls. At the north- and south wall, they have approximately the same value for all test cases, while at the east- and west wall the values differ more. As expected, the vertical velocities at the east- and west wall decrease with increasing Δx (case v4 and v5). This, however, does not lead to much better results. Case v3 and case v4 -same basin with different grid sizes- give exactly the same results.

Those vertical velocities influence the horizontal velocities via the advective terms $w\partial u/\partial z$ and $w\partial v/\partial z$ in the horizontal momentum equations, and their effect is stronger as w and/or $\partial u/\partial z$, $\partial v/\partial z$ are larger. As can be seen from the Figures 8.28-8.33, this effect is the strongest near the south wall. There, the vertical velocities are upward, and the bed velocities near this wall are directed against the wind direction, while at the surface the velocities should be in the wind direction.

Due to this large upward velocities, u-momentum and v-momentum with the direction and magnitude as at the bed layer is transported upwards from layer to layer until it reaches the surface, where the wind stress acts in the opposite direction. The surface velocities, together with the wind stress must balance the upward transported matter. Simply said, the surface velocities are the sum of wind stress- and bed velocity vector, as depicted in Figure 8.9. This process influences the whole circulation pattern, resulting in physically unrealistic patterns.

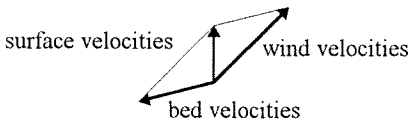

Figure 8.9: Surface velocities near the south wall, constructed in the x,y-plane

At the other walls similar effects take place: at the north- and east wall, (to much) horizontal momentum from the surface is transported downwards, while at the south- and west wall (to much) momentum from the bottom is transported upwards. To model flows like this, for which the shallow-water assumptions are no longer valid, the complete momentum equation in vertical direction must be

solved. The thus obtained set of equations is much more difficult to solve, because both the water level and the pressure are unknown, and must be computed in an implicit manner.

A much less accurate, but effective measure is just switching off the vertical advection at the closed boundaries. The vertical velocities at the closed boundaries remain large, but can not effect the horizontal velocities, and thus the velocity patterns anymore. This way, the obtained velocity patterns are similar to those from Figure 8.8 (below), and are believed to be realistic. Figures 8.34a and 8.34b show the resulting velocity patterns at the surface and at the bottom, for the test case v1 and for v5: both patterns are similar, except for the horizontal axis.

8.3.3 Effects on the Bosbaan model

The Bosbaan model has got a large aspect ration, as do the grid cells with Δx = 100 m and Δy = 4.6 m. At the east- and west wall: $w \sim u\Delta z/\Delta x$ and at the north- and south wall: $w \sim v\Delta z/\Delta y$. The latter will result in the largest vertical transports of horizontal momentum, provided that there are velocities in y-direction, which can only result from wind blowing at an angle with the course axis. The flow in the Bosbaan model was computed with the same wind force as for the above described test, 10 m/s, and an angle of 45° with the course axis. The resulting surface velocities are presented below, in Figure 8.10.

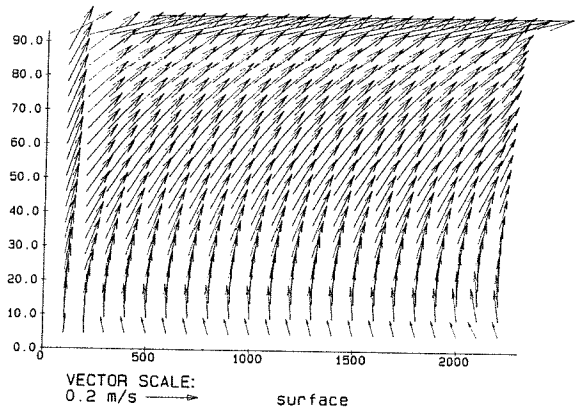

Figure 8.10: Bosbaan surface velocities with a constant south-west wind

The strong non-physical horizontal circulation occurs, again caused by the to high rate of vertical u-momentum transport. For this wind condition, the flow in the Bosbaan can therefore not be modelled correctly with a hydrostatic model.

Fortunately, velocities in y-direction on the Bosbaan remain small, especially at the windward side where the influence of the vertical transport of the horizontal momentum is the largest. It is therefore expected that the non-physical horizontal circulation will be much smaller then it would be for the constant wind oblique at the course as described above.

To verify this, the velocities in the Bosbaan were computed with the hydrostatic model, both with and without vertical advection at the closed boundaries, for the wind field related to 195° and 10 m/s at Schiphol. The local wind direction then has an angle of 30° to the course axis. The resulting surface velocities are presented in Figure 8.11. In addition to the physical horizontal circulation caused by the space-varying wind field, there is a (very) small non-physical horizontal circulation due to vertical transport of u-momentum at the south wall. However, the surface velocities are approximately equal to those computed without the vertical advection terms (see Figure 8.11), thus this non-physical circulation has only minor effect. At the windward side (the south wall), the velocities in y-direction

remain small, resulting in small w-velocities, and there is almost no wind. For situations like this, the hydrostatic pressure assumption leads to reasonable results.

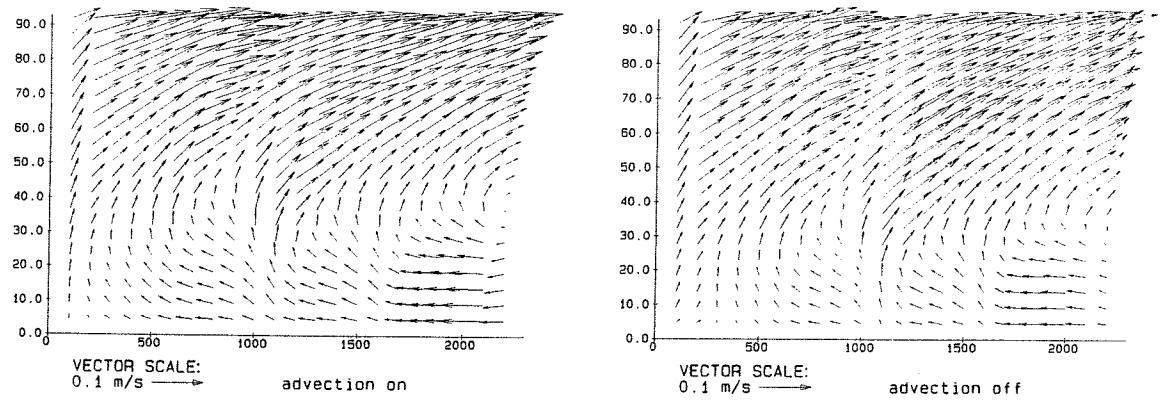

Figure 8.11: Bosbaan surface velocities for the wind field related to 195° and 10m/s at Schiphol, computed with and without vertical advection at the walls

For all normative wind conditions at the Bosbaan (wind conditions that cause the largest lane differences), the local wind velocities are in the course direction (see section 2.3.2). For those cases with a wind blowing in the direction of the course axis, velocities in y-direction remain approximately equal to zero, and so does w near the north- and south wall. The only influence the vertical advection terms may have is near the north- and south walls, when u is relatively large. In spite of the rather large Δx, w might then be of importance.

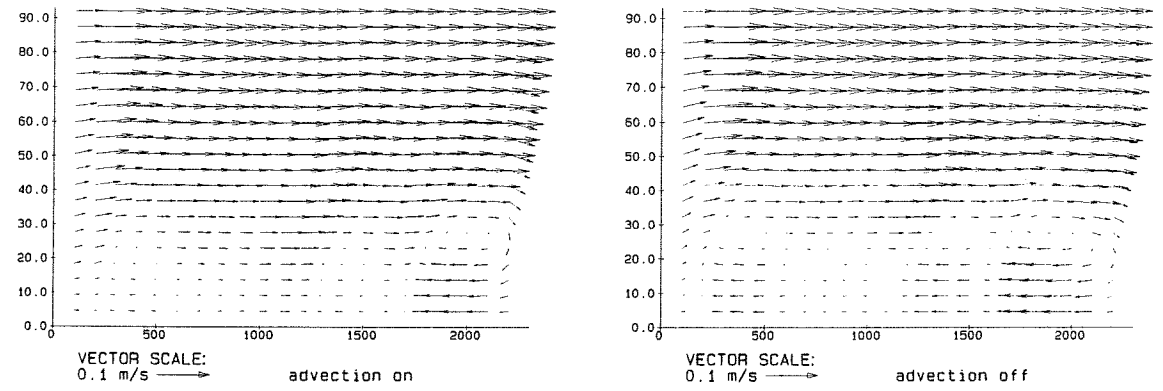

Figure 8.12: Bosbaan surface velocities for the wind field related to 210° and 10m/s at Schiphol, computed with and without vertical advection at the walls

The magnitude of this importance is determined for the wind field related to 210° and 10m/s at Schiphol. Computations were performed, both with and without vertical advection at the walls. The resulting surface velocities are presented in Figure 8.12. The two circulation patterns are similar; just the exact values differ. The most remarkable difference is that, for the calculations without advection, both the velocities at the lee side, and the velocities at the windward side increase, resulting in a stronger horizontal circulation, see Figure 8.13. Without this vertical advection terms at the wall, the vertical mixing is reduced, resulting in a less strong vertical circulation. The water, which would have gone downwards at the east wall, now turns in horizontal direction and thus increases the horizontal circulation.

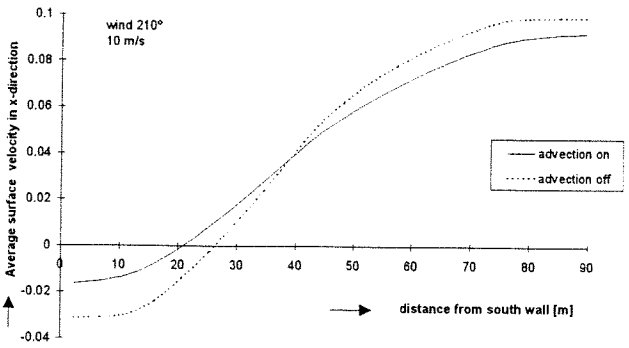

Figure 8.13: Influence of vertical advection near the walls on the surface velocity distribution over the width of the course at wind 210°, 10 m/s.

Only measurements and calibration of the model can determine which of those two computations gives the most realistic results for the Bosbaan. In absence of these measurements, the hydrostatic model with vertical advection terms at the walls was chosen to compute the wind-induced flow in the Bosbaan.

8.4 Results

The most important model parameters are summarised below.

- Grid: x-direction (in DELFT3D M-direction) 24 grid points, Δx is 100 meters;
  y-direction (in DELFT3D N-direction) 22 grid points, Δy is 4.6 meters;
  z-direction (in DELFT3D K-direction) 20 non-equidistant layers with the layer-distribution nu8 as shown in Table 8.1 and in Figure 8.35 (Appendix 'Figures') . In this chapter the depth was taken 2 meters. The exact depth of 2.2 meters will be used for all 'real' Bosbaan computations.

  Figure 8.36 (Appendix 'Figures') shows the horizontal grid together with the 6 lanes.
- Turbulence model: k-ε;
- Roughness height $z_0 = 0.002$ meters;
- Horizontal eddy viscosity $\nu^{2D} = 0.05$ m^2/s;
- Wind stress coefficient $C_d = 0.005$

Chapter 3 presents the results of flow computations for the widened Bosbaan. For this wider Bosbaan model (118 meters wide in stead of 92 meters), all model parameters were kept the same, except for the grid sizes in y-direction. Those grid sizes, however, may not differ much from the ones in the present Bosbaan, in order to estimate the effects of this widening as accurately as possible. The new grid sizes in y-direction are 4.72 meters (compared with 4.6 meters in the present situation). Figure 8.37 (Appendix 'Figures') shows the model grid for this widened course together with the 8 lanes.

REFERENCES

ANONYMOUS, 1971, Bootweerstand (Boat resistance), "Roeien" (Rowing), official magazine of the K.N.R.B., Vol. 25, no. 323, p 4-10.

ANONYMOUS, 1993, Numerical experiments with Trisula in case of wind driven currents, summary, NUFFIC report.

ANATONOPOULOS, K, 1995, Hull-form and comparison with slender body and a Kelvin-Neumann code, Masters' thesis, Department of Ship Science, Faculty of Engineering and Applied Science, University of Southampton.

BOOIJ, R., 1992, Turbulentie in de waterloopkunde (Turbulence in hydraulics), Lecture notes b82, Department of Civil Engineering, Delft University of Technology (in Dutch).

BRUIJNEN, T. and H. Lageweg, 1985, Bepaling C_d-waarde kruizen (Determination of C_d coefficient of the crosses, HTS Wiltzanglaan Amsterdam (in Dutch).

DEKKERS, K. and J. KERSSENS, 1985, De Bosbaan (The Bosbaan), final exam HTS Haarlem (in Dutch).

DUNSBERGEN, D.W., 1994, Particle models for the transport in three-dimensional shallow water flow, Ph.D. Thesis, Delft University of Technology.

ELK, VAN, E. and M. HULSMANN, 1983, Stromingsonderzoek in de Bosbaan (Flow study in the Bosbaan), HTS Wiltzanghlaan Amsterdam (in Dutch).

FISA, 12th and 13th April 1997, Report on the FISA inspection of the Bosbaan.

GAARTHUIS, J., 1995, A non-hydrostatic pressure model for shallow water flow, Final report of the postgraduate programme Mathematics for the Industry, Eindhoven University of Technology.

HEAPS, N.S., 1984, Vertical Structure of current in homogeneous and stratified waters: in Hydrodynamics of lakes, CISM Lectures, edited by K. Hutter.

HOERNER, S.F., 1965, Fluid dynamic drag

HOLTHUIJSEN, L.H., 1980, Methoden voor golfvoorspelling, (Methods for wave prediction), Technische adviescommissie voor de waterkeringen (in Dutch).

KLERKS, J, 1997, Hoe eerlijk is de Bosbaan bij schuin inkomende wind? (Is the Bosbaan fair with wind under an angle with the course axis? (in Dutch).

LAZAUKAS, L., 1997, Rowing shell drag comparisons, Technical Report L9701, University of Adelaide.

LIGGETT, J.A., 1975, Lake circulation, in Unsteady flow in open channels, Vol. 2, p 879-923, (K. Mahmood and V. yevjevich).

LIGGETT, J.A. and C. HADJITHEODOROU, 1969, Circulation in shallow homogeneous lakes, Journal of the Hydraulics Division, ACSE, Vol. 95, no. HY2, Proc. Paper 6454, March, p 609-620.

LIU, H., and H.J. PEREZ, 1971, Wind-induced circulation in shallow water, Journal of the Hydraulics Division, ASCE, Vol. 97, no. HY7, Proc. Paper 8235, July, p923-935.

KOWALIK, Z., and T. S. MURTY, 1993, Numerical modeling of ocean dynamics, Advanced Series on Ocean Engineering, Vol. 5

MELLE van, A, 1989, Windtunnelonderzoek naar windklimaat en windsnelheidsverschillen of de roeibaan in het Amsterdamse Bos (Wind tunnel research into the wind climate and wind velocity differences on the rowing course in Amsterdam), TNO-report (in Dutch).

MELLE van, A, 1997, The frequency of the appearance of unfair wind conditions on the rowing course "Bosbaan" in Amsterdam.

OORT, VAN, W.P., 1986, Driftsnelheidsmetingen op de Bosbaan (Drift measurements at the Bosbaan) (in Dutch).

OP DEN VELDE, J, 1992, Lane (dis-)advantage.

OP DEN VELDE, W, 1988, Literatuur en opinie onderzoek tot verbetering van de Bosbaan (Literature and opinion search to improve the Bosbaan (in Dutch).

RODI, W., 1984, Turbulence models and their application in hydraulics, State-of-the-art paper, IAHR, Delft.

SCHIERECK, G. J., 1995, Introduction to bed, bank and shore protection, Lecture notes f4, Department of Civil Engineering, Delft University of Technology.

STELLING, G.S. and BOOIJ, N., Computational modelling in open channel hydraulics, Lecture notes b84, Department of Civil Engineering, Delft University of Technology.

TSANIS, I.K., 1989, Simulation of wind-induced water currents, Journal of Hydraulic Engineering ASCE, 115(8), 1113-1134.

TUCK, E.O., and LAZAUKAS, L., 1996, Low drag rowing shells, Dept. of Applied Mathematics, University of Adelaide.

UITTENBOGAARD, R.E., VAN KESTER, J.A.Th.M, STELLING, G.S., 1992, Implementation of three turbulence models in 3D-TRISULA for rectangular grids, report Z81, DELFT HYDRAULICS.

VREUGDENHIL, C.B., 1977, The formulation of wind influence in shallow water, report S114 part V, DELFT HYDRAULICS.

VREUGDENHIL, C. B., 1993, Numerical methods for shallow water flow.

WIERINGA, J., and RIJKOORT, P.J.,1983, Windklimaat van Nederland (Wind climate of the Netherlands)

ZEE, VAN DER, F., 1985, Boeiverschil in de Bosbaan (Lane difference in the Bosbaan), Graduation Thesis, Department of Civil Engineering, Delft University of Technology (in Dutch).

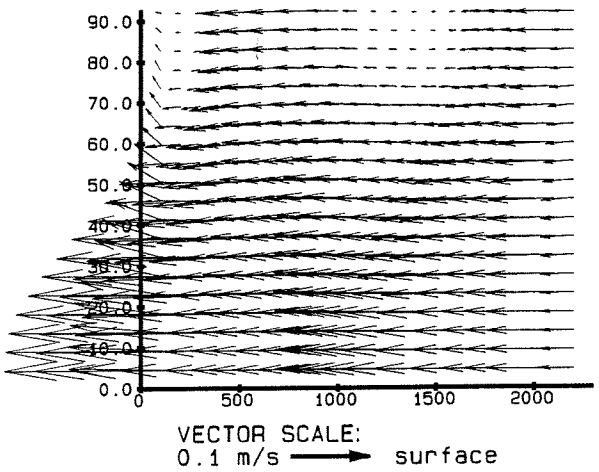

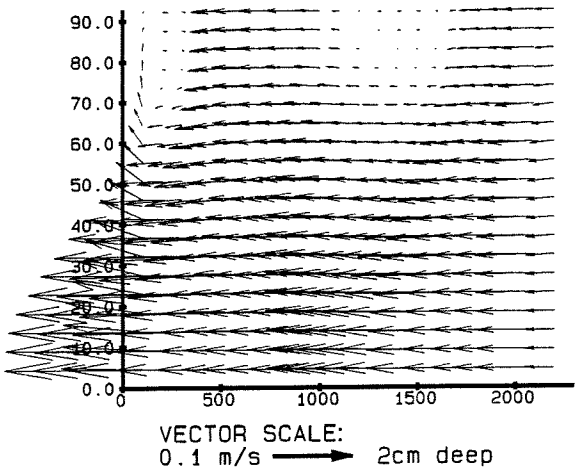

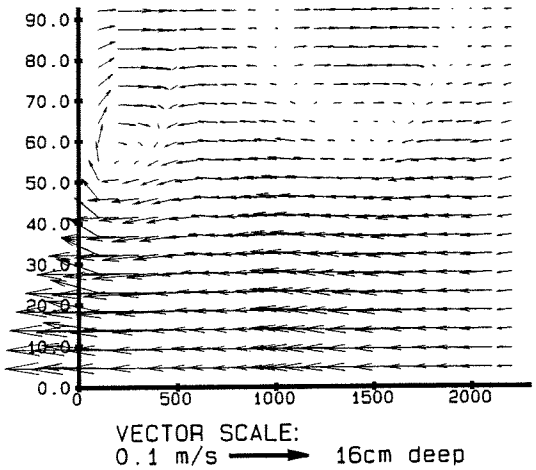

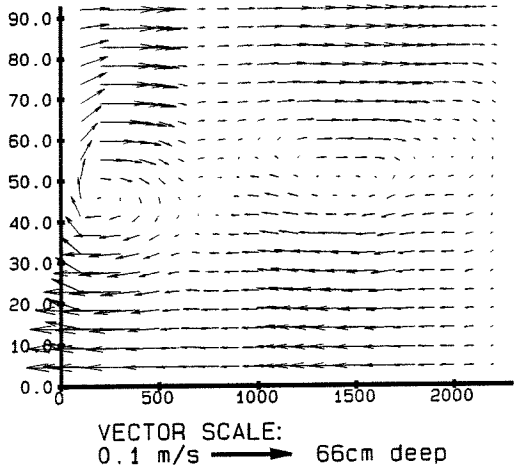

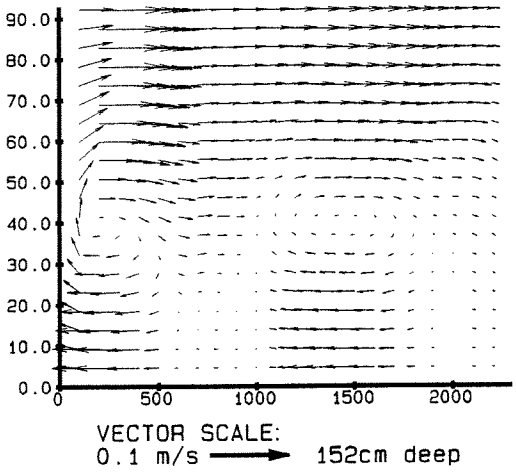

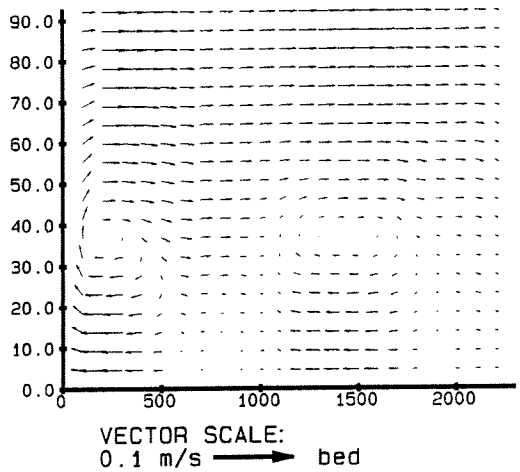

Bosbaan, wind 45 degrees, 10 m/s
Velocity vectors at different depths

fig 2.15a

DELFT HYDRAULICS

fig-1

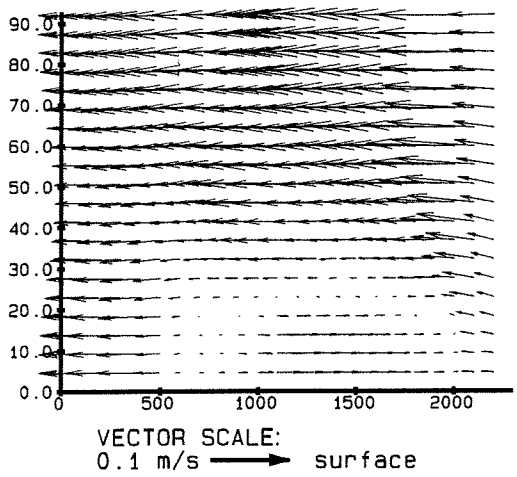

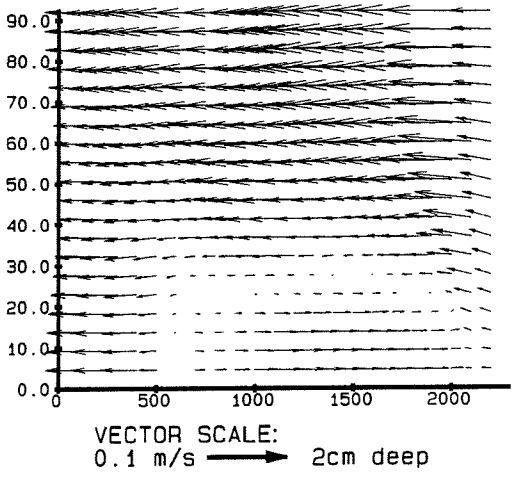

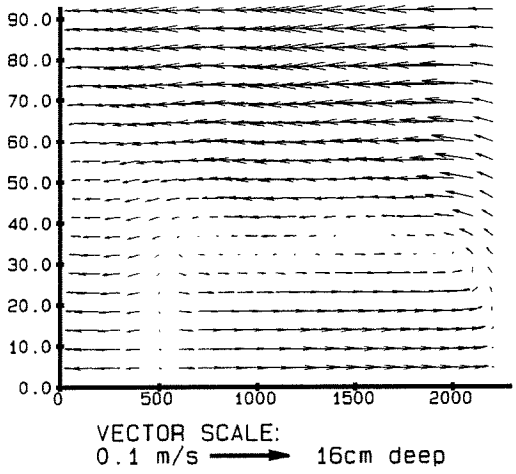

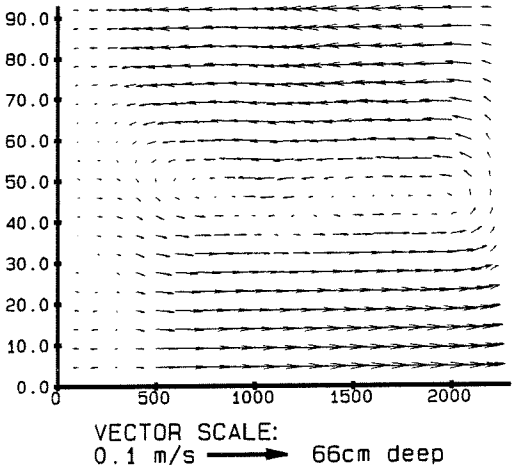

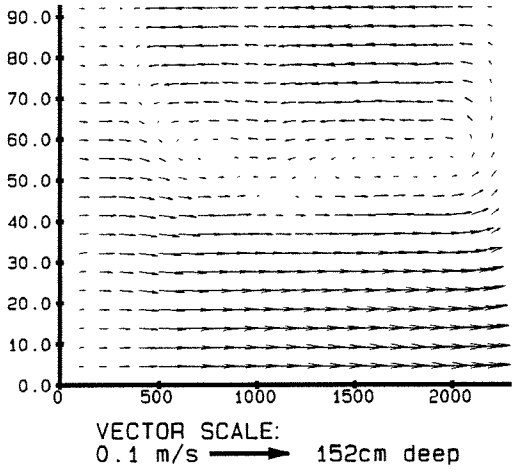

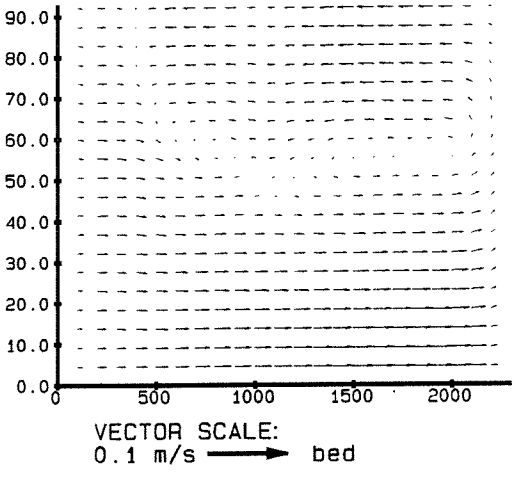

Bosbaan, wind 120 degrees, 10 m/s
Velocity vectors at different depths

fig 2.15b

DELFT HYDRAULICS

fig-2

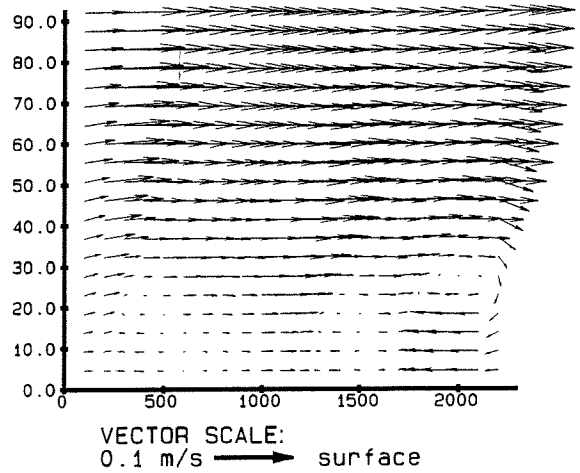

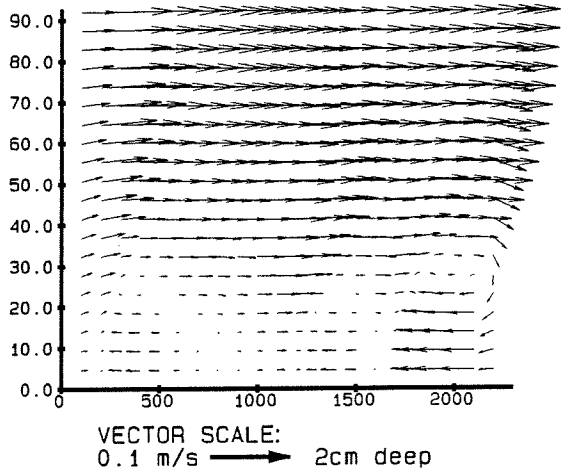

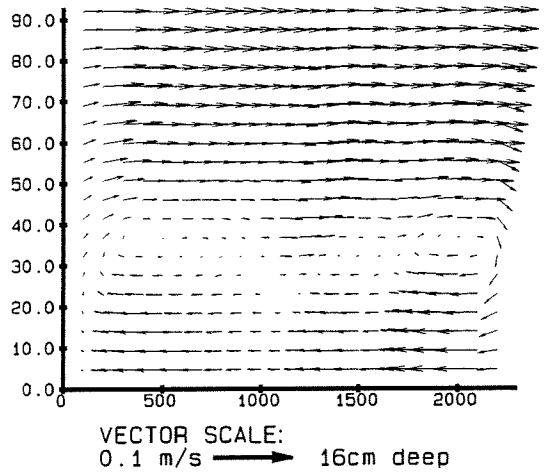

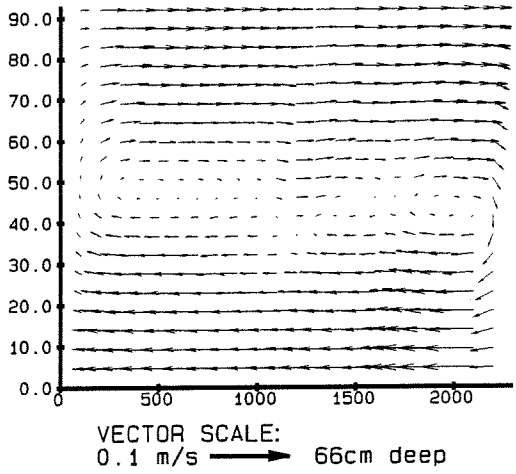

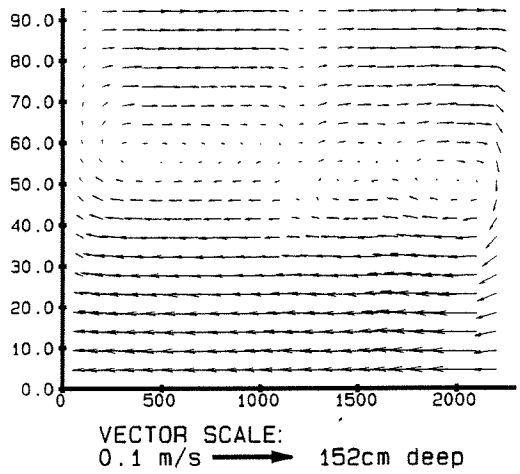

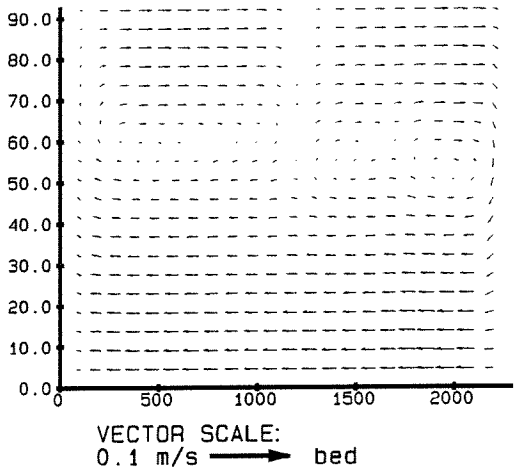

Bosbaan, wind 210 degrees, 10 m/s
Velocity vectors at different depths

fig 2.15c

DELFT HYDRAULICS

fig-3

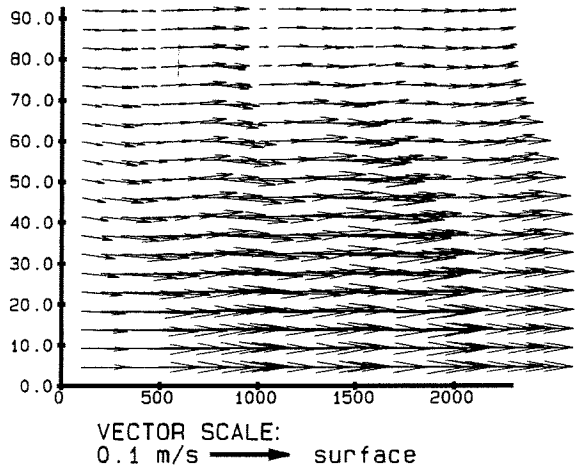

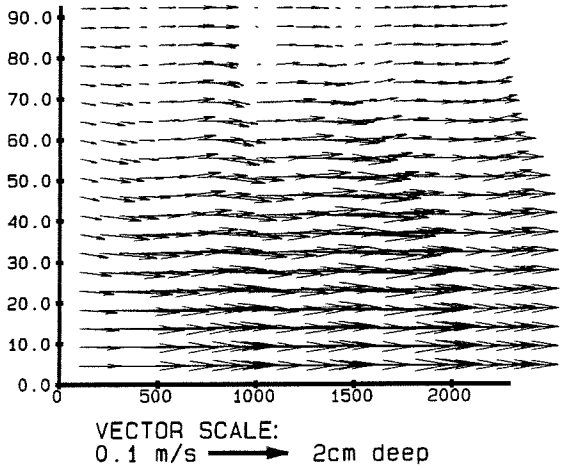

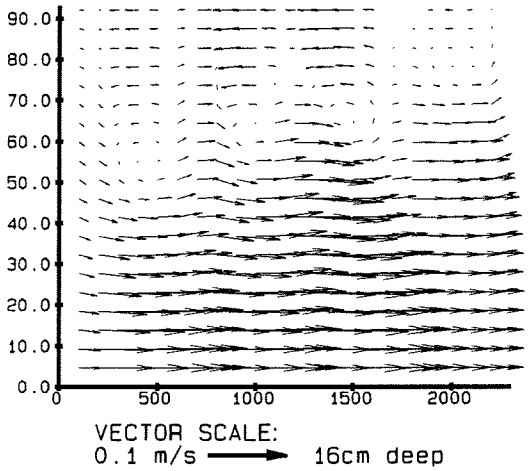

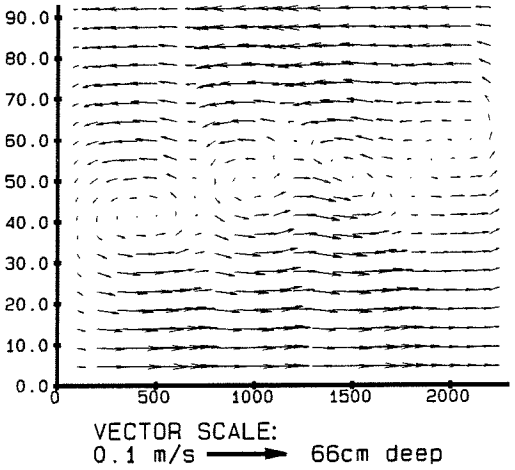

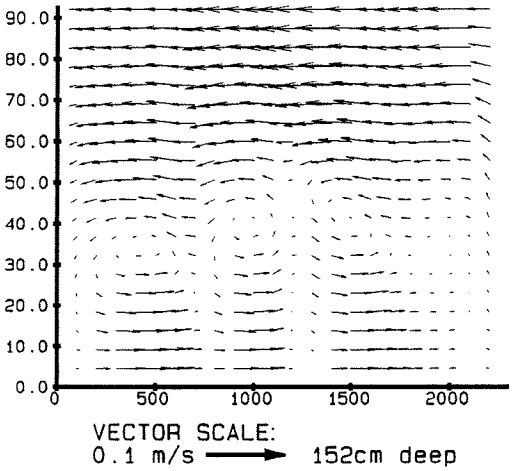

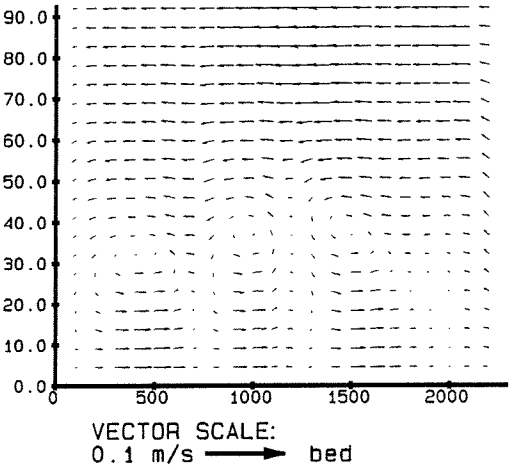

Bosbaan, wind 300 degrees, 10 m/s
Velocity vectors at different depths

fig 2.15d

DELFT HYDRAULICS

fig-4

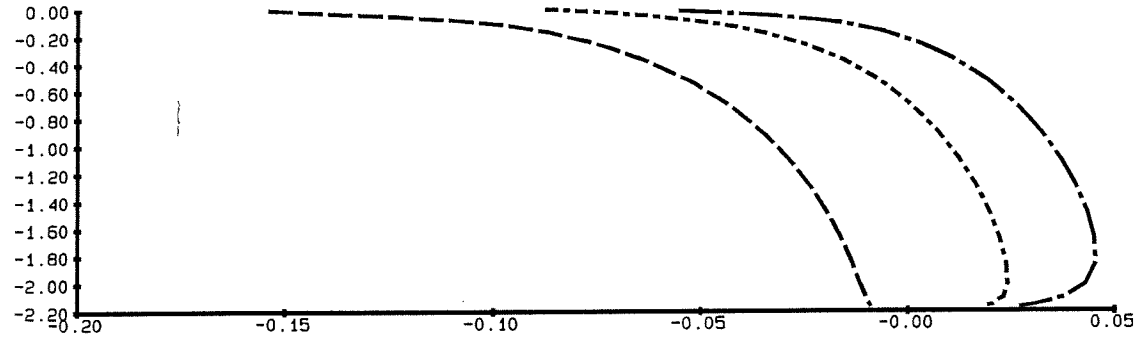

lane 6, 500m
lane 3/4, 500m
lane 1, 500m

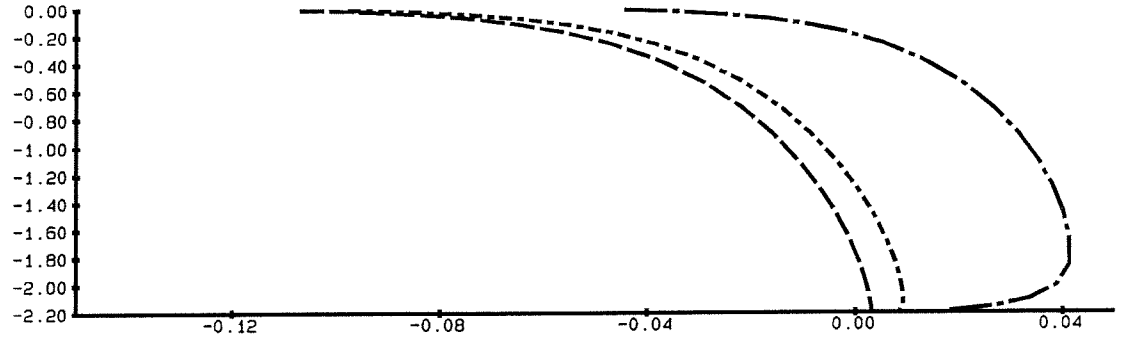

lane 6, 1000m
lane 3/4, 1000m
lane 1, 1000m

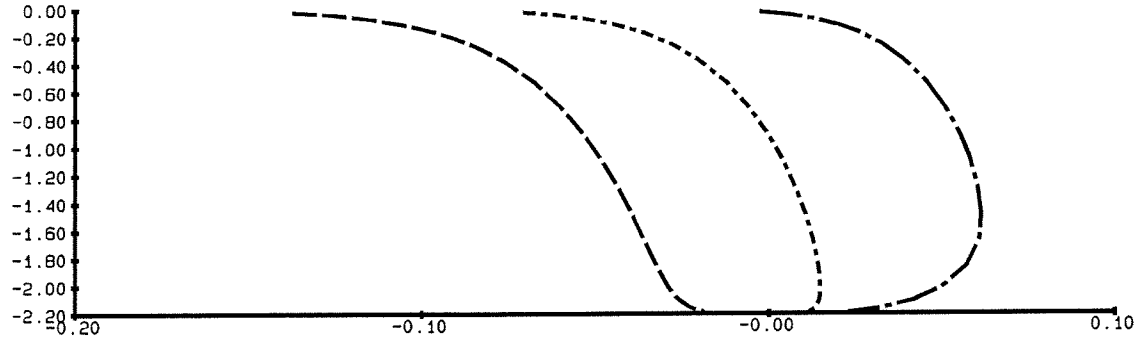

lane 6, 1500m
lane 3/4, 1500m
lane 1, 1500m

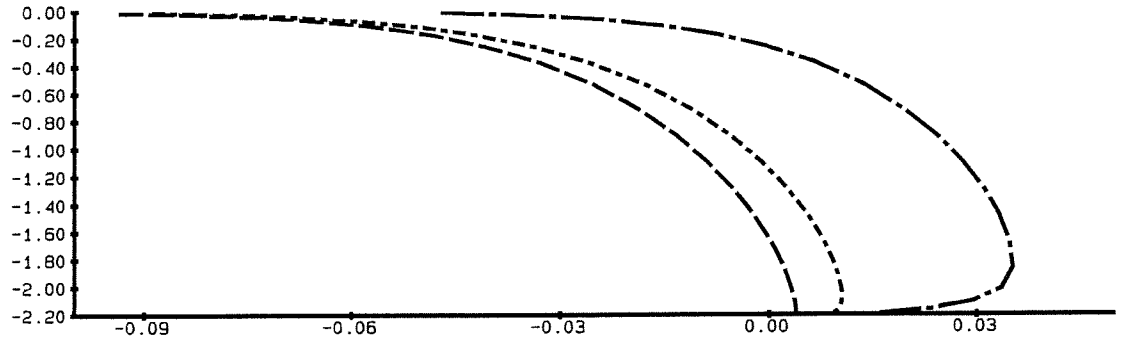

lane 6, 2000m
lane 3/4, 2000m
lane 1, 2000m

Bosbaan, wind 45 degrees, 10m/s
Vertical distributions velocity (u) [m/s]

fig 2.16a

DELFT HYDRAULICS

fig-5

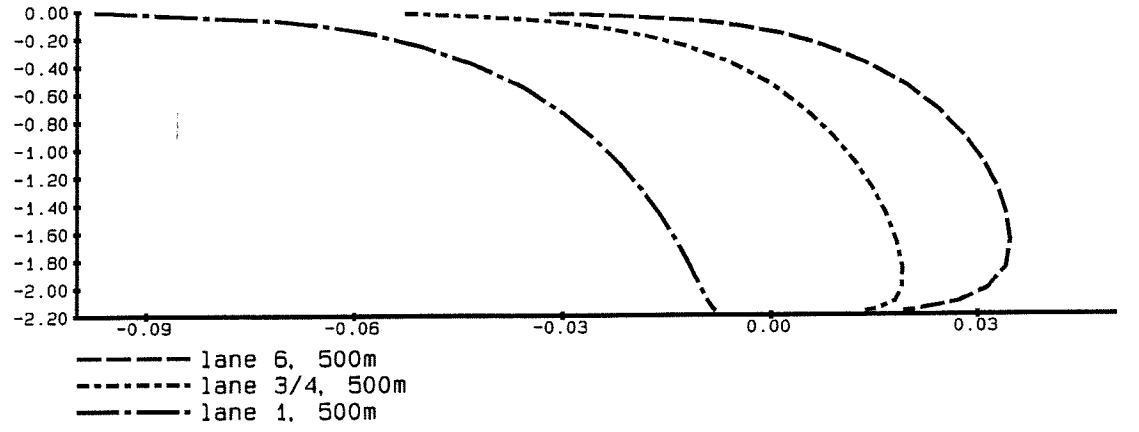

lane 6, 500m
lane 3/4, 500m
lane 1, 500m

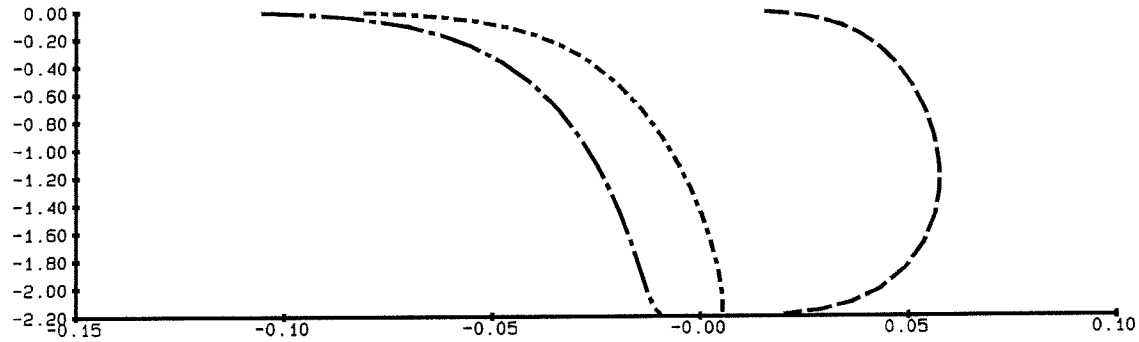

lane 6, 1000m
lane 3/4, 1000m
lane 1, 1000m

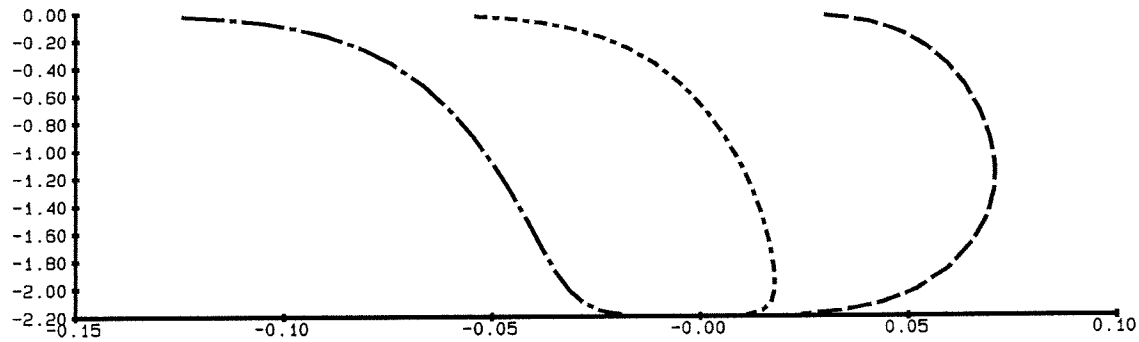

lane 6, 1500m
lane 3/4, 1500m
lane 1, 1500m

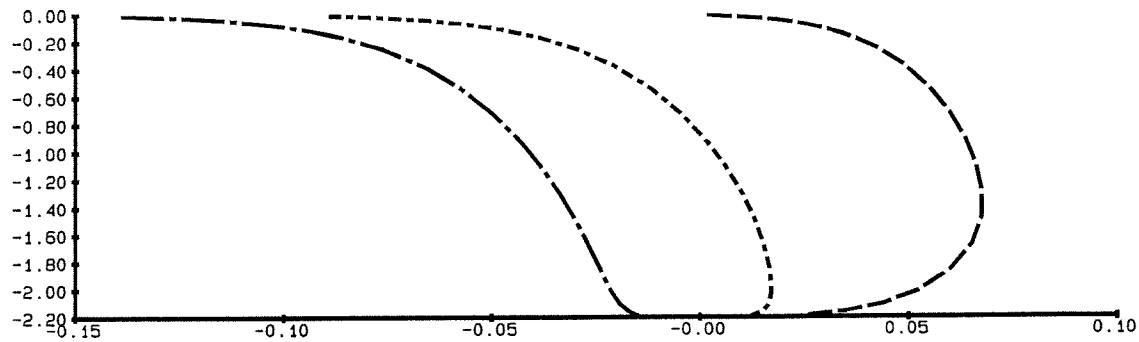

lane 6, 2000m
lane 3/4, 2000m
lane 1, 2000m

Bosbaan, wind 120 degrees, 10m/s
Vertical distributions of velocity (u) [m/s]

fig 2.16b

DELFT HYDRAULICS

fig-6

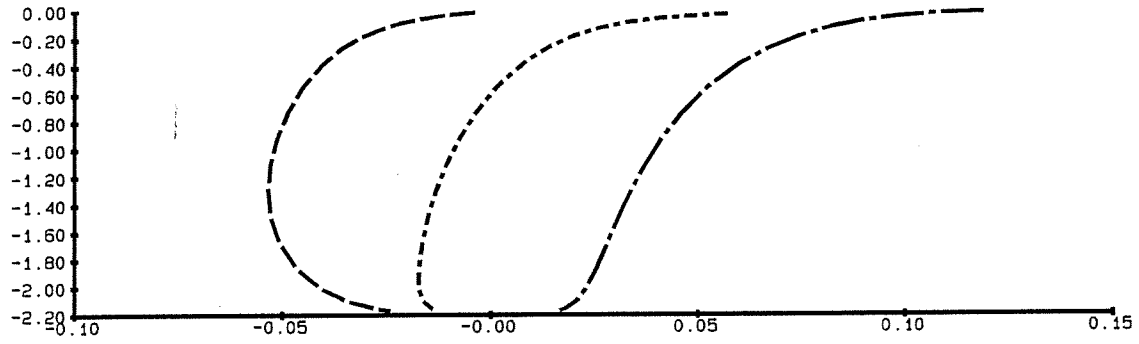

lane 6, 500m
lane 3/4, 500m
lane 1, 500m

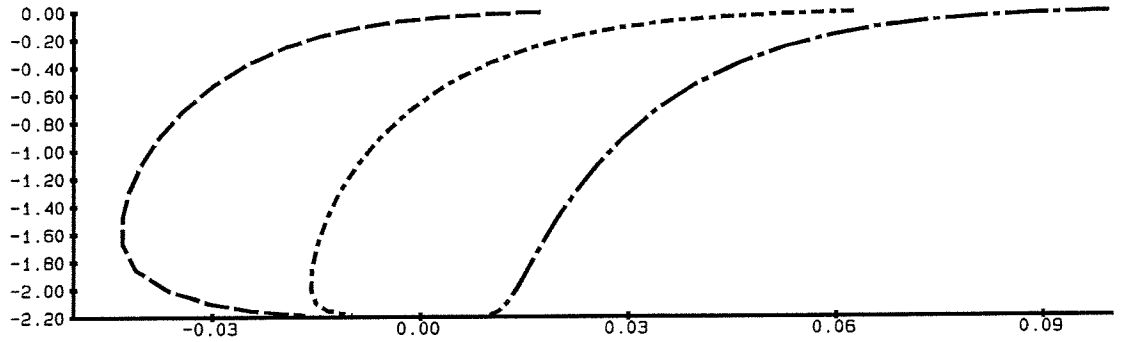

lane 6, 1000m
lane 3/4, 1000m
lane 1, 1000m

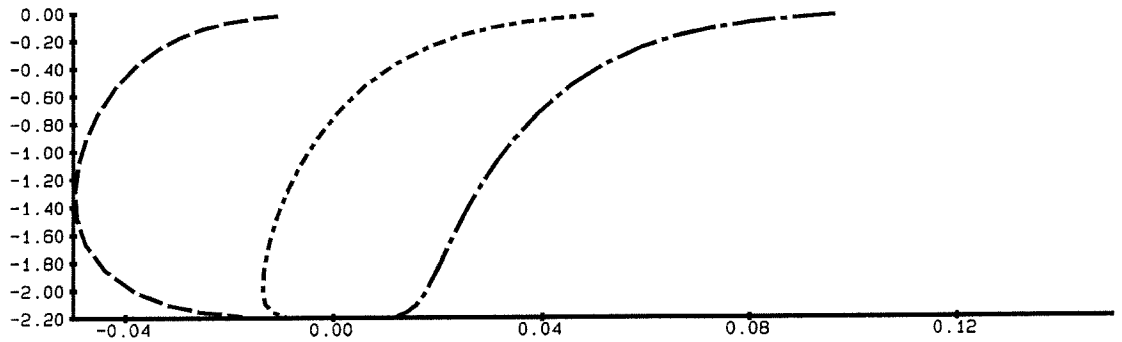

lane 6, 1500m
lane 3/4, 1500m
lane 1, 1500m

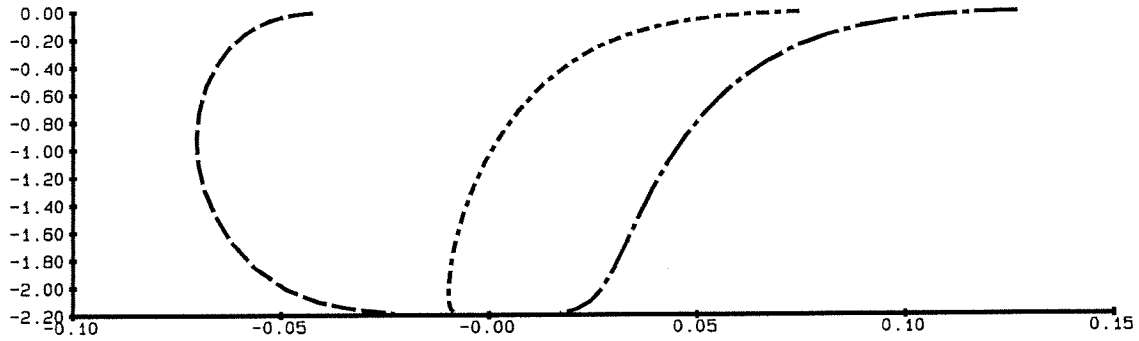

lane 6, 2000m
lane 3/4, 2000m
lane 1, 2000m

Bosbaan, wind 210 degrees, 10m/s
Vertical distributions of velocity (u) [m/s]

fig 2.16c

DELFT HYDRAULICS

fig-7

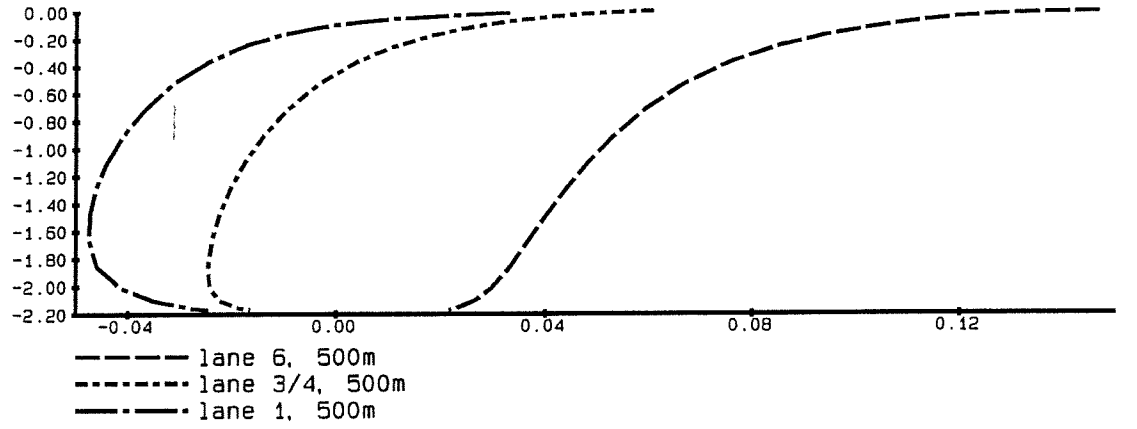

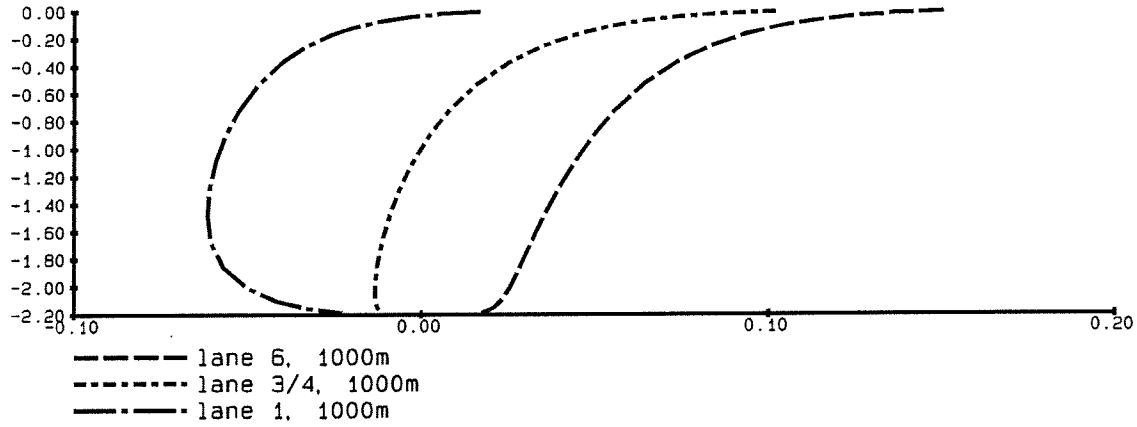

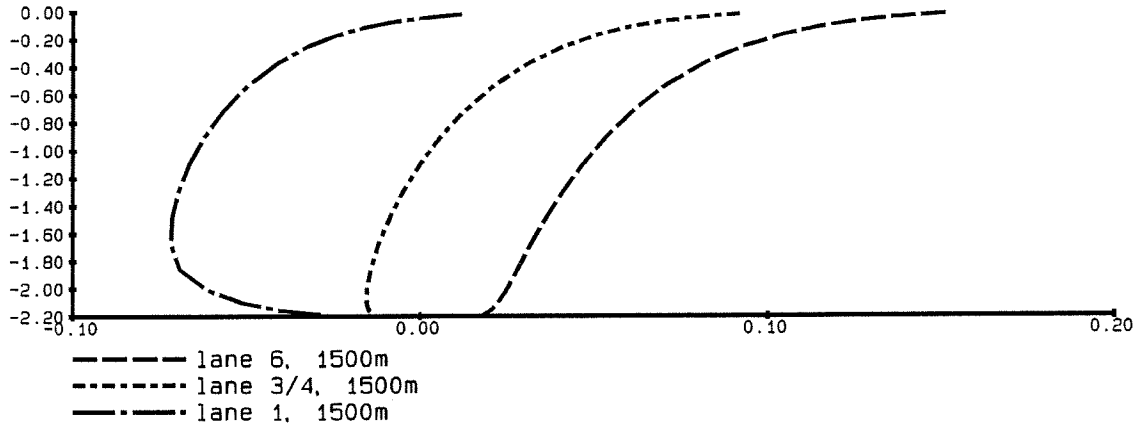

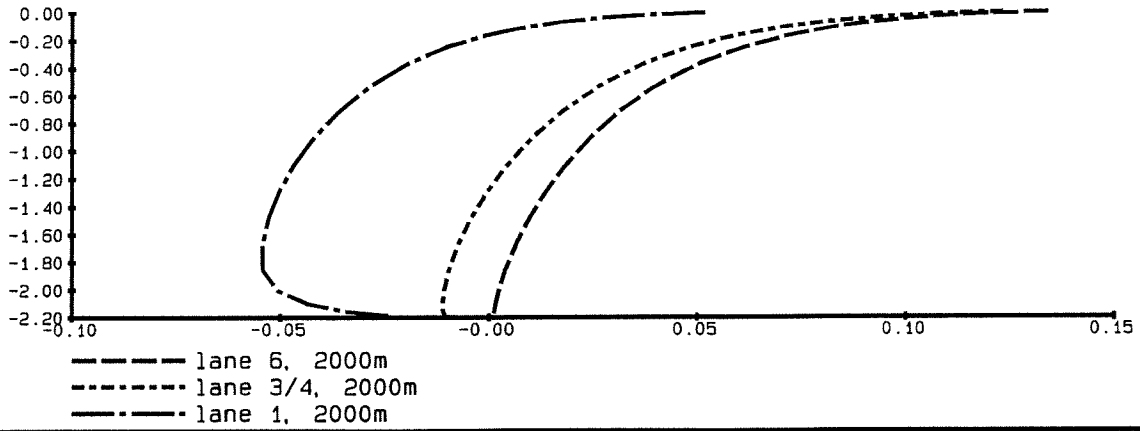

Bosbaan, wind 300 degrees, 10m/s
Vertical distributions of velocity (u) [m/s]

fig 2.16d

DELFT HYDRAULICS

fig-8

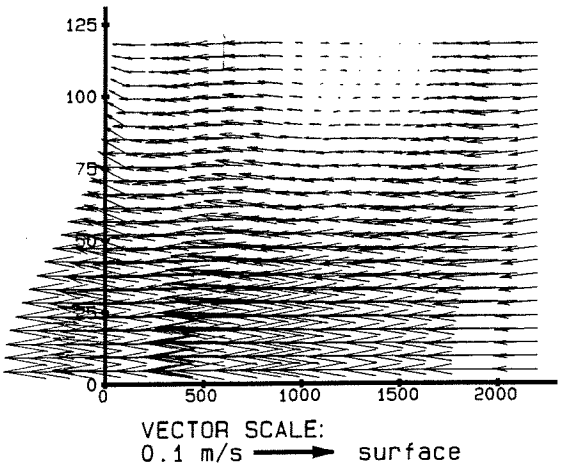

VECTOR SCALE:
0.1 m/s ⟶ surface

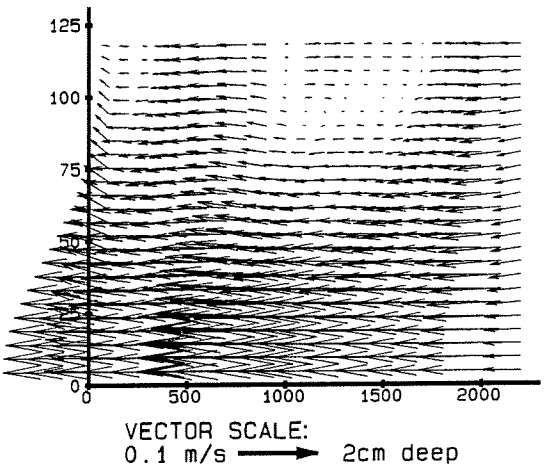

VECTOR SCALE:
0.1 m/s ⟶ 2cm deep

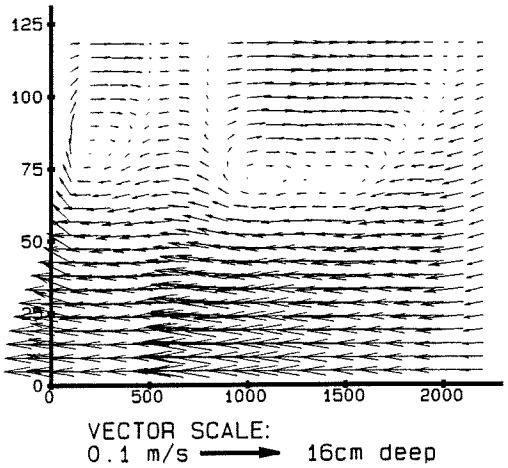

VECTOR SCALE:
0.1 m/s ⟶ 16cm deep

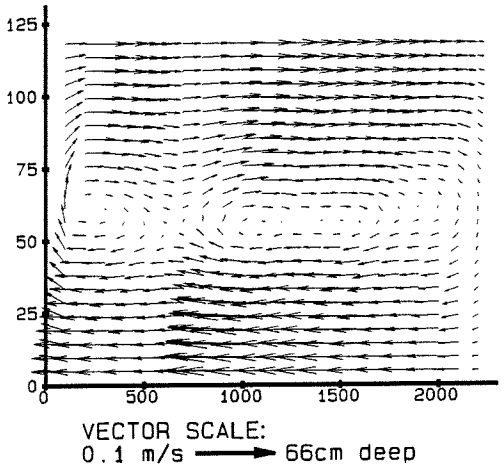

VECTOR SCALE:
0.1 m/s ⟶ 66cm deep

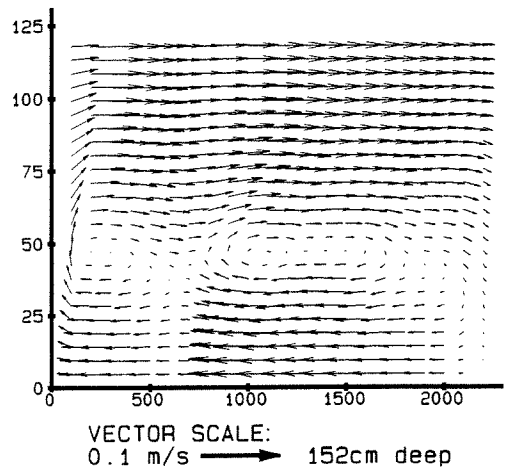

VECTOR SCALE:
0.1 m/s ⟶ 152cm deep

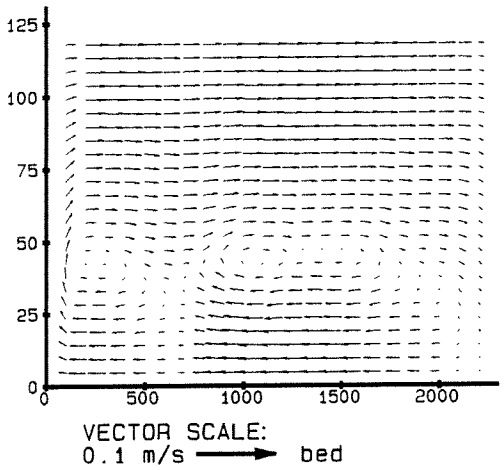

VECTOR SCALE:
0.1 m/s ⟶ bed

Widened Bosbaan, wind 45 degrees, 10 m/s
Velocity vectors at different depths

fig 3.6a

DELFT HYDRAULICS

fig-9

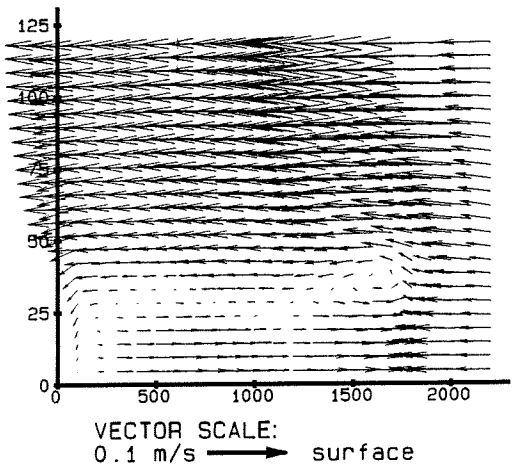

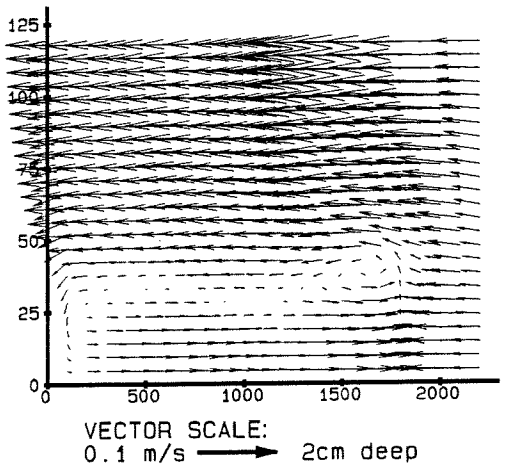

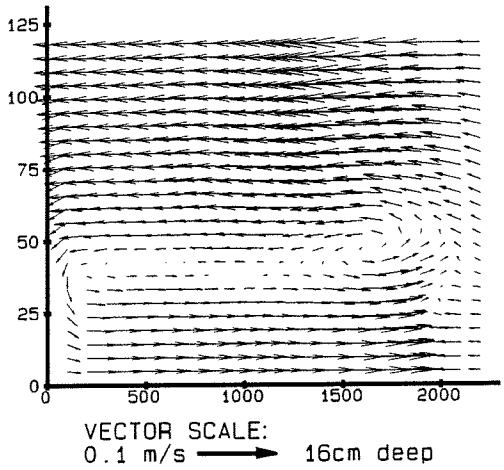

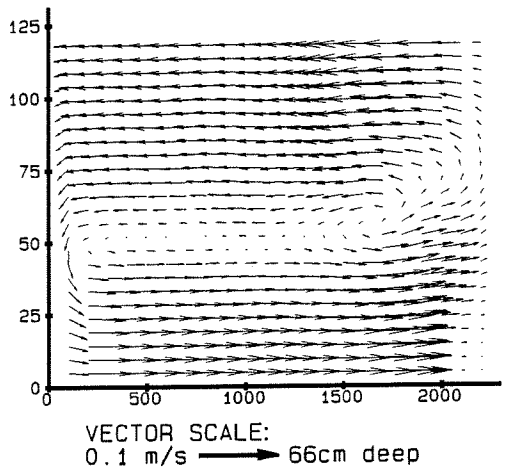

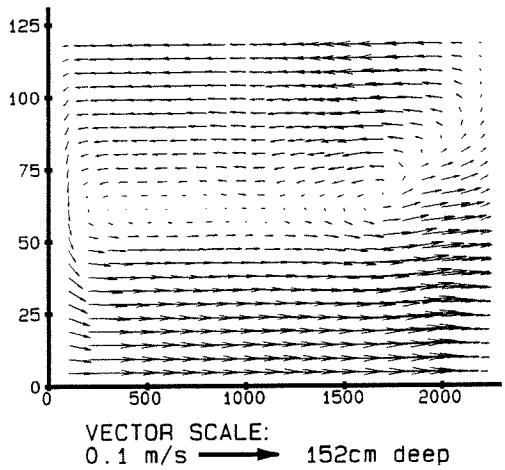

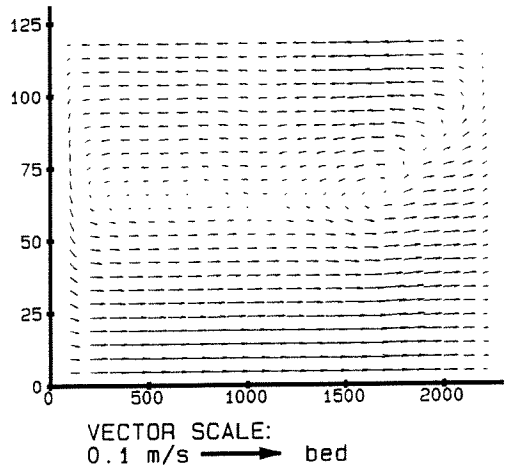

Widened Bosbaan, wind 120 degrees, 10 m/s
Velocity vectors at different depths

fig 3.6b

DELFT HYDRAULICS

fig-10

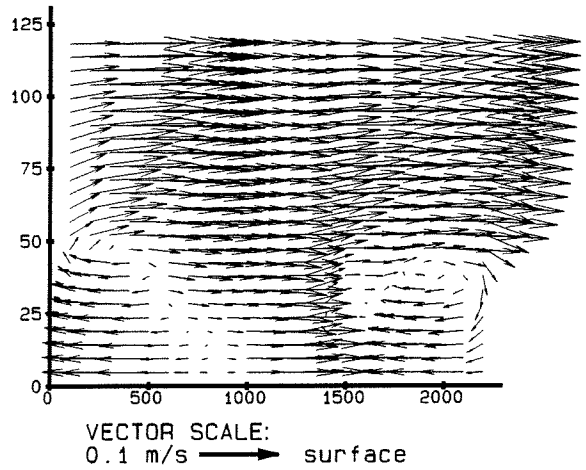

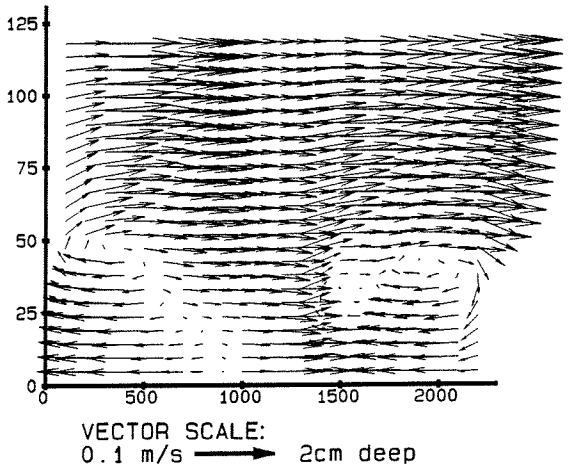

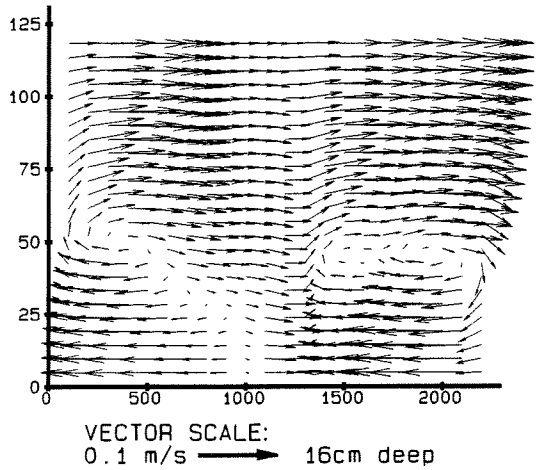

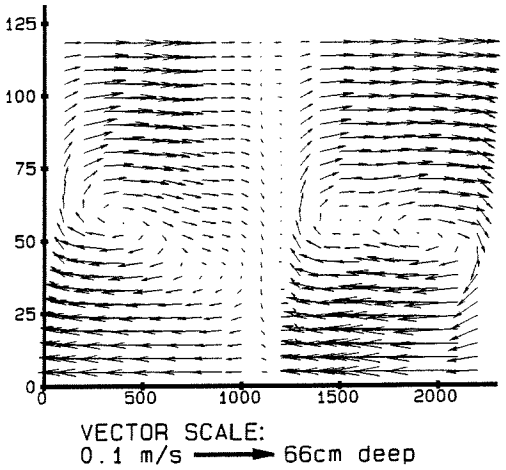

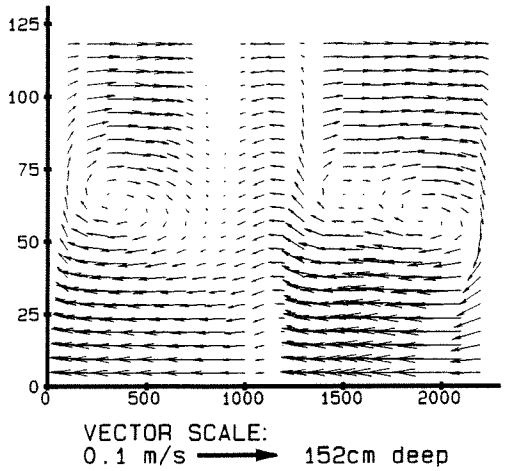

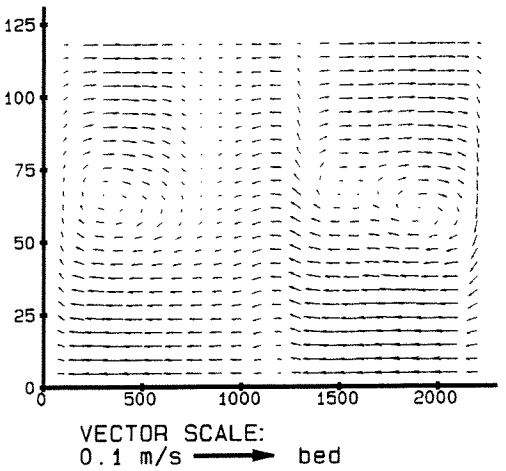

Widened Bosbaan, wind 210 degrees, 10 m/s
Velocity vectors at different depths

fig 3.6c

DELFT HYDRAULICS

fig-11

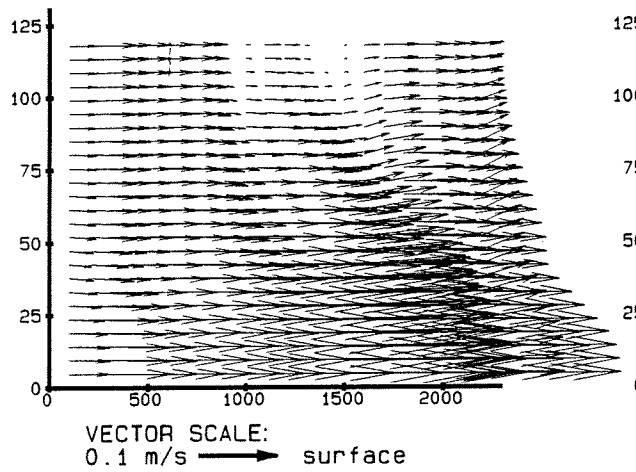

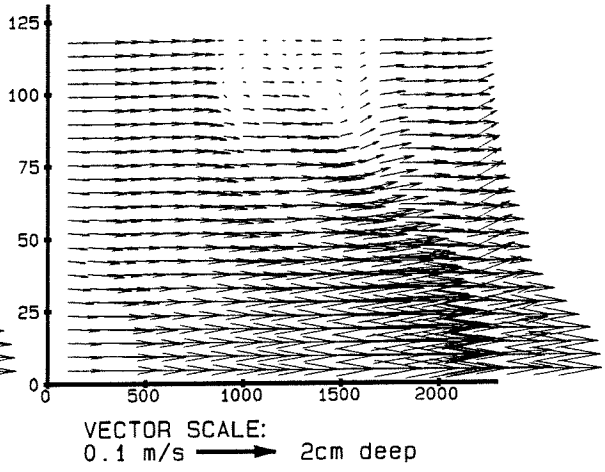

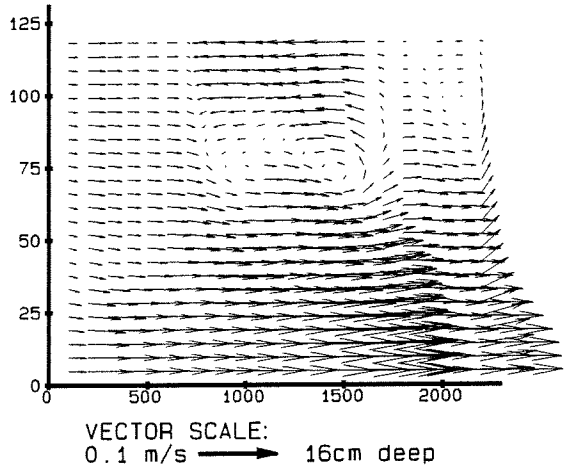

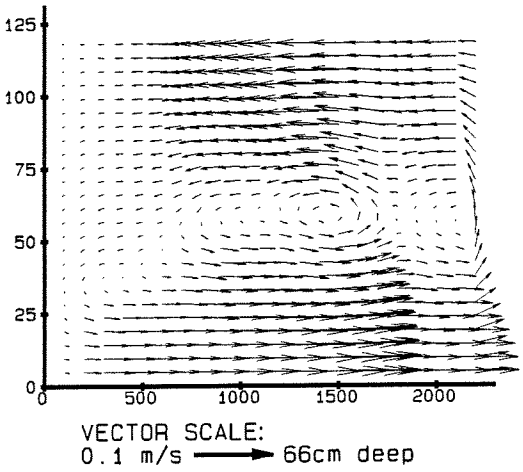

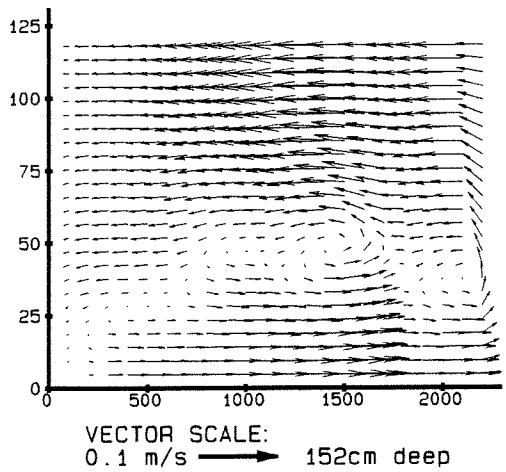

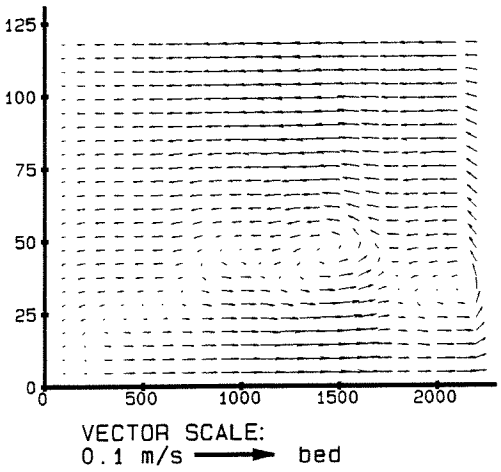

Widened Bosbaan, wind 300 degrees, 10 m/s
Velocity vectors at different depths

fig 3.6d

DELFT HYDRAULICS

fig-12

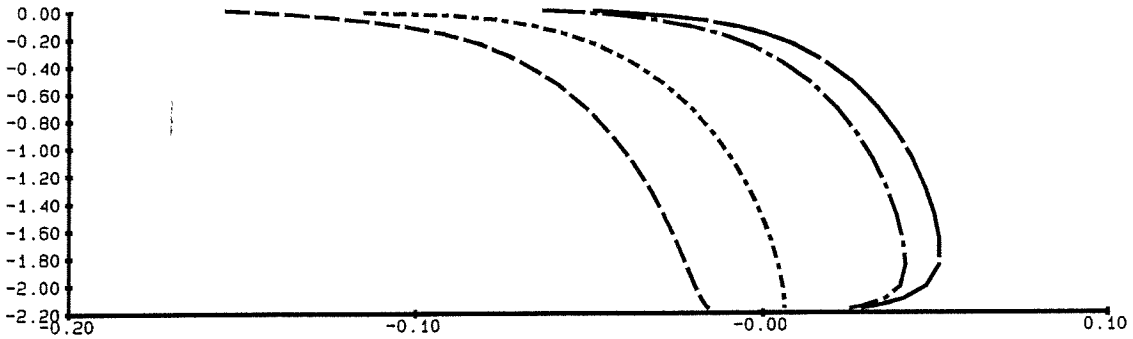

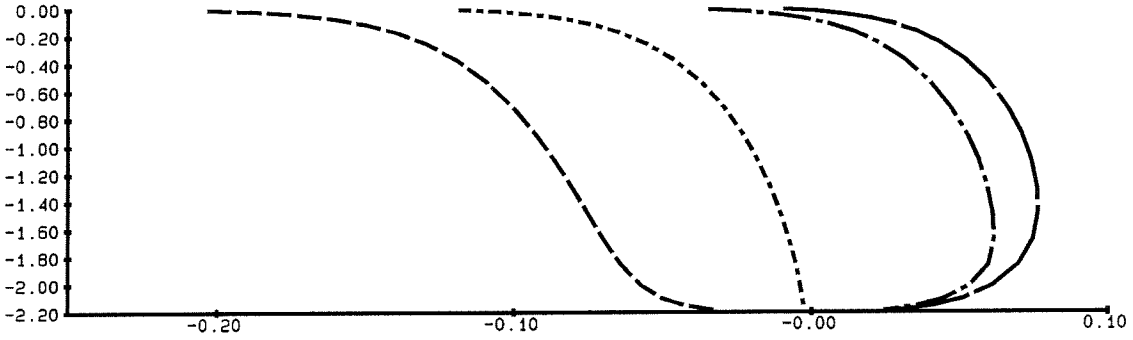

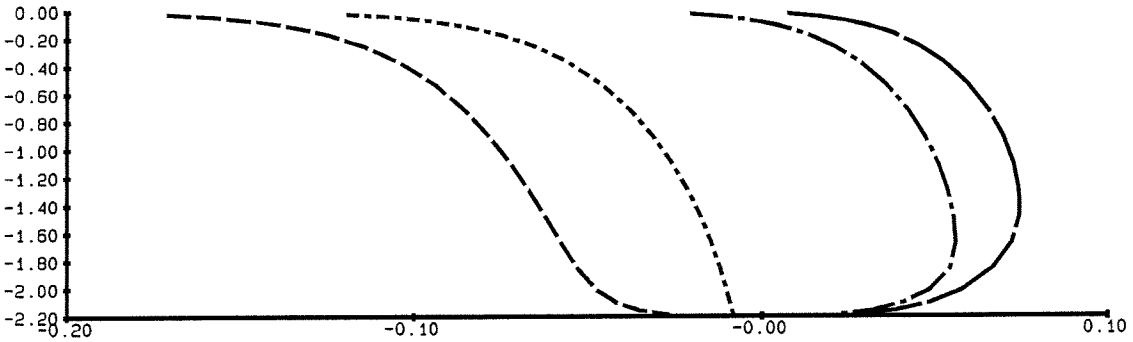

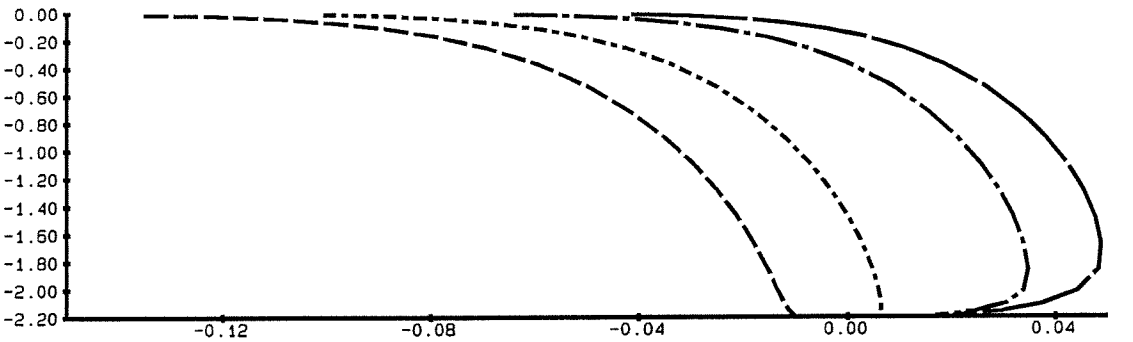

Widened Bosbaan, wind 45 degrees, 10 m/s
Vertical distributions of velocity (u) [m/s]

fig 3.7a

DELFT HYDRAULICS

fig-13

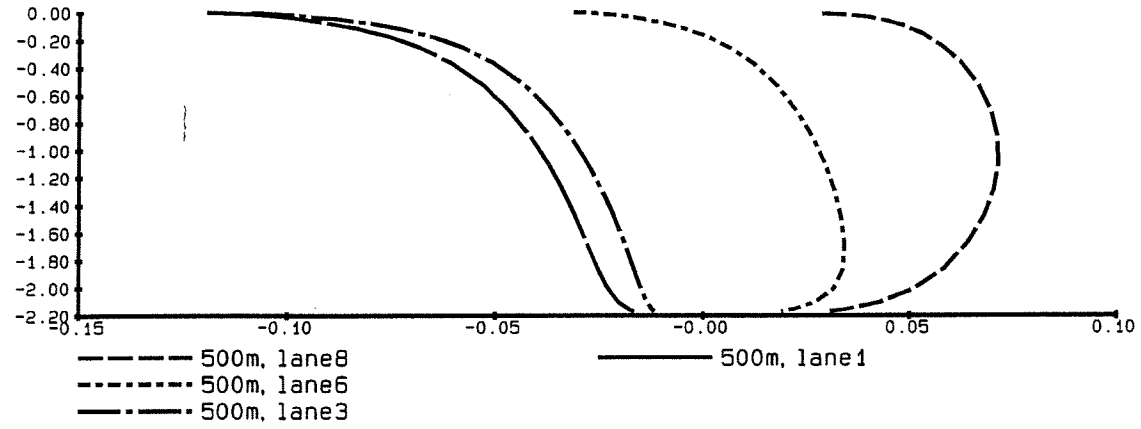

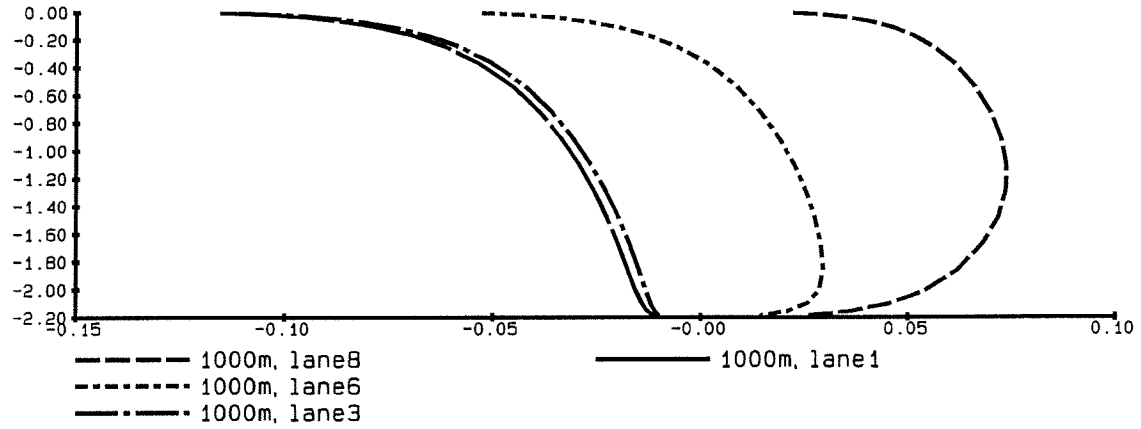

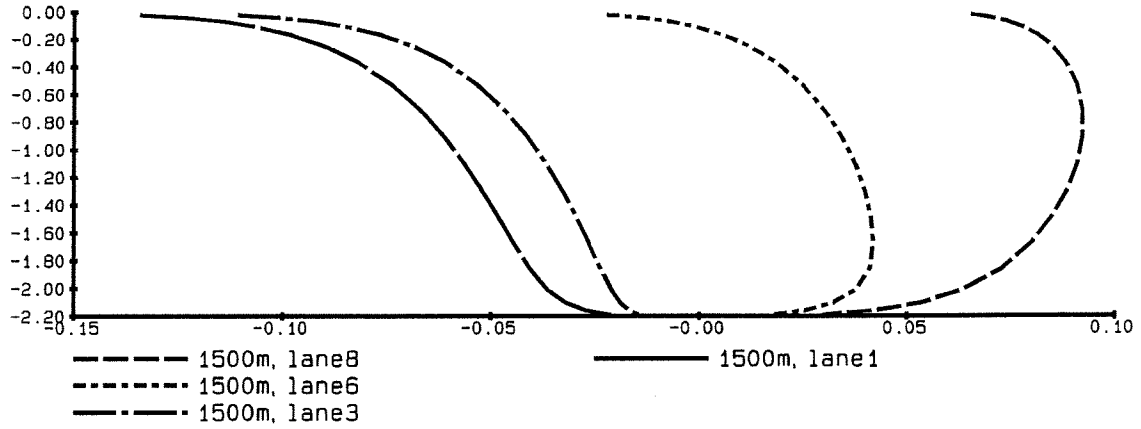

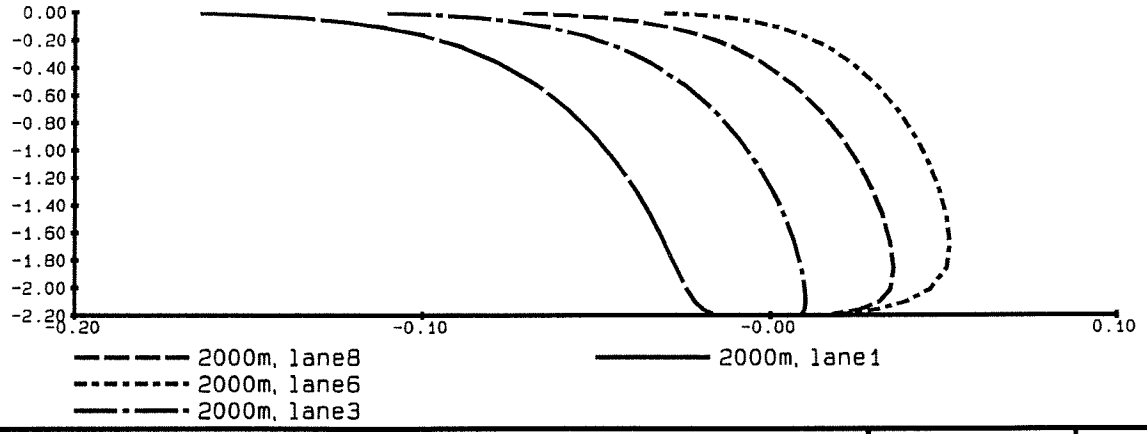

Widened Bosbaan, wind 120 degrees, 10 m/s
Vertical distributions of velocity (u) [m/s]

fig 3.7b

DELFT HYDRAULICS

fig-14

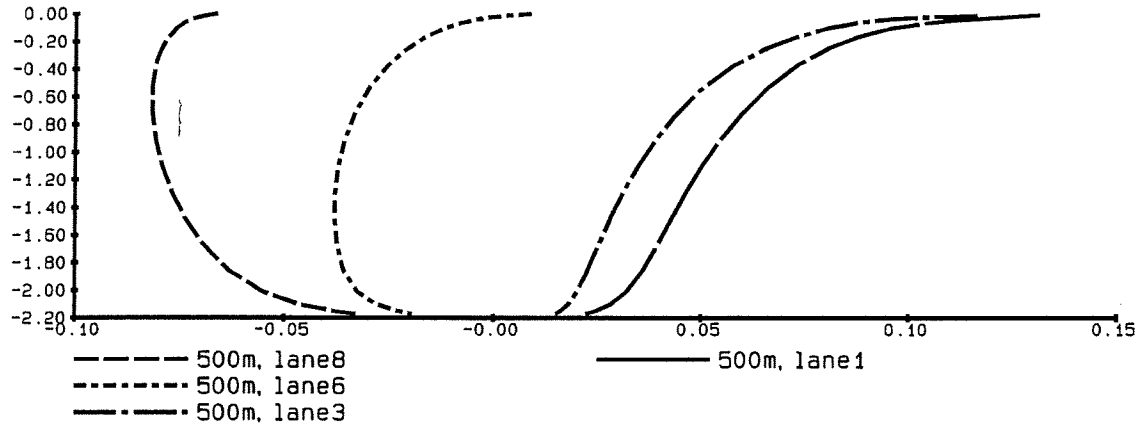

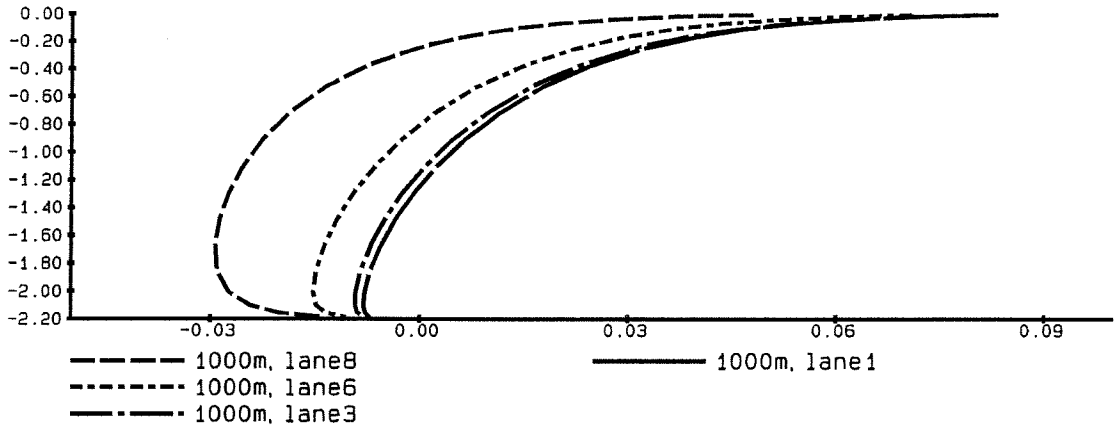

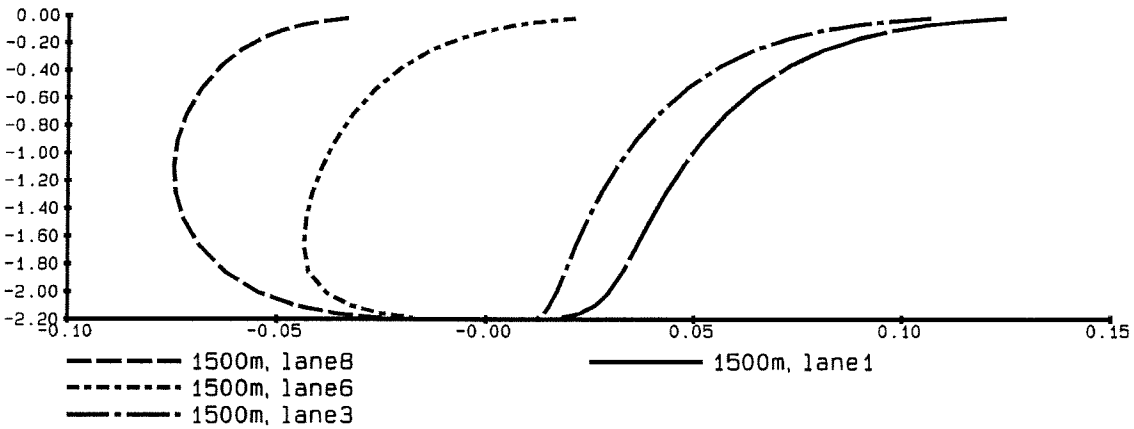

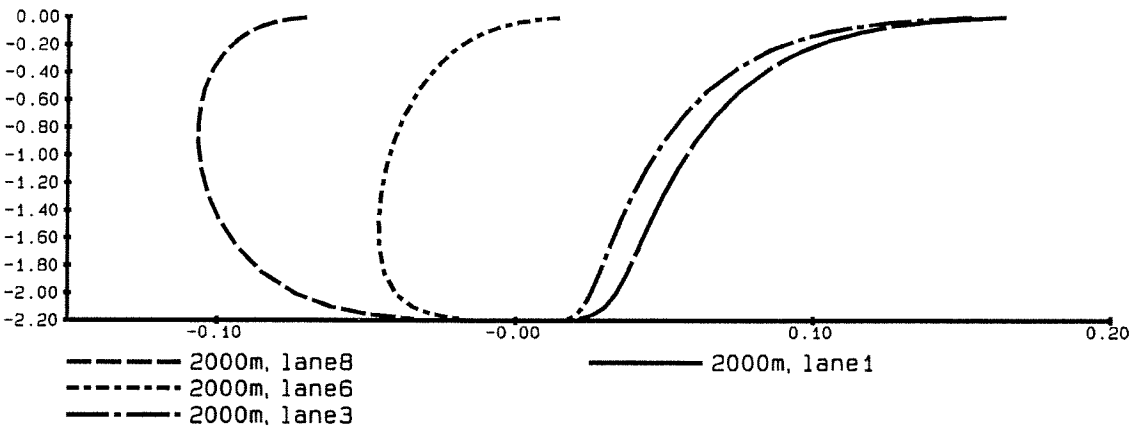

Widened Bosbaan, wind 210 degrees, 10 m/s
Vertical distributions of velocity (u) [m/s]

fig 3.7c

DELFT HYDRAULICS

fig-15

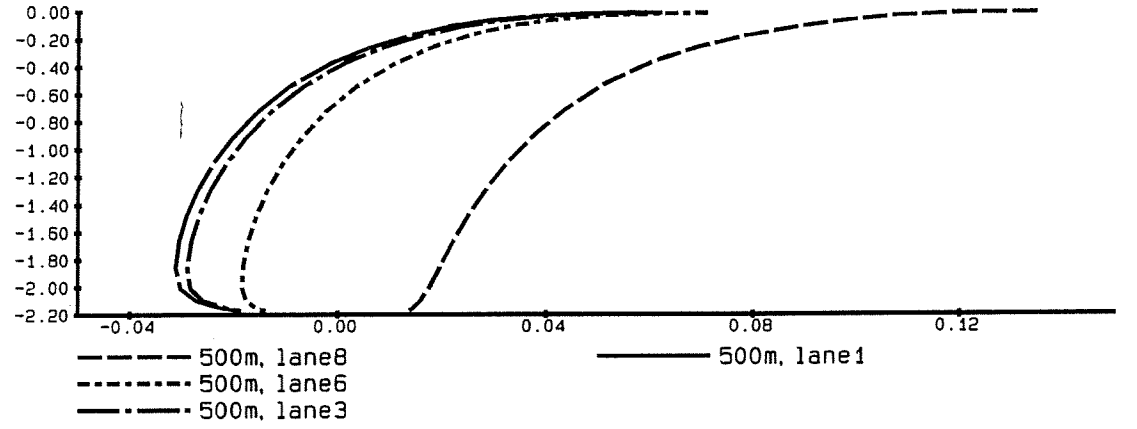

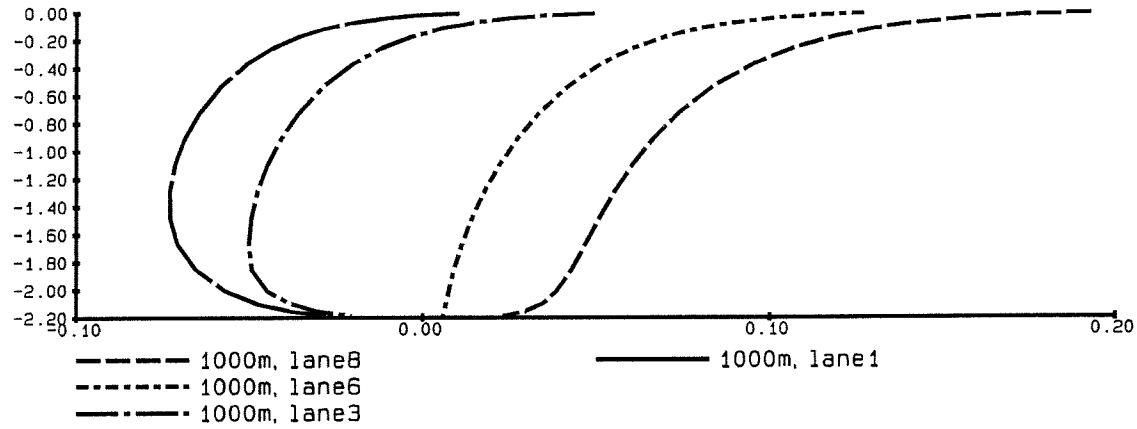

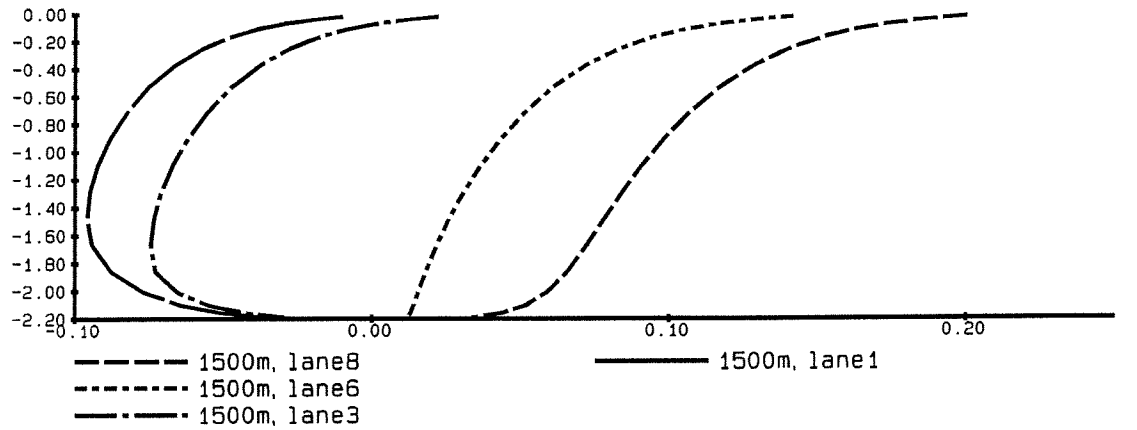

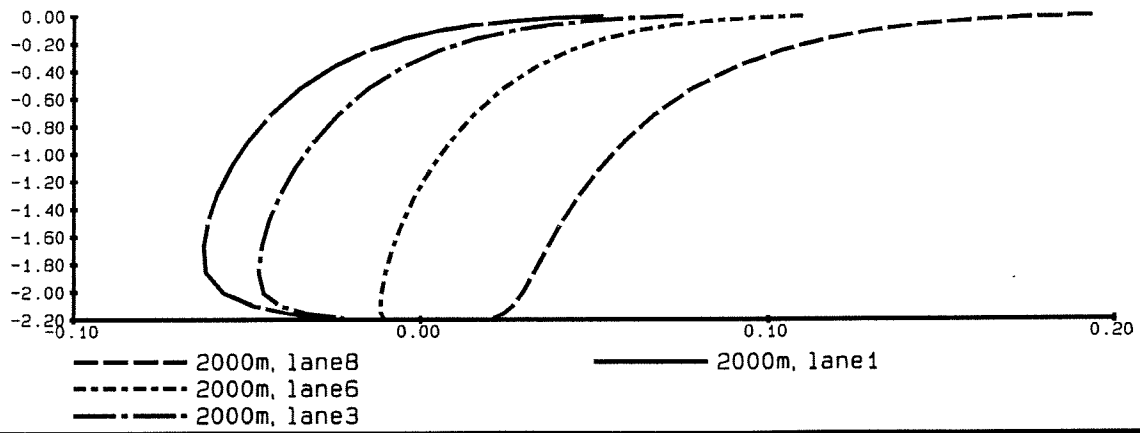

Widened Bosbaan, wind 300 degrees, 10 m/s
Vertical distributions of velocity (u) [m/s]

fig 3.7d

DELFT HYDRAULICS

fig-16

Figure 3.8a: Average flow velocity distribution over the width of the course at north-east wind (45°), 10 m/s

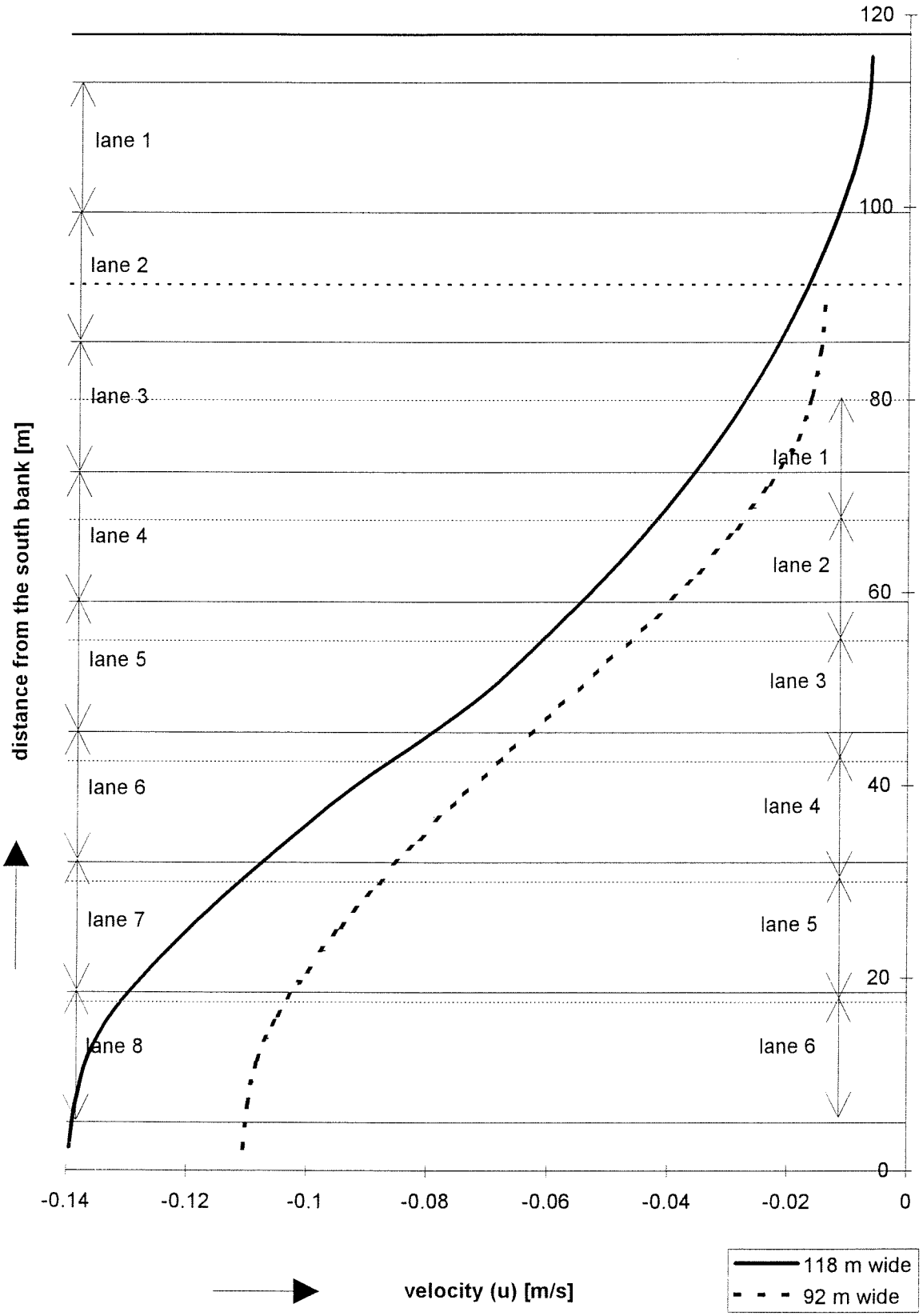

Figure 3.8b: Average flow velocity distribution over the width of the course at south-east wind (120°), 10 m/s

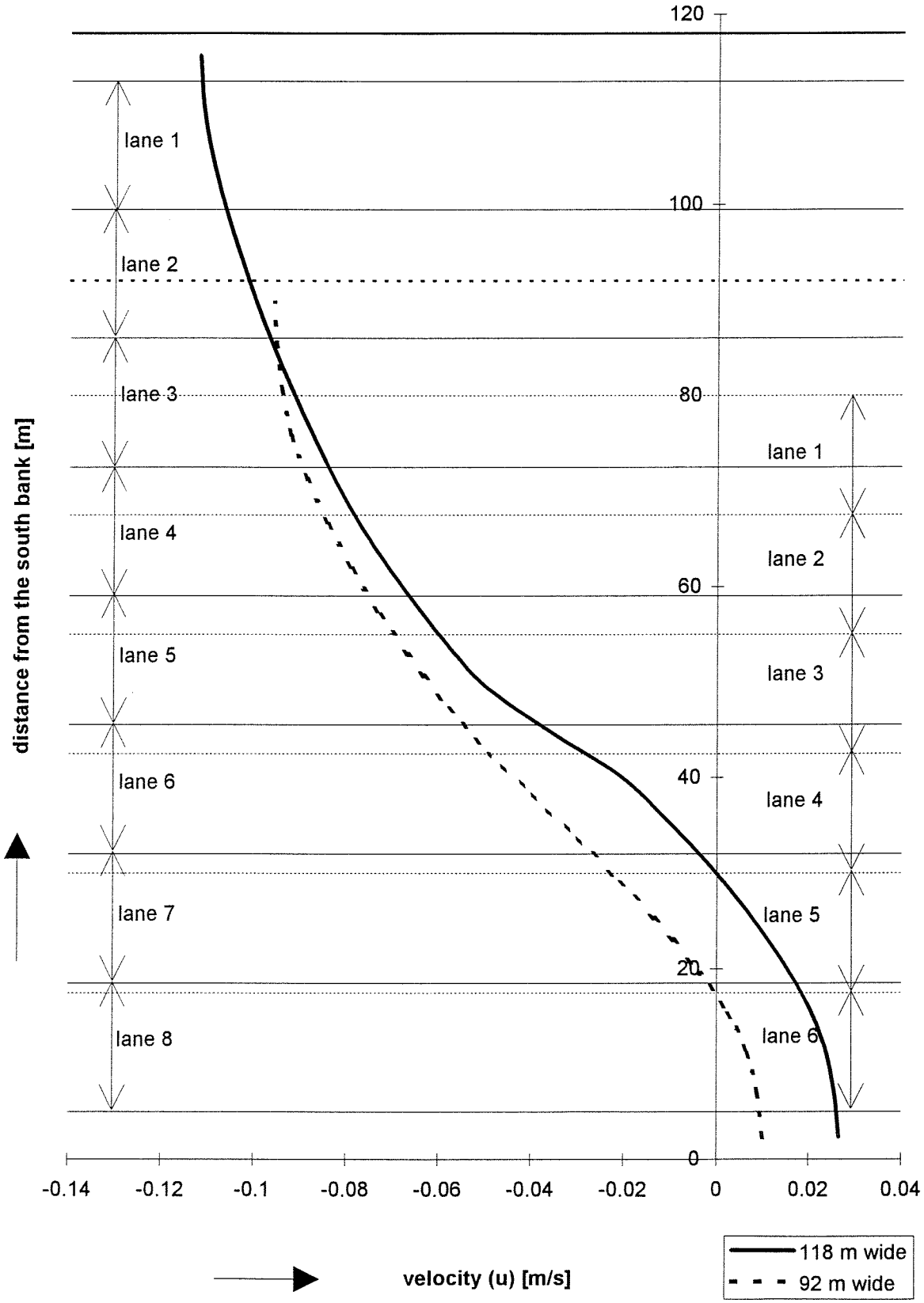

Figure 3.8c: Average flow velocity distribution over the width of the course at south-west wind (210°), 10 m/s

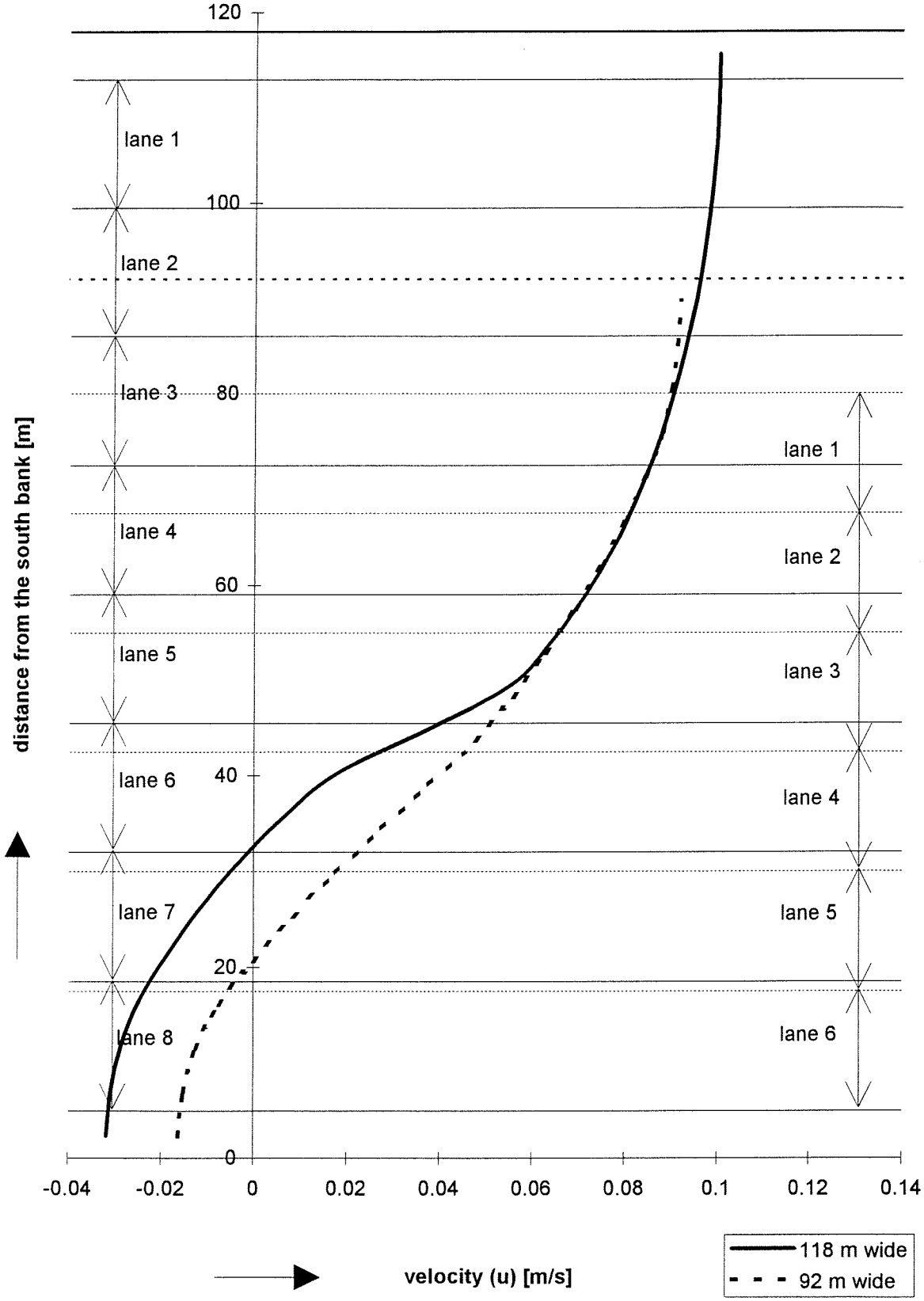

Figure 3.8d: Average flow velocity distribution over the width of the course at north-west wind (300°), 10 m/s

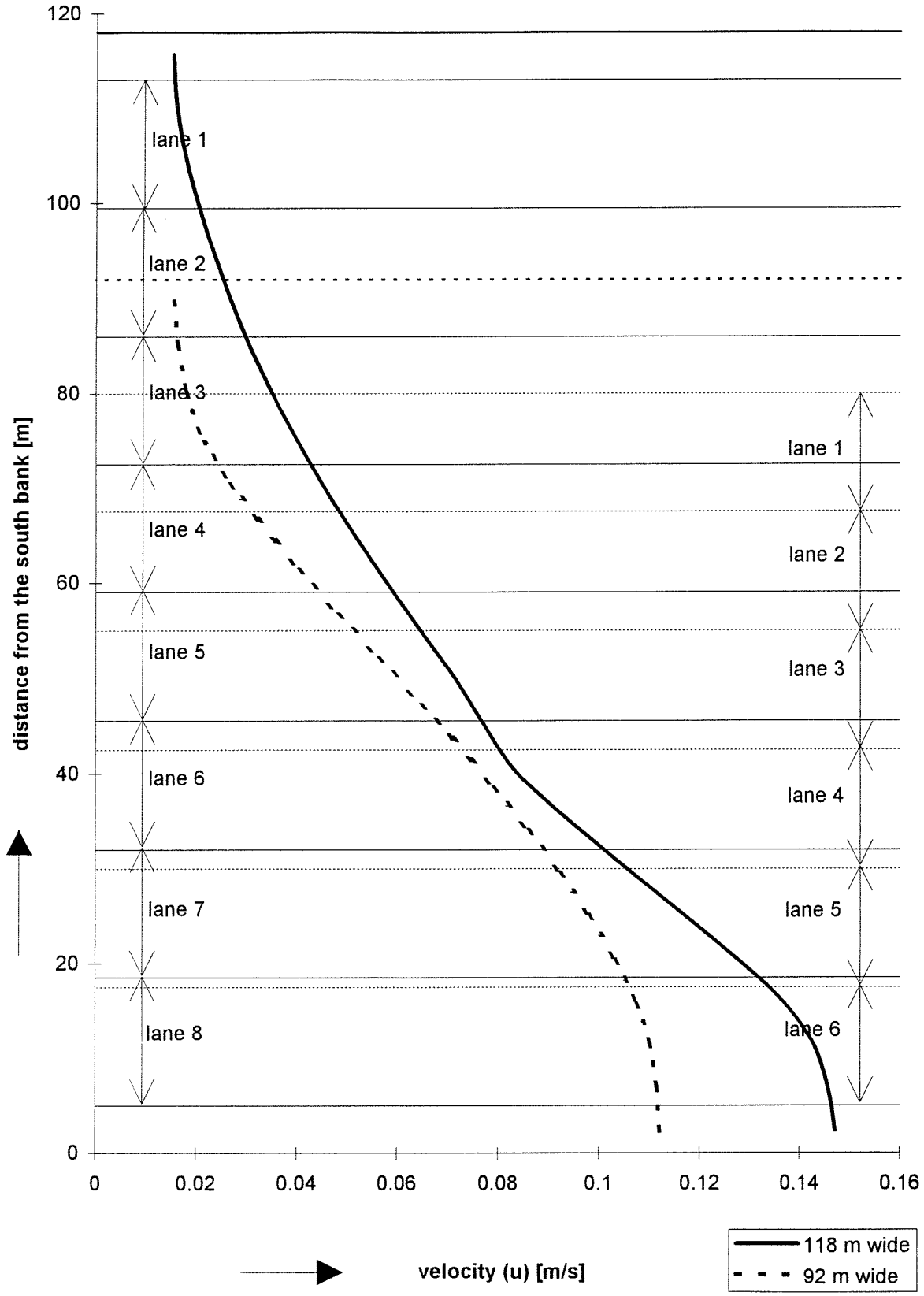

fig 8.14: 2DV-Bosbaan grid

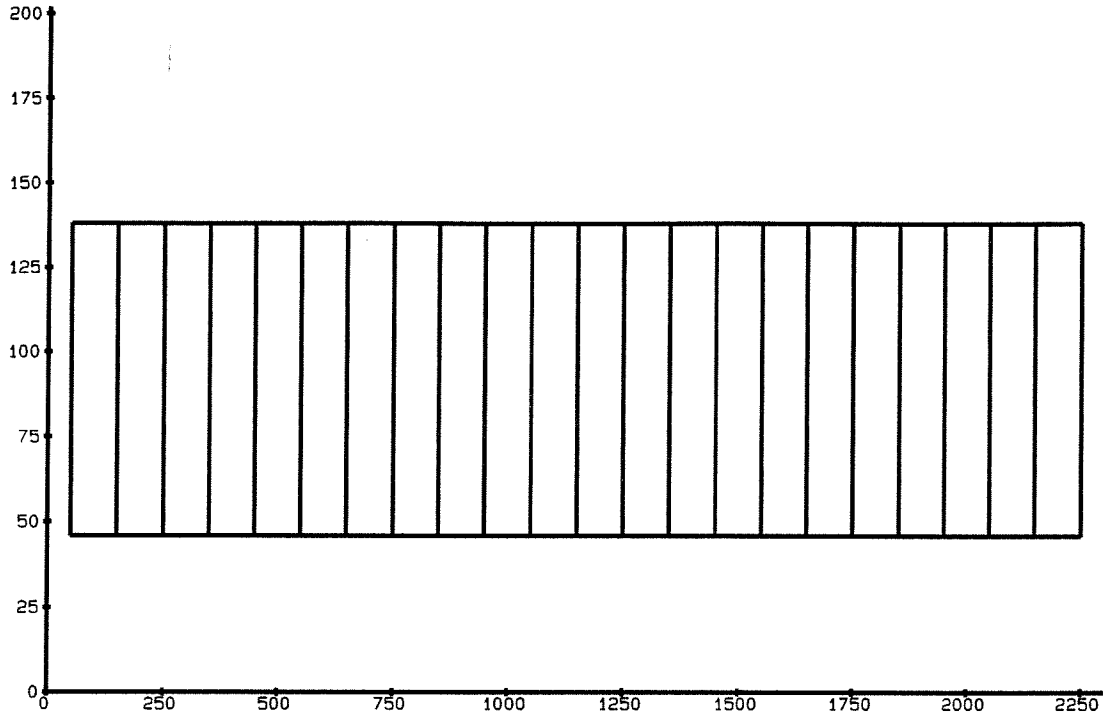

2DV grid (x, y) [m]

fig 8.15: k-epsilon (ke) and algebraic (a) turbulence model

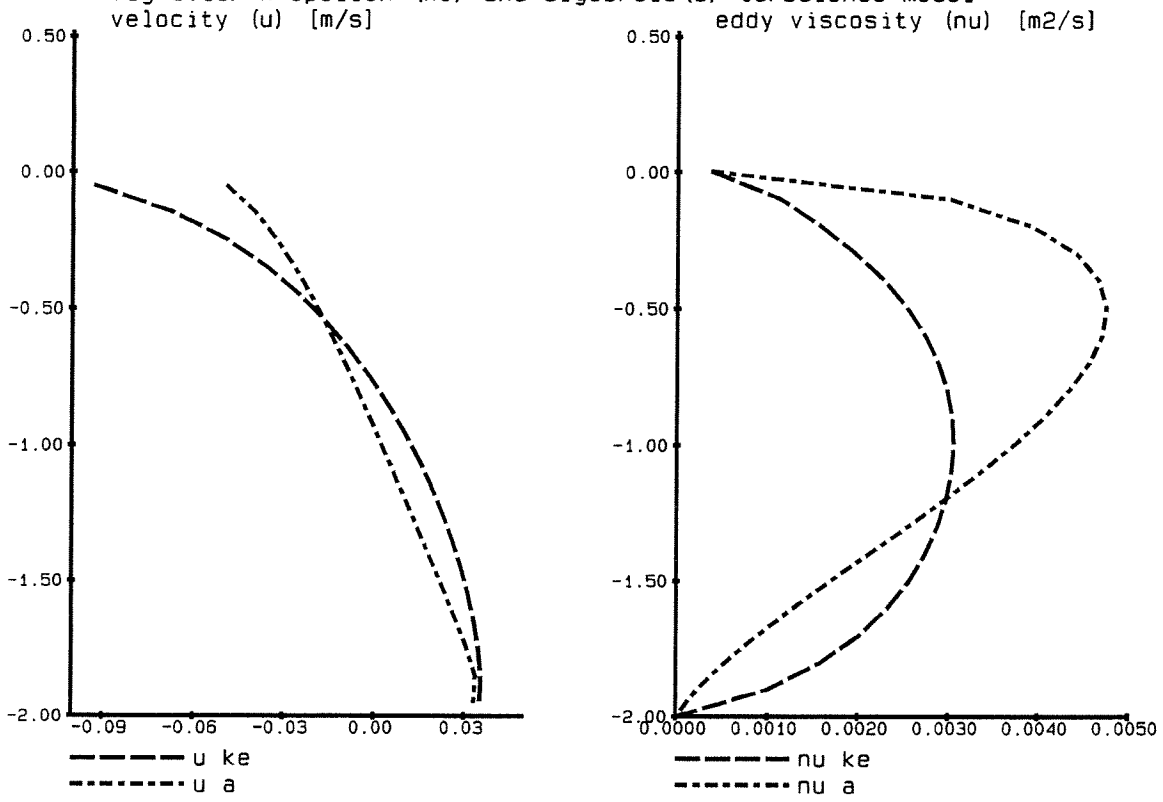

2DV-Bosbaan sensitivity analysis grid + turbulence model vertical distributions of velocity and viscosity		fig 8.14 fig 8.15
DELFT HYDRAULICS		fig-21

fig 8.16: Equidistant layer distributions

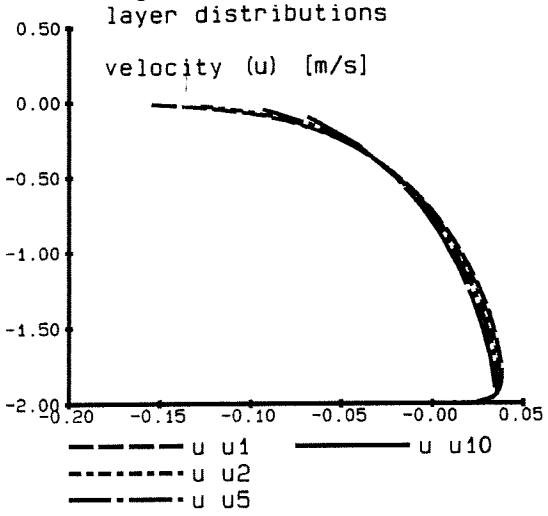

fig 8.17: Several layer distributions with 20 layers

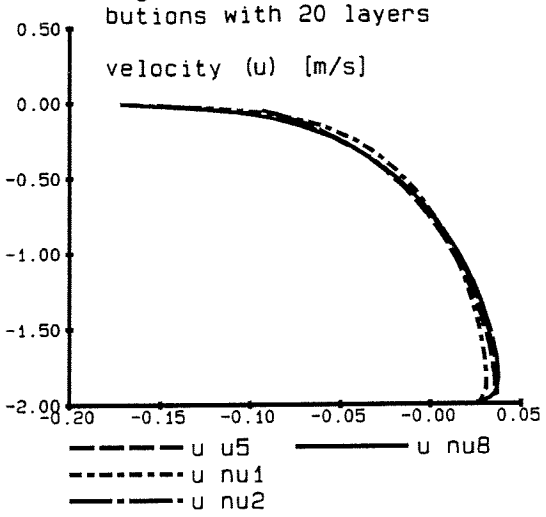

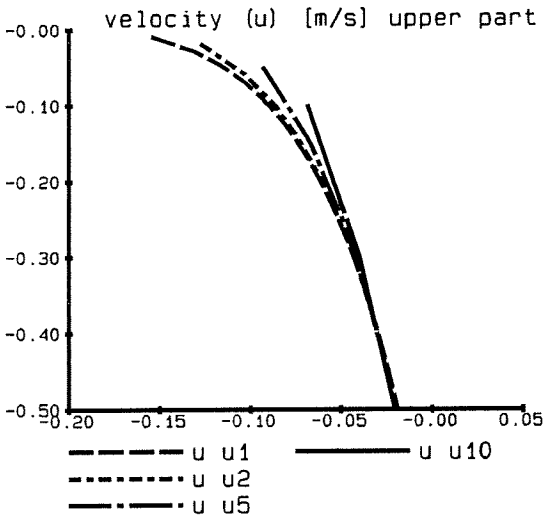

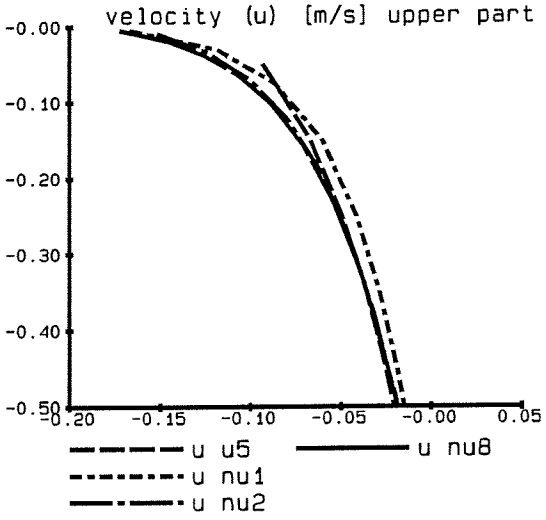

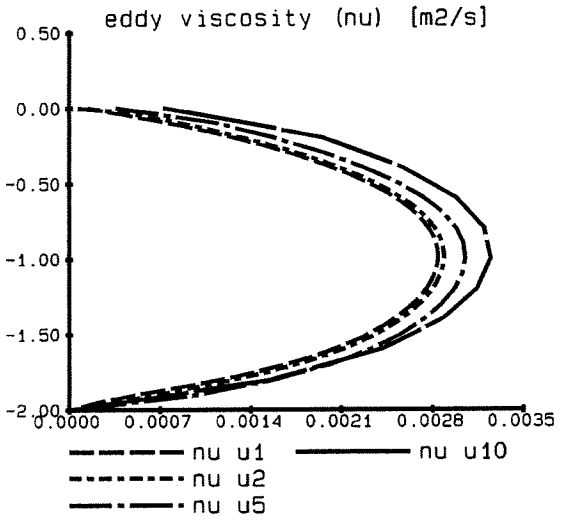

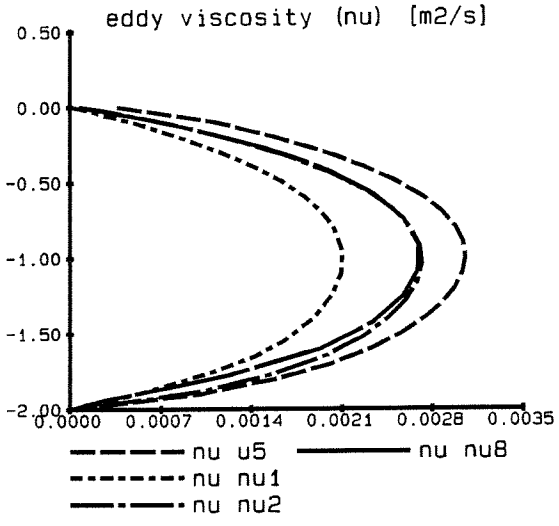

2DV-Bosbaan sensitivity analysis
layer distribution
vertical distributions of velocity and viscosity

fig 8.16
fig 8.17

DELFT HYDRAULICS

fig-22

fig 8.18: Large variation in layer thickness, different numbers of layers

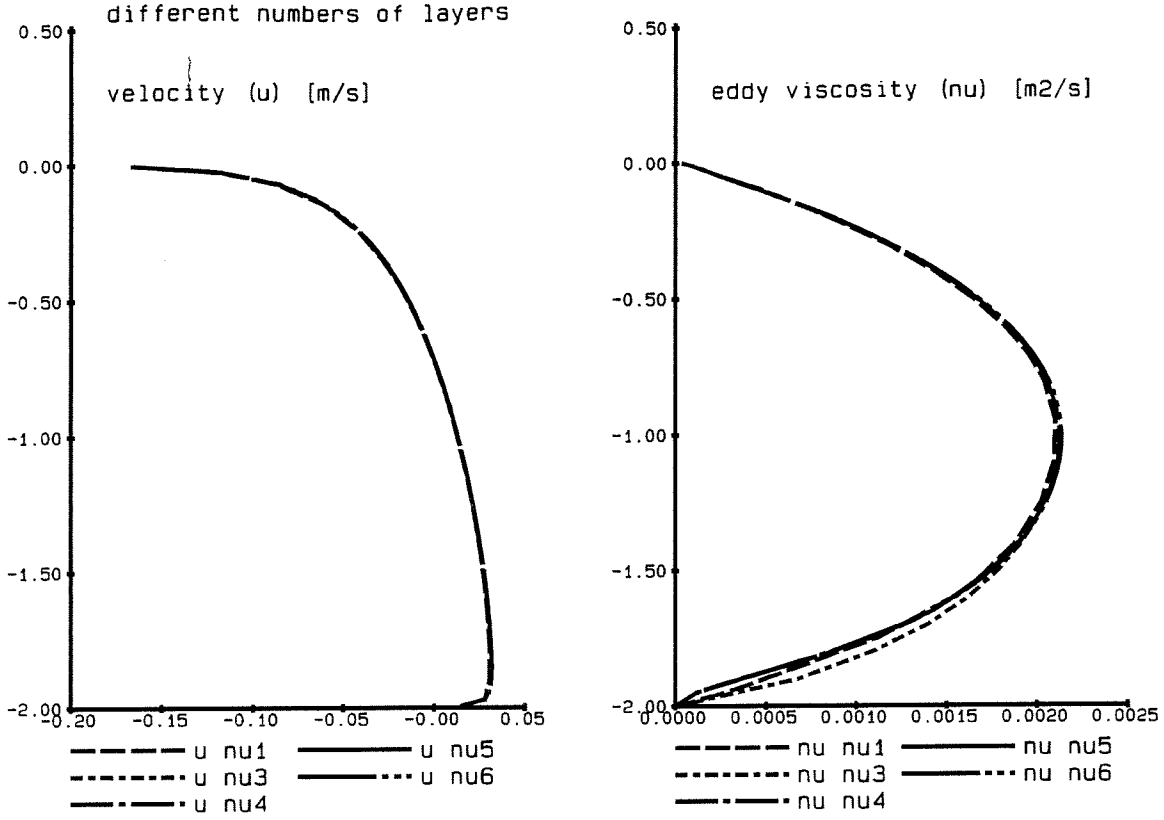

fig 8.19: Different smooth layer distributions

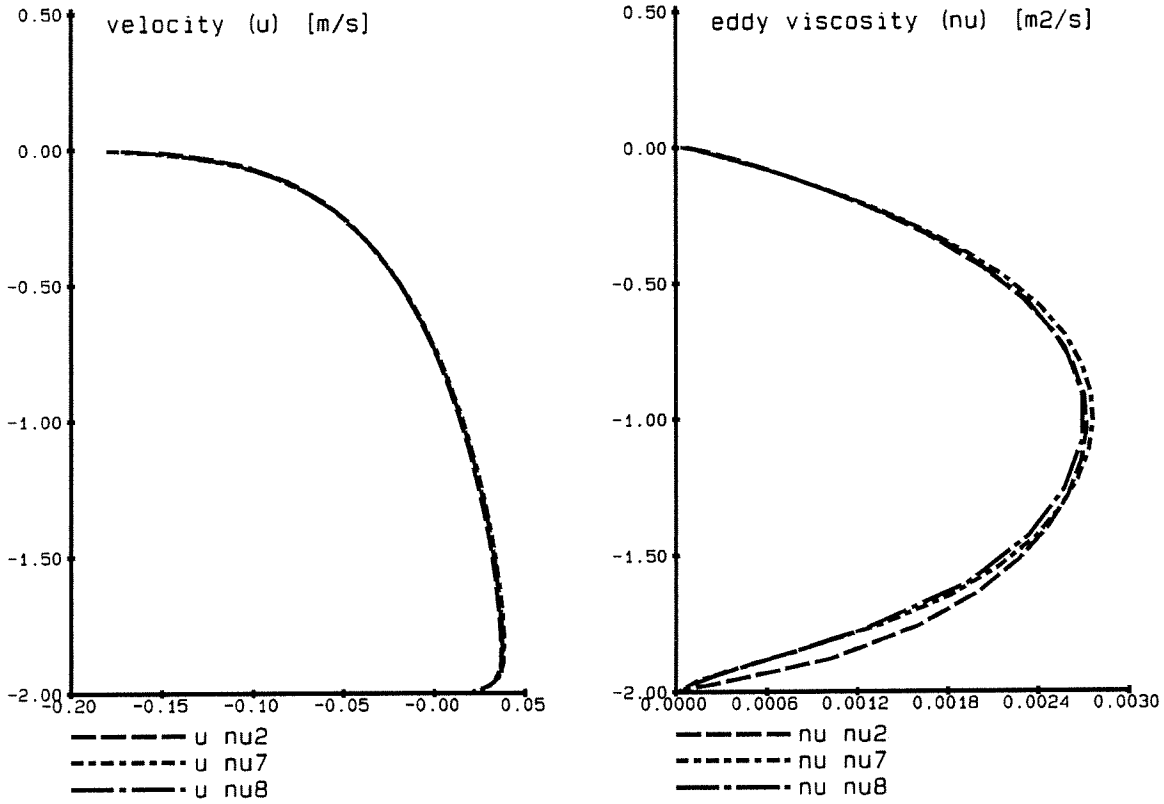

2DV-Bosbaan sensitivity analysis layer distribution vertical distributions of velocity and viscosity		fig 8.18 fig 8.19
D E L F T H Y D R A U L I C S		fig-23

fig 8.20a: Smooth layer distribution and 100 equidistant

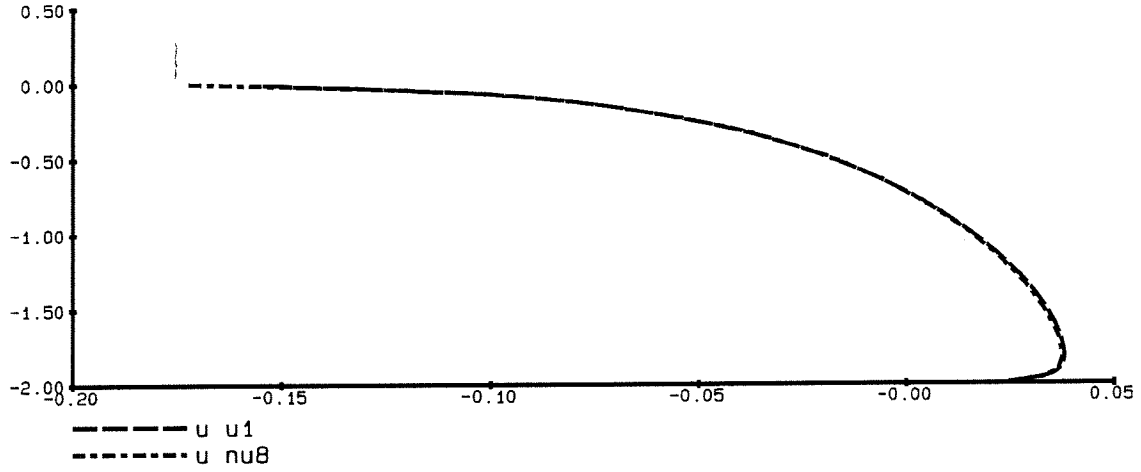

fig 8.20b: Large variation in layer thickness and 100 equidistant

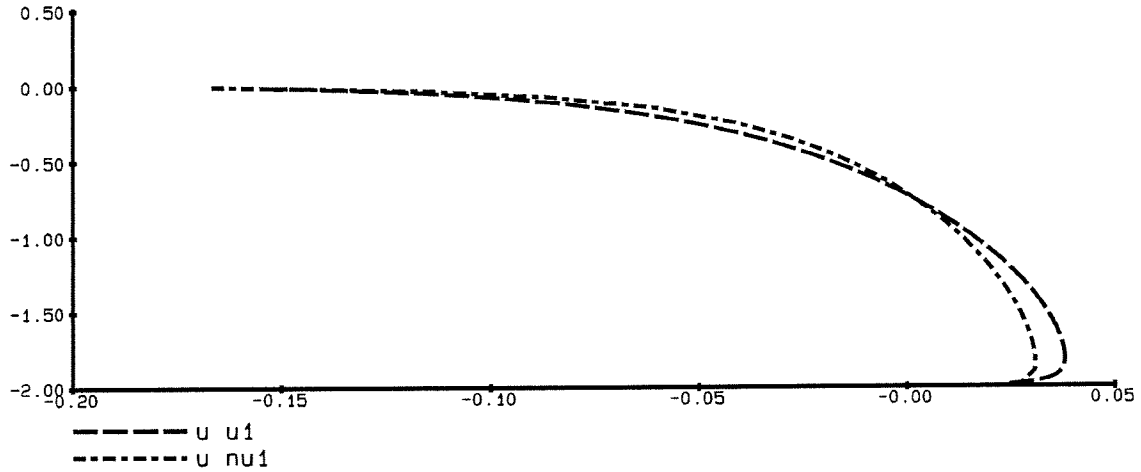

fig 8.20c: Smooth + non-smooth + 100 equidisant, upper part

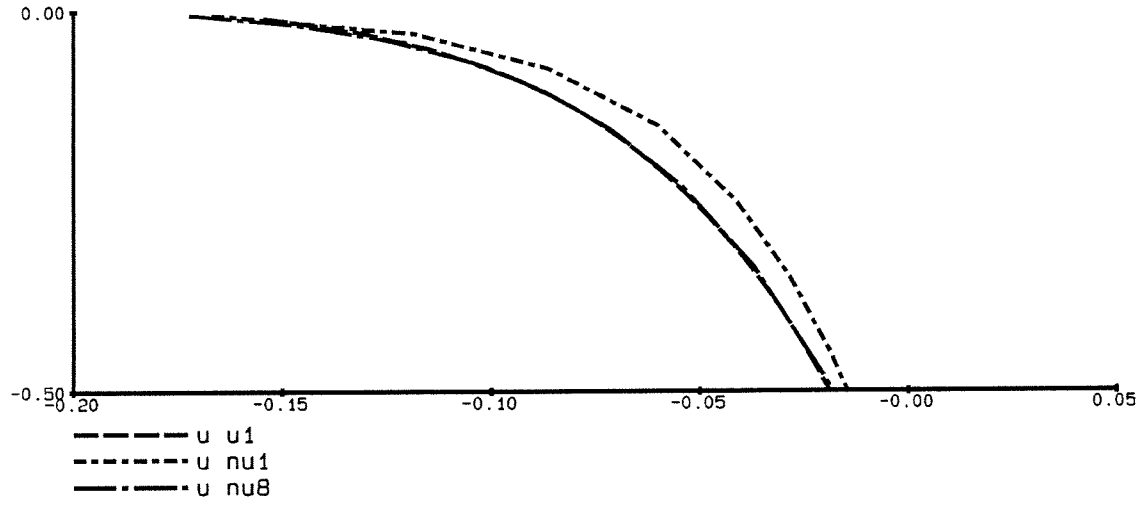

2DV-Bosbaan sensitivity analysis layer distribution vertical distributions of velocity [m/s]		fig 8.20
D E L F T H Y D R A U L I C S		fig-24

fig 8.21: Several roughness heights

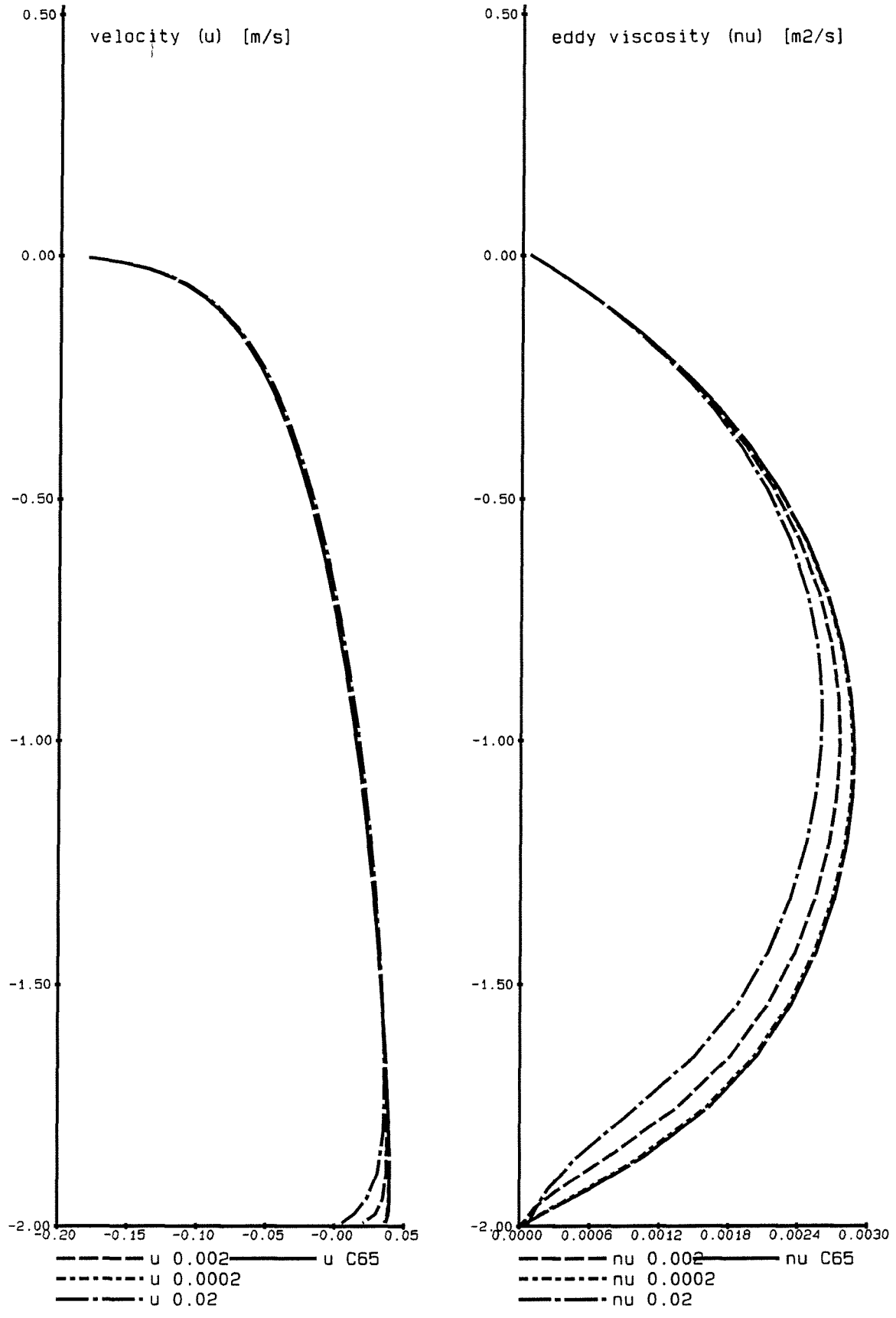

2DV-Bosbaan sensitivity analysis
roughness height
vertical distributions of velocity and viscosity

fig 8.21

DELFT HYDRAULICS

fig-25

fig 8.22a: spin-up time mm1

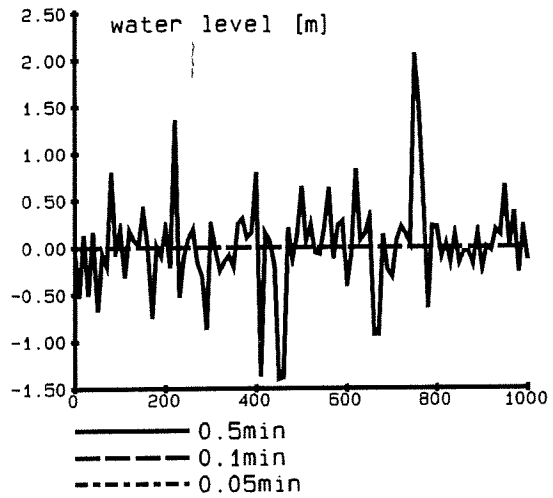

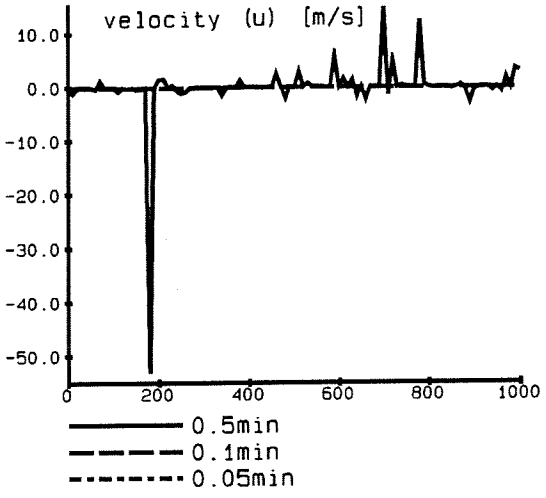

fig 8.22b: spin-up time sw

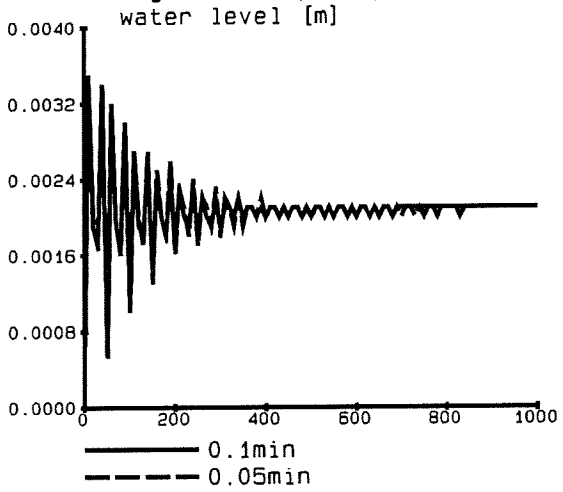

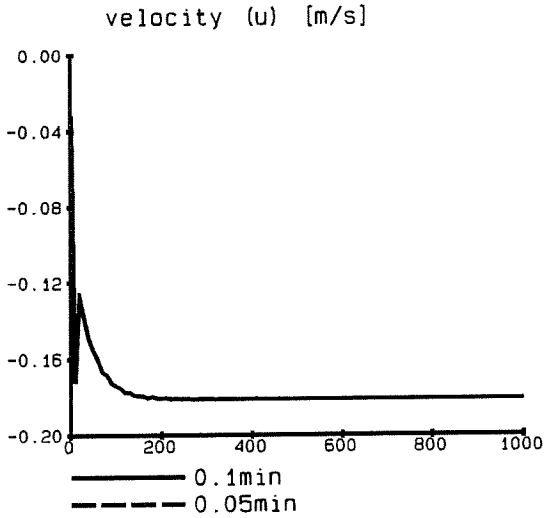

fig 8.22c: spin-up time ne

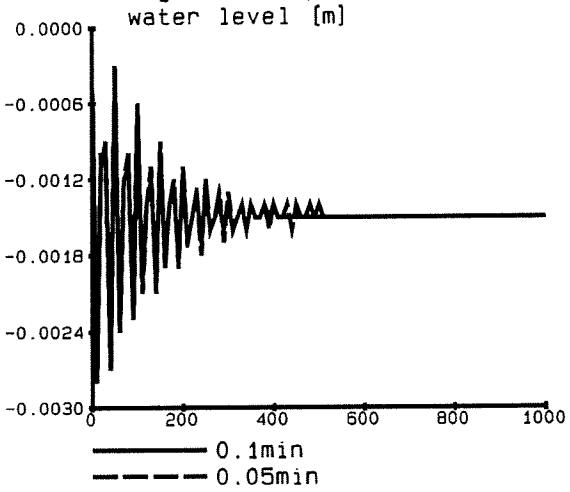

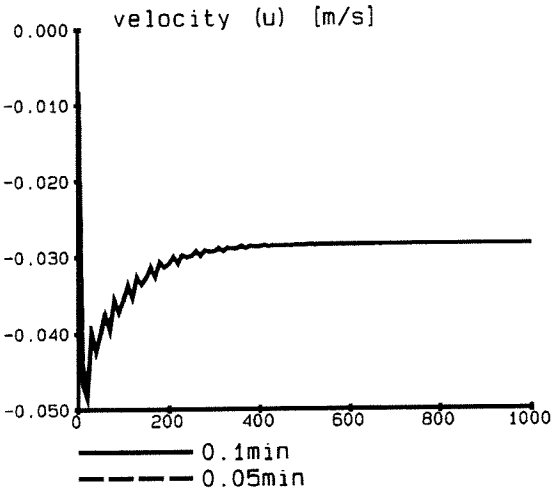

Bosbaan sensitivity analysis
time step 0.5, 0.1 and 0.05 min
spin-up time

fig 8.22

DELFT HYDRAULICS

fig-26

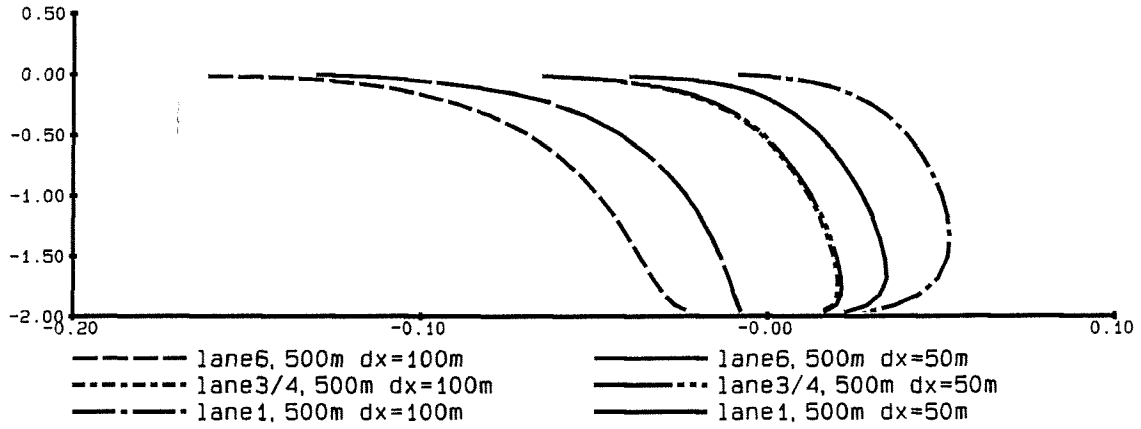

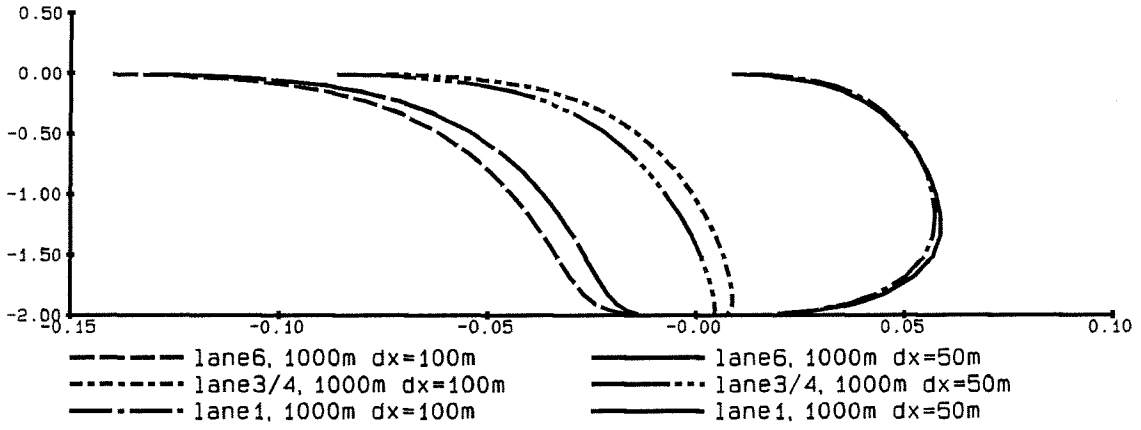

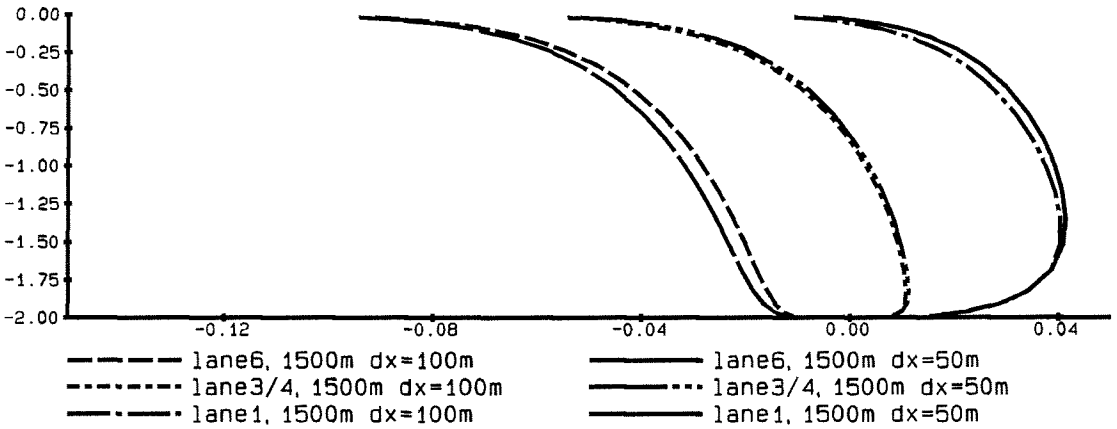

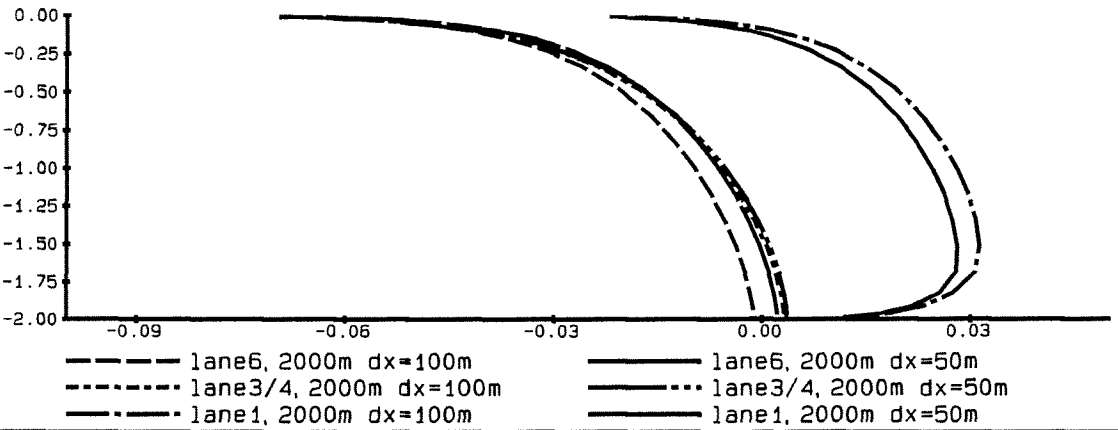

Bosbaan sensitivity analysis
grid sizes, delta x 50m or 100m
vertical distributions of velocity (u) [m/s]

fig 8.23

DELFT HYDRAULICS

fig-27

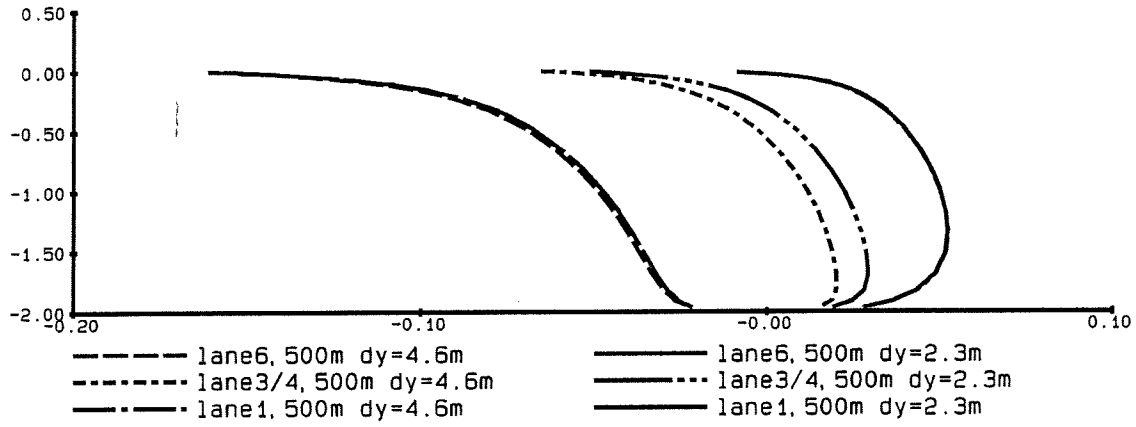

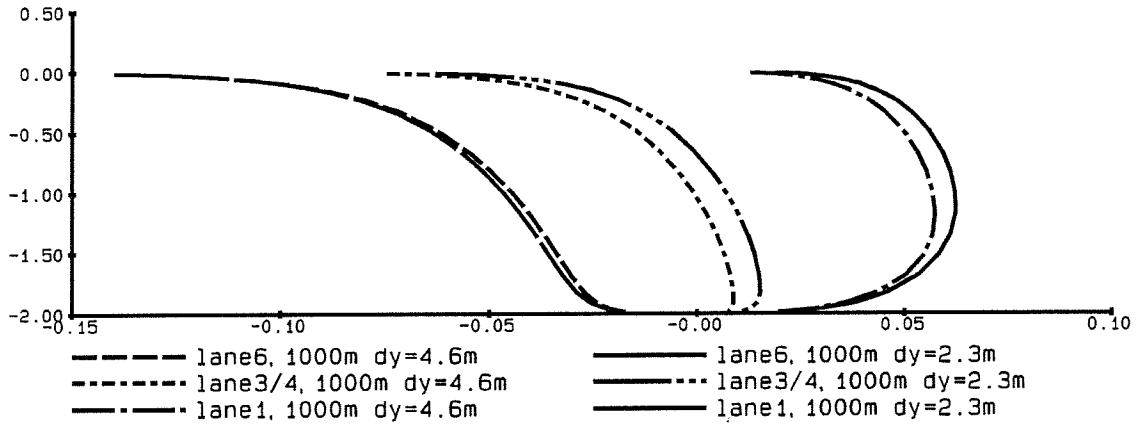

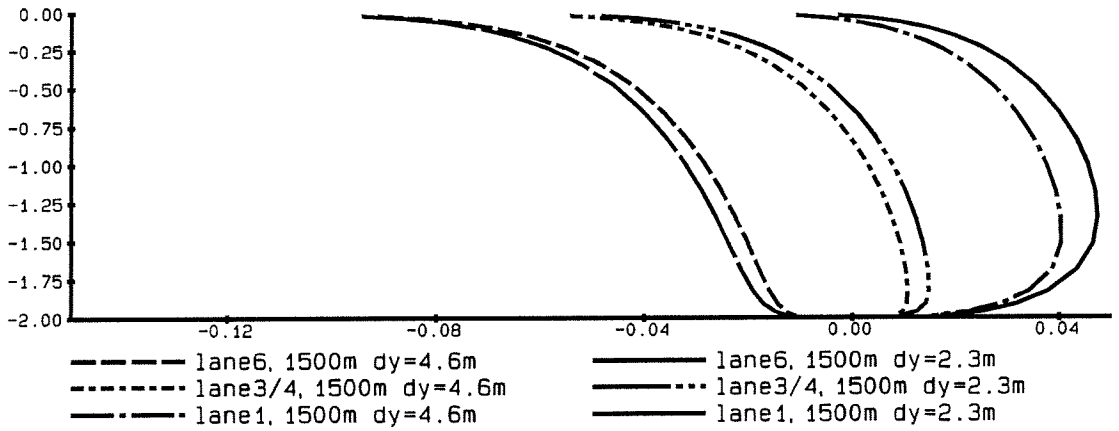

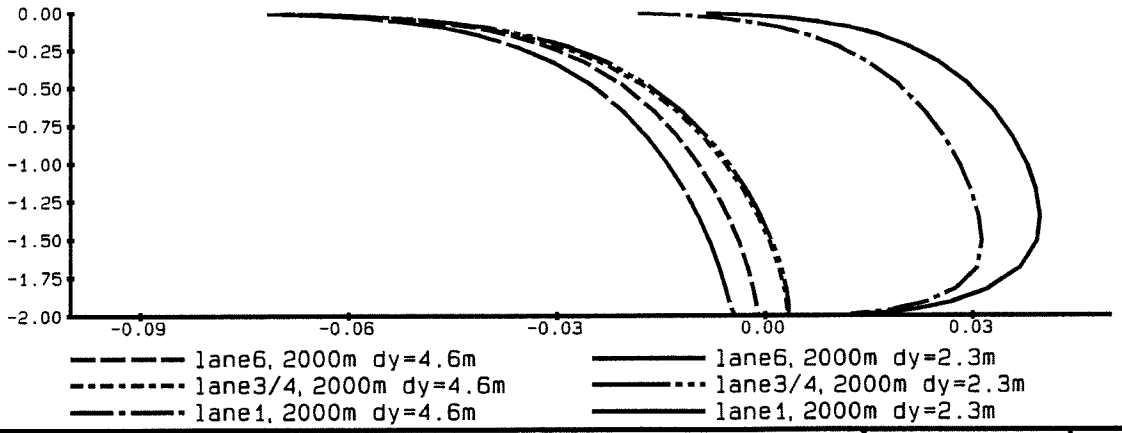

Bosbaan sensitivity analysis, grid sizes
delta y 4.6m or 2.3m, with scaling NU2D
vertical distributions of velocity (u) [m/s]

fig 8.24a

DELFT HYDRAULICS

fig-28

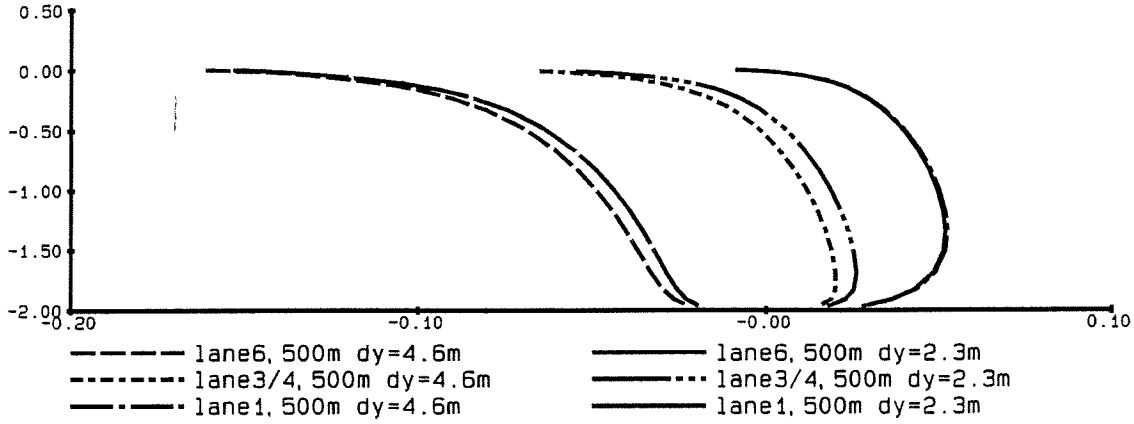

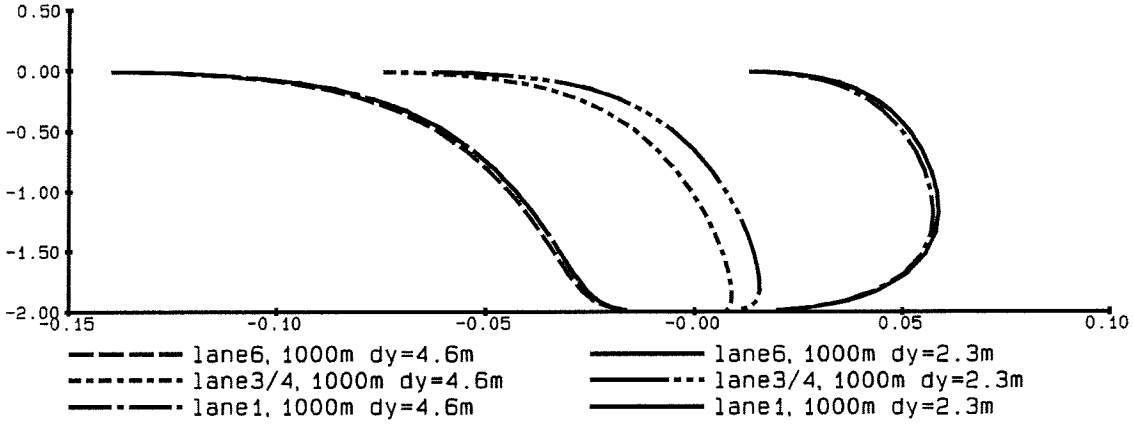

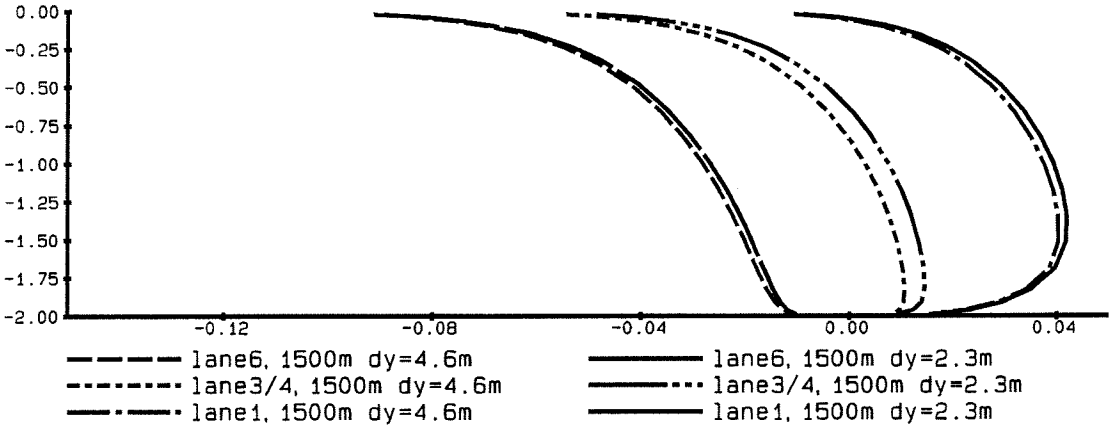

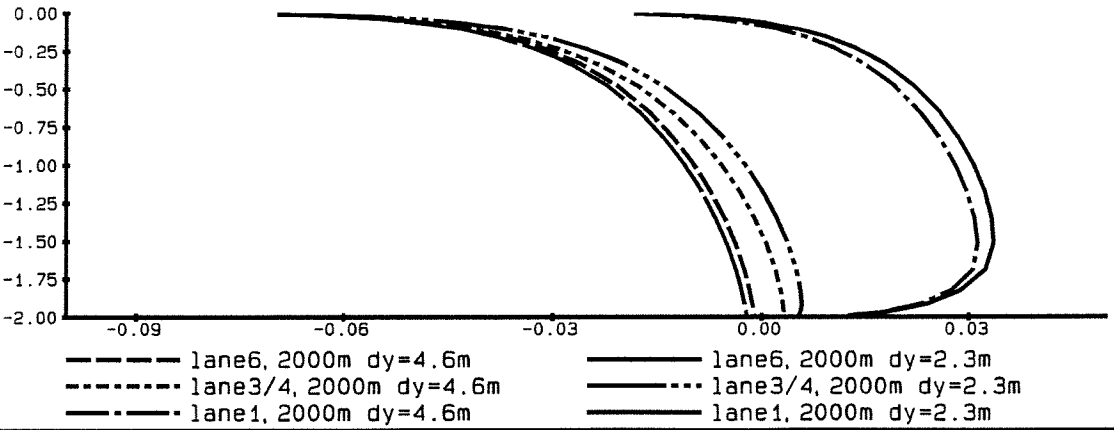

Bosbaan sensitivity analysis, grid sizes
delta y 4.6m or 2.3m, constant NU2D
vertical distributions of velocity (u) [m/s]

fig 8.24b

DELFT HYDRAULICS

fig-29

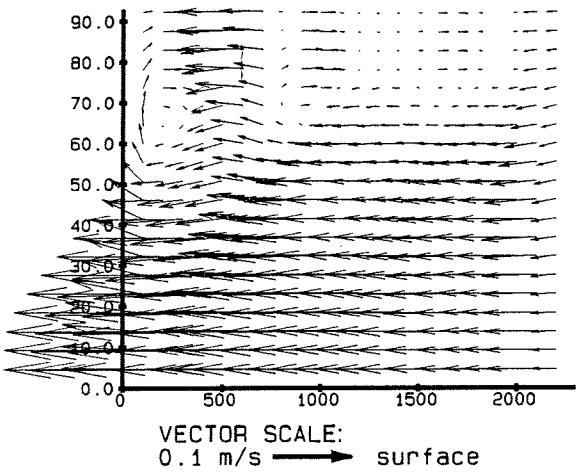

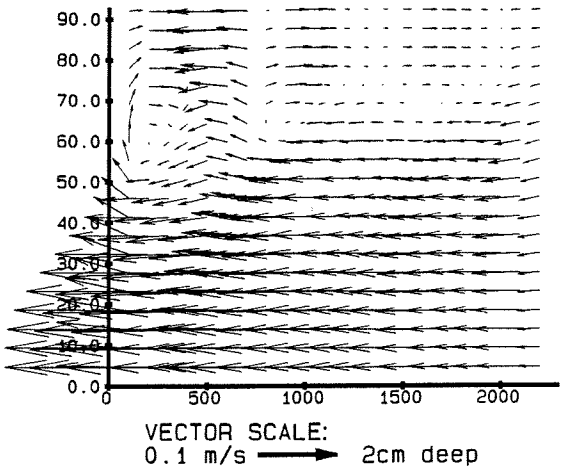

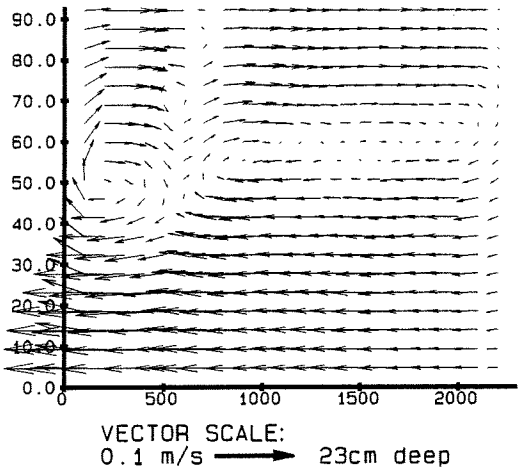

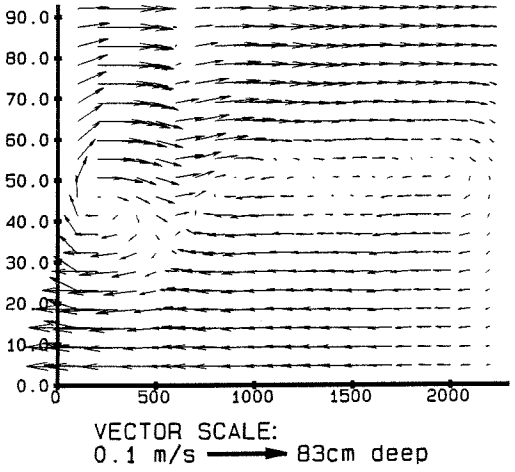

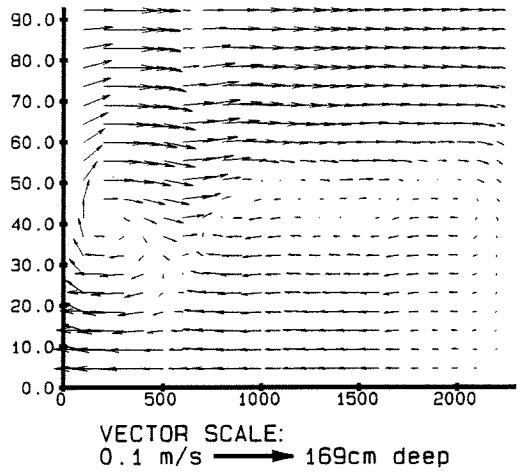

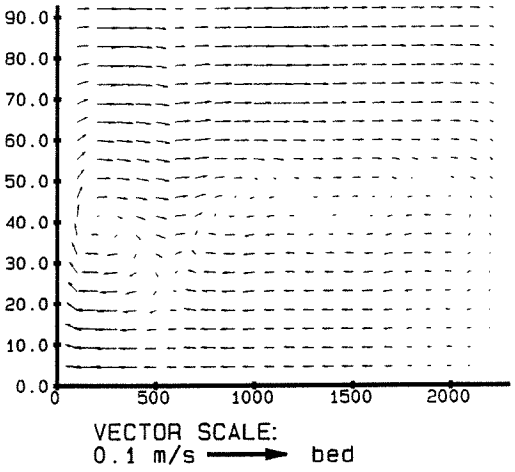

Bosbaan sensitivisty analysis
horizontal eddy viscosity 0 m2/s
velocity vectors at several depths

fig 8.25a

DELFT HYDRAULICS

fig-30

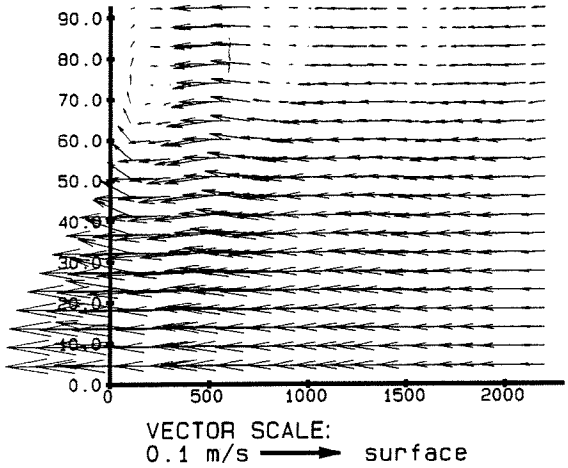

VECTOR SCALE:
0.1 m/s ⟶ surface

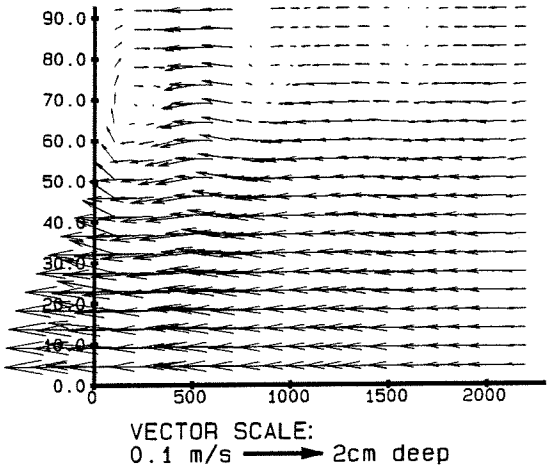

VECTOR SCALE:
0.1 m/s ⟶ 2cm deep

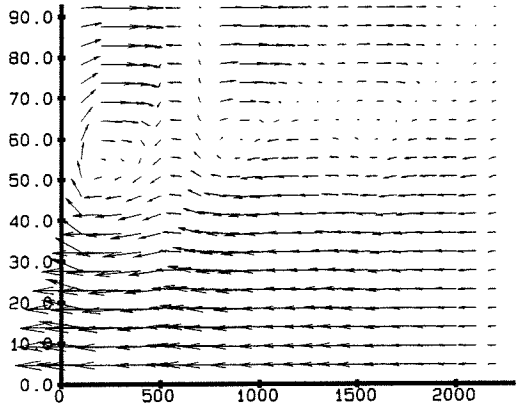

VECTOR SCALE:
0.1 m/s ⟶ 23cm deep

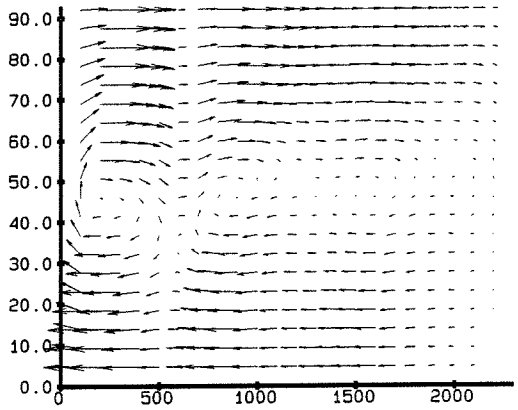

VECTOR SCALE:
0.1 m/s ⟶ 83cm deep

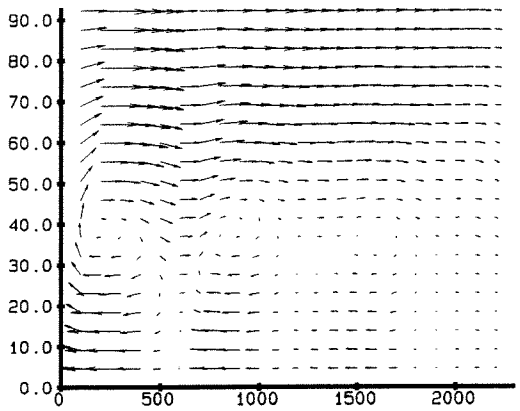

VECTOR SCALE:
0.1 m/s ⟶ 169cm deep

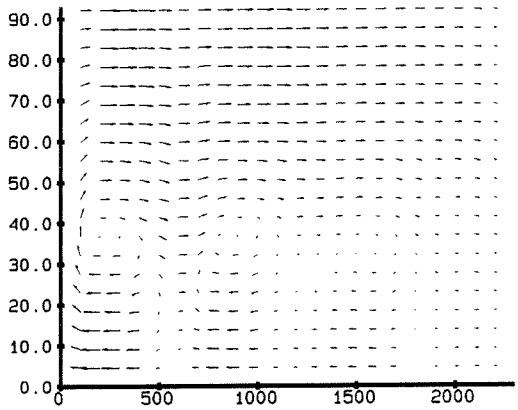

VECTOR SCALE:
0.1 m/s ⟶ bed

Bosbaan sensitivisty analysis
horizontal eddy viscosity 0.1 m2/s
velocity vectors at several depths

fig 8.25b

DELFT HYDRAULICS

fig-31

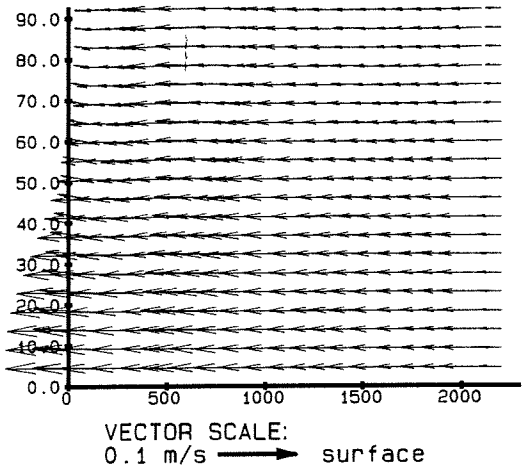

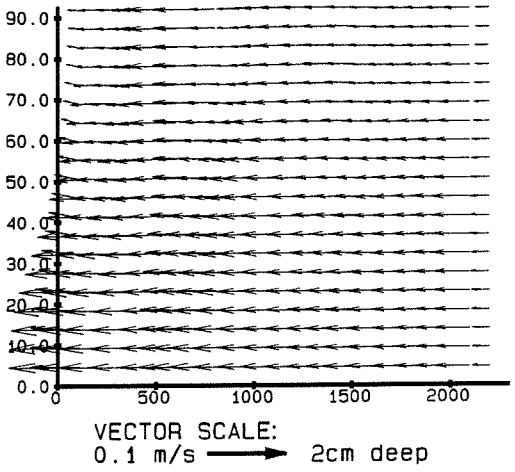

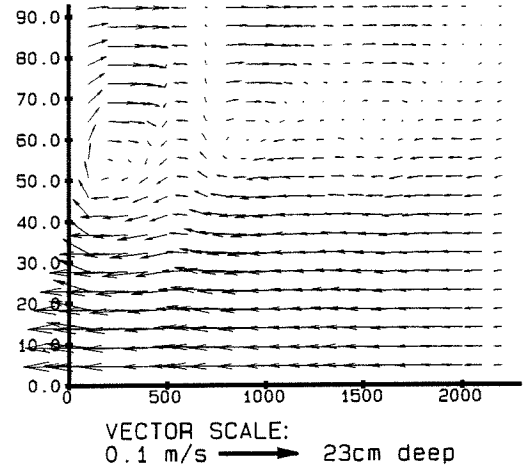

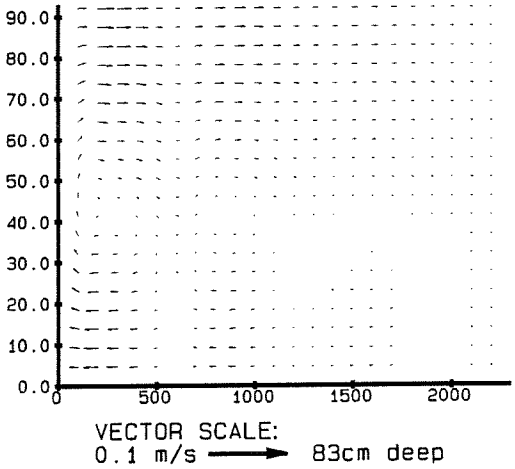

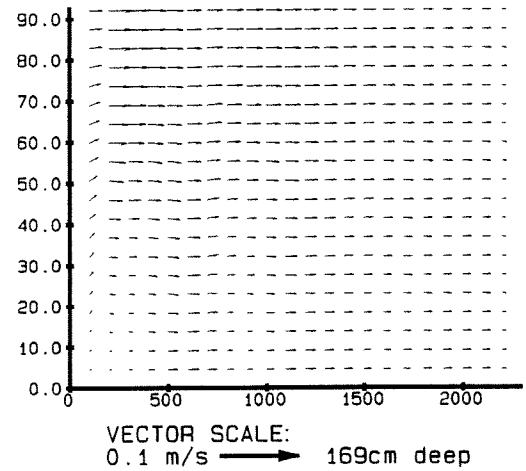

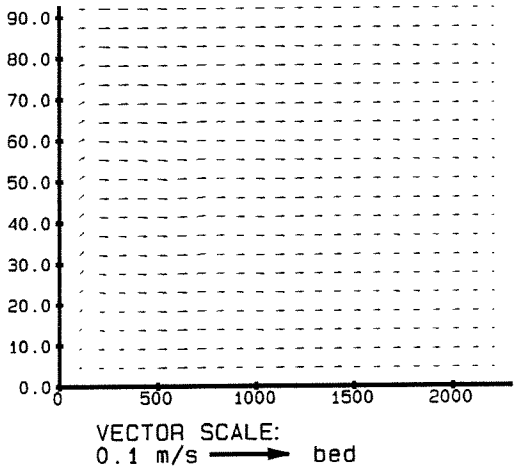

Bosbaan sensitivisty analysis
horizontal eddy viscosity 1 m2/s
velocity vectors at several depths

fig 8.25c

DELFT HYDRAULICS

fig-32

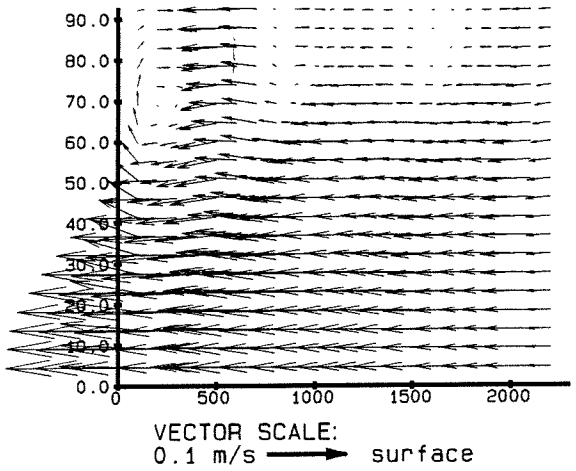

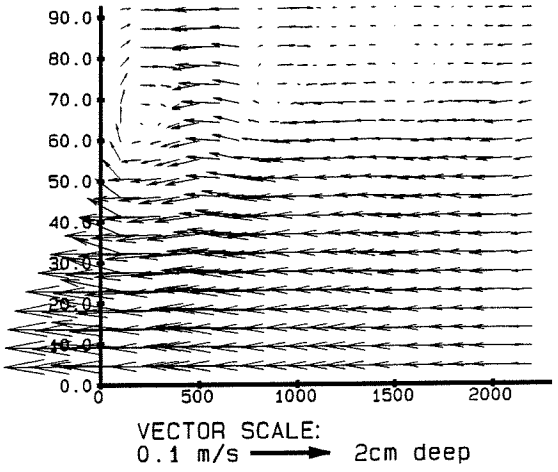

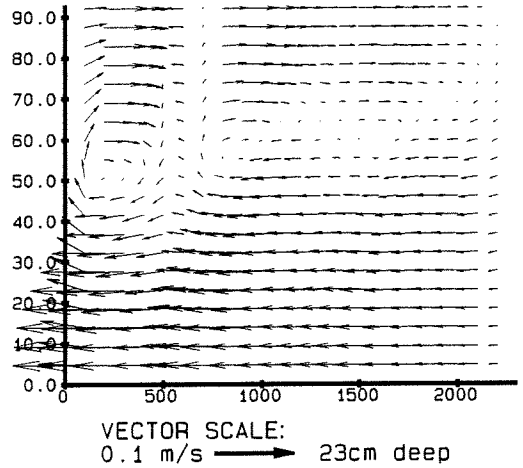

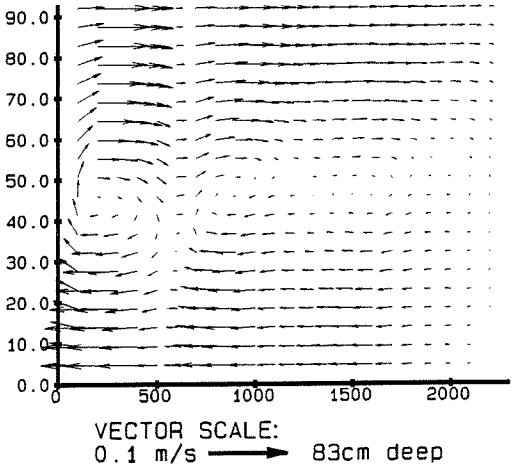

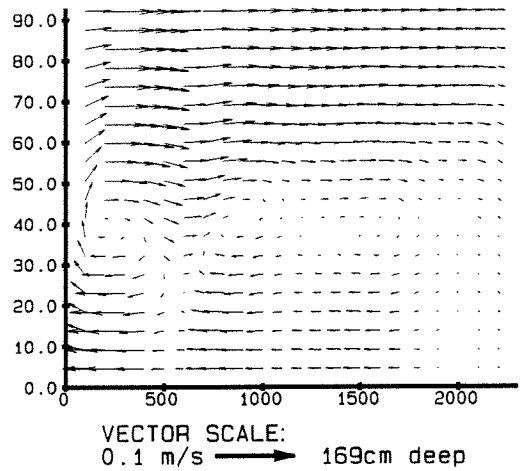

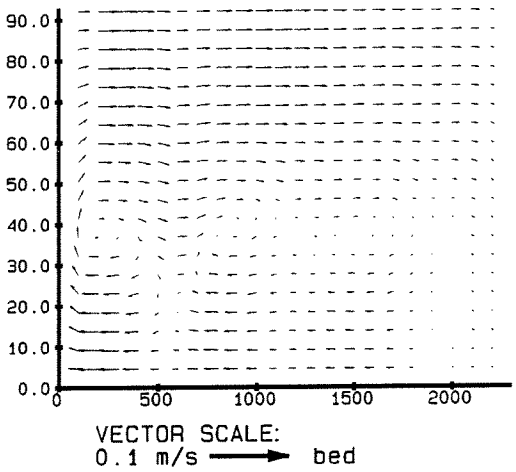

Bosbaan sensitivisty analysis
horizontal eddy viscosity 0.05 m2/s
velocity vectors at several depths

fig 8.25d

DELFT HYDRAULICS

fig-33

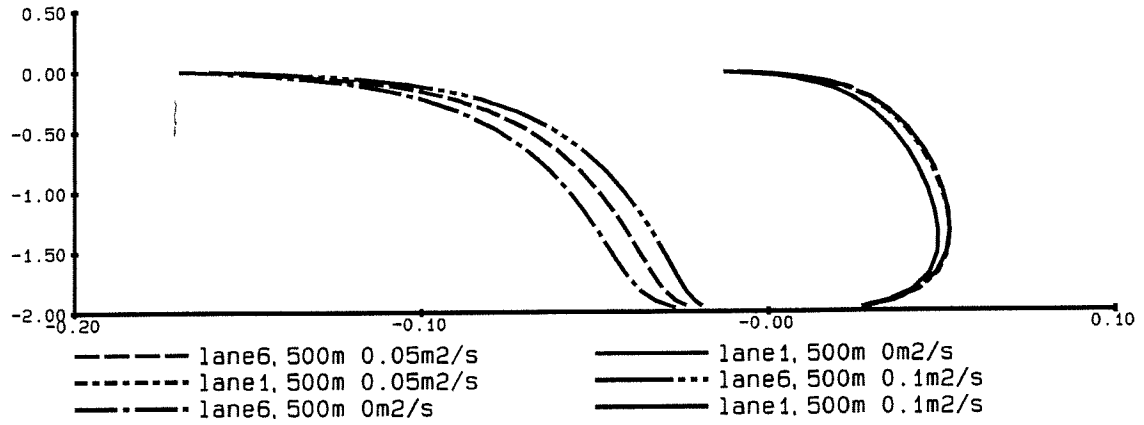

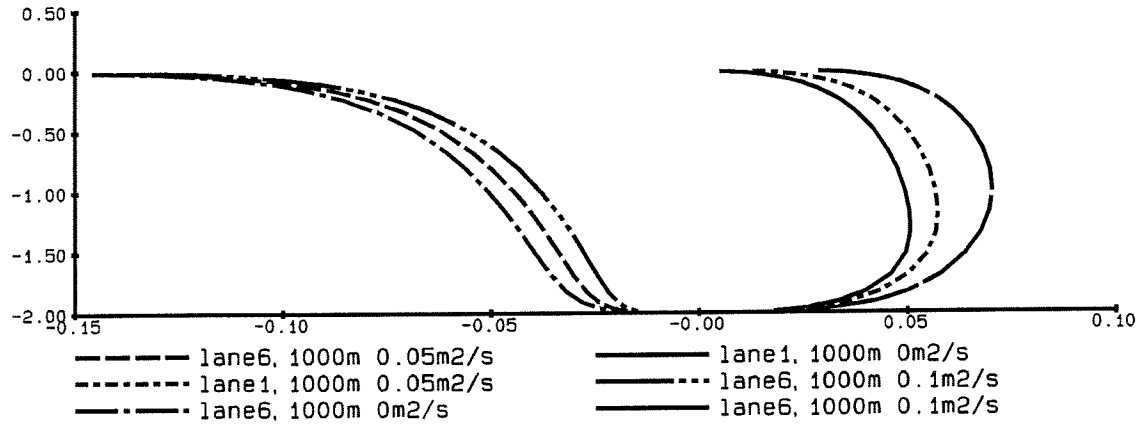

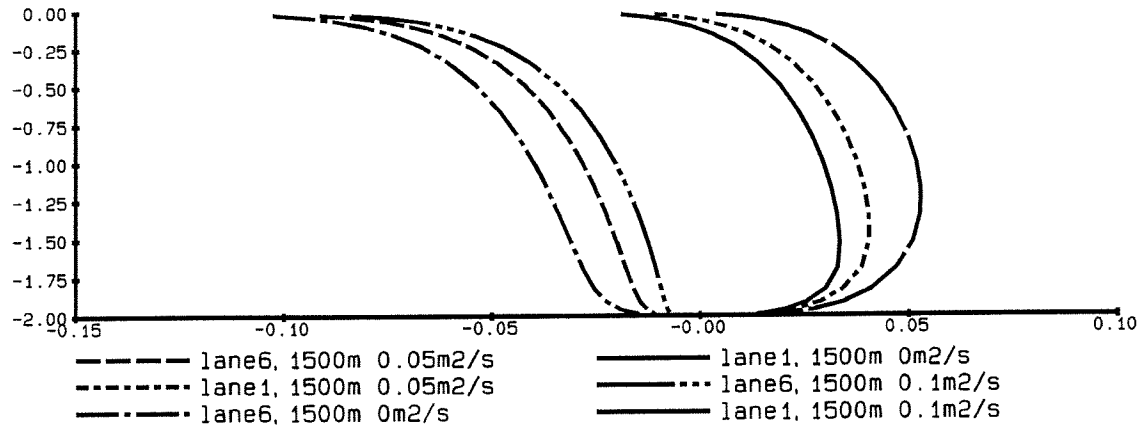

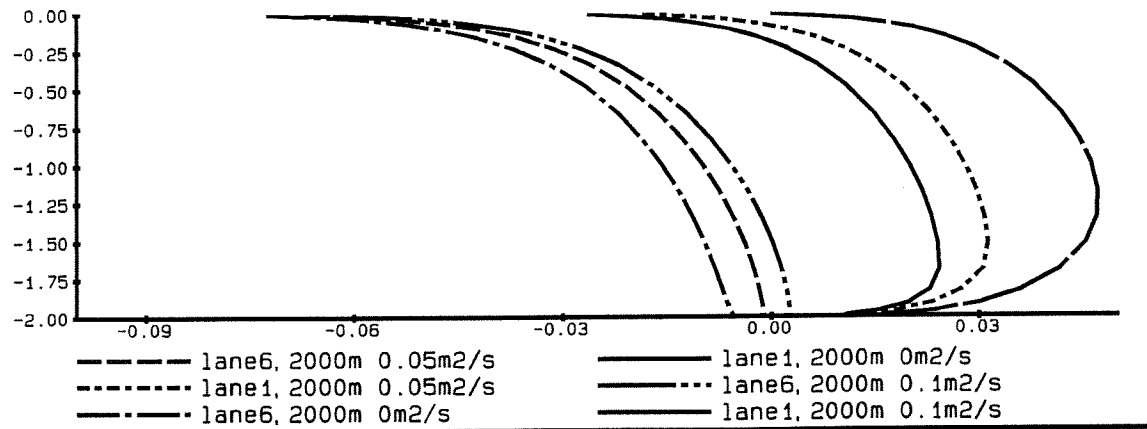

Bosbaan sensitivity analysis
horizontal eddy viscosity
vertical distributions of velocity (u) [m/s]

fig 8.26a

DELFT HYDRAULICS

fig-34

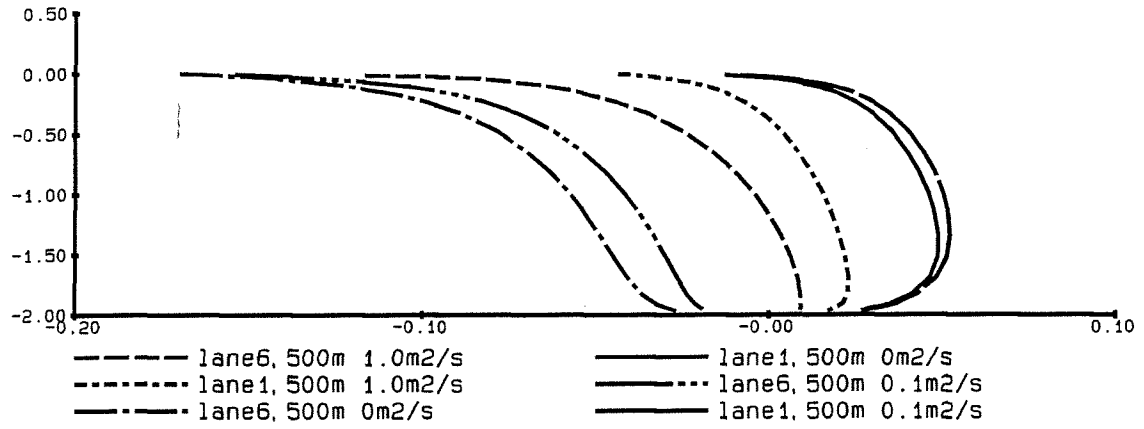

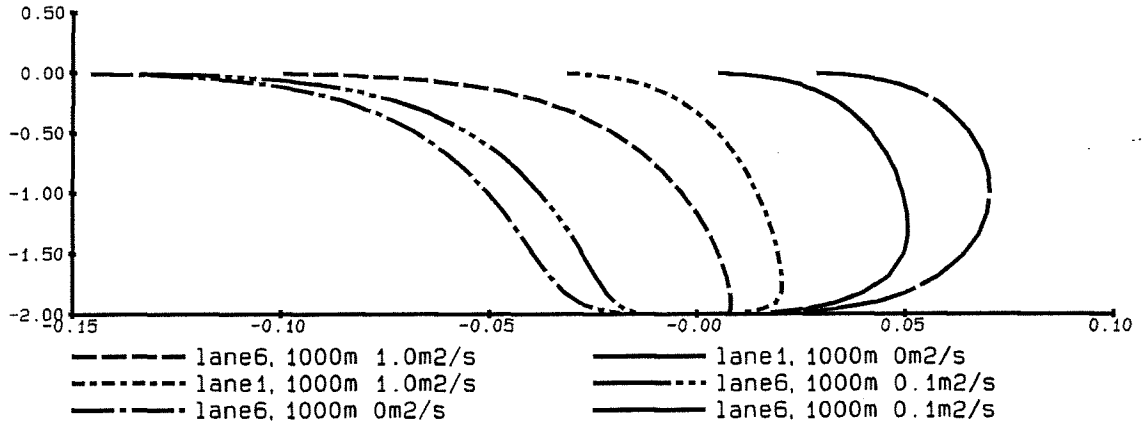

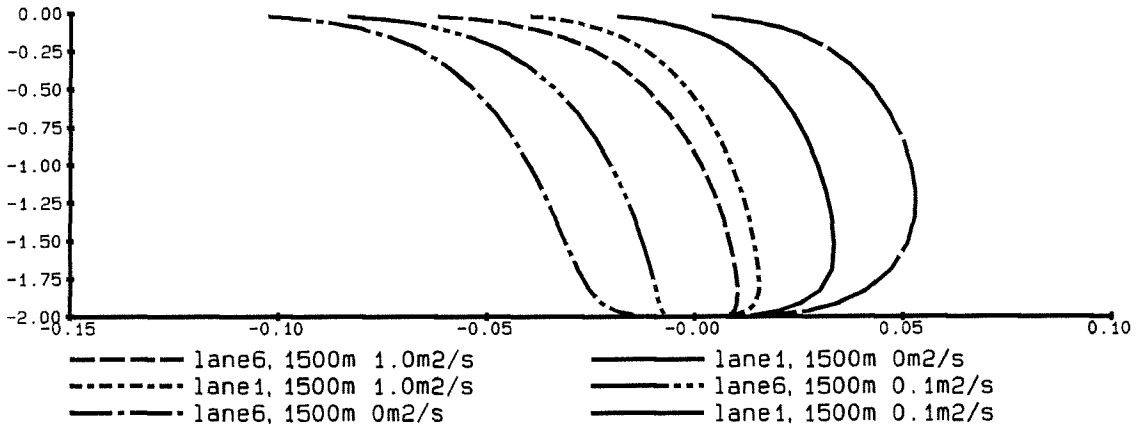

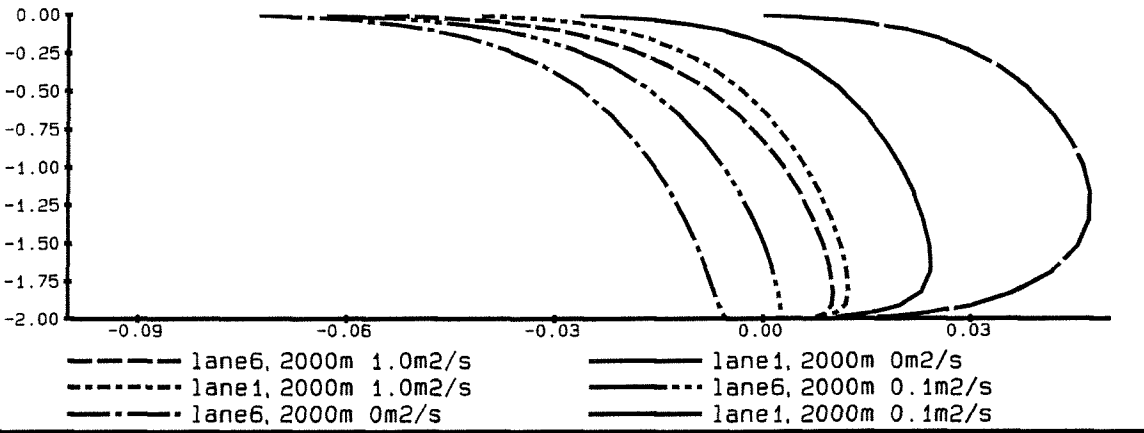

Bosbaan sensitivity analysis
horizontal eddy viscosity
vertical distributions of velocity (u) [m/s]

fig 8.26b

DELFT HYDRAULICS

fig-35

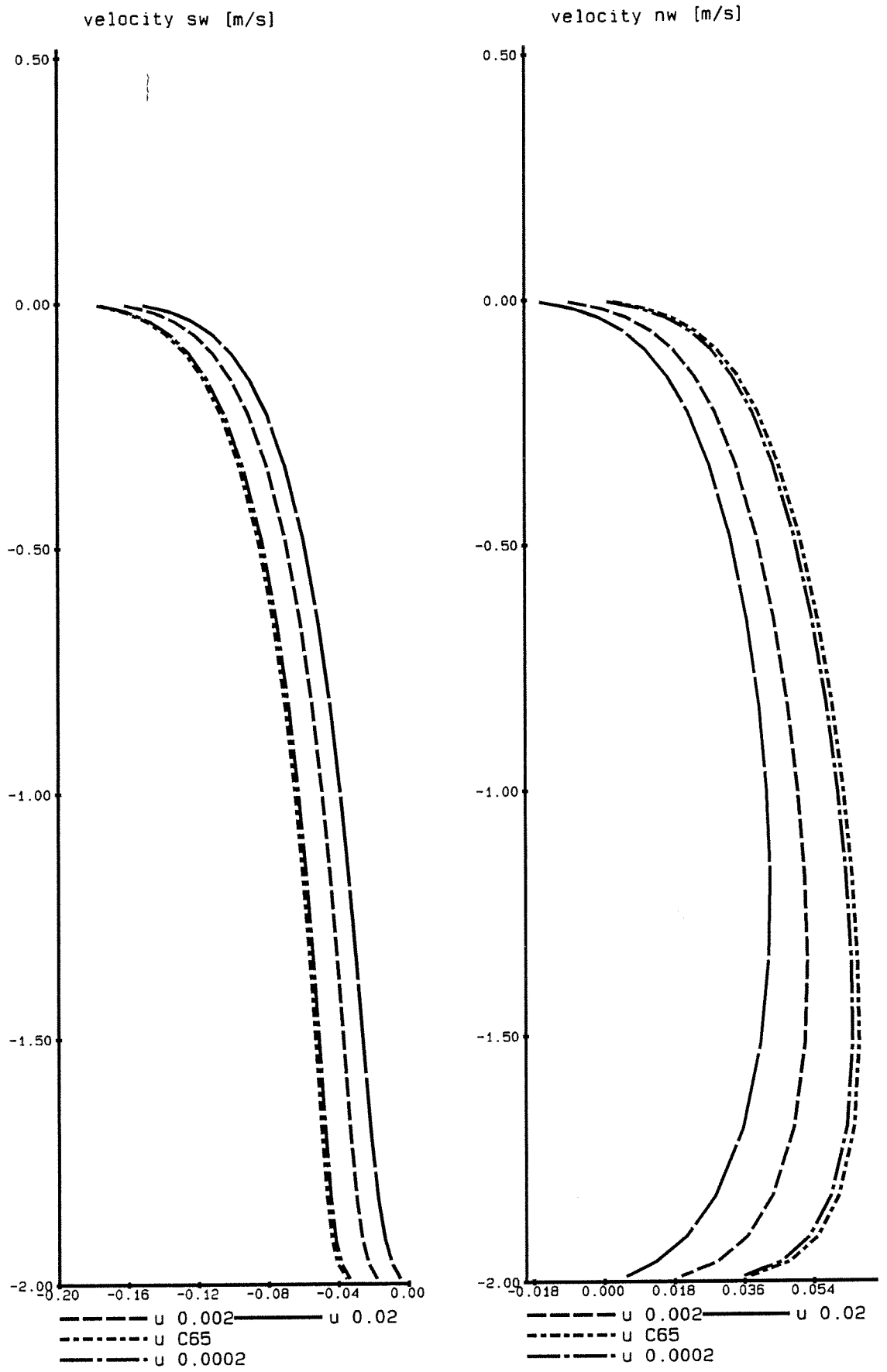

Bosbaan sensitivity analysis
roughness height
vertical distributions of velocity (u) [m/s]

fig 8.27

DELFT HYDRAULICS

fig-36

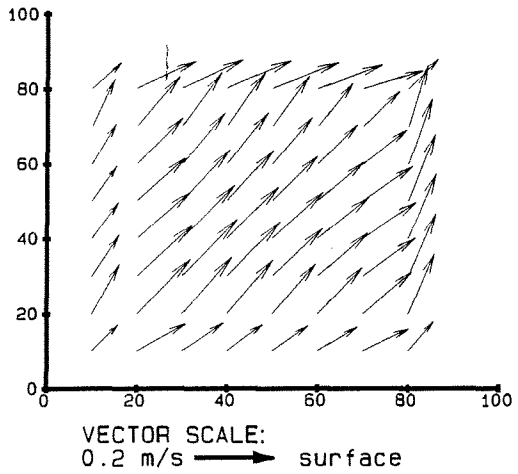

VECTOR SCALE:
0.2 m/s → surface

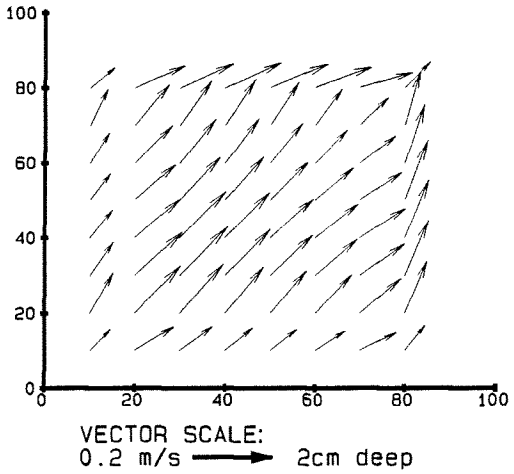

VECTOR SCALE:
0.2 m/s → 2cm deep

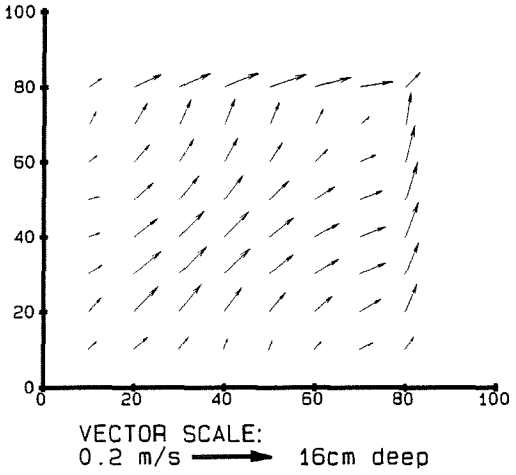

VECTOR SCALE:
0.2 m/s → 16cm deep

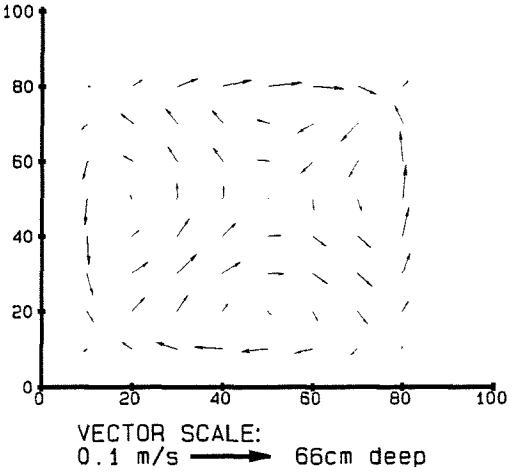

VECTOR SCALE:
0.1 m/s → 66cm deep

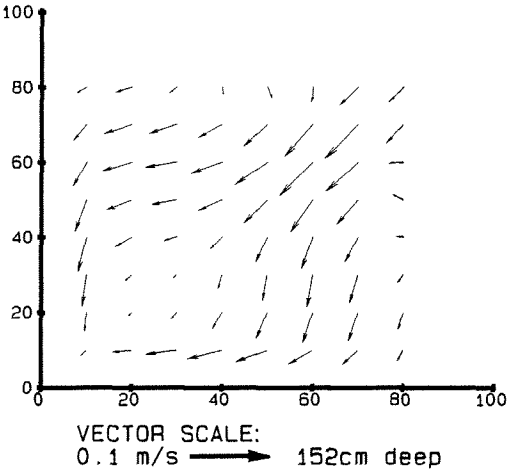

VECTOR SCALE:
0.1 m/s → 152cm deep

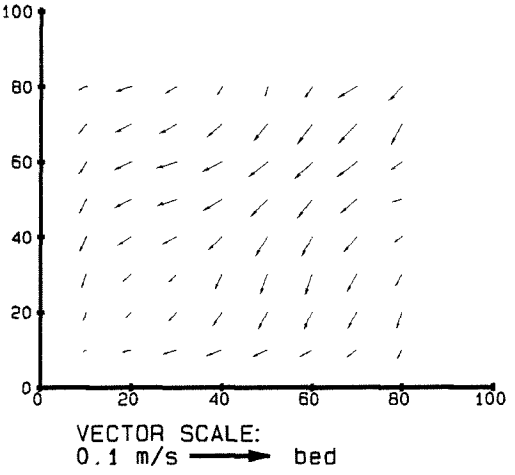

VECTOR SCALE:
0.1 m/s → bed

test basin 100m*100m dx*dy=10m*10m
v1
velocity vectors

fig 8.28

DELFT HYDRAULICS

fig-37

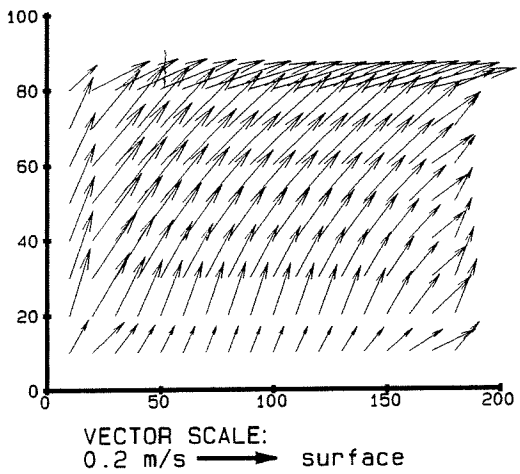

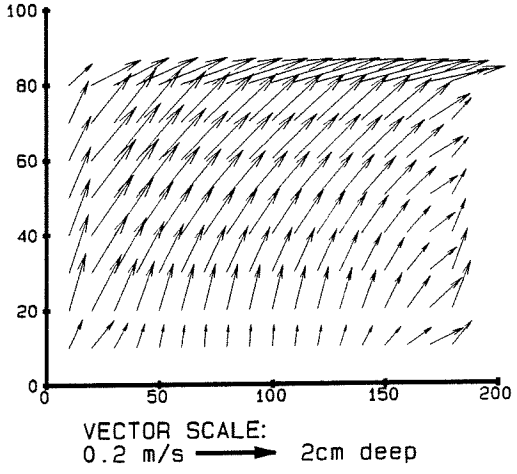

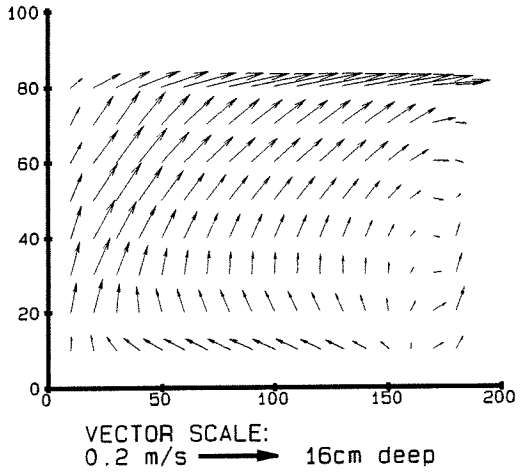

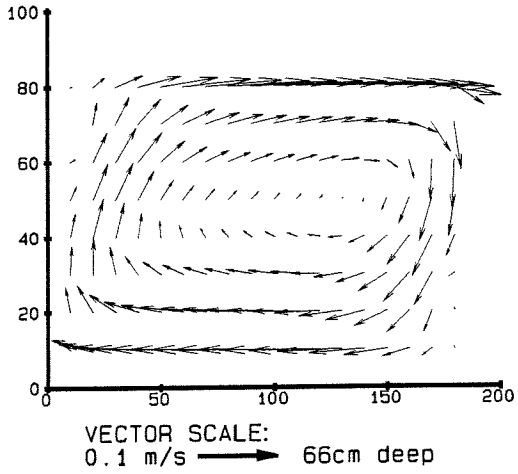

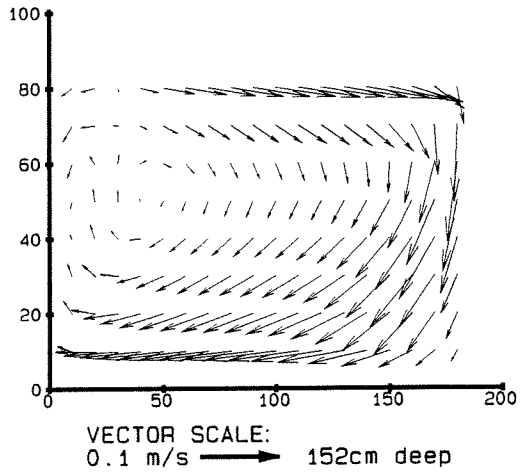

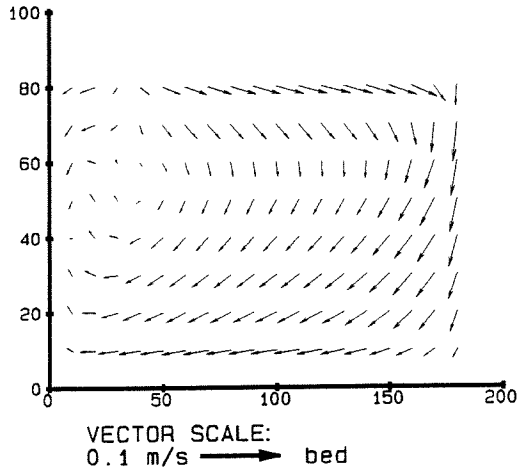

test basin 200m*100m, dx*dy=10m*10m
v2
velocity vectors

fig 8.29

DELFT HYDRAULICS

fig-38

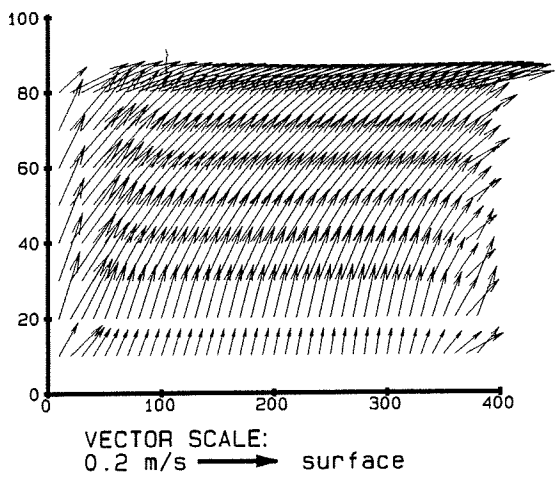

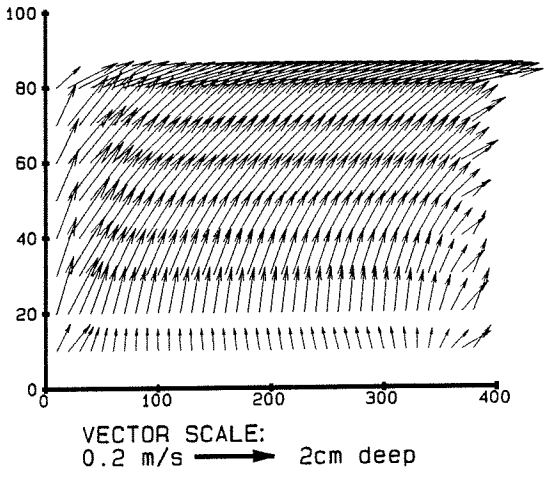

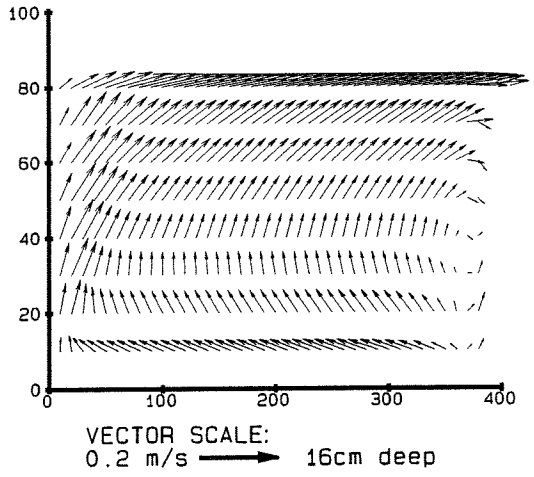

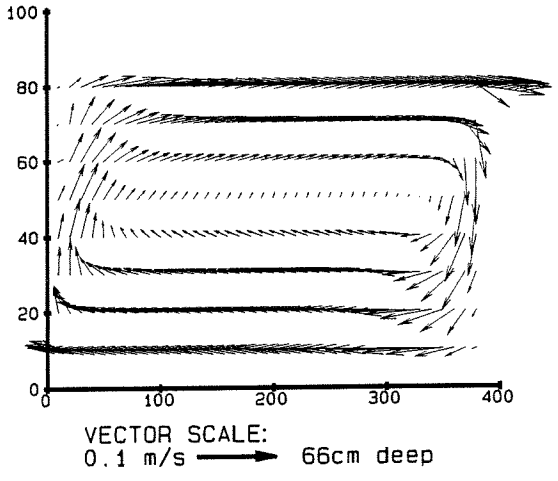

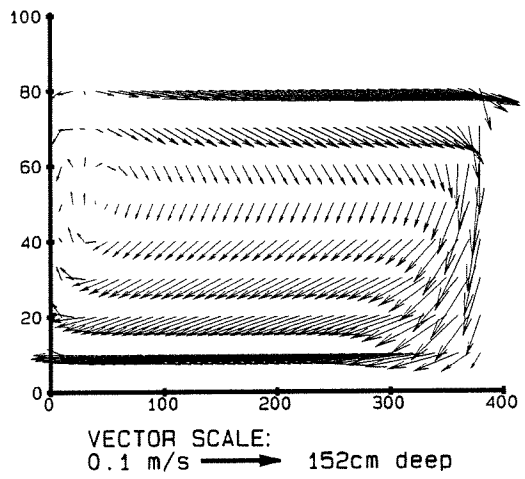

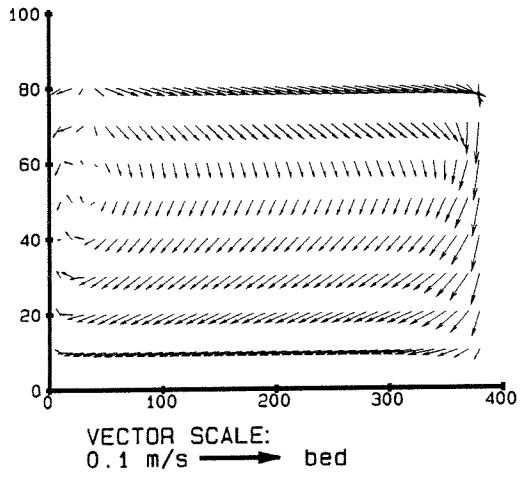

test basin 400m*100m, dx*dy=10m*10m
v3
velocity vectors

fig 8.30

DELFT HYDRAULICS

fig-39

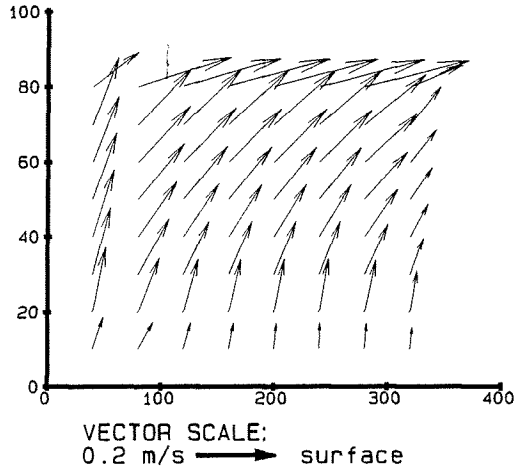

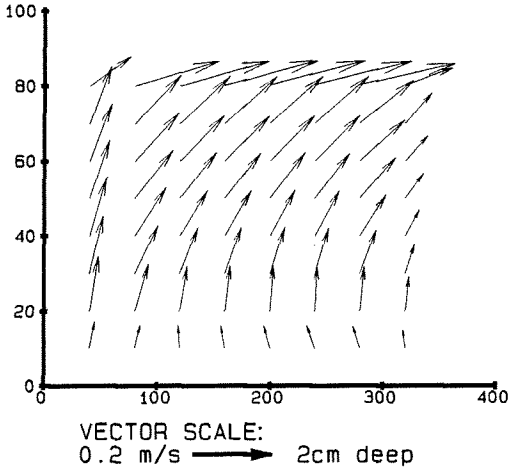

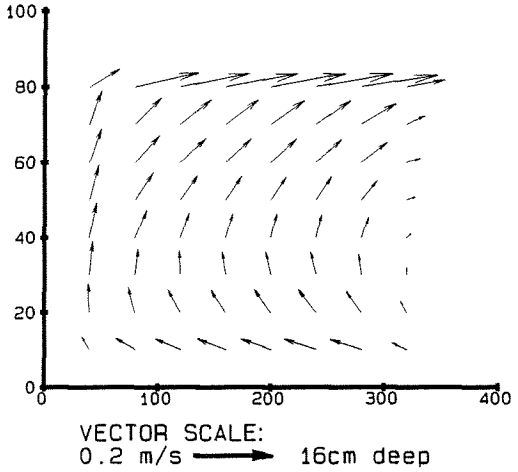

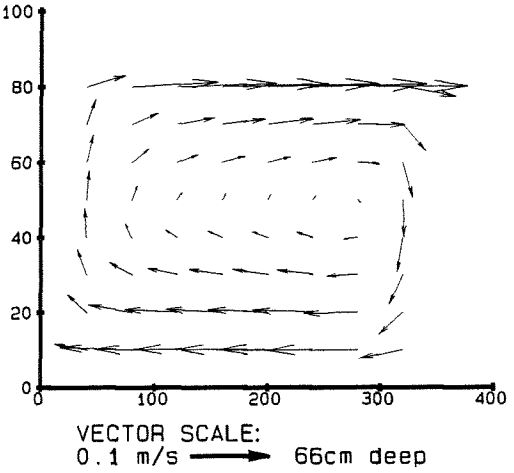

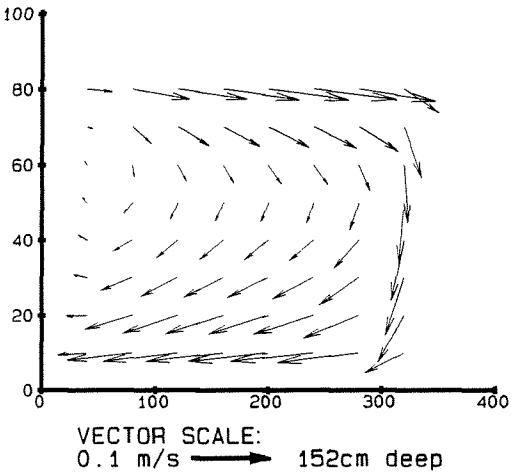

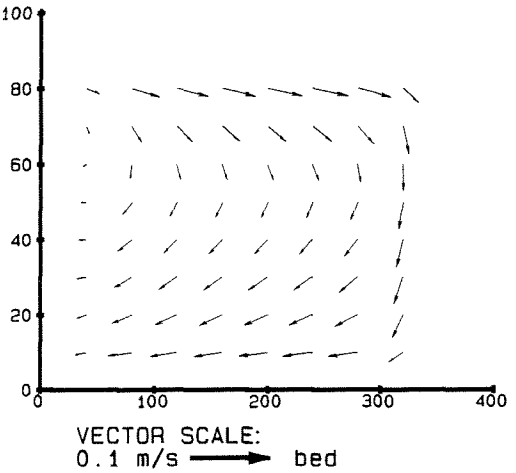

test basin 400m*100m, dx*dy=40m*10m
v4
velocity vectors

fig 8.31

DELFT HYDRAULICS

fig-40

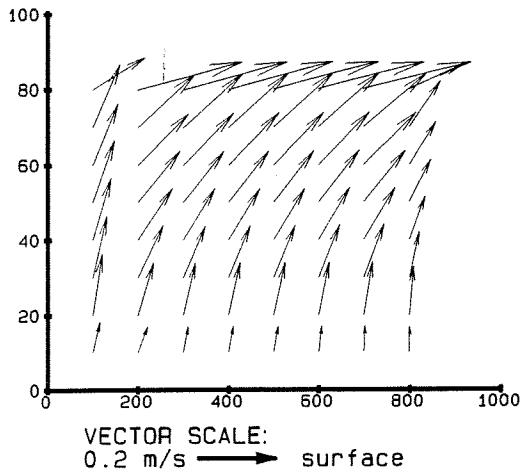

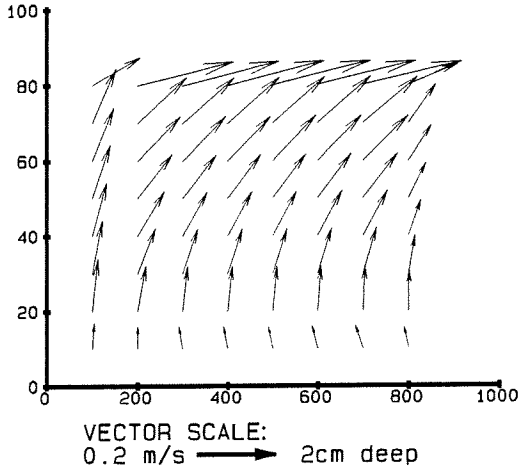

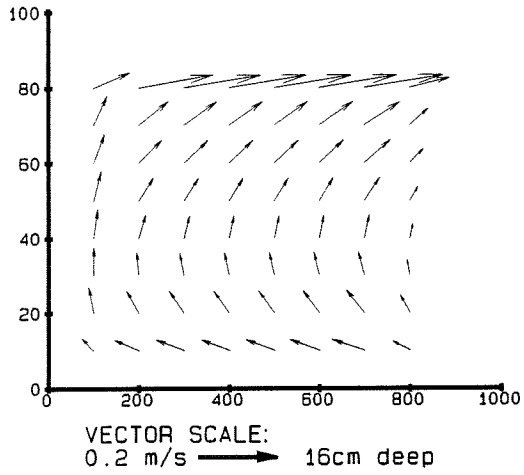

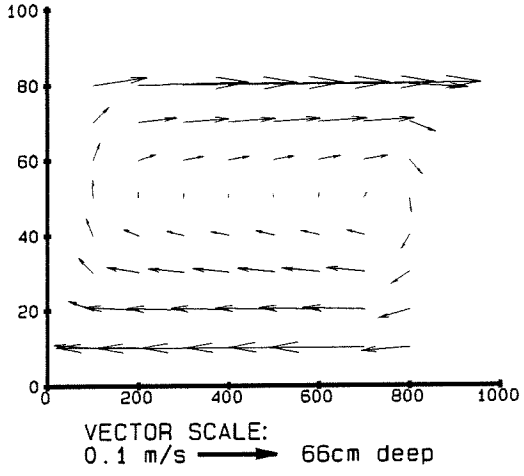

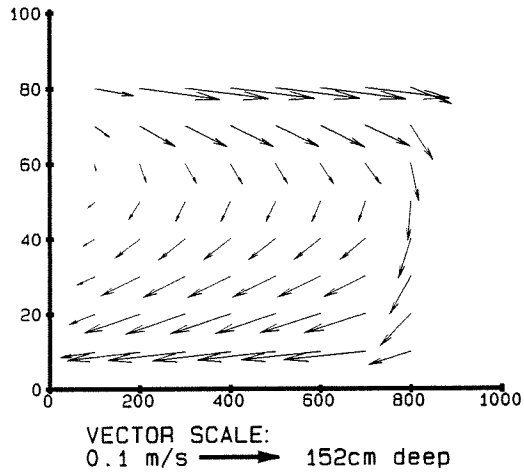

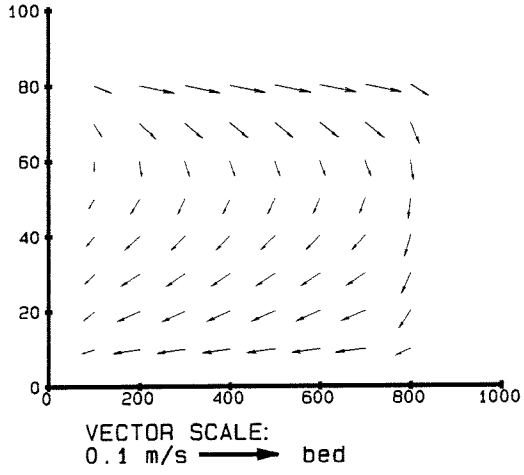

test basin 1000m*100m, dx*dy=100m*10m
v5
velocity vectors

fig 8.32

DELFT HYDRAULICS

fig-41

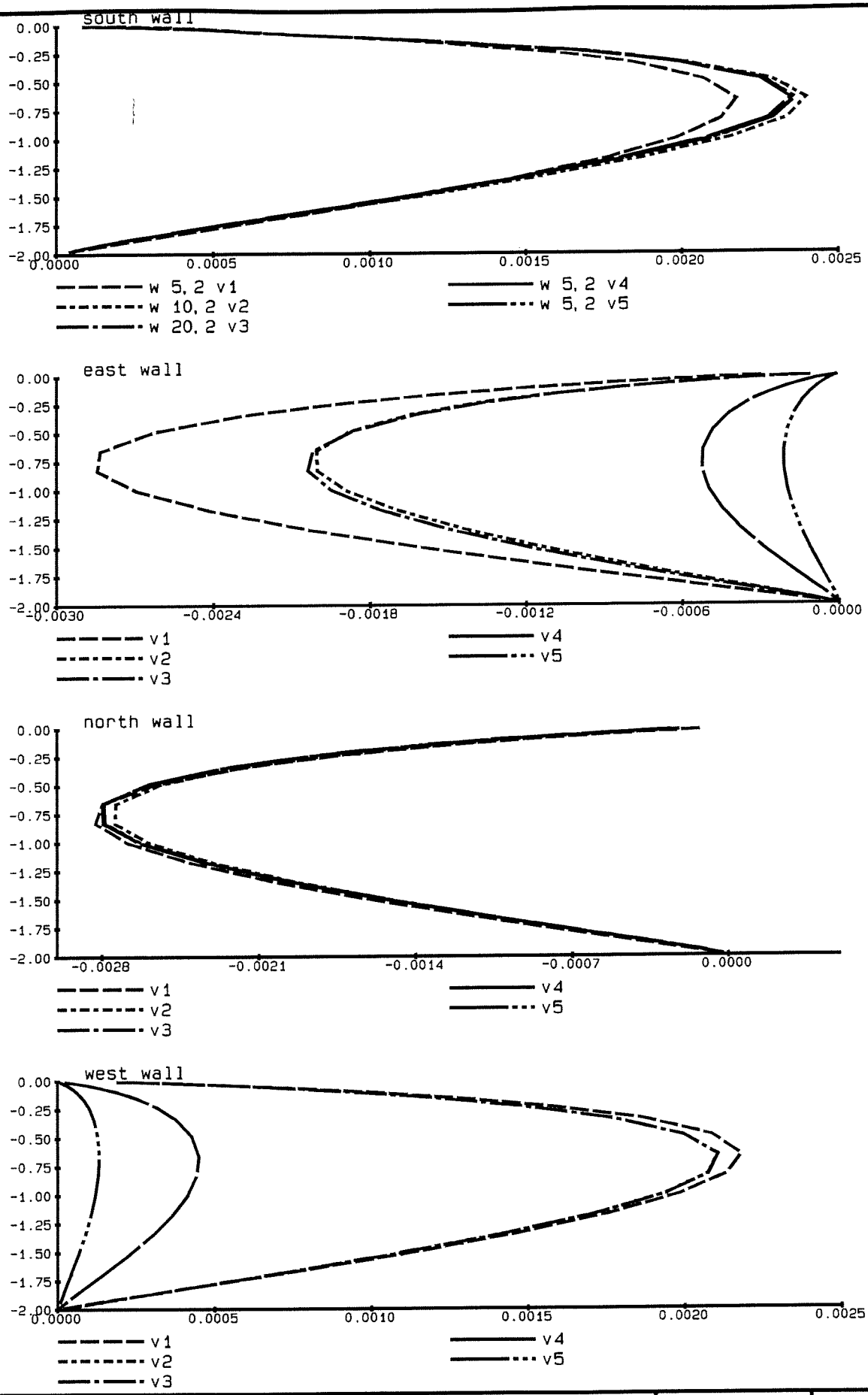

test basins		fig 8.33
velocities (w) [m/s] at closed boundaries		
DELFT HYDRAULICS		fig-42

fig 8.34a: test basin v1

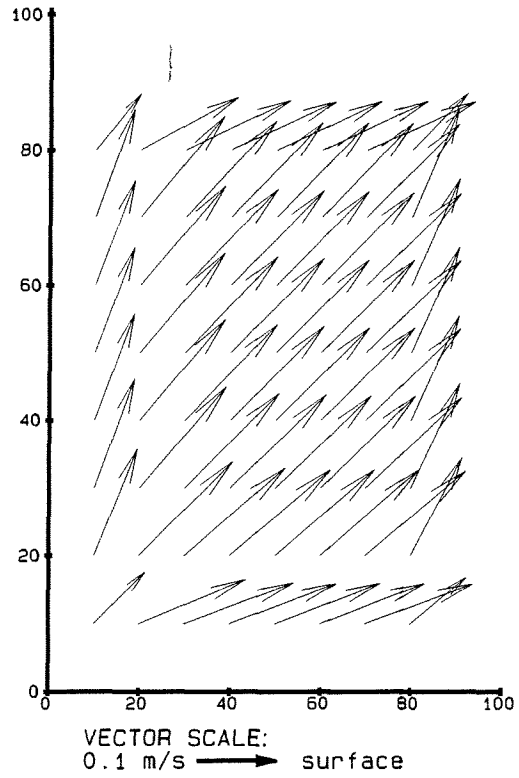

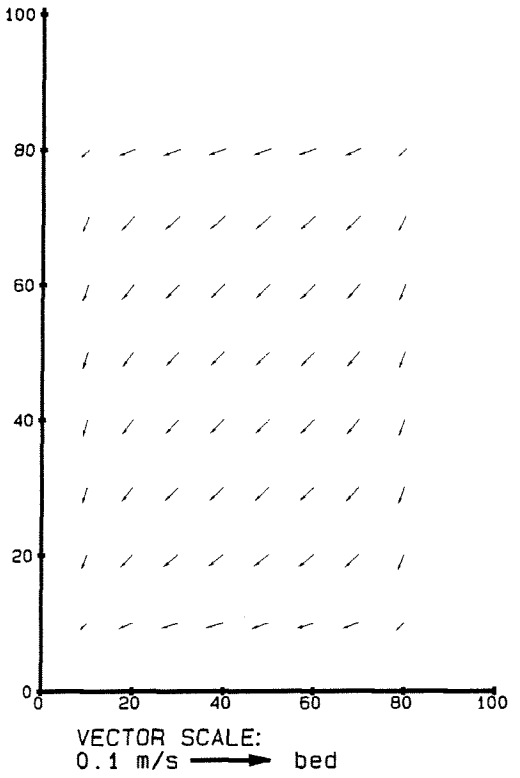

fig 8.34b: test basin v5

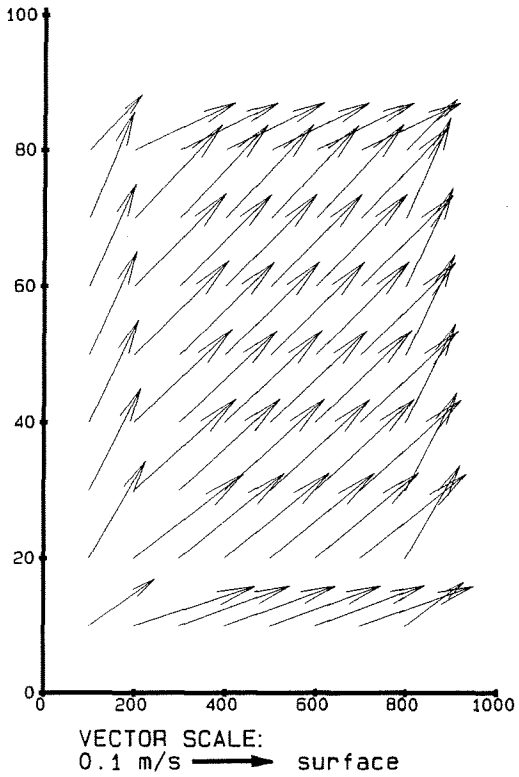

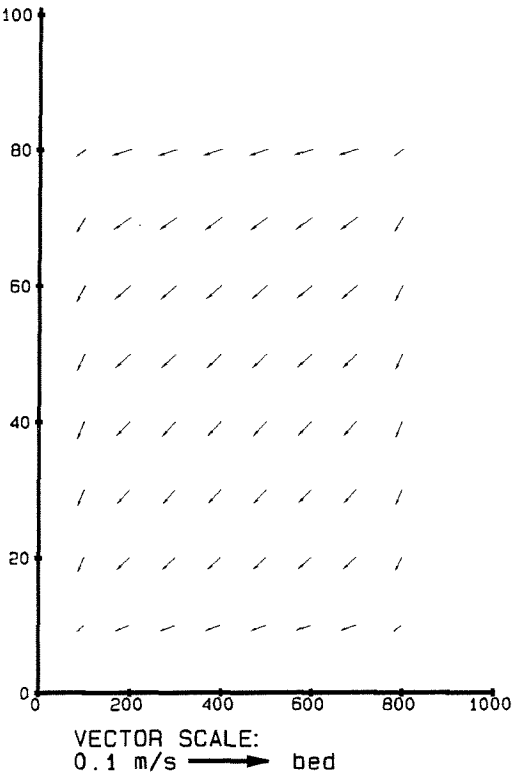

test basins v1 and v5 without vertical advection at closed boundaries velocity vectors at surface and bed		fig 8.34
DELFT HYDRAULICS		fig-43

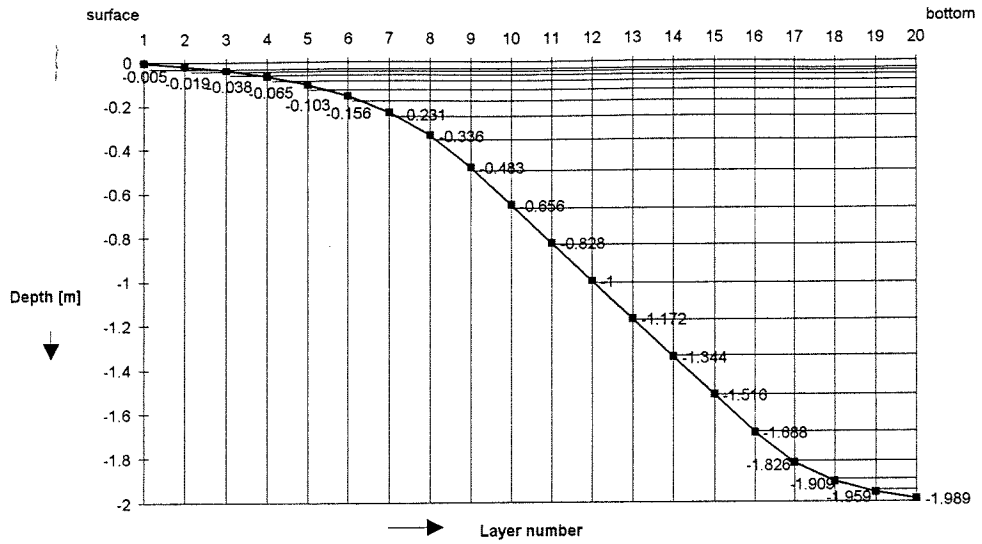

Figure 8.35: Vertical layer distribution nu8

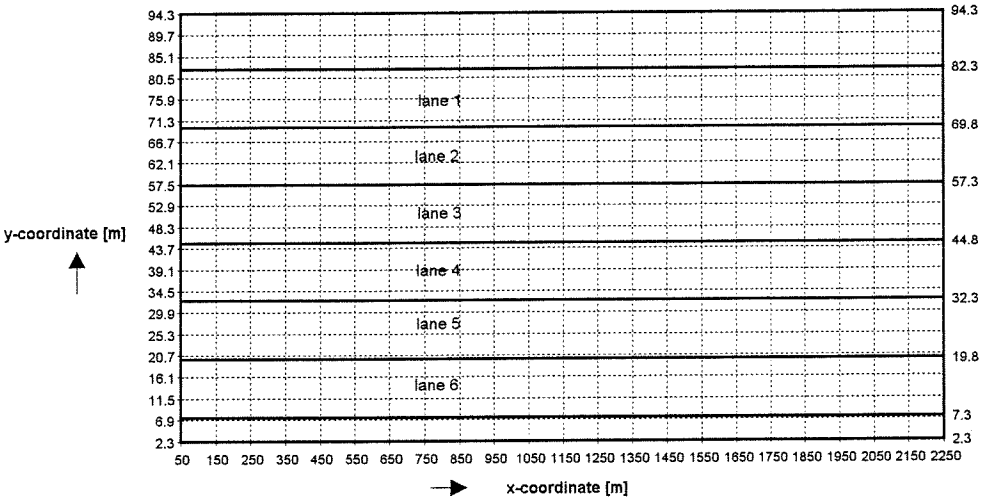

Figure 8.36: Grid coordinates Bosbaan

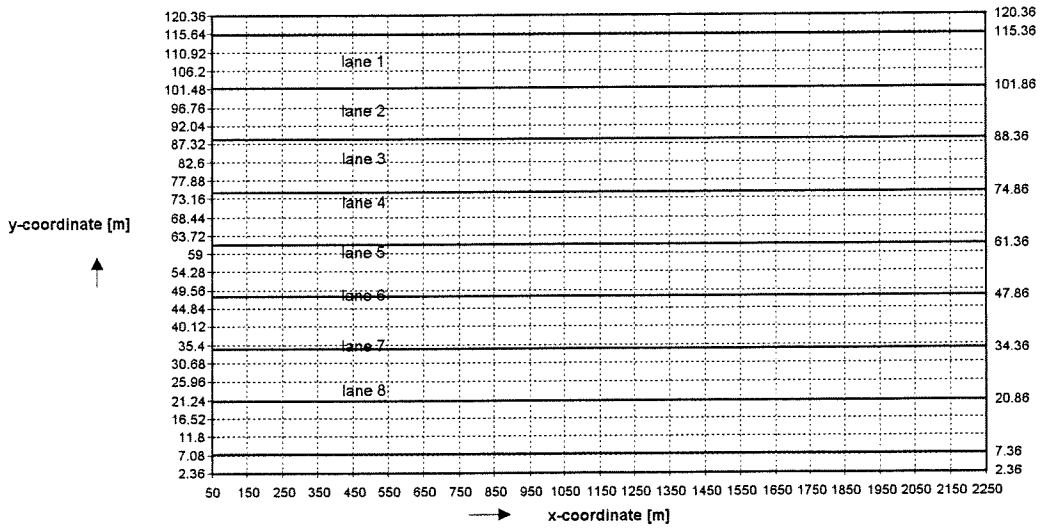

Figure 8.37: Grid coordinates widened Bosbaan

Table 2.2: Wind velocity coefficients [%], referring to wind at 10m at Schiphol

length of the course: distances from start: 250-1750 meters in steps of 250 m
width of the course: distances from north wall: 18.25 m (lane 1), 49.5 m (in between lane 3 and lane 4), and 80.75 m (lane 6)

wind dir. 0°

	18.25	49.5	80.75
250	16	19	26
500	31	29	26
750	0	1	18
1000	10	36	38
1250	17	18	23
1500	13	16	18
1750	14	16	7
mean	14.4	19.3	22.3

wind dir. 15°

	18.25	49.5	80.75
250	16	16	29
500	35	29	29
750	6	13	25
1000	29	43	35
1250	14	19	24
1500	12	18	24
1750	7	15	15
mean	17	21.9	25.9

wind dir. 30°

	18.25	49.5	80.75
250	21	29	45
500	35	29	34
750	15	27	38
1000	26	37	34
1250	22	25	28
1500	16	24	29
1750	18	25	22
mean	21.9	28	32.9

wind dir. 45°

	18.25	49.5	80.75
250	33	39	55
500	38	37	41
750	34	34	39
1000	27	39	35
1250	27	32	39
1500	27	35	42
1750	29	34	33
mean	30.7	35.7	40.6

wind dir. 60°

	18.25	49.5	80.75
250	36	40	56
500	38	40	45
750	37	37	42
1000	33	47	43
1250	36	40	47
1500	42	45	47
1750	42	46	44
mean	37.7	42.1	46.3

wind dir. 75°

	18.25	49.5	80.75
250	57	60	75
500	62	58	63
750	68	57	56
1000	52	66	55
1250	59	59	61
1500	64	65	61
1750	63	63	58
mean	60.7	61.1	61.3

wind dir. 90°

	18.25	49.5	80.75
250	37	35	41
500	45	39	36
750	45	35	37
1000	37	43	34
1250	44	34	27
1500	51	46	35
1750	47	46	39
mean	43.7	39.7	35.6

wind dir. 105°

	18.25	49.5	80.75
250	34	30	31
500	39	33	25
750	38	28	25
1000	35	41	25
1250	34	30	25
1500	46	40	29
1750	44	44	32
mean	38.6	35.1	27.4

wind dir. 120°

	18.25	49.5	80.75
250	30	27	30
500	29	23	18
750	34	26	19
1000	28	34	14
1250	30	28	17
1500	39	30	21
1750	39	37	25
mean	32.7	29.3	20.6

wind dir. 135°

	18.25	49.5	80.75
250	23	20	19
500	25	19	9
750	21	16	10
1000	21	22	3
1250	19	19	10
1500	26	23	11
1750	28	26	17
mean	23.3	20.7	11.3

wind dir. 150°

	18.25	49.5	80.75
250	14	11	13
500	18	16	5
750	15	11	7
1000	12	16	2
1250	16	15	6
1500	22	16	4
1750	21	17	0
mean	16.9	14.6	5.3

wind dir. 165°

	18.25	49.5	80.75
250	21	16	15
500	16	14	3
750	13	10	5
1000	17	19	3
1250	14	13	4
1500	17	14	9
1750	19	13	0
mean	16.7	14.1	5.6

wind dir. 180°

	18.25	49.5	80.75
250	21	17	15
500	16	14	5
750	11	8	4
1000	19	26	8
1250	17	15	6
1500	19	17	8
1750	20	13	0
mean	17.6	15.7	6.6

wind dir. 195°

	18.25	49.5	80.75
250	21	17	12
500	30	24	13
750	17	12	7
1000	23	30	17
1250	27	22	8
1500	22	19	14
1750	27	21	2
mean	23.9	20.7	10.4

wind dir. 210°

	18.25	49.5	80.75
250	30	24	16
500	34	29	23
750	28	22	20
1000	30	35	25
1250	30	25	14
1500	30	27	23
1750	33	30	12
mean	30.7	27.4	19

continuation table 2.2

wind dir. 225°

	18.25	49.5	80.75
250	31	27	24
500	40	34	30
750	40	29	27
1000	38	40	29
1250	38	34	26
1500	38	34	30
1750	43	38	25
mean	38.3	33.7	27.3

wind dir. 240°

	18.25	49.5	80.75
250	41	41	43
500	50	44	42
750	56	44	45
1000	50	55	43
1250	52	47	44
1500	50	50	48
1750	55	49	38
mean	50.6	47.1	43.3

wind dir. 255°

	18.25	49.5	80.75
250	49	49	62
500	66	61	63
750	76	62	64
1000	68	78	65
1250	70	71	72
1500	75	75	84
1750	73	77	69
mean	68.1	67.6	68.4

wind dir. 270°

	18.25	49.5	80.75
250	30	33	42
500	34	38	44
750	39	37	44
1000	35	49	46
1250	43	48	51
1500	47	48	54
1750	43	46	44
mean	38.7	42.7	46.4

wind dir. 285°

	18.25	49.5	80.75
250	24	29	44
500	34	34	38
750	37	36	41
1000	34	45	40
1250	43	42	45
1500	33	42	52
1750	36	40	41
mean	34.4	38.3	43

wind dir. 300°

	18.25	49.5	80.75
250	23	24	38
500	38	37	39
750	21	32	41
1000	40	50	42
1250	37	49	56
1500	33	32	37
1750	38	46	45
mean	32.9	38.6	42.6

wind dir. 315°

	18.25	49.5	80.75
250	20	25	32
500	33	29	30
750	3	18	28
1000	33	45	37
1250	17	27	30
1500	25	24	28
1750	21	28	30
mean	21.7	28	30.7

wind dir. 330°

	18.25	49.5	80.75
250	18	20	29
500	22	25	27
750	0	1	23
1000	9	34	32
1250	10	18	24
1500	24	21	24
1750	14	16	15
mean	13.9	19.3	24.9

wind dir. 345°

	18.25	49.5	80.75
250	14	17	25
500	17	17	18
750	0	0	15
1000	5	23	18
1250	23	25	27
1500	20	18	19
1750	8	12	4
mean	12.4	16	18

Table 2.3: Differences between average velocity coefficients in lane 1 and in lane 6 for all measured wind directions
The last column gives the differences in the rowing direction.

	Schiphol angle [°]	angle course axis [°]	difference Cu1-Cu6	*cos
north	0	30	-7.86	-6.8
	15	30	-8.86	-7.67
	30	30	-11	-9.53
	45	0	-9.86	-9.86
	60	0	-8.57	-8.57
	75	0	-0.57	-0.57
east	90	0	8.14	8.14
	105	0	11.14	11.14
	120	0	12.14	12.14
	135	0	12	12
	150	90	11.57	0
	165	90	11.14	0
south	180	240	11	5.5
	195	210	13.43	11.63
	210	180	11.71	11.71
	225	180	11	11
	240	180	7.29	7.29
	255	180	-0.29	-0.29
west	270	180	-7.71	-7.71
	285	180	-8.57	-8.57
	300	180	-9.71	-9.71
	315	180	-9	-9
	330	225	-11	-7.78
	345	270	-5.57	0

Table 2.4a : Wind velocities on lane 6 and lane 1 for north-east wind [m/s]

	45°,2.5m/s		45°,5m/s		45°,7.5m/s		45°,10m/s		45°,12.5m/s		45°,15m/s	
	lane 6	lane1	lane 6	lane1	lane 6	lane1	lane 6	lane1	lane 6	lane1	lane 6	lane1
100	-1.375	-0.8258	-2.75	-1.6515	-4.125	-2.4773	-5.5	-3.303	-6.875	-4.1288	-8.25	-4.9545
200	-1.375	-0.8258	-2.75	-1.6515	-4.125	-2.4773	-5.5	-3.303	-6.875	-4.1288	-8.25	-4.9545
300	-1.375	-0.8258	-2.75	-1.6515	-4.125	-2.4773	-5.5	-3.303	-6.875	-4.1288	-8.25	-4.9545
400	-1.305	-0.8505	-2.61	-1.701	-3.915	-2.5515	-5.22	-3.402	-6.525	-4.2525	-7.83	-5.103
500	-1.165	-0.9003	-2.33	-1.8005	-3.495	-2.7008	-4.66	-3.601	-5.825	-4.5013	-6.99	-5.4015
600	-1.025	-0.95	-2.05	-1.9	-3.075	-2.85	-4.1	-3.8	-5.125	-4.75	-6.15	-5.7
700	-1.005	-0.91	-2.01	-1.82	-3.015	-2.73	-4.02	-3.64	-5.025	-4.55	-6.03	-5.46
800	-0.985	-0.87	-1.97	-1.74	-2.955	-2.61	-3.94	-3.48	-4.925	-4.35	-5.91	-5.22
900	-0.955	-0.8153	-1.91	-1.6305	-2.865	-2.4458	-3.82	-3.261	-4.775	-4.0763	-5.73	-4.8915
1000	-0.915	-0.7458	-1.83	-1.4915	-2.745	-2.2373	-3.66	-2.983	-4.575	-3.7288	-5.49	-4.4745
1100	-0.875	-0.6765	-1.75	-1.353	-2.625	-2.0295	-3.5	-2.706	-4.375	-3.3825	-5.25	-4.059
1200	-0.915	-0.676	-1.83	-1.352	-2.745	-2.028	-3.66	-2.704	-4.575	-3.38	-5.49	-4.056
1300	-0.955	-0.6758	-1.91	-1.3515	-2.865	-2.0273	-3.82	-2.703	-4.775	-3.3788	-5.73	-4.0545
1400	-0.99	-0.6758	-1.98	-1.3515	-2.97	-2.0273	-3.96	-2.703	-4.95	-3.3788	-5.94	-4.0545
1500	-1.02	-0.6758	-2.04	-1.3515	-3.06	-2.0273	-4.08	-2.703	-5.1	-3.3788	-6.12	-4.0545
1600	-1.05	-0.676	-2.1	-1.352	-3.15	-2.028	-4.2	-2.704	-5.25	-3.38	-6.3	-4.056
1700	-0.96	-0.6958	-1.92	-1.3915	-2.88	-2.0873	-3.84	-2.783	-4.8	-3.4788	-5.76	-4.1745
1800	-0.87	-0.7158	-1.74	-1.4315	-2.61	-2.1473	-3.48	-2.863	-4.35	-3.5788	-5.22	-4.2945
1900	-0.825	-0.7255	-1.65	-1.451	-2.475	-2.1765	-3.3	-2.902	-4.125	-3.6275	-4.95	-4.353
2000	-0.825	-0.7255	-1.65	-1.451	-2.475	-2.1765	-3.3	-2.902	-4.125	-3.6275	-4.95	-4.353
mean	-1.0383	-0.7719	-2.0765	-1.5437	-3.1148	-2.3156	-4.153	-3.0875	-5.1913	-3.8593	-6.2295	-4.6312
v6-v1	-0.2664		-0.5328		-0.7992		-1.0656		-1.3319		-1.5983	

Table 2.4b: Wind velocities on lane 6 and lane 1 for south-east wind [m/s]

	120°,2.5m/s		120°,5m/s		120°,7.5m/s		120°,10m/s		120°,12.5m/s		120°,15m/s	
	lane 6	lane1	lane 6	lane1	lane 6	lane1	lane 6	lane1	lane 6	lane1	lane 6	lane1
100	-0.75	-0.7498	-1.5	-1.4995	-2.25	-2.2493	-3	-2.999	-3.75	-3.75	-4.5	-4.4985
200	-0.75	-0.7498	-1.5	-1.4995	-2.25	-2.2493	-3	-2.999	-3.75	-3.75	-4.5	-4.4985
300	-0.75	-0.7498	-1.5	-1.4995	-2.25	-2.2493	-3	-2.999	-3.75	-3.75	-4.5	-4.4985
400	-0.69	-0.7445	-1.38	-1.489	-2.07	-2.2335	-2.76	-2.978	-3.45	-3.725	-4.14	-4.467
500	-0.57	-0.7345	-1.14	-1.469	-1.71	-2.2035	-2.28	-2.938	-2.85	-3.675	-3.42	-4.407
600	-0.45	-0.7243	-0.9	-1.4485	-1.35	-2.1728	-1.8	-2.897	-2.25	-3.625	-2.7	-4.3455
700	-0.46	-0.7743	-0.92	-1.5485	-1.38	-2.3228	-1.84	-3.097	-2.3	-3.875	-2.76	-4.6455
800	-0.47	-0.824	-0.94	-1.648	-1.41	-2.472	-1.88	-3.296	-2.35	-4.125	-2.82	-4.944
900	-0.45	-0.8195	-0.9	-1.639	-1.35	-2.4585	-1.8	-3.278	-2.25	-4.1	-2.7	-4.917
1000	-0.4	-0.76	-0.8	-1.52	-1.2	-2.28	-1.6	-3.04	-2	-3.8	-2.4	-4.56
1100	-0.35	-0.7008	-0.7	-1.4015	-1.05	-2.1023	-1.4	-2.803	-1.75	-3.5	-2.1	-4.2045
1200	-0.38	-0.7203	-0.76	-1.4405	-1.14	-2.1608	-1.52	-2.881	-1.9	-3.6	-2.28	-4.3215
1300	-0.41	-0.74	-0.82	-1.48	-1.23	-2.22	-1.64	-2.96	-2.05	-3.7	-2.46	-4.44
1400	-0.445	-0.7945	-0.89	-1.589	-1.335	-2.3835	-1.78	-3.178	-2.225	-3.975	-2.67	-4.767
1500	-0.485	-0.8843	-0.97	-1.7685	-1.455	-2.6528	-1.94	-3.537	-2.425	-4.425	-2.91	-5.3055
1600	-0.525	-0.974	-1.05	-1.948	-1.575	-2.922	-2.1	-3.896	-2.625	-4.875	-3.15	-5.844
1700	-0.565	-0.9743	-1.13	-1.9485	-1.695	-2.9228	-2.26	-3.897	-2.825	-4.875	-3.39	-5.8455
1800	-0.605	-0.9745	-1.21	-1.949	-1.815	-2.9235	-2.42	-3.898	-3.025	-4.875	-3.63	-5.847
1900	-0.625	-0.9748	-1.25	-1.9495	-1.875	-2.9243	-2.5	-3.899	-3.125	-4.875	-3.75	-5.8485
2000	-0.625	-0.9748	-1.25	-1.9495	-1.875	-2.9243	-2.5	-3.899	-3.125	-4.875	-3.75	-5.8485
mean	-0.5378	-0.8171	-1.0755	-1.6342	-1.6133	-2.4513	-2.151	-3.2685	-2.6888	-4.0875	-3.2265	-4.9027
v6-v1	0.27936		0.55873		0.83809		1.11745		1.39875		1.67618	

Table 2.4c : Wind velocities on lane 6 and lane 1 for south-west wind [m/s]

	210°,2.5m/s		210°,5m/s		210°,7.5m/s		210°,10m/s		210°,12.5m/s		210°,15m/s	
	lane 6	lane1	lane 6	lane1	lane 6	lane1	lane 6	lane1	lane 6	lane1	lane 6	lane1
100	0.4	0.74925	0.8	1.4985	1.2	2.24775	1.6	2.997	2	3.74625	2.4	4.4955
200	0.4	0.74925	0.8	1.4985	1.2	2.24775	1.6	2.997	2	3.74625	2.4	4.4955
300	0.4	0.74925	0.8	1.4985	1.2	2.24775	1.6	2.997	2	3.74625	2.4	4.4955
400	0.435	0.76925	0.87	1.5385	1.305	2.30775	1.74	3.077	2.175	3.84625	2.61	4.6155
500	0.505	0.80925	1.01	1.6185	1.515	2.42775	2.02	3.237	2.525	4.04625	3.03	4.8555
600	0.575	0.8495	1.15	1.699	1.725	2.5485	2.3	3.398	2.875	4.2475	3.45	5.097
700	0.545	0.78925	1.09	1.5785	1.635	2.36775	2.18	3.157	2.725	3.94625	3.27	4.7355
800	0.515	0.72925	1.03	1.4585	1.545	2.18775	2.06	2.917	2.575	3.64625	3.09	4.3755
900	0.525	0.7095	1.05	1.419	1.575	2.1285	2.1	2.838	2.625	3.5475	3.15	4.257
1000	0.575	0.73	1.15	1.46	1.725	2.19	2.3	2.92	2.875	3.65	3.45	4.38
1100	0.625	0.7505	1.25	1.501	1.875	2.2515	2.5	3.002	3.125	3.7525	3.75	4.503
1200	0.515	0.75	1.03	1.5	1.545	2.25	2.06	3	2.575	3.75	3.09	4.5
1300	0.405	0.74975	0.81	1.4995	1.215	2.24925	1.62	2.999	2.025	3.74875	2.43	4.4985
1400	0.395	0.7495	0.79	1.499	1.185	2.2485	1.58	2.998	1.975	3.7475	2.37	4.497
1500	0.485	0.7495	0.97	1.499	1.455	2.2485	1.94	2.998	2.425	3.7475	2.91	4.497
1600	0.575	0.74975	1.15	1.4995	1.725	2.24925	2.3	2.999	2.875	3.74875	3.45	4.4985
1700	0.465	0.77975	0.93	1.5595	1.395	2.33925	1.86	3.119	2.325	3.89875	2.79	4.6785
1800	0.355	0.80975	0.71	1.6195	1.065	2.42925	1.42	3.239	1.775	4.04875	2.13	4.8585
1900	0.3	0.82475	0.6	1.6495	0.9	2.47425	1.2	3.299	1.5	4.12375	1.8	4.9485
2000	0.3	0.82475	0.6	1.6495	0.9	2.47425	1.2	3.299	1.5	4.12375	1.8	4.9485
mean	0.46475	0.76859	0.9295	1.53718	1.39425	2.30576	1.859	3.07435	2.32375	3.84294	2.7885	4.61153
v6-v1	-0.3038		-0.6077		-0.9115		-1.2154		-1.5192		-1.823	

Table 2.4d: Wind velocities on lane 6 and lane 1 for north-west wind [m/s]

	300°,2.5m/s		300°,5m/s		300°,7.5m/s		300°,10m/s		300°,12.5m/s		300°,15m/s	
	lane 6	lane1	lane 6	lane1	lane 6	lane1	lane 6	lane1	lane 6	lane1	lane 6	lane1
100	0.95	0.575	1.9	1.15	2.85	1.725	3.8	2.3	4.75	2.875	5.7	3.45
200	0.95	0.575	1.9	1.15	2.85	1.725	3.8	2.3	4.75	2.875	5.7	3.45
300	0.95	0.575	1.9	1.15	2.85	1.725	3.8	2.3	4.75	2.875	5.7	3.45
400	0.955	0.65	1.91	1.3	2.865	1.95	3.82	2.6	4.775	3.25	5.73	3.9
500	0.965	0.8	1.93	1.6	2.895	2.4	3.86	3.2	4.825	4	5.79	4.8
600	0.975	0.95	1.95	1.9	2.925	2.85	3.9	3.8	4.875	4.75	5.85	5.7
700	0.995	0.7805	1.99	1.561	2.985	2.3415	3.98	3.122	4.975	3.9025	5.97	4.683
800	1.015	0.611	2.03	1.222	3.045	1.833	4.06	2.444	5.075	3.055	6.09	3.666
900	1.03	0.62125	2.06	1.2425	3.09	1.86375	4.12	2.485	5.15	3.10625	6.18	3.7275
1000	1.04	0.81125	2.08	1.6225	3.12	2.43375	4.16	3.245	5.2	4.05625	6.24	4.8675
1100	1.05	1.00125	2.1	2.0025	3.15	3.00375	4.2	4.005	5.25	5.00625	6.3	6.0075
1200	1.19	0.97125	2.38	1.9425	3.57	2.91375	4.76	3.885	5.95	4.85625	7.14	5.8275
1300	1.33	0.9415	2.66	1.883	3.99	2.8245	5.32	3.766	6.65	4.7075	7.98	5.649
1400	1.305	0.90625	2.61	1.8125	3.915	2.71875	5.22	3.625	6.525	4.53125	7.83	5.4375
1500	1.115	0.8655	2.23	1.731	3.345	2.5965	4.46	3.462	5.575	4.3275	6.69	5.193
1600	0.925	0.825	1.85	1.65	2.775	2.475	3.7	3.3	4.625	4.125	5.55	4.95
1700	1.005	0.87525	2.01	1.7505	3.015	2.62575	4.02	3.501	5.025	4.37625	6.03	5.2515
1800	1.085	0.92575	2.17	1.8515	3.255	2.77725	4.34	3.703	5.425	4.62875	6.51	5.5545
1900	1.125	0.951	2.25	1.902	3.375	2.853	4.5	3.804	5.625	4.755	6.75	5.706
2000	1.125	0.951	2.25	1.902	3.375	2.853	4.5	3.804	5.625	4.755	6.75	5.706
mean	1.054	0.80814	2.108	1.61628	3.162	2.42441	4.216	3.23255	5.27	4.04069	6.324	4.84883
v6-v1	0.24586		0.49173		0.73759		0.98345		1.22931		1.47518	

Table 2.5a: Flow velocities on lane 6 and lane 1 for north-east wind [m/s]

	45°, 2.5m/s		45°, 5m/s		45°, 7.5m/s		45°, 10m/s		45°, 12.5m/s		45°, 15m/s	
	lane6	lane1	lane 6	lane1	lane6	lane1	lane 6	lane1	lane6	lane1	lane 6	lane1
100	-0.0216	-0.0013	-0.0468	0.00092	-0.072	0.00313	-0.098	0.00541	-0.1229	0.00739	-0.1495	0.00987
200	-0.0409	-0.0019	-0.0897	0.00261	-0.139	0.0078	-0.1895	0.0125	-0.2386	0.01737	-0.2902	0.02215
300	-0.0381	-0.0023	-0.0838	0.00086	-0.1311	0.00533	-0.1784	0.00809	-0.226	0.01243	-0.2737	0.01465
400	-0.0346	-0.0057	-0.075	-0.007	-0.1172	-0.0069	-0.1583	-0.0097	-0.2014	-0.0094	-0.2421	-0.0133
500	-0.0278	-0.0104	-0.0596	-0.0181	-0.0933	-0.0242	-0.1254	-0.0337	-0.1602	-0.0392	-0.1916	-0.05
600	-0.0219	-0.0144	-0.0465	-0.0271	-0.0728	-0.0387	-0.0982	-0.0529	-0.1255	-0.0638	-0.1509	-0.0791
700	-0.0203	-0.0148	-0.0429	-0.0282	-0.0671	-0.0408	-0.0912	-0.0551	-0.1163	-0.0673	-0.1409	-0.0824
800	-0.021	-0.0132	-0.0438	-0.0248	-0.0684	-0.0353	-0.0927	-0.0474	-0.1178	-0.0577	-0.1422	-0.0702
900	-0.0208	-0.0117	-0.0428	-0.021	-0.0659	-0.0294	-0.0887	-0.0388	-0.1115	-0.0467	-0.1337	-0.0564
1000	-0.0201	-0.0098	-0.0415	-0.0157	-0.0631	-0.0207	-0.085	-0.0264	-0.105	-0.0306	-0.1265	-0.0364
1100	-0.02	-0.0078	-0.0426	-0.0096	-0.065	-0.0103	-0.0889	-0.0115	-0.1091	-0.0114	-0.1336	-0.0123
1200	-0.0214	-0.0065	-0.0478	-0.0057	-0.0743	-0.0034	-0.1033	-0.0012	-0.128	0.00192	-0.1584	0.00464
1300	-0.0238	-0.006	-0.0537	-0.0043	-0.0846	-0.0011	-0.1178	0.00232	-0.1477	0.00627	-0.1826	0.01041
1400	-0.0255	-0.0052	-0.0571	-0.0031	-0.0902	0.00031	-0.125	0.00384	-0.1577	0.00801	-0.194	0.01234
1500	-0.0265	-0.0047	-0.0587	-0.0024	-0.0921	0.00104	-0.1271	0.00426	-0.1604	0.00844	-0.1965	0.01222
1600	-0.0265	-0.005	-0.0577	-0.0034	-0.0905	-0.0005	-0.1238	0.00163	-0.1566	0.00545	-0.1907	0.00776
1700	-0.0236	-0.007	-0.0511	-0.0079	-0.0802	-0.0071	-0.1093	-0.0076	-0.1386	-0.0057	-0.1683	-0.006
1800	-0.0196	-0.0094	-0.0418	-0.0136	-0.0655	-0.0158	-0.0897	-0.0194	-0.1137	-0.0203	-0.1388	-0.0232
1900	-0.0174	-0.0107	-0.0363	-0.0167	-0.0564	-0.0211	-0.078	-0.0262	-0.0986	-0.0291	-0.1212	-0.0333
2000	-0.0167	-0.0109	-0.0348	-0.0181	-0.0536	-0.0236	-0.0741	-0.03	-0.0935	-0.0339	-0.1149	-0.0395
mean	-0.0244	-0.0079	-0.0527	-0.0111	-0.0821	-0.0131	-0.1121	-0.0161	-0.1415	-0.0174	-0.172	-0.0204
v6-v1	-0.0165		-0.0416		-0.0691		-0.096		-0.1241		-0.1516	

Table 2.5b: Flow velocities on lane 6 and lane 1 for south-east wind [m/s]

	120°, 2.5m/s		120°, 5m/s		120°, 7.5m/s		120°, 10m/s		120°, 12.5m/s		120°, 15m/s	
	lane6	lane1	lane 6	lane1	lane6	lane1	lane 6	lane1	lane6	lane1	lane 6	lane1
100	-0.0084	-0.0084	-0.0158	-0.0156	-0.0239	-0.0236	-0.0327	-0.0323	-0.0408	-0.0405	-0.0498	-0.0496
200	-0.0149	-0.015	-0.0292	-0.0293	-0.0441	-0.0445	-0.0602	-0.0611	-0.0749	-0.0768	-0.0911	-0.0945
300	-0.0133	-0.0142	-0.0261	-0.0287	-0.0388	-0.0441	-0.0522	-0.0613	-0.0644	-0.0776	-0.0777	-0.0961
400	-0.0118	-0.0156	-0.0212	-0.032	-0.0303	-0.0499	-0.0395	-0.0701	-0.0479	-0.0888	-0.0568	-0.1103
500	-0.0079	-0.0169	-0.0119	-0.0361	-0.015	-0.0569	-0.0179	-0.08	-0.0205	-0.1013	-0.0232	-0.1253
600	-0.0052	-0.0181	-0.0024	-0.0398	0.0002	-0.0627	0.00307	-0.0879	0.00581	-0.1111	0.00893	-0.137
700	-0.0041	-0.0197	0.0024	-0.0432	0.00769	-0.0679	0.01343	-0.0947	0.01871	-0.1194	0.02469	-0.147
800	-0.003	-0.0213	0.00319	-0.046	0.00895	-0.0715	0.01525	-0.0992	0.02101	-0.1246	0.02761	-0.1528
900	-0.0028	-0.0213	0.00438	-0.0453	0.01102	-0.0699	0.01842	-0.0962	0.02532	-0.1201	0.03323	-0.1466
1000	-0.002	-0.0197	0.00665	-0.0417	0.01527	-0.0638	0.02492	-0.0871	0.03412	-0.1082	0.04455	-0.1314
1100	-0.0032	-0.0178	0.00953	-0.0386	0.02083	-0.0594	0.03335	-0.0813	0.04536	-0.101	0.05887	-0.1226
1200	-0.0035	-0.0179	0.01013	-0.0397	0.02284	-0.0623	0.03692	-0.0861	0.05049	-0.1078	0.06577	-0.1317
1300	-0.0023	-0.0191	0.00909	-0.0429	0.02167	-0.0683	0.03583	-0.0954	0.04957	-0.1204	0.06508	-0.1479
1400	-0.0025	-0.0207	0.00917	-0.0469	0.02144	-0.0748	0.03534	-0.1049	0.04902	-0.1326	0.06433	-0.1635
1500	-0.0019	-0.0233	0.00956	-0.0524	0.02127	-0.0828	0.03453	-0.1159	0.04765	-0.1465	0.06219	-0.1806
1600	-0.0013	-0.0257	0.009	-0.0567	0.01955	-0.0888	0.03189	-0.1239	0.04369	-0.1562	0.05713	-0.1922
1700	-0.0006	-0.026	0.00734	-0.0567	0.01675	-0.0884	0.02817	-0.1232	0.03879	-0.1551	0.0513	-0.1907
1800	-0.0013	-0.0252	0.00555	-0.055	0.0143	-0.0858	0.02501	-0.1195	0.03504	-0.1506	0.04692	-0.1853
1900	-0.0024	-0.0248	0.00446	-0.0545	0.01258	-0.0851	0.02258	-0.1187	0.03192	-0.1497	0.04299	-0.1844
2000	-0.0028	-0.0243	0.00243	-0.0533	0.00872	-0.083	0.01654	-0.1157	0.02362	-0.1458	0.03208	-0.1797
mean	-0.0048	-0.0197	-0.0007	-0.0427	0.00355	-0.0667	0.00864	-0.0927	0.01357	-0.1167	0.01935	-0.1435
v6-v1	0.01498		0.04203		0.07024		0.10137		0.13028		0.16281	

Table 2.5c : Flow velocities on lane 6 and lane 1 for south-west wind [m/s]

	210°, 2.5m/s		210°, 5m/s		210°, 7.5m/s		210°, 10m/s		210°, 12.5m/s		210°, 15m/s	
	lane6	lane1	lane 6	lane1	lane6	lane1	lane 6	lane1	lane6	lane1	lane 6	lane1
100	0.00279	0.00835	0.0039	0.01765	0.00466	0.02698	0.00574	0.03713	0.00687	0.04648	0.00807	0.05679
200	0.00454	0.01819	0.00266	0.03847	0.00123	0.05934	-9E-05	0.08222	-0.0011	0.10325	-0.0023	0.12654
300	0.00254	0.02011	-0.004	0.04254	-0.0097	0.06657	-0.0161	0.09299	-0.0219	0.1174	-0.0284	0.14448
400	0.00205	0.02058	-0.0048	0.04396	-0.0118	0.06941	-0.0197	0.09724	-0.0271	0.12318	-0.0353	0.15195
500	0.00365	0.02061	-0.0026	0.04492	-0.0087	0.07109	-0.0158	0.09958	-0.0226	0.12624	-0.0302	0.1559
600	0.00487	0.02071	0.00062	0.04596	-0.0037	0.07258	-0.0091	0.10144	-0.0142	0.12848	-0.0204	0.15865
700	0.00427	0.02037	0.00225	0.04473	-0.0013	0.07058	-0.0055	0.09857	-0.0098	0.1248	-0.0149	0.15408
800	0.00471	0.01927	0.00286	0.04111	-0.0003	0.06512	-0.004	0.09119	-0.0079	0.11567	-0.0125	0.14297
900	0.00738	0.01752	0.00481	0.03821	0.00286	0.06077	-0.0002	0.08554	-0.0034	0.10882	-0.0076	0.13482
1000	0.008	0.01627	0.00725	0.03643	0.00628	0.05808	0.00359	0.08212	0.00059	0.10469	-0.0035	0.12986
1100	0.00797	0.01605	0.00989	0.03429	0.01003	0.05429	0.00777	0.07694	0.00504	0.09818	0.00126	0.12157
1200	0.00698	0.01622	0.00749	0.03321	0.00621	0.05167	0.00251	0.07264	-0.0014	0.0922	-0.0065	0.11352
1300	0.00451	0.01761	-0.0002	0.03614	-0.0053	0.05569	-0.0122	0.07723	-0.0188	0.09716	-0.0268	0.11903
1400	0.00356	0.01912	-0.0044	0.04014	-0.0113	0.0621	-0.0193	0.08587	-0.027	0.10779	-0.036	0.1321
1500	0.0038	0.01925	-0.0025	0.04143	-0.0082	0.06473	-0.0148	0.08985	-0.0213	0.11317	-0.0287	0.13905
1600	0.006	0.01833	0.00362	0.04013	0.00066	0.06353	-0.0032	0.08887	-0.0074	0.11262	-0.0122	0.13897
1700	0.00623	0.01819	0.00333	0.04012	-0.0009	0.06417	-0.0063	0.09036	-0.012	0.11504	-0.0188	0.14248
1800	0.00408	0.01969	-0.0062	0.04393	-0.0166	0.07014	-0.0282	0.09855	-0.04	0.12521	-0.0531	0.15487
1900	0.00144	0.02177	-0.0149	0.0485	-0.0297	0.07656	-0.0461	0.10682	-0.0618	0.13477	-0.0792	0.16586
2000	-0.0004	0.02268	-0.0179	0.04984	-0.033	0.07756	-0.0495	0.10728	-0.0649	0.13428	-0.0819	0.16423
mean	0.00445	0.01855	-0.0004	0.04009	-0.0054	0.06305	-0.0115	0.08812	-0.0175	0.11147	-0.0245	0.13739
v6-v1	-0.0141		-0.0405		-0.0685		-0.0997		-0.129		-0.1618	

Table 2.5d: Flow velocities on lane 6 and lane 1 for north-west wind [m/s]

	300°, 2.5m/s		300°, 5m/s		300°, 7.5m/s		300°, 10m/s		300°, 12.5m/s		300°, 15m/s	
	lane6	lane1	lane 6	lane1	lane6	lane1	lane 6	lane1	lane6	lane1	lane 6	lane1
100	0.01072	0.00481	0.02231	0.00783	0.03365	0.01158	0.04584	0.01569	0.05705	0.01971	0.06948	0.02399
200	0.02335	0.007	0.049	0.01111	0.0746	0.01639	0.10213	0.02223	0.12736	0.02818	0.15542	0.0345
300	0.02582	0.0037	0.05537	0.00429	0.08566	0.00566	0.11831	0.00732	0.14822	0.00964	0.18158	0.01205
400	0.02621	0.00397	0.0576	0.00363	0.09044	0.0035	0.12585	0.00358	0.15875	0.00426	0.19529	0.00506
500	0.02493	0.00711	0.05563	0.00992	0.08826	0.01192	0.12387	0.01395	0.15721	0.01587	0.19431	0.01813
600	0.02196	0.01245	0.0484	0.02221	0.07739	0.03017	0.11025	0.03759	0.14117	0.04404	0.1753	0.05126
700	0.0203	0.01361	0.04267	0.02545	0.06723	0.03579	0.09611	0.04501	0.12422	0.05252	0.1548	0.06104
800	0.02257	0.00825	0.04759	0.01221	0.0732	0.01578	0.10259	0.01803	0.13107	0.01916	0.16261	0.02045
900	0.0261	0.00373	0.05653	0.00115	0.08719	-0.0019	0.12078	-0.0061	0.15229	-0.0105	0.18754	-0.0157
1000	0.02688	0.00472	0.05869	0.00357	0.09095	0.00106	0.12562	-0.0023	0.15784	-0.006	0.19375	-0.0106
1100	0.02373	0.01037	0.05148	0.01567	0.07983	0.01866	0.11005	0.02117	0.13795	0.02255	0.16879	0.02376
1200	0.02245	0.01306	0.04735	0.02104	0.07246	0.02637	0.09919	0.03117	0.12371	0.03487	0.15064	0.03865
1300	0.02719	0.01015	0.05716	0.01427	0.08642	0.01638	0.11758	0.01792	0.14617	0.01888	0.17784	0.01958
1400	0.03207	0.00676	0.0684	0.00695	0.1036	0.00622	0.14128	0.00494	0.17592	0.0033	0.21434	0.00129
1500	0.03114	0.0061	0.06757	0.00579	0.10298	0.00527	0.14115	0.00403	0.17607	0.00281	0.2149	0.00116
1600	0.02524	0.00844	0.05611	0.01128	0.08706	0.01357	0.12023	0.01563	0.15063	0.01767	0.18444	0.01931
1700	0.02147	0.01174	0.04816	0.01878	0.07657	0.02438	0.10668	0.02992	0.13467	0.03511	0.16542	0.04016
1800	0.02206	0.01322	0.0484	0.02214	0.07711	0.02888	0.10774	0.03504	0.13635	0.04073	0.16766	0.04642
1900	0.02368	0.01258	0.05049	0.02074	0.07914	0.02657	0.10992	0.03178	0.13871	0.03648	0.17005	0.04126
2000	0.02413	0.01137	0.05086	0.01859	0.07823	0.02385	0.10729	0.02895	0.13453	0.03353	0.1639	0.0384
mean	0.0241	0.00866	0.05199	0.01283	0.0806	0.01601	0.11162	0.01878	0.1405	0.02114	0.1724	0.02351
v6-v1	0.01544		0.03916		0.06459		0.09284		0.11936		0.14889	

Table 2.6: Travel times and lane differences for a four, wind + flow, just wind

wind direction 45°

	wind+flow: arrival times [s]		
wind vel.	lane 6	lane 1	T6-T1 [s]
0	390.37	390.37	0
2.5	395.47	393.6	1.87
5	401.5	397.01	4.49
7.5	408.4	400.75	7.65
10	416.16	404.99	11.17
12.5	424.86	409.61	15.25
15	434.58	414.79	19.79

wind direction 45°

	just wind: arrival times [s]		
wind vel.	lane 6	lane 1	T6-T1 [s]
0	390.37	390.37	0
2.5	394.3	393.23	1.07
5	398.98	396.46	2.52
7.5	404.43	400.13	4.3
10	410.74	404.24	6.5
12.5	417.91	408.75	9.16
15	426.03	413.8	12.23

wind direction 120°

	wind+flow: arrival times [s]		
wind vel.	lane 6	lane 1	T6-T1 [s]
0	390.37	390.37	0
2.5	392.58	394.34	-1.76
5	394.51	398.92	-4.41
7.5	396.65	404.01	-7.36
10	398.96	409.72	-10.76
12.5	401.53	415.88	-14.35
15	404.26	422.7	-18.44

wind direction 120°

	just wind: arrival times [s]		
wind vel.	lane 6	lane 1	T6-T1 [s]
0	390.37	390.37	0
2.5	392.34	393.43	-1.09
5	394.48	396.88	-2.4
7.5	396.82	400.82	-4
10	399.38	405.26	-5.88
12.5	402.15	410.21	-8.06
15	405.16	415.68	-10.52

wind direction 210°

	wind+flow: arrival times [s]		
wind vel.	lane 6	lane 1	T6-T1 [s]
0	390.37	390.37	0
2.5	388.69	387.11	1.58
5	387.57	384.06	3.51
7.5	386.59	381.33	5.26
10	385.81	378.88	6.93
12.5	385.17	376.88	8.29
15	384.73	375.1	9.63

wind direction 210°

	just wind: arrival times [s]		
wind vel.	lane 6	lane 1	T6-T1 [s]
0	390.37	390.37	0
2.5	388.91	387.99	0.92
5	387.54	385.98	1.56
7.5	386.33	384.33	2
10	385.28	383.04	2.24
12.5	384.33	382.17	2.16
15	383.56	381.63	1.93

wind direction 300°

	wind+flow: arrival times [s]		
wind vel.	lane 6	lane 1	T6-T1 [s]
0	390.37	390.37	0
2.5	386.05	387.47	-1.42
5	382.25	385.19	-2.94
7.5	379.14	383.38	-4.24
10	376.6	382.03	-5.43
12.5	374.77	381.14	-6.37
15	372.86	380.62	-7.76

wind direction 300°

	just wind: arrival times [s]		
wind vel.	lane 6	lane 1	T6-T1 [s]
0	390.37	390.37	0
2.5	387.2	387.89	-0.69
5	384.71	385.79	-1.08
7.5	382.94	384.14	-1.2
10	381.92	382.93	-1.01
12.5	381.48	382.15	-0.67
15	380.98	381.75	-0.77

Table 3.4: Wind velocity coefficients [%] widened course, referring to wind at 10m at Schiphol

length of the course: distances from start: 250-1750 meters in steps of 250 m
width of the course: distances from north wall: 18.25 m (lane 1), 49.5 m (in between lane 3 and lane 4), 80.75 m (lane 6), and 106.25 m (lane 8)

wind dir. 0°

	11.75	45.5	79.25	106.3
250	19	21	10	26
500	31	36	25	30
750	0	1	23	25
1000	10	35	34	25
1250	19	21	23	27
1500	12	17	20	24
1750	14	17	7	20
mean	15	21.14	20.29	25.29

wind dir. 15°

	11.75	45.5	79.25	106.3
250	19	20	10	25
500	37	31	27	30
750	6	12	24	28
1000	29	41	33	50
1250	17	21	21	26
1500	13	23	28	33
1750	8	18	18	31
mean	18.43	23.71	23	31.86

wind dir. 30°

	11.75	45.5	79.25	106.3
250	23	35	30	40
500	36	27	32	39
750	14	27	37	37
1000	25	38	33	52
1250	25	24	24	27
1500	18	26	30	35
1750	20	27	22	28
mean	23	29.14	29.71	36.86

wind dir. 45°

	11.75	45.5	79.25	106.3
250	33	39	41	47
500	38	37	41	44
750	37	37	42	38
1000	27	39	35	56
1250	30	34	41	43
1500	27	35	42	47
1750	32	37	36	41
mean	32	36.86	39.71	45.14

wind dir. 60°

	11.75	45.5	79.25	106.3
250	37	44	43	49
500	43	43	45	49
750	39	39	43	39
1000	33	45	41	61
1250	36	40	47	47
1500	39	44	48	49
1750	46	51	46	49
mean	39	43.71	44.71	49

wind dir. 75°

	11.75	45.5	79.25	106.3
250	61	63	59	60
500	64	60	65	62
750	68	57	56	48
1000	57	69	59	84
1250	59	60	66	64
1500	62	64	69	61
1750	60	64	67	66
mean	61.57	62.43	63	63.57

wind dir. 90°

	11.75	45.5	79.25	106.3
250	37	35	32	28
500	49	44	46	39
750	48	38	42	33
1000	38	45	40	44
1250	49	40	37	28
1500	50	47	47	36
1750	46	51	52	45
mean	45.29	42.86	42.29	36.14

wind dir. 105°

	11.75	45.5	79.25	106.3
250	35	34	22	18
500	41	33	30	19
750	43	31	30	23
1000	42	46	37	37
1250	37	34	33	23
1500	45	43	42	30
1750	46	50	39	42
mean	41.29	38.71	33.29	27.43

wind dir. 120°

	11.75	45.5	79.25	106.3
250	34	32	24	20
500	30	30	23	15
750	36	30	32	18
1000	31	35	26	23
1250	33	28	27	12
1500	39	36	27	18
1750	47	35	29	37
mean	35.71	32.29	26.86	20.43

wind dir. 135°

	11.75	45.5	79.25	106.3
250	26	21	10	10
500	33	26	20	8
750	25	15	19	2
1000	24	26	16	13
1250	25	17	18	12
1500	30	23	19	9
1750	30	25	17	27
mean	27.57	21.86	17	11.57

wind dir. 150°

	11.75	45.5	79.25	106.3
250	17	15	5	6
500	22	15	20	5
750	23	14	12	5
1000	16	18	9	8
1250	24	20	16	6
1500	24	20	17	4
1750	27	21	4	7
mean	21.86	17.57	11.86	5.857

wind dir. 165°

	11.75	45.5	79.25	106.3
250	24	22	9	8
500	24	16	12	2
750	15	10	15	4
1000	27	26	14	11
1250	16	14	13	5
1500	23	18	14	8
1750	27	21	10	5
mean	22.29	18.14	12.43	6.143

wind dir. 180°

	11.75	45.5	79.25	106.3
250	25	21	8	7
500	18	14	15	9
750	20	13	11	0
1000	24	27	18	13
1250	20	17	16	4
1500	20	16	15	8
1750	24	17	6	0
mean	21.57	17.86	12.71	5.857

wind dir. 195°

	11.75	45.5	79.25	106.3
250	25	22	4	0
500	32	28	20	4
750	17	17	14	3
1000	23	29	24	19
1250	34	31	14	5
1500	20	20	21	13
1750	30	29	6	5
mean	25.86	25.14	14.71	7

wind dir. 210°

	11.75	45.5	79.25	106.3
250	32	29	6	0
500	32	35	33	20
750	29	27	29	18
1000	34	37	31	41
1250	36	34	27	17
1500	35	32	28	24
1750	43	42	23	16
mean	34.43	33.71	25.29	19.43

continuation table 3.4

wind dir. 225°

	11.75	45.5	79.25	106.3
250	34	32	18	9
500	37	37	39	28
750	45	33	35	21
1000	38	39	26	34
1250	37	39	40	32
1500	42	36	30	24
1750	42	39	33	30
mean	39.29	36.43	31.57	25.43

wind dir. 240°

	11.75	45.5	79.25	106.3
250	41	45	39	36
500	52	48	49	45
750	60	51	56	42
1000	50	53	44	55
1250	50	49	55	51
1500	51	56	59	54
1750	56	55	50	42
mean	51.43	51	50.29	46.43

wind dir. 255°

	11.75	45.5	79.25	106.3
250	46	55	51	57
500	71	68	72	69
750	77	66	76	68
1000	72	79	70	94
1250	69	70	75	71
1500	78	73	87	80
1750	72	75	68	69
mean	69.29	69.43	71.29	72.57

wind dir. 270°

	11.75	45.5	79.25	106.3
250	31	35	27	29
500	34	37	41	41
750	42	40	46	43
1000	33	45	43	64
1250	42	48	51	52
1500	48	51	56	52
1750	43	45	43	46
mean	39	43	43.86	46.71

wind dir. 285°

	11.75	45.5	79.25	106.3
250	25	30	27	39
500	34	31	32	36
750	38	33	44	41
1000	36	47	42	61
1250	42	44	46	50
1500	32	42	48	53
1750	34	37	37	42
mean	34.43	37.71	39.43	46

wind dir. 300°

	11.75	45.5	79.25	106.3
250	27	27	22	35
500	38	39	42	45
750	23	31	38	40
1000	42	53	43	65
1250	39	51	57	62
1500	35	34	37	38
1750	41	45	41	55
mean	35	40	40	48.57

wind dir. 315°

	11.75	45.5	79.25	106.3
250	24	25	14	26
500	35	29	30	32
750	3	21	29	35
1000	33	47	39	55
1250	18	32	34	44
1500	27	24	26	32
1750	26	29	28	45
mean	23.71	29.57	28.57	38.43

wind dir. 330°

	11.75	45.5	79.25	106.3
250	19	18	8	18
500	22	28	25	29
750	0	2	26	27
1000	9	39	37	51
1250	12	21	28	34
1500	26	23	29	22
1750	18	16	14	24
mean	15.14	21	23.86	29.29

wind dir. 345°

	11.75	45.5	79.25	106.3
250	16	15	4	15
500	17	21	19	23
750	0	0	15	17
1000	5	24	15	31
1250	25	30	34	38
1500	19	16	17	17
1750	13	15	4	15
mean	13.57	17.29	15.43	22.29

Table 3.5a: Wind velocities on widened Bosbaan for north-east wind (45°) [m/s]

	45°,2.5m/s				45°, 5m/s				45°,7.5m/s			
	lane8	lane6	lane3	lane1	lane8	lane6	lane3	lane1	lane8	lane6	lane3	lane1
100	-1.175	-1.0305	-0.901	-0.831	2.35	2.061	1.802	1.662	-3.525	-3.0915	-2.703	-2.493
200	-1.175	-1.0305	-0.901	-0.831	2.35	2.061	1.802	1.662	-3.525	-3.0915	-2.703	-2.493
300	-1.175	-1.0305	-0.901	-0.831	2.35	2.061	1.802	1.662	-3.525	-3.0915	-2.703	-2.493
400	-1.16	-1.03	-0.90825	-0.8545	2.32	2.06	1.8165	1.709	-3.48	-3.09	-2.72475	-2.5635
500	-1.13	-1.02875	-0.92275	-0.90175	2.26	2.0575	1.8455	1.8035	-3.39	-3.08625	-2.76825	-2.70525
600	-1.1	-1.02775	-0.93725	-0.949	2.2	2.0555	1.8745	1.898	-3.3	-3.08325	-2.81175	-2.847
700	-1.04	-1.03525	-0.9325	-0.9395	2.08	2.0705	1.865	1.879	-3.12	-3.10575	-2.7975	-2.8185
800	-0.98	-1.0425	-0.9275	-0.92975	1.96	2.085	1.855	1.8595	-2.94	-3.1275	-2.7825	-2.78925
900	-1.04	-1.016	-0.90525	-0.8775	2.08	2.032	1.8105	1.755	-3.12	-3.048	-2.71575	-2.6325
1000	-1.22	-0.955	-0.866	-0.78225	2.44	1.91	1.732	1.5645	-3.66	-2.865	-2.598	-2.34675
1100	-1.4	-0.89425	-0.82675	-0.687	2.8	1.7885	1.6535	1.374	-4.2	-2.68275	-2.48025	-2.061
1200	-1.27	-0.94725	-0.81625	-0.71375	2.54	1.8945	1.6325	1.4275	-3.81	-2.84175	-2.44875	-2.14125
1300	-1.14	-1.00025	-0.80575	-0.7405	2.28	2.0005	1.6115	1.481	-3.42	-3.00075	-2.41725	-2.2215
1400	-1.095	-1.0325	-0.79575	-0.73975	2.19	2.065	1.5915	1.4795	-3.285	-3.0975	-2.38725	-2.21925
1500	-1.135	-1.0435	-0.786	-0.71125	2.27	2.087	1.572	1.4225	-3.405	-3.1305	-2.358	-2.13375
1600	-1.175	-1.0545	-0.77625	-0.683	2.35	2.109	1.5525	1.366	-3.525	-3.1635	-2.32875	-2.049
1700	-1.115	-0.9945	-0.811	-0.73175	2.23	1.989	1.622	1.4635	-3.345	-2.9835	-2.433	-2.19525
1800	-1.055	-0.9345	-0.84575	-0.7805	2.11	1.869	1.6915	1.561	-3.165	-2.8035	-2.53725	-2.3415
1900	-1.025	-0.9045	-0.86325	-0.805	2.05	1.809	1.7265	1.61	-3.075	-2.7135	-2.58975	-2.415
2000	-1.025	-0.9045	-0.86325	-0.805	2.05	1.809	1.7265	1.61	-3.075	-2.7135	-2.58975	-2.415
mean	-1.1315	-0.99685	-0.86463	-0.80624	2.263	1.9937	1.72925	1.612475	-3.3945	-2.99055	-2.59388	-2.41871
v8-v3	-0.26688				0.53375				-0.80063			
v6-v1	-0.19061				0.381225				-0.57184			

	45°,10m/s				45°,12.5m/s				45°,15m/s			
	lane8	lane6	lane3	lane1	lane8	lane6	lane3	lane1	lane8	lane6	lane3	lane1
100	4.7	4.122	3.604	3.324	-5.875	-5.1525	-4.505	-4.155	7.05	6.183	5.406	4.986
200	4.7	4.122	3.604	3.324	-5.875	-5.1525	-4.505	-4.155	7.05	6.183	5.406	4.986
300	4.7	4.122	3.604	3.324	-5.875	-5.1525	-4.505	-4.155	7.05	6.183	5.406	4.986
400	4.64	4.12	3.633	3.418	-5.8	-5.15	-4.54125	-4.2725	6.96	6.18	5.4495	5.127
500	4.52	4.115	3.691	3.607	-5.65	-5.14375	-4.61375	-4.50875	6.78	6.1725	5.5365	5.4105
600	4.4	4.111	3.749	3.796	-5.5	-5.13875	-4.68625	-4.745	6.6	6.1665	5.6235	5.694
700	4.16	4.141	3.73	3.758	-5.2	-5.17625	-4.6625	-4.6975	6.24	6.2115	5.595	5.637
800	3.92	4.17	3.71	3.719	-4.9	-5.2125	-4.6375	-4.64875	5.88	6.255	5.565	5.5785
900	4.16	4.064	3.621	3.51	-5.2	-5.08	-4.52625	-4.3875	6.24	6.096	5.4315	5.265
1000	4.88	3.82	3.464	3.129	-6.1	-4.775	-4.33	-3.91125	7.32	5.73	5.196	4.6935
1100	5.6	3.577	3.307	2.748	-7	-4.47125	-4.13375	-3.435	8.4	5.3655	4.9605	4.122
1200	5.08	3.789	3.265	2.855	-6.35	-4.73625	-4.08125	-3.56875	7.62	5.6835	4.8975	4.2825
1300	4.56	4.001	3.223	2.962	-5.7	-5.00125	-4.02875	-3.7025	6.84	6.0015	4.8345	4.443
1400	4.38	4.13	3.183	2.959	-5.475	-5.1625	-3.97875	-3.69875	6.57	6.195	4.7745	4.4385
1500	4.54	4.174	3.144	2.845	-5.675	-5.2175	-3.93	-3.55625	6.81	6.261	4.716	4.2675
1600	4.7	4.218	3.105	2.732	-5.875	-5.2725	-3.88125	-3.415	7.05	6.327	4.6575	4.098
1700	4.46	3.978	3.244	2.927	-5.575	-4.9725	-4.055	-3.65875	6.69	5.967	4.866	4.3905
1800	4.22	3.738	3.383	3.122	-5.275	-4.6725	-4.22875	-3.9025	6.33	5.607	5.0745	4.683
1900	4.1	3.618	3.453	3.22	-5.125	-4.5225	-4.31625	-4.025	6.15	5.427	5.1795	4.83
2000	4.1	3.618	3.453	3.22	-5.125	-4.5225	-4.31625	-4.025	6.15	5.427	5.1795	4.83
mean	4.526	3.9874	3.4585	3.22495	-5.6575	-4.98425	-4.32313	-4.03119	6.789	5.9811	5.18775	4.837425
v8-v3	1.0675				-1.33438				1.60125			
v6-v1	0.76245				-0.95306				1.143675			

Table 3.5b: Wind velocities on widened Bosbaan for south-east wind (120°) [m/s]

	120°,2.5m/s				120°, 5m/s				120°,7.5m/s			
	lane8	lane6	lane3	lane1	lane8	lane6	lane3	lane1	lane8	lane6	lane3	lane1
100	-0.5	-0.59625	-0.82475	-0.848	1	1.1925	1.6495	1.696	-1.5	-1.78875	-2.47425	-2.544
200	-0.5	-0.59625	-0.82475	-0.848	1	1.1925	1.6495	1.696	-1.5	-1.78875	-2.47425	-2.544
300	-0.5	-0.59625	-0.82475	-0.848	1	1.1925	1.6495	1.696	-1.5	-1.78875	-2.47425	-2.544
400	-0.475	-0.5905	-0.80975	-0.8285	0.95	1.181	1.6195	1.657	-1.425	-1.7715	-2.42925	-2.4855
500	-0.425	-0.57925	-0.78	-0.78925	0.85	1.1585	1.56	1.5785	-1.275	-1.73775	-2.34	-2.36775
600	-0.375	-0.56775	-0.75	-0.75	0.75	1.1355	1.5	1.5	-1.125	-1.70325	-2.25	-2.25
700	-0.405	-0.6555	-0.77975	-0.8075	0.81	1.311	1.5595	1.615	-1.215	-1.9665	-2.33925	-2.4225
800	-0.435	-0.74325	-0.80925	-0.86525	0.87	1.4865	1.6185	1.7305	-1.305	-2.22975	-2.42775	-2.59575
900	-0.475	-0.75925	-0.8245	-0.871	0.95	1.5185	1.649	1.742	-1.425	-2.27775	-2.4735	-2.613
1000	-0.525	-0.70325	-0.825	-0.825	1.05	1.4065	1.65	1.65	-1.575	-2.10975	-2.475	-2.475
1100	-0.575	-0.64725	-0.8255	-0.779	1.15	1.2945	1.651	1.558	-1.725	-1.94175	-2.4765	-2.337
1200	-0.465	-0.65275	-0.8	-0.7955	0.93	1.3055	1.6	1.591	-1.395	-1.95825	-2.4	-2.3865
1300	-0.355	-0.6585	-0.7745	-0.81175	0.71	1.317	1.549	1.6235	-1.065	-1.9755	-2.3235	-2.43525
1400	-0.33	-0.66225	-0.79675	-0.8505	0.66	1.3245	1.5935	1.701	-0.99	-1.98675	-2.39025	-2.5515
1500	-0.39	-0.6645	-0.867	-0.91125	0.78	1.329	1.734	1.8225	-1.17	-1.9935	-2.601	-2.73375
1600	-0.45	-0.66675	-0.937	-0.972	0.9	1.3335	1.874	1.944	-1.35	-2.00025	-2.811	-2.916
1700	-0.64	-0.693	-0.9715	-1.0485	1.28	1.386	1.943	2.097	-1.92	-2.079	-2.9145	-3.1455
1800	-0.83	-0.71925	-1.006	-1.125	1.66	1.4385	2.012	2.25	-2.49	-2.15775	-3.018	-3.375
1900	-0.925	-0.73225	-1.02325	-1.163	1.85	1.4645	2.0465	2.326	-2.775	-2.19675	-3.06975	-3.489
2000	-0.925	-0.73225	-1.02325	-1.163	1.85	1.4645	2.0465	2.326	-2.775	-2.19675	-3.06975	-3.489
mean	-0.525	-0.66081	-0.85386	-0.895	1.05	1.321625	1.707725	1.79	-1.575	-1.98244	-2.56159	-2.685
v8-v3	0.328863				-0.65773				0.986588			
v6-v1	0.234188				-0.46838				0.702562			

	120°,10m/s				120°,12.5m/s				120°,15m/s			
	lane8	lane6	lane3	lane1	lane8	lane6	lane3	lane1	lane8	lane6	lane3	lane1
100	2	2.385	3.299	3.392	-2.5	-2.98125	-4.12375	-4.24	3	3.5775	4.9485	5.088
200	2	2.385	3.299	3.392	-2.5	-2.98125	-4.12375	-4.24	3	3.5775	4.9485	5.088
300	2	2.385	3.299	3.392	-2.5	-2.98125	-4.12375	-4.24	3	3.5775	4.9485	5.088
400	1.9	2.362	3.239	3.314	-2.375	-2.9525	-4.04875	-4.1425	2.85	3.543	4.8585	4.971
500	1.7	2.317	3.12	3.157	-2.125	-2.89625	-3.9	-3.94625	2.55	3.4755	4.68	4.7355
600	1.5	2.271	3	3	-1.875	-2.83875	-3.75	-3.75	2.25	3.4065	4.5	4.5
700	1.62	2.622	3.119	3.23	-2.025	-3.2775	-3.89875	-4.0375	2.43	3.933	4.6785	4.845
800	1.74	2.973	3.237	3.461	-2.175	-3.71625	-4.04625	-4.32625	2.61	4.4595	4.8555	5.1915
900	1.9	3.037	3.298	3.484	-2.375	-3.79625	-4.1225	-4.355	2.85	4.5555	4.947	5.226
1000	2.1	2.813	3.3	3.3	-2.625	-3.51625	-4.125	-4.125	3.15	4.2195	4.95	4.95
1100	2.3	2.589	3.302	3.116	-2.875	-3.23625	-4.1275	-3.895	3.45	3.8835	4.953	4.674
1200	1.86	2.611	3.2	3.182	-2.325	-3.26375	-4	-3.9775	2.79	3.9165	4.8	4.773
1300	1.42	2.634	3.098	3.247	-1.775	-3.2925	-3.8725	-4.05875	2.13	3.951	4.647	4.8705
1400	1.32	2.649	3.187	3.402	-1.65	-3.31125	-3.98375	-4.2525	1.98	3.9735	4.7805	5.103
1500	1.56	2.658	3.468	3.645	-1.95	-3.3225	-4.335	-4.55625	2.34	3.987	5.202	5.4675
1600	1.8	2.667	3.748	3.888	-2.25	-3.33375	-4.685	-4.86	2.7	4.0005	5.622	5.832
1700	2.56	2.772	3.886	4.194	-3.2	-3.465	-4.8575	-5.2425	3.84	4.158	5.829	6.291
1800	3.32	2.877	4.024	4.5	-4.15	-3.59625	-5.03	-5.625	4.98	4.3155	6.036	6.75
1900	3.7	2.929	4.093	4.652	-4.625	-3.66125	-5.11625	-5.815	5.55	4.3935	6.1395	6.978
2000	3.7	2.929	4.093	4.652	-4.625	-3.66125	-5.11625	-5.815	5.55	4.3935	6.1395	6.978
mean	2.1	2.64325	3.41545	3.58	-2.625	-3.30406	-4.26931	-4.475	3.15	3.964875	5.123175	5.37
v8-v3	-1.31545				1.644313				-1.97318			
v6-v1	-0.93675				1.170938				-1.40513			

Table 3.5c: Wind velocities on widened Bosbaan for south-west wind (210°) [m/s]

	210°,2.5m/s				210°, 5m/s				210°,7.5m/s			
	lane8	lane6	lane3	lane1	lane8	lane6	lane3	lane1	lane8	lane6	lane3	lane1
100	0	0.1445	0.762	0.797	0	0.289	1.524	1.594	0	0.4335	2.286	2.391
200	0	0.1445	0.762	0.797	0	0.289	1.524	1.594	0	0.4335	2.286	2.391
300	0	0.1445	0.762	0.797	0	0.289	1.524	1.594	0	0.4335	2.286	2.391
400	0.1	0.27825	0.77725	0.79825	0.2	0.5565	1.5545	1.5965	0.3	0.83475	2.33175	2.39475
500	0.3	0.54575	0.8075	0.8005	0.6	1.0915	1.615	1.601	0.9	1.63725	2.4225	2.4015
600	0.5	0.813	0.838	0.803	1	1.626	1.676	1.606	1.5	2.439	2.514	2.409
700	0.48	0.77375	0.78275	0.771	0.96	1.5475	1.5655	1.542	1.44	2.32125	2.34825	2.313
800	0.46	0.7345	0.72725	0.739	0.92	1.469	1.4545	1.478	1.38	2.2035	2.18175	2.217
900	0.565	0.72875	0.73725	0.749	1.13	1.4575	1.4745	1.498	1.695	2.18625	2.21175	2.247
1000	0.795	0.7565	0.81275	0.801	1.59	1.513	1.6255	1.602	2.385	2.2695	2.43825	2.403
1100	1.025	0.78425	0.888	0.853	2.05	1.5685	1.776	1.706	3.075	2.35275	2.664	2.559
1200	0.785	0.73675	0.88275	0.871	1.57	1.4735	1.7655	1.742	2.355	2.21025	2.64825	2.613
1300	0.545	0.6895	0.87725	0.889	1.09	1.379	1.7545	1.778	1.635	2.0685	2.63175	2.667
1400	0.46	0.672	0.86725	0.89275	0.92	1.344	1.7345	1.7855	1.38	2.016	2.60175	2.67825
1500	0.53	0.68425	0.852	0.8825	1.06	1.3685	1.704	1.765	1.59	2.05275	2.556	2.6475
1600	0.6	0.69625	0.837	0.872	1.2	1.3925	1.674	1.744	1.8	2.08875	2.511	2.616
1700	0.52	0.64525	0.92725	0.95275	1.04	1.2905	1.8545	1.9055	1.56	1.93575	2.78175	2.85825
1800	0.44	0.59425	1.01725	1.0335	0.88	1.1885	2.0345	2.067	1.32	1.78275	3.05175	3.1005
1900	0.4	0.5685	1.06225	1.074	0.8	1.137	2.1245	2.148	1.2	1.7055	3.18675	3.222
2000	0.4	0.5685	1.06225	1.074	0.8	1.137	2.1245	2.148	1.2	1.7055	3.18675	3.222
mean	0.44525	0.58518	0.8521	0.86236	0.8905	1.17035	1.7042	1.72473	1.33575	1.75553	2.5563	2.58709
v8-v3	-0.40685				-0.8137				-1.22055			
v6-v1	-0.27719				-0.55438				-0.83156			

	210°, 10m/s				210°,12.5m/s				210°, 15m/s			
	lane8	lane6	lane3	lane1	lane8	lane6	lane3	lane1	lane8	lane6	lane3	lane1
100	0	0.578	3.048	3.188	0	0.7225	3.81	3.985	0	0.867	4.572	4.782
200	0	0.578	3.048	3.188	0	0.7225	3.81	3.985	0	0.867	4.572	4.782
300	0	0.578	3.048	3.188	0	0.7225	3.81	3.985	0	0.867	4.572	4.782
400	0.4	1.113	3.109	3.193	0.5	1.39125	3.88625	3.99125	0.6	1.6695	4.6635	4.7895
500	1.2	2.183	3.23	3.202	1.5	2.72875	4.0375	4.0025	1.8	3.2745	4.845	4.803
600	2	3.252	3.352	3.212	2.5	4.065	4.19	4.015	3	4.878	5.028	4.818
700	1.92	3.095	3.131	3.084	2.4	3.86875	3.91375	3.855	2.88	4.6425	4.6965	4.626
800	1.84	2.938	2.909	2.956	2.3	3.6725	3.63625	3.695	2.76	4.407	4.3635	4.434
900	2.26	2.915	2.949	2.996	2.825	3.64375	3.68625	3.745	3.39	4.3725	4.4235	4.494
1000	3.18	3.026	3.251	3.204	3.975	3.7825	4.06375	4.005	4.77	4.539	4.8765	4.806
1100	4.1	3.137	3.552	3.412	5.125	3.92125	4.44	4.265	6.15	4.7055	5.328	5.118
1200	3.14	2.947	3.531	3.484	3.925	3.68375	4.41375	4.355	4.71	4.4205	5.2965	5.226
1300	2.18	2.758	3.509	3.556	2.725	3.4475	4.38625	4.445	3.27	4.137	5.2635	5.334
1400	1.84	2.688	3.469	3.571	2.3	3.36	4.33625	4.46375	2.76	4.032	5.2035	5.3565
1500	2.12	2.737	3.408	3.53	2.65	3.42125	4.26	4.4125	3.18	4.1055	5.112	5.295
1600	2.4	2.785	3.348	3.488	3	3.48125	4.185	4.36	3.6	4.1775	5.022	5.232
1700	2.08	2.581	3.709	3.811	2.6	3.22625	4.63625	4.76375	3.12	3.8715	5.5635	5.7165
1800	1.76	2.377	4.069	4.134	2.2	2.97125	5.08625	5.1675	2.64	3.5655	6.1035	6.201
1900	1.6	2.274	4.249	4.296	2	2.8425	5.31125	5.37	2.4	3.411	6.3735	6.444
2000	1.6	2.274	4.249	4.296	2	2.8425	5.31125	5.37	2.4	3.411	6.3735	6.444
mean	1.781	2.3407	3.4084	3.44945	2.22625	2.92588	4.2605	4.31181	2.6715	3.51105	5.1126	5.17418
v8-v3	-1.6274				-2.03425				-2.4411			
v6-v1	-1.10875				-1.38594				-1.66313			

Table 3.5d: Wind velocities on widened Bosbaan for north-west wind (300°) [m/s]

	300°,2.5m/s				300°, 5m/s				300°,7.5m/s			
	lane8	lane6	lane3	lane1	lane8	lane6	lane3	lane1	lane8	lane6	lane3	lane1
100	0.875	0.562	0.675	0.675	1.75	1.124	1.35	1.35	2.625	1.686	2.025	2.025
200	0.875	0.562	0.675	0.675	1.75	1.124	1.35	1.35	2.625	1.686	2.025	2.025
300	0.875	0.562	0.675	0.675	1.75	1.124	1.35	1.35	2.625	1.686	2.025	2.025
400	0.925	0.66	0.7325	0.73125	1.85	1.32	1.465	1.4605	2.775	1.98	2.1975	2.19075
500	1.025	0.8565	0.8475	0.844	2.05	1.713	1.695	1.681	3.075	2.5695	2.5425	2.5215
600	1.125	1.05275	0.96275	0.95675	2.25	2.1055	1.9255	1.902	3.375	3.15825	2.88825	2.853
700	1.075	1.0125	0.848	0.826	2.15	2.025	1.696	1.6075	3.225	3.0375	2.544	2.41125
800	1.025	0.972	0.7335	0.695	2.05	1.944	1.467	1.313	3.075	2.916	2.2005	1.9695
900	1.125	0.9805	0.77875	0.72875	2.25	1.961	1.5575	1.357	3.375	2.9415	2.33625	2.0355
1000	1.375	1.03775	0.984	0.92675	2.75	2.0755	1.968	1.7395	4.125	3.11325	2.952	2.60925
1100	1.625	1.09525	1.189	1.125	3.25	2.1905	2.378	2.122	4.875	3.28575	3.567	3.183
1200	1.595	1.229	1.16425	1.09775	3.19	2.458	2.3285	2.0625	4.785	3.687	3.49275	3.09375
1300	1.565	1.36275	1.13925	1.0705	3.13	2.7255	2.2785	2.0035	4.695	4.08825	3.41775	3.00525
1400	1.43	1.32875	1.07375	1.019	2.86	2.6575	2.1475	1.9285	4.29	3.98625	3.22125	2.89275
1500	1.19	1.1275	0.968	0.94375	2.38	2.255	1.936	1.8385	3.57	3.3825	2.904	2.75775
1600	0.95	0.926	0.86225	0.86825	1.9	1.852	1.7245	1.748	2.85	2.778	2.58675	2.622
1700	1.12	0.97075	0.94775	0.94175	2.24	1.9415	1.8955	1.872	3.36	2.91225	2.84325	2.808
1800	1.29	1.0155	1.033	1.0155	2.58	2.031	2.066	1.996	3.87	3.0465	3.099	2.994
1900	1.375	1.03775	1.0755	1.05225	2.75	2.0755	2.151	2.058	4.125	3.11325	3.2265	3.087
2000	1.375	1.03775	1.0755	1.05225	2.75	2.0755	2.151	2.058	4.125	3.11325	3.2265	3.087
mean	1.19075	0.96945	0.922013	0.895975	2.3815	1.9389	1.844025	1.739875	3.57225	2.90835	2.766038	2.609813
v8-v3	0.268738				0.537475				0.806213			
v6-v1	0.073475				0.199025				0.298538			

	300°,10m/s				300°,12.5m/s				300°,15m/s			
	lane8	lane6	lane3	lane1	lane8	lane6	lane3	lane1	lane8	lane6	lane3	lane1
100	3.5	2.248	2.7	2.7	4.375	2.81	3.375	3.375	5.25	3.372	4.05	4.05
200	3.5	2.248	2.7	2.7	4.375	2.81	3.375	3.375	5.25	3.372	4.05	4.05
300	3.5	2.248	2.7	2.7	4.375	2.81	3.375	3.375	5.25	3.372	4.05	4.05
400	3.7	2.64	2.93	2.921	4.625	3.3	3.6625	3.65125	5.55	3.96	4.395	4.3815
500	4.1	3.426	3.39	3.362	5.125	4.2825	4.2375	4.2025	6.15	5.139	5.085	5.043
600	4.5	4.211	3.851	3.804	5.625	5.26375	4.81375	4.755	6.75	6.3165	5.7765	5.706
700	4.3	4.05	3.392	3.215	5.375	5.0625	4.24	4.01875	6.45	6.075	5.088	4.8225
800	4.1	3.888	2.934	2.626	5.125	4.86	3.6675	3.2825	6.15	5.832	4.401	3.939
900	4.5	3.922	3.115	2.714	5.625	4.9025	3.89375	3.3925	6.75	5.883	4.6725	4.071
1000	5.5	4.151	3.936	3.479	6.875	5.18875	4.92	4.34875	8.25	6.2265	5.904	5.2185
1100	6.5	4.381	4.756	4.244	8.125	5.47625	5.945	5.305	9.75	6.5715	7.134	6.366
1200	6.38	4.916	4.657	4.125	7.975	6.145	5.82125	5.15625	9.57	7.374	6.9855	6.1875
1300	6.26	5.451	4.557	4.007	7.825	6.81375	5.69625	5.00875	9.39	8.1765	6.8355	6.0105
1400	5.72	5.315	4.295	3.857	7.15	6.64375	5.36875	4.82125	8.58	7.9725	6.4425	5.7855
1500	4.76	4.51	3.872	3.677	5.95	5.6375	4.84	4.59625	7.14	6.765	5.808	5.5155
1600	3.8	3.704	3.449	3.496	4.75	4.63	4.31125	4.37	5.7	5.556	5.1735	5.244
1700	4.48	3.883	3.791	3.744	5.6	4.85375	4.73875	4.68	6.72	5.8245	5.6865	5.616
1800	5.16	4.062	4.132	3.992	6.45	5.0775	5.165	4.99	7.74	6.093	6.198	5.988
1900	5.5	4.151	4.302	4.116	6.875	5.18875	5.3775	5.145	8.25	6.2265	6.453	6.174
2000	5.5	4.151	4.302	4.116	6.875	5.18875	5.3775	5.145	8.25	6.2265	6.453	6.174
mean	4.763	3.8778	3.68805	3.47975	5.95375	4.84725	4.610063	4.349688	7.1445	5.8167	5.532075	5.219625
v8-v3	1.07495				1.343688				1.612425			
v6-v1	0.39805				0.497563				0.597075			

Table 3.6a: Flow velocities on widened Bosbaan for north-east wind (45°) [m/s]

	45°,2.5m/s				45°,5m/s				45°,7.5m/s			
	lane8	lane6	lane3	lane1	lane8	lane6	lane3	lane1	lane8	lane6	lane3	lane1
100	-0.01787	-0.01325	-0.00636	-0.00331	-0.03792	-0.02692	-0.01063	-0.00406	-0.05841	-0.04127	-0.01502	-0.00499
200	-0.03417	-0.02503	-0.01125	-0.00495	-0.07321	-0.05143	-0.01912	-0.00545	-0.11329	-0.07891	-0.02667	-0.00565
300	-0.03271	-0.02372	-0.01026	-0.00414	-0.07039	-0.0489	-0.01775	-0.0041	-0.10946	-0.07506	-0.02464	-0.00335
400	-0.03154	-0.02306	-0.01135	-0.00645	-0.06741	-0.04733	-0.01992	-0.00883	-0.10471	-0.07252	-0.02818	-0.01072
500	-0.02875	-0.02167	-0.0127	-0.00982	-0.0612	-0.04451	-0.02298	-0.01638	-0.09526	-0.06808	-0.03293	-0.02266
600	-0.02591	-0.02073	-0.01408	-0.01309	-0.0549	-0.04253	-0.02575	-0.02355	-0.08638	-0.06528	-0.03678	-0.03338
700	-0.02353	-0.02056	-0.01476	-0.01429	-0.05073	-0.04276	-0.02658	-0.02536	-0.08119	-0.06686	-0.03679	-0.03474
800	-0.02325	-0.02114	-0.0142	-0.0131	-0.05295	-0.04535	-0.02357	-0.02028	-0.08538	-0.07195	-0.03129	-0.02591
900	-0.02804	-0.02219	-0.01162	-0.0089	-0.06512	-0.04779	-0.01701	-0.01008	-0.10409	-0.07495	-0.02158	-0.011
1000	-0.03626	-0.02295	-0.00816	-0.00268	-0.0819	-0.04738	-0.01088	0.00128	-0.12915	-0.07235	-0.01323	0.004735
1100	-0.04207	-0.02283	-0.00644	0.001585	-0.0926	-0.04574	-0.00843	0.008838	-0.14442	-0.06866	-0.01031	0.015546
1200	-0.04038	-0.02303	-0.00694	0.001185	-0.08819	-0.04691	-0.00953	0.00861	-0.13724	-0.07128	-0.012	0.015729
1300	-0.03548	-0.02381	-0.00767	-0.00108	-0.07789	-0.05006	-0.01058	0.004679	-0.12174	-0.07732	-0.01335	0.010322
1400	-0.03396	-0.02453	-0.00734	-0.00148	-0.07455	-0.05226	-0.00973	0.003806	-0.11673	-0.08075	-0.01204	0.008825
1500	-0.0347	-0.02512	-0.00674	-0.0006	-0.07575	-0.05299	-0.00893	0.004825	-0.11835	-0.08127	-0.01114	0.009756
1600	-0.03497	-0.02523	-0.00688	-0.00023	-0.07566	-0.05241	-0.00985	0.004793	-0.11773	-0.07991	-0.01303	0.009317
1700	-0.03235	-0.02365	-0.00869	-0.0026	-0.06943	-0.04887	-0.01414	2.89E-05	-0.1078	-0.07437	-0.01978	0.002169
1800	-0.0286	-0.02119	-0.0111	-0.00611	-0.06132	-0.04359	-0.01928	-0.00693	-0.09543	-0.06633	-0.02767	-0.00807
1900	-0.02639	-0.01976	-0.01224	-0.008	-0.05653	-0.0403	-0.0219	-0.01115	-0.08822	-0.0614	-0.0316	-0.01413
2000	-0.02525	-0.01919	-0.01261	-0.00896	-0.05351	-0.03919	-0.02356	-0.01386	-0.08326	-0.05985	-0.03407	-0.01846
average	-0.03081	-0.02213	-0.01007	-0.00535	-0.06706	-0.04586	-0.0165	-0.00566	-0.10491	-0.07042	-0.0226	-0.00583
v8-v3	-0.02074				-0.05055				-0.08231			
v6-v1	-0.01678				-0.0402				-0.06459			

	45°,10m/s				45°,12.5m/s				45°,15m/s			
	lane8	lane6	lane3	lane1	lane8	lane6	lane3	lane1	lane8	lane6	lane3	lane1
100	-0.07869	-0.05565	-0.01933	-0.00604	-0.09927	-0.06995	-0.02364	-0.0072	-0.02383	-0.08437	-0.02785	-0.00824
200	-0.15314	-0.10643	-0.03395	-0.00606	-0.19349	-0.13383	-0.04121	-0.00669	-0.04575	-0.16141	-0.04819	-0.00707
300	-0.14855	-0.10122	-0.03121	-0.00277	-0.188	-0.12733	-0.03782	-0.00243	-0.04391	-0.15353	-0.04411	-0.00188
400	-0.14231	-0.09768	-0.03633	-0.01279	-0.18003	-0.12282	-0.04456	-0.01494	-0.13816	-0.14798	-0.05267	-0.01717
500	-0.12963	-0.09181	-0.0428	-0.0288	-0.16393	-0.11539	-0.05276	-0.03495	-0.22673	-0.13914	-0.06289	-0.0413
600	-0.1178	-0.08863	-0.0476	-0.04293	-0.14905	-0.11215	-0.05851	-0.05236	-0.2192	-0.13604	-0.06931	-0.06206
700	-0.1112	-0.09186	-0.04676	-0.04408	-0.14094	-0.11771	-0.05663	-0.05315	-0.20922	-0.1439	-0.06617	-0.0625
800	-0.11758	-0.09954	-0.0386	-0.03143	-0.14972	-0.12793	-0.04565	-0.03677	-0.19458	-0.15686	-0.05238	-0.04213
900	-0.14345	-0.1026	-0.02556	-0.01173	-0.18301	-0.13075	-0.02936	-0.01236	-0.1865	-0.15928	-0.03279	-0.01281
1000	-0.17694	-0.09699	-0.01509	0.008368	-0.22499	-0.12179	-0.01693	0.011919	-0.18796	-0.14634	-0.01865	0.01564
1100	-0.19666	-0.09117	-0.01196	0.022304	-0.24914	-0.11334	-0.01343	0.029024	-0.2036	-0.13531	-0.01498	0.035665
1200	-0.18661	-0.09554	-0.0143	0.022653	-0.23615	-0.11967	-0.01622	0.02967	-0.23481	-0.14368	-0.01828	0.036615
1300	-0.16585	-0.10467	-0.01583	0.015634	-0.21013	-0.13226	-0.01813	0.021039	-0.26997	-0.1597	-0.02042	0.026292
1400	-0.1592	-0.10934	-0.01408	0.013474	-0.20179	-0.13807	-0.01625	0.018136	-0.29075	-0.1667	-0.01828	0.022439
1500	-0.16097	-0.10951	-0.01324	0.014216	-0.20389	-0.1378	-0.0156	0.018668	-0.2782	-0.16584	-0.01805	0.022817
1600	-0.15964	-0.10743	-0.01625	0.013527	-0.20198	-0.13477	-0.01951	0.017593	-0.25289	-0.16211	-0.02314	0.021431
1700	-0.14637	-0.09996	-0.02552	0.004211	-0.18503	-0.12518	-0.03118	0.006097	-0.24133	-0.15075	-0.03725	0.00796
1800	-0.12983	-0.08912	-0.03603	-0.00932	-0.16437	-0.11151	-0.04456	-0.01058	-0.23845	-0.13434	-0.05309	-0.01164
1900	-0.11967	-0.08259	-0.04132	-0.0175	-0.15172	-0.1034	-0.05128	-0.02073	-0.23315	-0.12461	-0.06098	-0.02373
2000	-0.1125	-0.08062	-0.04475	-0.02356	-0.14245	-0.10115	-0.05562	-0.0284	-0.21448	-0.12201	-0.06628	-0.03299
average	-0.14283	-0.09512	-0.02853	-0.00613	-0.18095	-0.11984	-0.03444	-0.00642	-0.19667	-0.14469	-0.04029	-0.00673
v8-v3	-0.11431				-0.14651				-0.15639			
v6-v1	-0.08899				-0.11342				-0.13796			

Table 3.6b: Flow velocities on widened Bosbaan for south-east wind (120°) [m/s]

	120°,2.5m/s				120°,5m/s				120°,7.5m/s			
	lane8	lane6	lane3	lane1	lane8	lane6	lane3	lane1	lane8	lane6	lane3	lane1
100	-0.00012	-0.00528	-0.01155	-0.01273	0.002035	-0.00815	-0.0226	-0.0252	0.004178	-0.01255	-0.03422	-0.03776
200	0.000329	-0.00865	-0.02173	-0.02457	0.006863	-0.01366	-0.04403	-0.04965	0.013026	-0.02073	-0.06721	-0.07469
300	0.00115	-0.00713	-0.02096	-0.02428	0.010549	-0.01093	-0.04371	-0.04993	0.019639	-0.01574	-0.06756	-0.07586
400	0.000934	-0.0073	-0.021	-0.02414	0.012	-0.01082	-0.04405	-0.0503	0.022819	-0.01486	-0.06857	-0.07727
500	0.000484	-0.00771	-0.02015	-0.023	0.013686	-0.01079	-0.04292	-0.04882	0.026009	-0.01459	-0.06707	-0.0756
600	0.001291	-0.00788	-0.01962	-0.02254	0.016132	-0.01057	-0.0417	-0.04773	0.030077	-0.01422	-0.06524	-0.07424
700	0.0011	-0.00792	-0.01972	-0.02342	0.01682	-0.01237	-0.04167	-0.04944	0.031419	-0.01753	-0.06513	-0.07681
800	0.000259	-0.0093	-0.02019	-0.0246	0.015392	-0.01656	-0.0426	-0.05176	0.029644	-0.02464	-0.0665	-0.08021
900	-0.00056	-0.01063	-0.02039	-0.02412	0.013093	-0.01928	-0.04311	-0.05052	0.026473	-0.02882	-0.06747	-0.07814
1000	-0.00097	-0.01072	-0.02037	-0.02228	0.009734	-0.01886	-0.04317	-0.04665	0.021397	-0.02768	-0.06777	-0.07209
1100	-0.00111	-0.00999	-0.02032	-0.02095	0.006693	-0.01664	-0.04305	-0.04405	0.016538	-0.02364	-0.06773	-0.0685
1200	-0.0002	-0.00913	-0.02012	-0.02191	0.009522	-0.01482	-0.04267	-0.04628	0.020488	-0.02096	-0.06698	-0.07216
1300	0.001805	-0.00836	-0.02	-0.0239	0.017162	-0.01357	-0.04248	-0.05058	0.031989	-0.01965	-0.06632	-0.07861
1400	0.00321	-0.00758	-0.02088	-0.02575	0.023334	-0.01187	-0.04436	-0.05467	0.041715	-0.01731	-0.06923	-0.08473
1500	0.004765	-0.00672	-0.02275	-0.02788	0.026678	-0.00965	-0.04872	-0.06001	0.047428	-0.01309	-0.07627	-0.09334
1600	0.005809	-0.00602	-0.02467	-0.03017	0.026993	-0.00684	-0.05301	-0.06611	0.048286	-0.00725	-0.08312	-0.10394
1700	0.003914	-0.00557	-0.02507	-0.03211	0.018246	-0.00508	-0.05339	-0.0712	0.033724	-0.00317	-0.08342	-0.11255
1800	-0.00261	-0.00584	-0.02408	-0.03317	0.000319	-0.00562	-0.05029	-0.07325	0.00272	-0.00405	-0.07725	-0.115
1900	-0.00817	-0.00632	-0.02307	-0.03317	-0.01395	-0.00708	-0.04717	-0.07176	-0.02277	-0.00742	-0.07065	-0.11116
2000	-0.01038	-0.00711	-0.02225	-0.03172	-0.021	-0.00991	-0.04494	-0.06703	-0.0352	-0.01251	-0.06635	-0.10259
average	4.75E-05	-0.00776	-0.02095	-0.02532	0.010515	-0.01165	-0.04398	-0.05375	0.02048	-0.01602	-0.0682	-0.08326
v8-v3	0.020993				0.054497				0.088684			
v6-v1	0.017563				0.042094				0.067241			

	120°,10m/s				120°,12.5m/s				120°,15m/s			
	lane8	lane6	lane3	lane1	lane8	lane6	lane3	lane1	lane8	lane6	lane3	lane1
100	0.005968	-0.01712	-0.04575	-0.05036	0.007638	-0.02195	-0.05706	-0.06288	0.009302	-0.02685	-0.06849	-0.07543
200	0.018729	-0.02811	-0.09025	-0.09956	0.024276	-0.03604	-0.11286	-0.12416	0.029805	-0.04417	-0.13562	-0.14871
300	0.028637	-0.02083	-0.09144	-0.10126	0.037649	-0.02636	-0.11495	-0.12635	0.046693	-0.03216	-0.13852	-0.15122
400	0.03364	-0.01911	-0.09323	-0.10352	0.044557	-0.02354	-0.1177	-0.12964	0.055783	-0.02818	-0.14221	-0.15548
500	0.038337	-0.01848	-0.09141	-0.10182	0.050789	-0.02241	-0.1157	-0.12793	0.063754	-0.02633	-0.14003	-0.15388
600	0.044244	-0.01798	-0.08898	-0.10049	0.058458	-0.02174	-0.11272	-0.12653	0.073154	-0.02543	-0.13654	-0.15248
700	0.046386	-0.02282	-0.08876	-0.10396	0.061343	-0.02829	-0.11241	-0.13096	0.076776	-0.03369	-0.13622	-0.15771
800	0.044116	-0.03303	-0.09062	-0.10813	0.058917	-0.04191	-0.11476	-0.13601	0.073948	-0.05069	-0.13911	-0.16347
900	0.040136	-0.03885	-0.0922	-0.10505	0.05431	-0.04928	-0.11682	-0.13197	0.06873	-0.05989	-0.14169	-0.1584
1000	0.033854	-0.03678	-0.09285	-0.0972	0.046605	-0.04618	-0.11789	-0.12215	0.059843	-0.05567	-0.14284	-0.1467
1100	0.027425	-0.03084	-0.09259	-0.09273	0.038403	-0.03809	-0.11766	-0.1167	0.049906	-0.04517	-0.14236	-0.14065
1200	0.03212	-0.02728	-0.09134	-0.09774	0.043848	-0.0336	-0.1157	-0.12328	0.056135	-0.04002	-0.13996	-0.14886
1300	0.047154	-0.02581	-0.0904	-0.10639	0.06263	-0.03248	-0.11408	-0.13417	0.078353	-0.03932	-0.13793	-0.16186
1400	0.060488	-0.02273	-0.09422	-0.11473	0.079603	-0.02871	-0.11871	-0.14461	0.098826	-0.03477	-0.14332	-0.17445
1500	0.068713	-0.01655	-0.10378	-0.12683	0.090293	-0.02007	-0.13099	-0.16039	0.112128	-0.02383	-0.158	-0.19374
1600	0.070035	-0.00733	-0.1133	-0.14187	0.092113	-0.00683	-0.14339	-0.18009	0.11437	-0.0065	-0.17338	-0.21809
1700	0.0491	-0.00053	-0.11362	-0.1538	0.064354	0.002849	-0.14363	-0.1955	0.079564	0.006225	-0.17378	-0.23703
1800	0.004132	-0.00187	-0.10388	-0.15648	0.004272	0.000637	-0.13	-0.19825	0.00427	0.003197	-0.15616	-0.23976
1900	-0.03284	-0.00724	-0.09347	-0.15038	-0.04503	-0.00684	-0.11549	-0.18959	-0.05713	-0.00628	-0.13743	-0.22861
2000	-0.05042	-0.01444	-0.0873	-0.13819	-0.06764	-0.01588	-0.10754	-0.17393	-0.08472	-0.01706	-0.12759	-0.20958
average	0.030498	-0.02039	-0.09247	-0.11252	0.040369	-0.02484	-0.1165	-0.14175	0.050474	-0.02933	-0.14056	-0.1708
v8-v3	0.122967				0.156873				0.191033			
v6-v1	0.092137				0.116918				0.141475			

Table 3.6c: Flow velocities on widened Bosbaan for south-west wind (210°) [m/s]

	210°,2.5m/s				210°,5m/s				210°,7.5m/s			
	lane8	lane6	lane3	lane1	lane8	lane6	lane3	lane1	lane8	lane6	lane3	lane1
100	-0.00172	0.002862	0.009314	0.010763	-0.01246	-0.00247	0.019763	0.024756	-0.01816	-0.00677	0.030432	0.037785
200	-0.00739	0.003441	0.020061	0.024227	-0.03103	-0.00903	0.042573	0.054586	-0.04656	-0.01977	0.066229	0.084654
300	-0.01254	0.00067	0.022114	0.027888	-0.03879	-0.01309	0.046355	0.06008	-0.06124	-0.02561	0.073063	0.094671
400	-0.01182	0.000424	0.022829	0.028532	-0.03777	-0.00951	0.04712	0.059024	-0.06291	-0.01853	0.074269	0.092481
500	-0.00818	0.00262	0.022617	0.027087	-0.0294	0.000572	0.046587	0.054683	-0.05051	-0.00082	0.07252	0.084282
600	-0.0042	0.00835	0.021861	0.024341	-0.01667	0.015781	0.044931	0.048303	-0.02968	0.024086	0.069028	0.073115
700	-0.00046	0.012307	0.020129	0.021138	-0.00774	0.025037	0.040963	0.041364	-0.01532	0.039394	0.062583	0.061333
800	0.002339	0.012342	0.017939	0.018858	-0.00395	0.025113	0.035721	0.036493	-0.00889	0.039991	0.054451	0.053573
900	0.004549	0.012404	0.016727	0.017914	0.002811	0.024691	0.032527	0.034596	0.002374	0.038946	0.049305	0.051222
1000	0.008831	0.013192	0.016502	0.017242	0.015771	0.025714	0.03182	0.033091	0.022967	0.039683	0.047902	0.049433
1100	0.017125	0.014444	0.016249	0.015539	0.034764	0.027563	0.031499	0.029546	0.053036	0.041207	0.047326	0.043795
1200	0.018522	0.014181	0.016115	0.014927	0.038969	0.026376	0.031445	0.028141	0.061261	0.038651	0.047025	0.041107
1300	0.009051	0.011527	0.01844	0.018958	0.015937	0.019795	0.037139	0.037492	0.025357	0.028022	0.056334	0.056539
1400	0.001151	0.008851	0.021343	0.024032	-0.00733	0.013263	0.0448	0.050145	-0.0136	0.017035	0.069637	0.078057
1500	-0.0004	0.008057	0.021762	0.025805	-0.01325	0.011577	0.046695	0.054918	-0.02521	0.01414	0.073608	0.086601
1600	0.000248	0.008395	0.020957	0.025423	-0.00974	0.012632	0.045145	0.055043	-0.02131	0.016028	0.071587	0.087572
1700	-0.00046	0.008045	0.022112	0.02646	-0.0125	0.011174	0.047492	0.058435	-0.02633	0.013466	0.075211	0.092996
1800	-0.00452	0.006115	0.025512	0.029837	-0.02438	0.005635	0.055385	0.066177	-0.04434	0.00428	0.087168	0.103953
1900	-0.01009	0.003832	0.028776	0.033131	-0.03429	0.001309	0.06214	0.071674	-0.05812	-0.00127	0.096755	0.11023
2000	-0.01166	0.002842	0.029582	0.033709	-0.0353	0.001552	0.062808	0.07033	-0.0576	0.001702	0.096352	0.105733
mean	-0.00058	0.007745	0.020547	0.023291	-0.01032	0.010684	0.042645	0.048444	-0.01874	0.014193	0.066039	0.074457
v8-v3	-0.02113				-0.05296				-0.08478			
v6-v1	-0.01555				-0.03776				-0.06026			

	210°,10m/s				210°,12.5m/s				210°,15m/s			
	lane8	lane6	lane3	lane1	lane8	lane6	lane3	lane1	lane8	lane6	lane3	lane1
100	-0.02348	-0.0103	0.04047	0.051214	-0.02919	-0.01427	0.050642	0.06472	-0.03501	-0.01831	0.060844	0.078401
200	-0.06213	-0.02989	0.088991	0.115334	-0.07836	-0.04077	0.111961	0.146159	-0.09476	-0.05182	0.134969	0.17737
300	-0.08426	-0.03851	0.099467	0.12949	-0.10777	-0.052	0.12599	0.16439	-0.13145	-0.06568	0.152572	0.199644
400	-0.08798	-0.02772	0.101396	0.125913	-0.11332	-0.03719	0.128499	0.159356	-0.13882	-0.04666	0.15547	0.192928
500	-0.07133	-0.00198	0.098365	0.113549	-0.09226	-0.00295	0.123993	0.142747	-0.11328	-0.00383	0.149224	0.171894
600	-0.04259	0.03301	0.092752	0.097285	-0.05562	0.042455	0.116132	0.121313	-0.06875	0.051958	0.139159	0.145509
700	-0.02277	0.054951	0.083623	0.080418	-0.03037	0.070945	0.104153	0.099645	-0.03816	0.087094	0.124647	0.118891
800	-0.01371	0.056321	0.072699	0.069628	-0.01868	0.072868	0.090475	0.085801	-0.02384	0.089848	0.108159	0.10177
900	0.001816	0.054132	0.065854	0.067131	0.001308	0.069678	0.08225	0.082655	0.000576	0.085709	0.09814	0.098365
1000	0.030268	0.053923	0.063904	0.065477	0.037504	0.068438	0.079907	0.081278	0.044742	0.083156	0.095722	0.097205
1100	0.071627	0.054889	0.063281	0.057851	0.090253	0.068376	0.079284	0.071856	0.108959	0.081894	0.095433	0.086001
1200	0.083534	0.050759	0.062811	0.054022	0.10638	0.062491	0.078465	0.066906	0.129388	0.074106	0.094282	0.079968
1300	0.035497	0.036057	0.075348	0.075531	0.046053	0.04394	0.094071	0.094588	0.057374	0.05175	0.112648	0.113355
1400	-0.01882	0.020409	0.094251	0.10589	-0.02385	0.023671	0.118795	0.133809	-0.02819	0.026896	0.142837	0.161614
1500	-0.03693	0.016202	0.100572	0.118341	-0.0486	0.017747	0.127724	0.15035	-0.06007	0.019256	0.154616	0.182691
1600	-0.03301	0.019049	0.098293	0.12009	-0.04499	0.021362	0.125251	0.152995	-0.05701	0.02372	0.15233	0.186174
1700	-0.04045	0.015031	0.103448	0.127529	-0.05506	0.01601	0.131992	0.162387	-0.06988	0.01669	0.160701	0.19748
1800	-0.06458	0.002205	0.1194	0.141476	-0.0853	-0.00039	0.151846	0.179201	-0.10624	-0.00321	0.184171	0.216806
1900	-0.08206	-0.0039	0.131275	0.148195	-0.10606	-0.00643	0.165541	0.185917	-0.1302	-0.00857	0.199523	0.223037
2000	-0.07953	0.002348	0.129185	0.140537	-0.10103	0.003768	0.161455	0.174741	-0.12256	0.005923	0.193389	0.208262
mean	-0.02704	0.017849	0.089269	0.100245	-0.03545	0.021388	0.112421	0.126041	-0.04386	0.024996	0.135442	0.151868
v8-v3	-0.11631				-0.14787				-0.1793			
v6-v1	-0.0824				-0.10465				-0.12687			

Table 3.6d: Flow velocities on widened Bosbaan for north-west wind (300°) [m/s]

	300°,2.5 m/s				300°,5m/s				300°, 7.5m/s			
	lane8	lane6	lane3	lane1	lane8	lane6	lane3	lane1	lane8	lane6	lane3	lane1
100	0.00959	0.006279	0.006684	0.006611	0.019549	0.010941	0.012222	0.012111	0.029599	0.015935	0.018473	0.018413
200	0.020258	0.012056	0.012203	0.011995	0.041504	0.020841	0.022551	0.022237	0.063418	0.029814	0.034243	0.03409
300	0.021711	0.011808	0.010748	0.010356	0.045042	0.019493	0.019578	0.019034	0.069792	0.02702	0.029734	0.029381
400	0.02272	0.012794	0.010948	0.010422	0.047893	0.021556	0.019508	0.018618	0.075006	0.02998	0.029311	0.028278
500	0.024097	0.015316	0.012293	0.011464	0.051951	0.028211	0.022215	0.020452	0.081914	0.040625	0.032804	0.03037
600	0.026095	0.019333	0.014009	0.012697	0.056597	0.03786	0.025945	0.022995	0.0893	0.056135	0.037774	0.033513
700	0.027572	0.021546	0.013028	0.010611	0.05901	0.04374	0.023873	0.018236	0.092696	0.065989	0.034294	0.025688
800	0.028266	0.021874	0.009482	0.005327	0.060488	0.045422	0.015773	0.005588	0.094706	0.06961	0.021822	0.006172
900	0.030831	0.02297	0.007779	0.001937	0.066065	0.047923	0.011873	-0.00212	0.103177	0.073939	0.015889	-0.00589
1000	0.036141	0.02438	0.009301	0.002081	0.077151	0.050319	0.015632	-0.00113	0.119842	0.077111	0.021646	-0.00478
1100	0.043097	0.025207	0.012891	0.004354	0.092274	0.050838	0.023684	0.003647	0.142888	0.076448	0.034173	0.00236
1200	0.047239	0.026753	0.013715	0.00392	0.101776	0.053239	0.025425	0.002519	0.157562	0.079029	0.037041	0.000856
1300	0.047937	0.030294	0.01151	0.001013	0.104203	0.061379	0.020138	-0.00356	0.161417	0.091788	0.028604	-0.00789
1400	0.046525	0.032445	0.009599	-0.00033	0.102253	0.067649	0.014811	-0.00689	0.158889	0.102558	0.019582	-0.01293
1500	0.040548	0.029624	0.008707	0.0014	0.090299	0.063936	0.011603	-0.00486	0.141071	0.098791	0.01364	-0.01069
1600	0.030638	0.023148	0.009609	0.006361	0.069509	0.051542	0.012851	0.004067	0.109234	0.081474	0.015476	0.001979
1700	0.025424	0.019538	0.012752	0.011692	0.057952	0.04264	0.020187	0.015779	0.091242	0.067509	0.027304	0.019832
1800	0.028194	0.020131	0.015434	0.013573	0.062541	0.041568	0.027636	0.021903	0.097885	0.064068	0.039563	0.02976
1900	0.033139	0.021341	0.015566	0.012165	0.071477	0.042768	0.029034	0.020586	0.111172	0.064334	0.042562	0.028437
2000	0.03611	0.021817	0.014341	0.009905	0.077241	0.043739	0.026797	0.016614	0.119904	0.065324	0.039201	0.023009
average	0.031307	0.020933	0.01153	0.007378	0.067739	0.04228	0.020067	0.010291	0.105536	0.063874	0.028657	0.013497
v8-v3	0.019777				0.047672				0.076879			
v6-v1	0.013555				0.03199				0.050377			

	300°,10m/s				300°, 12.5m/s				300°,15m/s			
	lane8	lane6	lane3	lane1	lane8	lane6	lane3	lane1	lane8	lane6	lane3	lane1
100	0.039682	0.0207	0.024779	0.024784	0.049896	0.02534	0.031273	0.03134	0.060085	0.029906	0.037683	0.037794
200	0.085403	0.038079	0.046059	0.046115	0.107642	0.045816	0.058317	0.058571	0.129852	0.053357	0.070432	0.070818
300	0.094654	0.033527	0.040065	0.03994	0.119747	0.039162	0.050966	0.051065	0.144887	0.044527	0.061713	0.061937
400	0.102245	0.0375	0.039248	0.038244	0.129758	0.04409	0.049662	0.048725	0.157341	0.05044	0.06	0.059031
500	0.111959	0.052403	0.043575	0.040612	0.14241	0.063204	0.054652	0.051177	0.172867	0.074034	0.06572	0.061652
600	0.121977	0.073921	0.049869	0.044322	0.155249	0.09101	0.062078	0.055502	0.188408	0.108354	0.074469	0.066432
700	0.126626	0.087891	0.04492	0.03362	0.161082	0.109479	0.055579	0.041662	0.195285	0.131222	0.066503	0.049512
800	0.129276	0.093546	0.027959	0.007129	0.164278	0.117256	0.034309	0.007855	0.198959	0.141009	0.040671	0.008774
900	0.140379	0.099924	0.019799	-0.00976	0.178087	0.125771	0.023762	-0.01356	0.21546	0.151706	0.027788	-0.01717
1000	0.162569	0.104202	0.027637	-0.00869	0.205786	0.131226	0.033352	-0.01241	0.248629	0.158465	0.03921	-0.01618
1100	0.193429	0.101921	0.044809	0.000935	0.244592	0.127259	0.055179	-0.0005	0.295313	0.152461	0.065508	-0.00178
1200	0.213522	0.10422	0.04883	-0.00065	0.269963	0.129011	0.06035	-0.00229	0.32628	0.153507	0.072005	-0.00372
1300	0.219215	0.121827	0.037075	-0.01195	0.277134	0.151516	0.045355	-0.01609	0.335383	0.181354	0.053872	-0.02015
1400	0.216163	0.137324	0.02417	-0.01875	0.273582	0.17191	0.028558	-0.02459	0.331366	0.20684	0.032894	-0.03021
1500	0.192497	0.13371	0.015407	-0.01638	0.244148	0.168585	0.016909	-0.02216	0.296202	0.203438	0.018266	-0.0278
1600	0.149495	0.111682	0.017561	-0.00021	0.189906	0.142236	0.019435	-0.00265	0.23078	0.172633	0.021155	-0.00528
1700	0.124637	0.092907	0.034115	0.023542	0.157993	0.118771	0.040727	0.027174	0.191684	0.144902	0.047155	0.030413
1800	0.133205	0.08668	0.05157	0.037573	0.168316	0.109659	0.063583	0.045423	0.203743	0.132749	0.075574	0.052957
1900	0.15095	0.08559	0.056045	0.036467	0.190706	0.106891	0.06982	0.044315	0.230656	0.128036	0.08347	0.052072
2000	0.16266	0.086887	0.051387	0.029283	0.205714	0.108253	0.063963	0.035419	0.248683	0.129576	0.076163	0.041614
average	0.143527	0.085222	0.037244	0.016809	0.181799	0.106322	0.045891	0.020198	0.220093	0.127426	0.054513	0.023536
v8-v3	0.106283				0.135908				0.165581			
v6-v1	0.068413				0.086124				0.10389			

Table 3.7: Travel times and lane differences for a four on the widened course.

wind direction 45° — 118 m — 92 m

wind vel.	wind+flow: arrival times [s] lane 8	lane 6	lane 3	lane 1	difference [s] T8-T3 [s]	T6-T1 [s]	T6-T1 [s]
2.5	396.44	395.23	393.94	393.45	2.07	1.55	1.87
5	403.07	400.72	398.09	397.05	4.98	3.67	4.49
7.5	411.01	407.02	402.62	400.91	8.39	6.11	7.65
10	420	414.11	407.66	405.29	12.34	8.82	11.17
12.5	430.04	421.96	413.3	410.14	16.74	11.82	15.25
15	440.19	430.71	419.55	415.51	20.64	15.2	19.79

wind direction 120 ° — 118 m — 92 m

wind vel.	wind+flow: arrival times [s] lane 8	lane 6	lane 3	lane 1	difference [s] T8-T3 [s]	T6-T1 [s]	T6-T1 [s]
2.5	391.88	393.09	393.86	395.06	2.26	1.76	1.76
5	393.89	396.06	399.3	400.17	5.41	4.11	4.41
7.5	395.72	399.25	404.65	406.04	8.93	6.79	7.36
10	397.77	402.77	410.53	412.56	12.76	9.79	10.76
12.5	400.06	406.62	417	419.7	16.94	13.08	14.35
15	402.55	410.8	424.08	427.54	21.53	16.74	18.44

wind direction 210° — 118 m — 92 m

wind vel.	wind+flow: arrival times [s] lane 8	lane 6	lane 3	lane 1	difference [s] T8-T3 [s]	T6-T1 [s]	T6-T1 [s]
2.5	389.38	388.31	386.64	386.55	2.24	1.57	1.58
5	388.22	386.45	383.55	383.24	4.67	3.21	3.51
7.5	387.55	384.93	380.75	380.31	6.8	4.62	5.26
10	387.04	383.64	378.41	377.87	8.63	5.77	6.93
12.5	386.73	382.62	376.54	375.88	10.19	6.74	8.29
15	386.56	381.82	375.05	374.27	11.51	7.55	9.63

wind direction 300 ° — 118 m — 92 m

wind vel.	wind+flow: arrival times [s] lane 8	lane 6	lane 3	lane 1	difference [s] T8-T3 [s]	T6-T1 [s]	T6-T1 [s]
2.5	379.11	380.88	381.34	381.7	1.8	0.77	1.42
5	381.04	383.13	384.34	385.04	3.3	1.91	2.94
7.5	377.57	380.39	382.21	383.17	4.64	2.78	4.24
10	374.94	378.32	380.66	381.81	5.72	3.49	5.43
12.5	378.38	382.46	385.4	386.69	7.02	4.23	6.37
15	369.51	375.18	378.74	380.42	9.23	5.24	7.76

no wind: arrival time is 390.37 s.

wind direction 45° — 118 m — 92 m

wind vel.	just wind: arrival times [s] lane 8	lane 6	lane 3	lane 1	difference [s] T8-T3 [s]	T6-T1 [s]	T6-T1 [s]
2.5	394.69	394.14	393.61	393.36	1.08	0.78	1.07
5	399.84	398.52	397.3	396.76	2.54	1.76	2.52
7.5	405.95	403.64	401.53	400.64	4.42	3	4.3
10	413.03	409.51	406.3	405	6.73	4.51	6.5
12.5	421.14	416.13	411.65	409.83	9.49	6.3	9.16
15	430.38	423.58	417.6	415.17	12.78	8.41	12.23

118 m — 92 m

differences, just flow [s] T8-T3	T6-T1	T6-T1
0.99	0.77	0.8
2.44	1.91	1.97
3.97	3.11	3.35
5.61	4.31	4.67
7.25	5.52	6.09
7.86	6.79	7.56

wind direction 120° — 118 m — 92 m

wind vel.	just wind: arrival times [s] lane 8	lane 6	lane 3	lane 1	difference [s] T8-T3 [s]	T6-T1 [s]	T6-T1 [s]
2.5	392.29	392.79	393.55	393.72	1.26	0.93	1.09
5	394.39	395.49	397.22	397.6	2.83	2.11	2.4
7.5	396.69	398.47	401.38	402.04	4.69	3.57	4
10	399.22	401.8	406.07	407.1	6.85	5.3	5.88
12.5	401.97	405.42	411.34	412.78	9.37	7.36	8.06
15	404.92	409.38	417.18	419.14	12.26	9.76	10.52

118 m — 92 m

differences, just flow [s] T8-T3	T6-T1	T6-T1
1	0.83	0.67
2.58	2	2.01
4.24	3.22	3.36
5.91	4.49	4.88
7.57	5.72	6.29
9.27	6.98	7.92

wind direction 210° — 118 m — 92 m

wind vel.	just wind: arrival times [s] lane 8	lane 6	lane 3	lane 1	difference [s] T8-T3 [s]	T6-T1 [s]	T6-T1 [s]
2.5	388.98	388.55	387.76	387.74	1.22	0.81	0.92
5	387.74	386.95	385.57	385.55	2.17	1.4	1.56
7.5	386.65	385.6	383.88	383.83	2.77	1.77	2
10	385.76	384.5	382.66	382.6	3.1	1.9	2.24
12.5	385.01	383.62	381.91	381.88	3.1	1.74	2.16
15	384.42	383.03	381.52	381.48	2.9	1.55	1.93

118 m — 92 m

differences, just flow [s] T8-T3	T6-T1	T6-T1
1.02	0.76	0.66
2.5	1.81	1.95
4.03	2.85	3.26
5.53	3.87	4.69
7.09	5	6.13
8.61	6	7.7

wind direction 300° — 118 m — 92 m

wind vel.	just wind: arrival times [s] lane 8	lane 6	lane 3	lane 1	difference [s] T8-T3 [s]	T6-T1 [s]	T6-T1 [s]
2.5	380.95	381.8	381.82	381.92	0.87	0.12	0.69
5	384.24	385.12	385.3	385.5	1.66	0.35	1.08
7.5	382.55	383.42	383.59	383.82	1.04	0.4	1.2
10	381.73	382.37	382.42	382.61	0.69	0.24	1.01
12.5	386.86	387.43	387.56	387.64	0.7	0.21	0.67
15	379.69	381.2	381.35	381.55	1.66	0.35	0.77

118 m — 92 m

differences, just flow [s] T8-T3	T6-T1	T6-T1
0.93	0.65	0.73
1.64	1.56	1.86
3.6	2.38	3.04
5.03	3.25	4.42
6.32	4.02	5.7
7.57	4.89	6.99

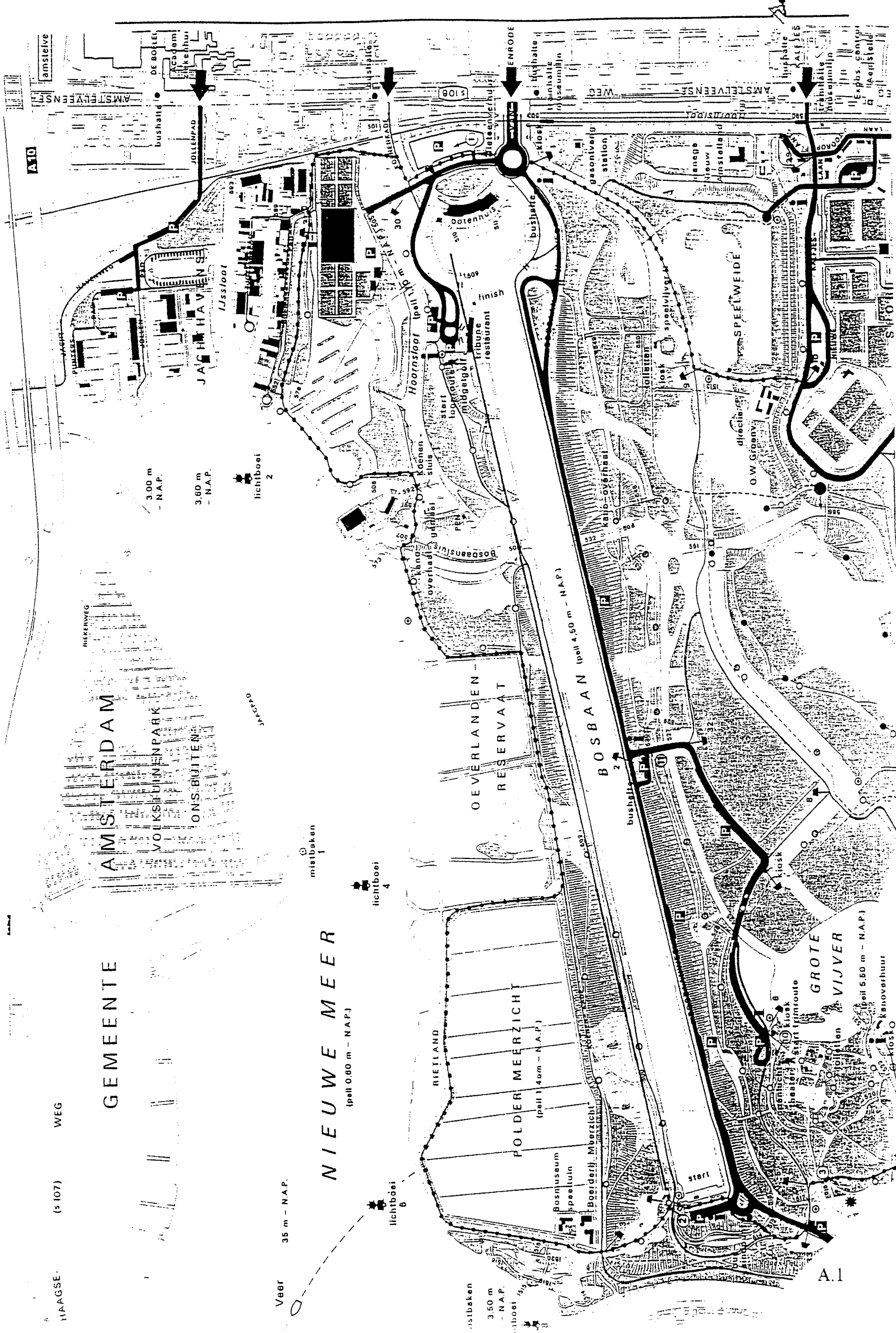
BOSBAAN
NIEUWE MEER
GEMEENTE AMSTERDAM
VOLKSTUINENPARK
ONS BUITEN
OEVERLANDEN-RESERVAAT
POLDER MEERZICHT
GROTE VIJVER
SPEELWEIDE
JACHTHAVEN
RIETLAND
AMSTELVEENSE WEG
HAAGSE WEG
finish
start
tribune restaurant
Bosbaansluis
lichtboei
kiosk
bushalte
A10

Distributions of frequencies of wind velocity and wind direction in July and August

wind force [Beaufort]	wind velocity U_{10} [m/s]
0-1	0-1.5
2	1.6-3.3
3	3.4-5.4
4	5.5-7.9
5	8.0-10.7
6	10.8-13.8
7	13.9-17.1

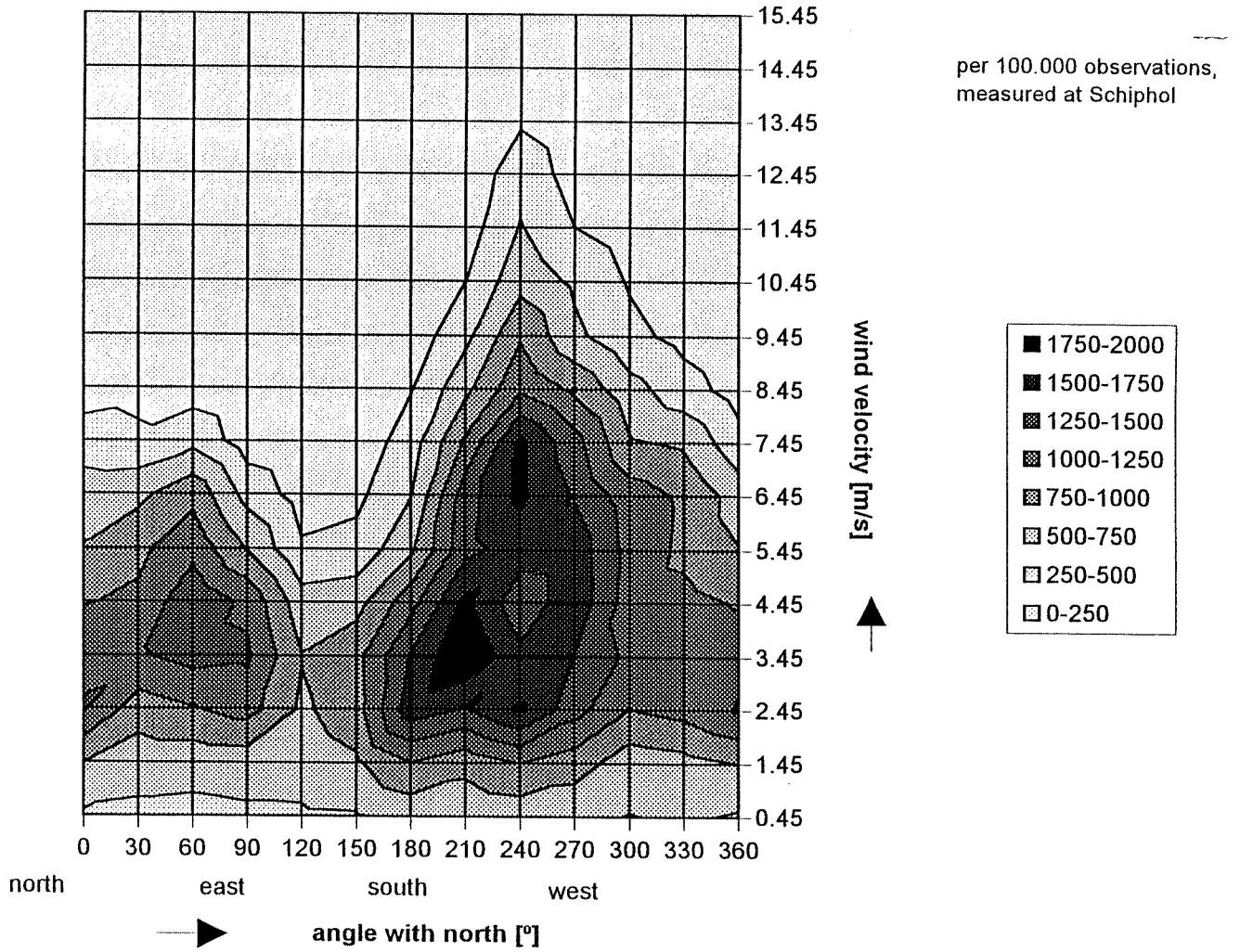

Appendix C ELEMENTS OF WATER RESISTANCE

A rowing combination on an undisturbed free surface of water with a constant speed, experiences a force, known as the total resistance, so that it opposes its motion and acts parallel to the motion of the boat. The actual forces acting directly on the hull are the normal pressure and the tangential shear forces, or skin friction, which when integrated over the hull result in the total resistance.

Frictional force is created by the forces between the surface of the hull and the water adjacent to it. These forces are so strong that the water can not slip along the body surface. Near the body surface, the water is at rest (in relation to the moving body), while the further out you get, the faster the speed of the water. The magnitude of the frictional force is determined by the rate at which the speed increases with the distance from the body surface, i.e. the velocity gradient.

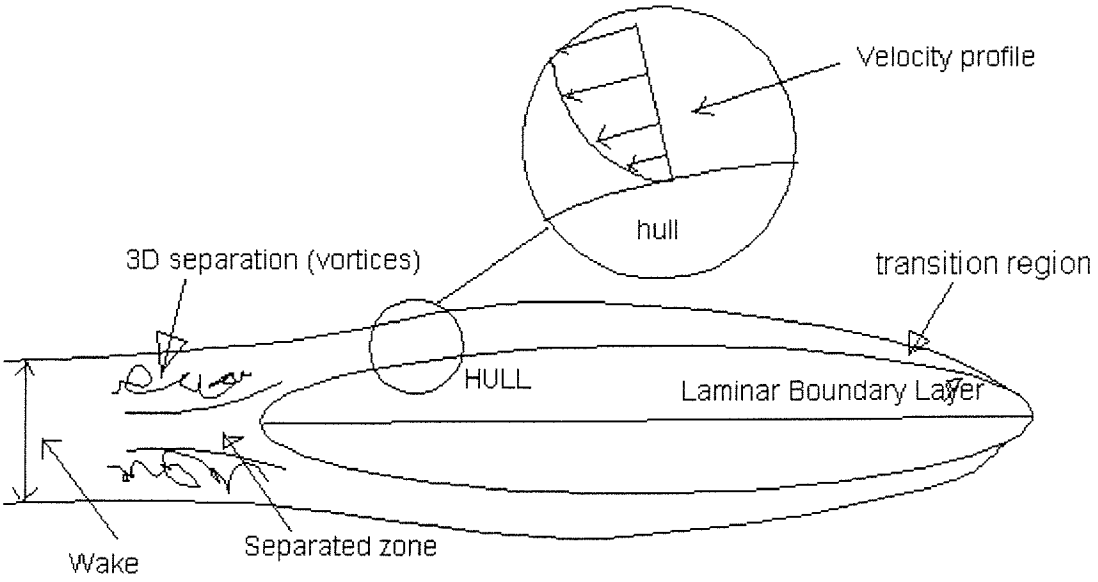

Figure C.1: The boundary layer around a hull.

To visualise this, a principal picture of the flow around the hull is shown in Figure C.1. Two main regions may be distinguished: one adjacent to the hull (the boundary layer), extending backward (the wake), and one outside this region, (the potential flow). There is one major difference between the two: viscosity may be neglected in the case of potential flow, while it is very important in the boundary layer.

From the above figure also appears that the boundary layer can be subdivided into several other regions. At the forward end of the hull the boundary layer is laminar, after a certain distance small disturbances in the flow can no longer be damped, but grow rapidly in a transition zone, leading to a seemingly irregular flow pattern which we call turbulence. The turbulent part of the boundary layer covers most of the hull and its characterised by a mean flow velocity growing from zero at the hull surface to a maximum value of about the speed of the hull at the boundary between the inner and outer regions.

If the hull has a blunt stern, separation may appear. In this region the mean flow velocity is very slow and may even be directed forwards. The eddies created are large and constitute a resistance on the movement of the hull. In the figure the thickness of the boundary layer is exaggerated, usually the thickness is about 2-3% of the hull length but has a dramatic effect in the resistance of the hull.

If the boundary layer is responsible for the friction, the potential flow may be considered responsible for the pressure forces. This may seem surprising, since one may consider that the pressure must be applied on the hull by the water particles closest to the hull surface, i.e. inside the boundary layer. However, the pressure is a quantity depended on the global flow picture, and is influenced by conditions everywhere in the fluid. The very thin boundary layer has a very minor influence on the global picture of the flow and in fact, in many applications, the pressure forces may be calculated without taking into account the boundary layer at all. On the other hand, it is impossible to determine frictional forces without taking into account the potential flow, since the pressure distribution determines the development of the boundary layer along the hull surface.

Hence, the total resistance can be split into a number of components -see Figure C.2- which although they interact with each other in a very complicated way, they may be assumed independent of each other for practical purposes.

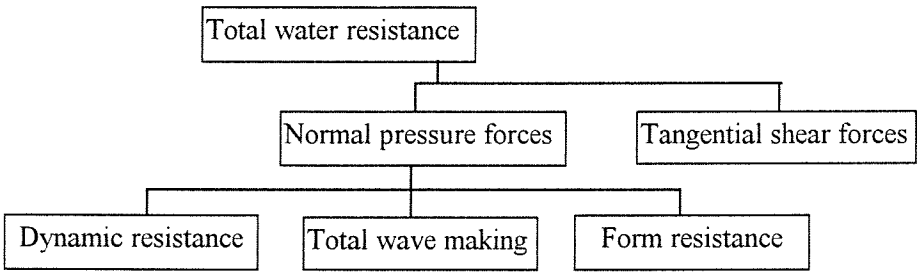

Figure C.2: Classifying total water resistance.

The tangential shear forces and the form resistance result both from the viscosity of the fluid and are further referred to as viscous resistance. Total wave making is referred to as wave resistance. Both wave resistance and viscous resistance are discussed below. The dynamic resistance also consists of differences in pressure force over the ship, and results from the motions of the ship. It is mostly taken into account as an extra component in the wave resistance.

The viscous resistance

The viscous resistance is considered to be equivalent to the sum of the frictional and a pressure resistance component of viscous origin. The frictional resistance is associated with the force required to overcome the tangential stresses developed between the hull and the viscous fluid. The pressure resistance is due to the pressure difference between the forebody and the aftbody as a consequence of the growth of the viscous boundary layer. This causes the pressure on the aftbody to be lower than on the forebody, leading to a resultant pressure force on the hull. Since this pressure force is of viscous origin, as distinct from forces associated with the pressure distribution over a body in potential flow, it is accordingly termed the viscous pressure resistance or form resistance.

The viscous resistance can be expressed as:

$$F_v = \frac{1}{2}\rho V^2 C_v A \tag{C.1}$$

where

$$C_v = (1+k)C_f \tag{C.2}$$

in which:

A is the wetted surface area of the body

C_f is the frictional resistance coefficient of the body, here assumed to be equivalent to that of a flat plate with the same Reynolds number as that of the subject body, i.e. using the ITTC 1957 formula:

$$C_f = \frac{0.075}{(\log \mathrm{Re} - 2)^2} \qquad (C.3)$$

1+k is the three-dimensional additional resistance of the body over that of the equivalent plate, and:

$$k = 0.0097(\theta_{entry} + \theta_{exit}) \qquad (C.4)$$

where θ_{entry} and θ_{exit} are the half angles (in degrees) of the bow and the stern, respectively, at the waterplane.

It should be noted that in the above expressions, the form factor, not only accounts for the viscous pressure resistance but also for the difference between the frictional coefficient of the equivalent flat plate and that of the body under investigation. This difference is due to the fact that the wall shear stress in the boundary layer along a three-dimensional body is different to that along a flat plate. 1+k also allows for changes of A with forward speed.

These relations are used to verify the values used in section 2.4.3, that were taken from 'Rowing' (1977). For the four-ours boat used for the calculations, the Reynolds number is $6.1 \cdot 10^7$. From equation (C.3) follows: $C_f = 0.0022$. The used four has a length-beam ratio of 1/24, resulting in an bow and stern angle of only 4.8°. With k = 0.046 (equation (C.4)), the viscous resistance coefficient $C_v = 0.00234$ (equations (C.1) and (C.2)). This is the same value as was used in section 2.4.3

The wave resistance

The wave resistance is the force required to maintain the energy of the wave pattern created by the boat. The flow around the body leads to an increase in pressure in the region of the bow, a decrease in pressure amidships and an increase in pressure astern. This leads to a wave peak at the bow, a wave trough amidships and a wave peak at the stern. Depending upon whether the bow and the stern wave are in phase or not, they can add to each other or they may partly cancel each other. As a consequence, the wave resistance coefficient of hulls shows "humps and hollows" as a function of speed. However, generally it can be said that wave resistance is a (rapidly) increasing function of the length-based Froude number, $Fr = v_b/\sqrt{gL}$, and thus decreases with increasing length.

After integration of the static pressure around a given hull, its possible to predict the wave resistance, e.g. the slender body theory of J.H. Mitchell, used by Tuck/Lazaukus (1996) to calculate the wave resistance of racing shells. They found that for all racing shells, wave resistance is generally only 10% of the total resistance. The anonymous article Boat Resistance in the Dutch rowing magazine "Rowing" gives a percentage of the same order of magnitude: 8%. The proportion of wave resistance to total resistance is lower than what is usually encountered with conventional ships, due to the high length/beam ratio.

This theory is wrongly based on deep water. Shallow water creates an additional hump in the wave resistance - Froude relation. The critical speed is when the boat velocity is approximately equal to the wave speed, which is the case for rowers on the Bosbaan - see van der Zee (1985). This is not further examined here, because of the small amount of wave resistance in comparison with the total resistance.

Appendix D WAVE GROWTH

Waves grow as a result of energy transferred from the wind to the water surface. Wave growth is strongly related to the strength and duration of the wind forces and to the distance (=fetch) over which the wind is blowing. A rough estimate of the wave height and wave period can be obtained from simple quasi-empirical, quasi-theoretical wave growth prediction formulae, which describe non-dimensional wave parameters in terms of non-dimensional wind parameters. The wave height H and the wave period T, and the wind fetch F and wind duration t were made non-dimensional through the wind velocity U and the gravity acceleration g.

$$F_{dim} = g\frac{F}{U^2} \quad , \quad t_{dim} = g\frac{t}{U} \quad , \quad H_{dim} = \frac{gH}{U^2} \quad , \quad T_{dim} = g\frac{T}{U} \tag{D.1}$$

In which: $U = U_{10}$ the wind velocity at a height of 10 meters above the surface.

The wave growth formulae in terms of non-dimensional quantities are of the following form:

$$H_{dim} = H_{\infty} \tanh\left(k_1 F_{dim}^{m_1}\right) \tag{D.2}$$

$$T_{dim} = T_{\infty} \tanh\left(k_2 F_{dim}^{m2}\right) \tag{D.3}$$

in which H_∞ and T_∞ are the values of H_{dim} and T_{dim} for unlimited fetch and duration.

In case of the Bosbaan, wind duration is assumed to have no influence, for only steady state computations are performed. The limiting parameter is the fetch. For wind parallel to the course axis, the fetch will be the largest. According to the wind tunnel tests performed by van Melle (1989), the local wind velocities above the course are parallel to the course axis for most of the weather bureau wind directions, resulting in the maximum possible fetch of 2000 meters. This is also the case for the normative situation: south-west wind of 10 m/s measured at Schiphol. For this case, the differences in wave growth between the lanes 1 and 6 as function of the fetch will be estimated.

The average wind velocity at lane 6 and at lane 1 (at 10 meters above the surface) amount to 2.6 m/s, and 4.4, respectively. For those two lanes the non-dimensional fetch is given in the columns 2 and 3 of Table D.1.The values vary between 50 and 3000. For this range, the empirical relations given by Groen/Dorrestein (1976) give the best results for the prediction of wave growth, according to Holthuijsen (1980). These relations are given by:

$$H_{dim} = 0.24 \tanh\left(0.015 F_{dim}^{0.45}\right) \qquad with\ F_{dim} > 10 \tag{D.5}$$

$$\begin{aligned} T_{dim} &= 0.502 \tanh\left(F_{dim}^{0.225}\right) \qquad with \quad 10 < F_{dim} < 400 \\ T_{dim} &= 2\pi \tanh\left(0.0345 F_{dim}^{0.37}\right) \qquad with \quad F_{dim} > 400 \end{aligned} \tag{D.6}$$

The columns 4 and 5 of Table D.1 give the values of the non-dimensional wave heights in the lanes 6 and 1. The columns 6 and 7 present the wave heights in dimensional form. The columns 8, 9, 10, and 11 present the wave periods in the same way.

F [m]	lane 6 Fdim	lane1 Fdim	lane 6 Hdim	lane1 Hdim	lane 6 H [m]	lane1 H [m]	lane 6 Tdim	lane1 Tdim	lane 6 T [s]	lane1 T [s]
0	0	0	0	0	0	0	0	0	0	0
100	148.53	50.9	0.03	0.02	0.02	0.04	1.55	1.22	0.28	0.38
200	297.05	101.81	0.05	0.03	0.03	0.06	1.81	1.42	0.33	0.44
300	445.58	152.71	0.06	0.03	0.04	0.07	2	1.56	0.37	0.49
400	594.1	203.61	0.06	0.04	0.04	0.08	2.2	1.66	0.4	0.52
500	742.63	254.51	0.07	0.04	0.05	0.08	2.38	1.75	0.44	0.55
600	891.16	305.42	0.07	0.05	0.05	0.09	2.52	1.82	0.46	0.57
700	1039.68	356.32	0.08	0.05	0.05	0.1	2.65	1.88	0.49	0.59
800	1188.21	407.22	0.08	0.05	0.06	0.1	2.77	1.94	0.51	0.61
900	1336.73	458.12	0.09	0.06	0.06	0.11	2.88	2.02	0.53	0.63
1000	1485.26	509.03	0.09	0.06	0.06	0.11	2.97	2.09	0.55	0.65
1100	1633.79	559.93	0.1	0.06	0.06	0.12	3.06	2.16	0.56	0.68
1200	1782.31	610.83	0.1	0.06	0.07	0.12	3.15	2.22	0.58	0.7
1300	1930.84	661.73	0.1	0.07	0.07	0.13	3.22	2.29	0.59	0.72
1400	2079.37	712.64	0.1	0.07	0.07	0.13	3.29	2.34	0.6	0.73
1500	2227.89	763.54	0.11	0.07	0.07	0.14	3.36	2.4	0.62	0.75
1600	2376.42	814.44	0.11	0.07	0.07	0.14	3.43	2.45	0.63	0.77
1700	2524.94	865.34	0.11	0.07	0.08	0.14	3.49	2.5	0.64	0.78
1800	2673.47	916.25	0.12	0.07	0.08	0.15	3.55	2.55	0.65	0.8
1900	2822	967.15	0.12	0.08	0.08	0.15	3.6	2.59	0.66	0.81
2000	2970.52	1018.05	0.12	0.08	0.08	0.15	3.65	2.64	0.67	0.82

Table D.1: wave growth on the lanes 6 and 1 for wind 210°, 10 m/s measured at Schiphol

The waves growth as a function of the distance from the west wall (fetch) is presented in Figure D.1. Waves in lane 1 are about twice as high as in lane 6. The wave period is in both cases very short, less than a second.

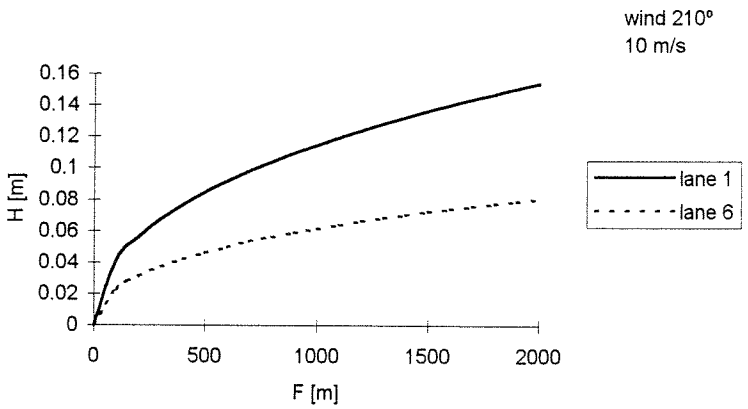

Figure D.1: Wave growth on the two outside lanes.

Water depth may affect wave generation: wave heights will be smaller and wave periods shorter if wave generation takes place in transitional or shallow water, rather than in deep water. The extend to which this effect takes place depends on the ratio wave length/ water depth. As this ratio increases, the bottom will influence waves stronger due to a greater influence of the bottom friction.

For the above described normative wind conditions, the deep water wave length, given by $L_0=gT^2/2\pi$ is at most 1 meter, resulting in a wave length/water depth ratio of 2. A ratio larger than 0.5 means

deep water, thus the waves on the Bosbaan can be treated as deep water waves, which will hardly affect the bottom friction, and thus the flow.

The wave propagation velocity in deep water is given by: $c_0 = gT/2\pi$, which amounts to 1.3 m/s at most.

In the same manner, the wave growth of waves oblique to the boat is estimated occurring at south or north wind. Those waves are found to have a maximum wave length of about 4 cm, which is much smaller than the width of the boats. The added resistance due to the rolling, and yawing motion of the boats is therefore neglected.

Appendix E PROGRAM LANE DIFFERENCES FOR A FOUR

```
      PROGRAM wind 45°, 10 m/s, lane 6
*     (Wind direction 45 degrees; wind velocity 10 m/s; lane 6)
*
      include 'variable'
      REAL TOL, getal1, getal2, getal3, getal4, sum,minuten,seconden
      REAL hulpb
      PARAMETER (TOL = 0.001)
      PARAMETER (max = 1000)
      REAL a(0:max), b(0:max), d(0:max), vb(0:max),Snelheid(20),tijd(20)
      OPEN (15,file='W45106.txt')
      OPEN (20,file='U45106.txt')
      DO i = 1, 20
        READ (15,*) w(i)
      ENDDO
      DO i = 1, 20
        READ (20,*) u(i)
      ENDDO
      DO i = 1, 20
        abegin = -6.0
        bbegin = 6.0
        getal1 = P(abegin)
        getal2 = P(bbegin)
        IF ((getal1*getal2).lt.0) THEN
          k = 1
          a(1) = abegin
          b(1) = bbegin
          d(0) = 1
            WHILE (d(k-1).ge.TOL) DO
              d(k) = 0.5*(b(k)-a(k))
              vb(k) = a(k)+d(k)
              hulpvb = vb(k)
              hulpa = a(k)
              hulpb = b(k)
              getal3 = P(hulpa)
              getal4 = P(hulpvb)
                IF ((getal3*getal4).gt.0) THEN
                  a(k+1) = vb(k)
                  b(k+1) = b(k)
                ENDIF
                IF ((getal3*getal4).le.0) THEN
                  a(k+1) =a(k)
                  b(k+1) =vb(k)
                ENDIF
              k = k+1
            ENDWHILE
```

```
      ELSE
        PRINT *,i
        PRINT *, 'kies ander interval'
      ENDIF
      Snelheid(i) = hulpvb
      PRINT *, Snelheid(i),i
    ENDDO
    DO i = 1, 20
      tijd(i) = 100/Snelheid(i)
    ENDDO
    sum = 0
    DO i = 1, 20
    sum = sum + tijd(i)
    ENDDO
    minuten = sum/60
    seconden = (minuten-INT(minuten))*60
    print *, sum
    print 11, sum,'seconden','=',INT(minuten),'.',NINT(seconden),
   $ 'minuten'
11   format (f6.2,1x,a8,1x,a1,1x,i1,a1,i2,1x,a7)
    END
*
*    Vermogen functie
*
    REAL FUNCTION P(x)
    include 'variable'
    REAL x, wa, wi
    wa = u(i)
    wi = w(i)
    Fw = 1.16*0.5*1000*2.3E-3*6*(x-wa)**2
    Flr = 0.8*0.8*0.5*1.2*(x-wi)**2
    Flb = 0.5*1.2*1*0.3*(x-wi)**2
    Ftot = Fw + Flr + Flb
    P = Ftot*x - 1157
    return
    END
```

Appendix F SOLVING THE SIMPLIFIED SHALLOW-WATER EQUATIONS

The shallow-water equations (6.17) can been linearised through the assumption of small Rossby number. The Rossby number is defined as the ratio of inertia to Coriolis forces. The water body is considered shallow, so that the dominant frictional forces are a result of bottom friction; horizontal diffusion of momentum is neglected. Due to the smallness of the water body, circulation is not affected by the rotation of the earth. The wind stress is prescribed as a boundary condition at the water surface (6.39). The motion is two-dimensional in the vertical *x-z* plane, so all terms in *y*-direction can be omitted. The eddy viscosity's are assumed to be constant over the water depth. With the above assumptions the shallow-water equations reduce to the following equations.

$$\frac{\partial u}{\partial x} + \frac{\partial w}{\partial z} = 0 \tag{F.1a}$$

$$0 = -\frac{1}{\rho}\frac{\partial P}{\partial x} + \frac{\partial}{\partial z}\left(\nu_t^{\nu}\frac{\partial u}{\partial z}\right) \tag{F.1b}$$

$$\frac{1}{\rho}\frac{\partial P}{\partial z} = -g \tag{F.1c}$$

Equation F.1c can be integrated, satisfying the surface condition

$$P = P_a \quad , \quad \text{yielding} \tag{F.2}$$

$$P(z) = P_a + \rho g(\zeta - z) \text{ and} \tag{F.3}$$

$$\frac{1}{\rho}\frac{\partial P}{\partial x} = g\frac{\partial \zeta}{\partial x} \tag{F.4}$$

Substitution into equation F.1b and integrating the result yields

$$\nu_t^{\nu}\frac{\partial u}{\partial z} = g\frac{\partial \zeta}{\partial x}z + A \tag{F.5}$$

$$\nu_t^{\nu}u = \frac{1}{2}g\frac{\partial \zeta}{\partial x}z^2 + Az + B \tag{F.6}$$

The constants A and B can be determined by satisfying the following bottom and surface boundary conditions

$$u = 0 \qquad at \qquad z = -d \tag{F.7}$$

$$\nu_t^{\nu}\frac{\partial u}{\partial z} = \frac{\tau_{sx}}{\rho} \qquad at \qquad z = \zeta \tag{F.8}$$

Combining F.7 and F.8 with F.5 and F.6 yields

$$A = \frac{\tau_{sx}}{\rho} - g\frac{\partial \zeta}{\partial x}\zeta \tag{F.9}$$

$$B = -\frac{1}{2}g\frac{\partial \zeta}{\partial x}d^2 + \frac{\tau_{sx}}{\rho}d - g\frac{\partial \zeta}{\partial x}\zeta d \tag{F.10}$$

ζ is assumed to be small in comparison with d, and can be neglected. This assumption yields the following distribution for u

$$u(z) = \frac{g}{2\nu_t^{\nu}}\frac{\partial \zeta}{\partial x}\left(z^2 - d^2\right) + \frac{\tau_{sx}}{\rho\nu_t^{\nu}}\left(z + d\right) \tag{F.11}$$

The surface elevation $\partial\zeta/\partial x$ can be calculated by using continuity for the water within a vertical column extending form the free surface to the bed

$$\frac{\partial}{\partial x}\int_{-d}^{\zeta} u\,dz = 0 \tag{F.12a}$$

which implies

$$\int_{-d}^{\zeta} u\,dz = \text{constant} \tag{F.12b}$$

which since there is no flow across the ends of the basin: $u = 0$ at $x = 0$ and $x = l$, reduces to

$$\int_{-d}^{\zeta} u\,dz = 0 \tag{F.12c}$$

Combining (F.11) and (F.12c) yields (again with neglecting of terms with ζ)

$$\frac{\partial \zeta}{\partial x} = \frac{3}{2dg}\frac{\tau_{sx}}{\rho} \tag{F.13}$$

and

$$u(z) = \frac{\tau_{sx}}{\rho\nu_t^{\nu}}\left(\frac{3}{4}\frac{z^2}{d} + \frac{1}{4}h + z\right) \tag{F.14}$$

The bottom stress τ_{bx} is for this situation equal to

$$\tau_{bx} = \rho\nu_t^{\nu}\left.\frac{\partial u}{\partial z}\right|_{z=-d} = \frac{1}{2}\tau_{sx} \tag{F.15}$$